INFORMATION TO USERS

This manuscript has been reproduced from the microfilm master. UMI films the text directly from the original or copy submitted. Thus, some thesis and dissertation copies are in typewriter face, while others may be from any type of computer printer.

The quality of this reproduction is dependent upon the quality of the copy submitted. Broken or indistinct print, colored or poor quality illustrations and photographs, print bleedthrough, substandard margins, and improper alignment can adversely affect reproduction.

In the unlikely event that the author did not send UMI a complete manuscript and there are missing pages, these will be noted. Also, if unauthorized copyright material had to be removed, a note will indicate the deletion.

Oversize materials (e.g., maps, drawings, charts) are reproduced by sectioning the original, beginning at the upper left-hand corner and continuing from left to right in equal sections with small overlaps.

ProQuest Information and Learning
300 North Zeeb Road, Ann Arbor, MI 48106-1346 USA
800-521-0600

University of Alberta

Analysis of Ice Jam Release Surges on the Athabasca River at Fort McMurray, AB

by

Twyla Kowalczyk

A thesis submitted to the Faculty of Graduate Studies and Research in partial fulfillment of the requirements for the degree of Master of Science

In

Water Resources Engineering

Department of Civil and Environmental Engineering

Edmonton, Alberta

Spring 2005

ABSTRACT

Past studies analyzing ice jam release events have been unable to capture surge propagation behaviour. Also, these studies have been inconclusive as to the effects of an ice cover on surge propagation. This research compiled all historical data (1977 to 1990) of ice jam release events documented along the Athabasca River near Fort McMurray. Measurements for breakup events of 2001, 2002 and 2003 were obtained using a remote monitoring network, and were compared to the historical events. The best event record (2002) was then modeled using River1-D. The celerity of the surge, and to a lesser degree, the peak magnitude attenuation were successfully modeled. Ice within the ice jam and in the downstream channel played a significant role in surge propagation. Additional studies of the ice processes associated with river ice breakup would further our knowledge of ice jam release.

ACKNOWLEDGEMENTS

The author gratefully acknowledges the support and friendship of her supervisor, Dr. Faye Hicks. The many hours of discussion and review have greatly improved the output of this thesis, as well as enhance the knowledge and experience attained by author. The opportunities of field work and to present the author's research at conferences was much appreciated.

Thank you to Dr. Thian Gan and Dr. David Chanasyk for their involvement in the thesis defense. Their comments and suggestions are much appreciated.

The many hours of work with Evan Friesenhan contributed to the development of the geometric dataset and made tedious tasks enjoyable. The author would also like to thank other graduate students for their assistance: Kristel Pelletier, Carin Meliefste, Karen Dow and Chandra Mahabir. For their assistance with field work, the Water Resources technical staff of Perry Fedun and Sheldon Lovell is gratefully acknowledged.

Golder Associates Ltd. (Golder) is acknowledged by the author for their support in the final stages of this thesis, including their assistance in printing the thesis and providing the opportunity to present the author's research to the Water Resources Group at Golder.

Financial assistance from NSERC is acknowledged. Cambell Scientific and Hoskins Instruments are appreciated for supplying various equipment as well as help in the installation phase. GIS base station data was provided by Pelaides Data Corps, and is gratefully acknowledged.

The love and support of Dean Hutchison is much appreciated; the author's many hours in front of the computer as well as the hours of frustration were made easier knowing that Dean was there through it all. The author's family is also acknowledged for their overwhelming support: Don, Viv, Kendra, Rhea and Murray.

TABLE OF CONTENTS

LIST OF TABLES

LIST OF FIGURES

LIST OF SYMBOLS

A	channel cross sectional area perpendicular to flow
B	channel width
c	celerity
C_*	non-dimensional Chezy coefficient
D	diffusive term of diffusive wave approximation
D_s	distance ice run has traveled
D_j	length of jam before release
F_r	Froude number
g	acceleration due to gravity
H	elevation of water surface above specified datum, known as stage
k	channel roughness height
k_b	channel roughness height for the bed of the channel
k_i	channel roughness height for the underside of an ice cover
L	length scale
m_o	relative backwater of ice jam
n	Manning coefficient
n_b	Manning coefficient for the bed of the channel
n_i	Manning coefficient for the underside of an ice cover
P	wetted perimeter
Q	discharge
R	hydraulic radius
S_f	longitudinal boundary friction slope
S_o	longitudinal channel bed slope
t	temporal coordinate
T	time scale
U	velocity scale
V	mean flow velocity
V_0	mean flow velocity downstream of ice jam
V_1	mean flow velocity of uniform flow section between surge and negative wave
V_S	velocity of surge
x	longitudinal coordinate
y	depth of flow
y_0	depth downstream of surge
y_1	depth of uniform flow section between surge and negative wave
y_2	depth upstream of ice jam
Y	depth scale
z	slope scale
α	kinematic wave speed coefficient
β	momentum flux correction coefficient

1 INTRODUCTION

River ice breakup is the manner in which an ice cover deteriorates and eventually disappears to create the open water condition experienced throughout the non-winter months. River ice can deteriorate both by thermally melting in place and by a mechanical process where the ice cracks into pieces and is carried along the river with the water flow. Which of these deterioration processes dominates is highly dependent on the meteorological conditions experienced. However, when mechanical processes dominate, ice runs typically result and ice jam formation and release become a flood risk issue.

Ice jams occur on many northern rivers, and in many cases are responsible for the most severe floods on record for rivers prone to ice jams. Canadian examples include: the Hay River, NT; the Saint John River, NB; and the Athabasca River, AB, to name only a few. North flowing rivers are particularly susceptible to mechanical breakups, since their southern headwaters are most likely to experience ice deterioration and snowmelt first, with the resulting runoff wave fracturing the deteriorated ice cover and carrying the resulting ice floes downstream towards strong competent ice in the north. Where the forces associated with the incoming ice run are not longer sufficient to push through this ice cover, this ice run will be arrested. Ice runs can also be hindered by a natural constriction to flow or bend along the channel, or by man-made obstacles such as bridge piers.

As an ice run is arrested, the ice floes consolidate and become densely packed forming an ice jam. An ice jam will grow in length with continued incoming ice floes but will also thicken as the accumulation compresses longitudinally. Not only are ice floes prevented from propagating downstream during such events, but the amount of passing water is also affected. If the ice run arrests with sufficient force, the ice floes may even ground out on the bed near the downstream end of the resulting jam (i.e., in the vicinity of the jam toe) creating what is called a grounded jam. An ice jam tends to store water within the spaces between ice floes in the accumulation. More significantly, the rough

texture decelerates the flow and results in a higher water level for a given discharge than is experienced under a smooth ice cover. Therefore, a substantial amount of water goes into storage underneath the ice jam as well. This deceleration creates backwater conditions upstream of the jam as well. Therefore, an ice jam involves a stationary accumulation of fractured ice that inhibits the passage of both ice and water. In the case of a grounded jam, this obstruction can be particularly severe.

Because of the significant obstruction to flow that an ice jam causes, water levels upstream can continue to build, especially if there is limited ability for the flow to escape overbank onto a floodplain. In such cases, if the building pressure forces on the ice jam exceed the resistive forces on the banks and/or the strength of the restraining ice cover, the ice jam will release. A surge of both ice and water will charge forth with drastic increases in water level experienced downstream of the release location (a surge becomes a wave when the stage hydrograph spreads out having a more gradual increase in water level). Ice jams may also release upon the arrival of a large increase in discharge, with its corresponding high water levels, and/or from an impacting ice run, both typically caused when upstream ice jams release. It is also common for ice jams to briefly reform and release as it propagates downstream creating a cascading effect of release events.

Due to the rapid water level increases that occur downstream of ice jam release locations, severe flooding can occur causing thousands to millions of dollars in damage to property and putting the lives of citizens in danger. One such event occurred in Badgar, NF, in 2003 where a 2 m high surge flooded the town. Residents of Badgar barely had enough time to flee for safety. During an event on the Saint John River in New Brunswick, ice entered and started flooded a town only 35 minutes after the release of the ice jam located about 5 km upstream (Beltaos *et al.*, 1994). The ice would have been traveling at about 2.4 m/s and the peak water level at 1.7 m/s giving the town little time to react.

The Athabasca River in Alberta frequently experiences ice jams that have been known to result in the flooding of the downtown section of Fort McMurray. Figure 1-1

shows the Athabasca River flowing northward towards Fort McMurray. The downtown sector is located on a low floodplain at the confluence of the Athabasca and Clearwater Rivers, as shown in an aerial view provided in Figure 1-2. Flooding within this downtown sector occurs when ice jams on the Athabasca River hinder the outflow from the Clearwater River. Water then backs up the Clearwater River and floods the city of Fort McMurray.

Historical documentation exists of ice jams and related flooding at Fort McMurray. The most significant events in the recent past occurred in 1977 and 1997, which both resulted in the flooding of the downtown sector. The ice jam of 1977 was documented by the Alberta Research Council in Figure 1-3 at the MacEwan Bridge, with flooding of the Clearwater River shown in Figure 1-4. Possibly the most dramatic of events was documented in 1875 by the Hudson's Bay Company, with its post (HBP) located on the right bank just downstream of where the current MacEwan Bridge crosses the Athabasca River (Figure 1-2). The following passage is extracted from a copy of the letter from Henry J. Moberly dated April 25th, 1875, from the archives of the Hudson's Bay Company:

"On the 20 Instant about 2 hours after daylight, the river suddenly gave signs of breaking up and in half an hour from that time the water had risen about 60 feet, and the whole place was flooded – the water and ice passing with fearful rapidity and carrying off everything before them. We had just enough time to escape to the hill, in our immediate vicinity, with the families, bedding and a little Provisions and Ammunition, and to throw up stairs the Furs and most of the valuable property, when the water was already rushing through the Fort. From the time the river first gave signs of starting hardly half an hour elapsed before there was 5 feet of water in the highest building in the Fort, and the Interpreter's house was carried bodily away and dashed to pieces in the Woods; the Workshop and Men's houses have been almost destroyed."

Clearly these are very dangerous events and it would be highly desirable to have some means of providing warning of there expected occurrence and severity. Analysis

has been performed on some ice jam release events, but data are scarce. Doyle and Andres (1979) measured a 3.6 m increase in water level on the Athabasca River at the MacEwan Bridge in Fort McMurray. This increase occurred within 45 minutes of the jam release, initially poised 11 km upstream of the MacEwan Bridge. These data were then used by Henderson and Gerard (1981) to study the applicability of the classic dam break scenario. A discrepancy was found between theory and observation in regards to the celerity of the surge with a theoretical value of 11 m/s compared to 4 m/s in the field. It was presumed that ice carried by the surge slowed it down considerably, as well as increased the height of the surge. A collection of more field data was recommended. Beltaos *et al.* (1994) obtained a much more detailed data set for a 1993 ice jam release on the Saint John River, NB, including channel geometry, a measured ice jam profile before release, and water levels downstream of the jam toe as the surge passed. However, significant propagation data was not possible due to a hydro-power facility downstream of the release location. These data were used in a numerical simulation using the unsteady flow model cdg-1D (Hicks *et al.*, 1997). Modeled results adequately reproduced surge propagation speed, but were relatively inaccurate at predicting stage. The resulting discrepancies were attributed to the effects of an ice cover downstream of the toe of the jam as well as the approximated geometry.

Laboratory studies have also been attempted, such as Wong *et al.* (1985) and Khan *et al.* (2000). Wong and his colleagues used polyethylene blocks to form an ice jam by obstructing the blocks with a retaining gate, which was lifted suddenly to simulate a jam release. The study concluded that moving ice has little effect on surge characteristics and that assuming one-dimensional flow is valid. The experiments performed by Khan *et al.* (2000) studied the effects of floating debris on dam-break surges using a similar method as Wong *et al.* (1985). This debris (again polyethylene blocks) was not only placed into an ice jam formation, but was also placed in the downstream channel with a uniform surface debris concentration. Debris was found to slow the celerity of the surge wave, with small debris particles causing the surge to slow even faster. It was also found that the average relative surge height increased with a higher concentration of debris. Laboratory experiments are limited due to the physical

constraints of a laboratory setting preventing full analysis of surge propagation. Therefore, more analysis was required to study the applicability of these findings to a field situation.

Further analysis has been performed on the 1993 release event on the Saint John River upstream of Grand Falls, NB. Blackburn and Hicks (2003) studied the applicability of one-dimensional dynamic hydraulic flow modeling techniques to an ice jam release. Field data consisted of a water surface profile along the length of the jam prior to its release, and a stage hydrograph about 5 km downstream of the jam toe following the release. Actual channel geometry was used but was found not to be essential to accurately predict the speed of the surge. Increasing resistance that could reflect remnant ice along the channel had no effect on the speed of the surge. To forecast the peak water level, actual channel geometry was beneficial. However, the recession portion of the stage hydrograph could not be accurately reproduced with the model. Recommendations included obtaining numerous stage hydrographs at sites upstream and downstream of the toe of a releasing jam. It was also recommended that these hydrographs should have stage measurements before and after the wave to get additional information on the true shape of the wave.

A two-dimensional ice dynamic model was used by Liu and Shen (2004) to look at the effects of ice on the surge propagation as a result of the same 1993 ice jam release event. This model considered internal ice resistance and boundary friction resistance. An idealized channel of the Saint John River was used due to inaccuracies with the field data (the actual channel geometry is proprietary to NB Power and so was not available to them). Results showed ice to have a significant effect on the stage and discharge hydrographs. The peak stage was very similar to a situation without ice resistance, but the occurrence of ice changed the shape of the hydrograph. The ice resistance significantly lowered the peak discharge experienced. Results also show the surge to reduce at a much slower rate. Although this study is lacking in verification data, it can be concluded that ice slows down the release process and thus ice cannot be neglected.

Thus far hydraulic models have been relatively successful in capturing the celerity of a release surge. However, more field data are required to adequately model and understand water levels associated with surge events, as well as the impact of an ice cover. Actual geometry data have aided forecasting capabilities, therefore surveyed data is required along the length of a study reach. Also, stage hydrograph data is required at various points along the channel complete with measurements before and after the event to see the true shape of the surge. Further analysis on the importance of an ice cover should be addressed thus providing a need for measuring the ice conditions in the field.

Ice jam release events along the Athabasca River have been documented for years. Measurements include water levels, surge celerities and surveyed cross sections. The Athabasca River experiences ice jams nearly every year with some years being more dynamic than others. It has been consistently observed that breakup is characterized by a cascade of releasing and reforming ice jams providing numerous events for data collection. Therefore, the Athabasca River presents an excellent location for further data collection and analysis of ice jam release events.

Ice jam release events are one of the most dangerous types of ice-related floods. Being able to predict the corresponding rapid water level increases downstream of the release location could aid in forecasting purposes. The Athabasca River near Fort McMurray is an ideal site to further the efforts in forecasting such events. Therefore the objectives of this study include:

1. to collate and analyze all of the historically documented ice jam release surge events at the study site;
2. to identify the inadequacies in that data and attempt to get more and better scientific data;
3. to use that data to assess the importance of ice on the nature of the propagating surge.

The equations of open channel unsteady flow are discussed in Chapter 2 and are applied to an ice jam release situation. The characteristics of kinematic, diffusive and

dynamic wave forms are presented from a non-dimensionalization of the equations. This theory is used to analyze ice jam release events on the Athabasca River. Field observations of the mechanics of an ice cover, as reported by Jasek (2003), are also discussed in Chapter 2.

Chapter 3 includes quantitative observations compiled from historical data on breakup events on the Athabasca River near Fort McMurray. The nature of breakup is studied and historical events are classified by patterns observed. Monitoring studies performed by Alberta Environment (AE), Alberta Research Council (ARC) and the Regional Municipality of Wood Buffalo (RMWB) are presented. This chapter also discusses a staff gauge network originally installed by ARC.

Upon analysis of the historical data, a plan is devised to obtain a more complete data set. Chapter 4 outlines the measurement method used to capture stage hydrographs of ice jam release events on the Athabasca River. A discussion of the field study includes the equipment used and the strategy for installation. The data successfully captured by this monitoring network is presented.

All the documented events were analyzed and compared in Chapter 5. Comparisons are made in terms of wave speed and wave peak attenuation in relation to theoretical values. The event with the most complete data set is then analyzed further using the dynamic open channel flow hydraulic model, River1-D. A description of this model, the input data required and the various applications performed are discussed along with the modeled results. Chapter 6 summarizes the major findings of this research and recommendations for continued study.

Upon completion of this research, it is desired to contribute to the body of knowledge regarding the physics of ice jam release surge propagation. It is also desirable to provide a flood forecasting tool, although preliminary in nature, to the people of Fort McMurray to prevent unnecessary damage to property and lives.

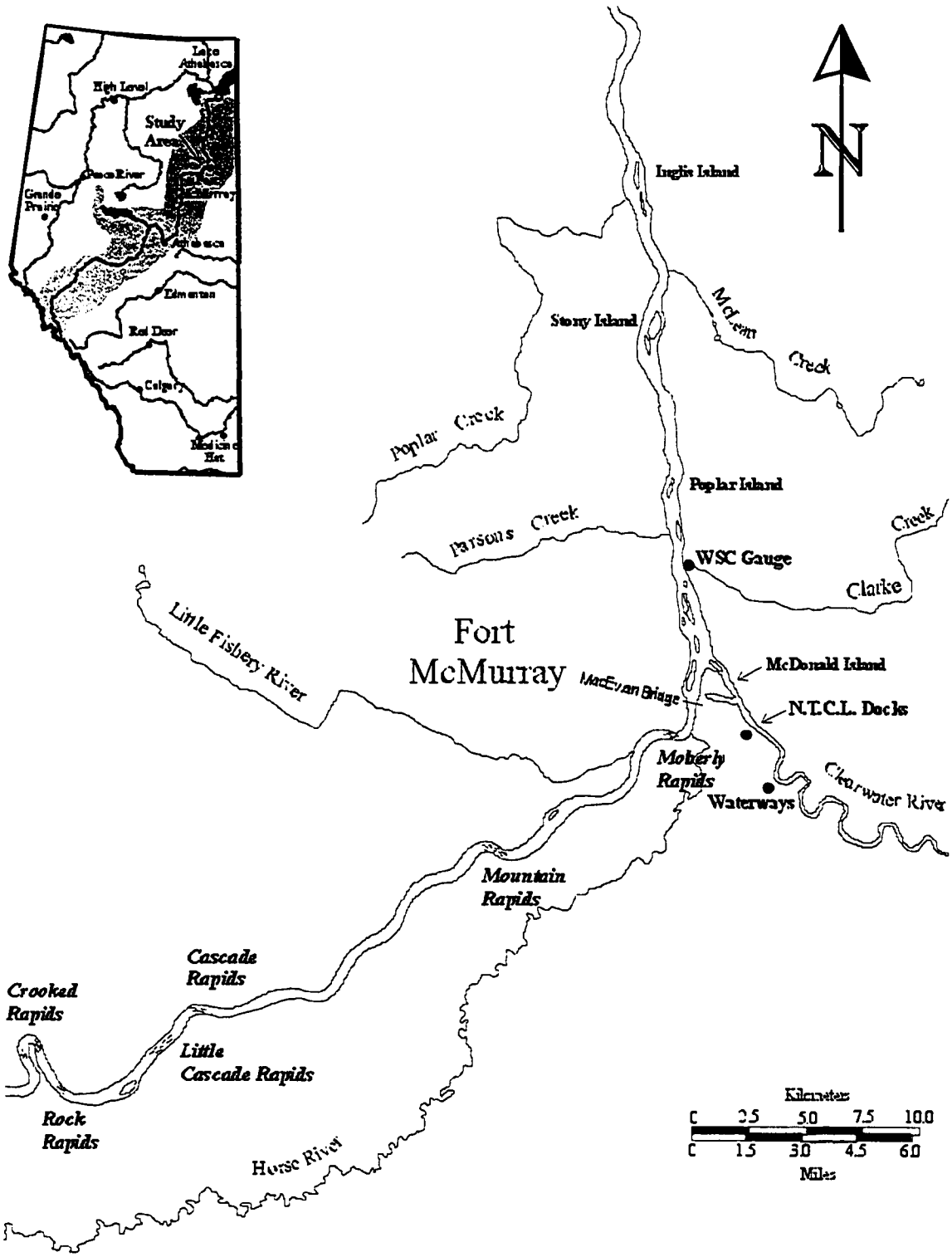

Figure 1-1. Study reach of the Athabasca River near Fort McMurray (adapted from Robichaud, 2003).

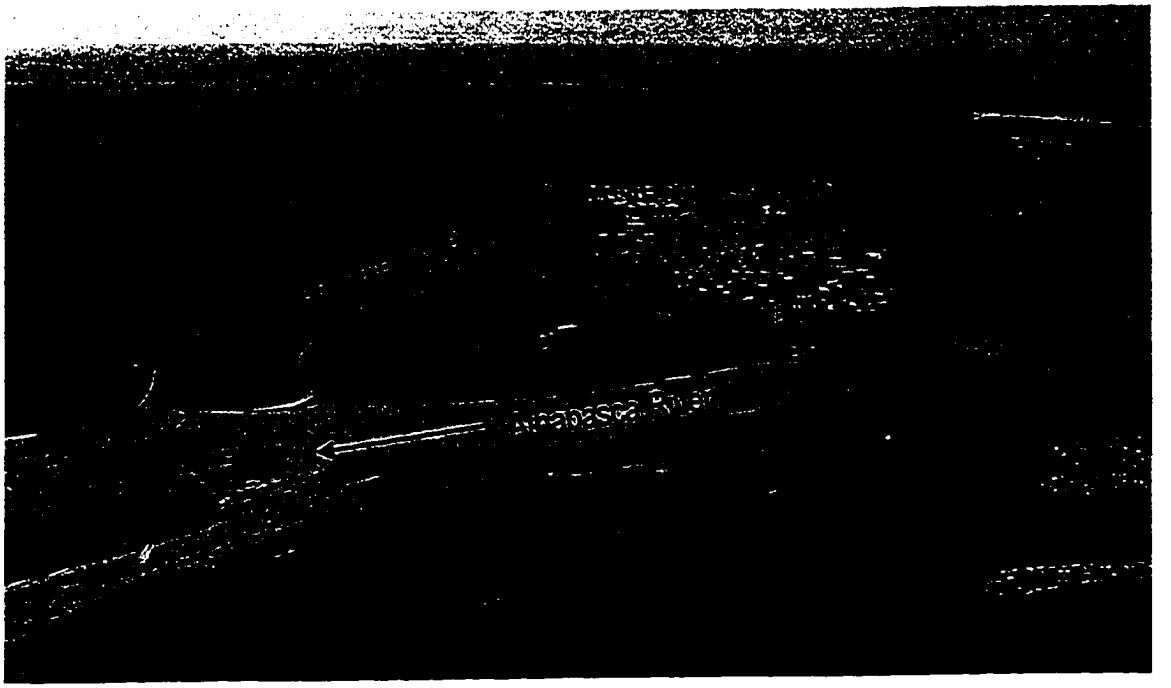

Figure 1-2. Aerial view of downtown Fort McMurray and the confluence of the Athabasca River and the Clearwater River.

Figure 1-3. Ice jam at MacEwan Bridge in 1977.

Figure 1-4. Flooding of the Clearwater River due to an ice jam on the Athabasca River in 1977.

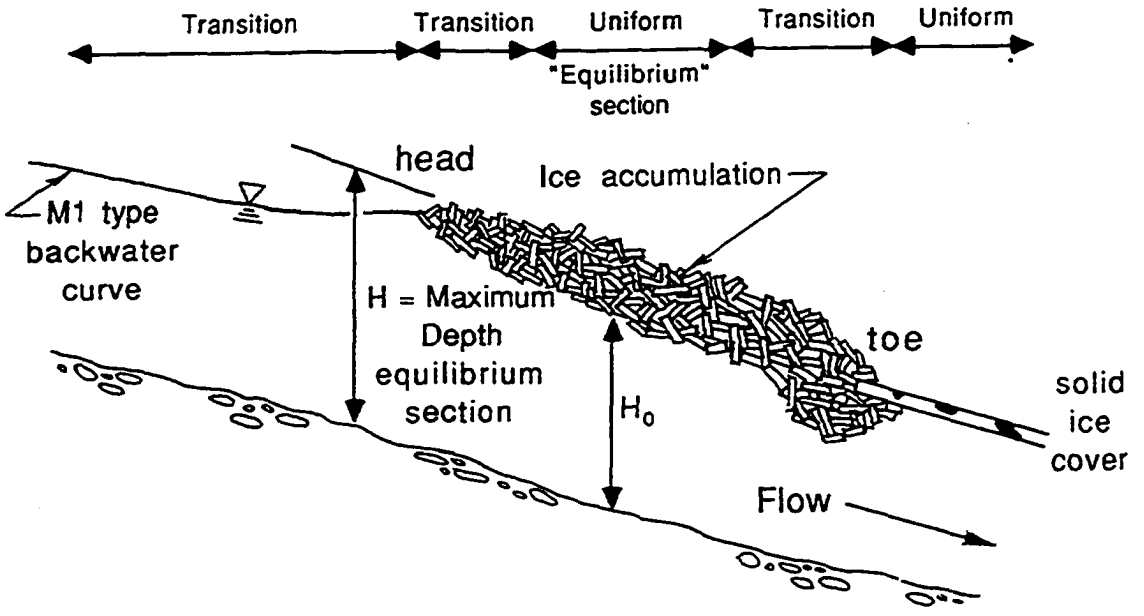

Figure 1-5. Typical ice jam profile with a solid ice cover downstream (adapted from Watt, 1989).

2 THEORY

Flow can be assumed to be one-dimensional in an open channel when the variations in flow parameters in the longitudinal dimension are more significant than those variations in the transverse and vertical directions (Cunge *et al.*, 1980). Although one-dimensional flow clearly does not exist in nature, an ice jam release surge event can be reasonably approximated using one-dimensional analysis. Surge wave propagation extends over several kilometers of channel length, and the issues of importance are the peak magnitude attenuation and celerity of propagation, rather than the variations across the width and depth of the channel.

As will be discussed in future chapters, in this study analysis of documented surge events along the Athabasca River employs the hydraulic model River1-D Version 1.00. This model solves the one-dimensional unsteady open channel flow equations, known as the Saint Venant equations. This version of River1-D is capable of modeling a rectangular channel approximation but does take into account varying width.

This chapter will look at the Saint Venant equations for a rectangular channel and their use to describe waves of either a kinematic, diffusive or dynamic nature. This theory will then be applied to the ice jam release scenario. This chapter also provides a summary of the ice mechanics of an ice jam release event according to the work of Jasek (2003).

2.1 SAINT VENANT EQUATIONS

The Saint Venant equations are used to describe unsteady open channel flow. Various forms of these equations exist depending on assumptions of either one or two-dimensional flow, or using natural or rectangular channel geometry. The derivation of these various forms of the equations can be found in Hicks and Steffler (1990). Only one-dimensional flow with rectangular channel approximations will be discussed in this section.

The Saint Venant equations contain two components: the principles of conservation of mass and momentum. River1-D Version 1.00 solves a conservative form of these equations:

$$\frac{\partial A}{\partial t}+\frac{\partial Q}{\partial x}=0 \qquad [1]$$

and,

$$\frac{\partial Q}{\partial t}+\frac{\partial (Q^2/A)}{\partial x}+\frac{\partial}{\partial x}\left(\frac{gAy}{2}\right)-\frac{gAy}{2B}\frac{dB}{dx}=gA\left(S_o-S_f\right) \qquad [2]$$

where,

A = cross sectional area perpendicular to the flow;

Q = discharge;

B = the channel width;

g = acceleration due to gravity;

y = depth of flow;

S_f = longitudinal boundary friction slope;

S_o = longitudinal channel bed slope;

t = temporal coordinate; and

x = longitudinal coordinate.

Since all of the dependent variables (i.e., A, Q, y and B) appear within the derivatives, these equations are described as a conservative formulation. River1-D Version 1.00 uses the *characteristic-dissipative-Galerkin* (CDG) finite element scheme to solve these equations. Hicks and Steffler (1990) found that only the conservation formulation was able to perfectly conserve both mass and longitudinal momentum, even

though the CDG finite element scheme is able to solve both the conservation and non-conservation formulations of the equations.

There is no analytical solution to these full equations; therefore flow approximations were commonly used in the past, and are still useful for interpreting wave propagation behaviour. A simplified formulation of the St. Venant equations is convenient to consider for this discussion:

$$\frac{\partial y}{\partial t}+\frac{\partial Vy}{\partial x}=0 \qquad [3]$$

and,

$$\frac{\partial V}{\partial t}+V\frac{\partial V}{\partial x}+g\frac{\partial y}{\partial x}=g\left(S_o-S_f\right) \qquad [4]$$

where V is mean flow velocity.

Acceleration, pressure and friction forces are all included in the Saint Venant equations. By comparing the relative magnitudes of each of these forces, these flow approximations can be examined. Scaling analysis applied to equations [3] and [4] involves the following:

- a length scale, L, (e.g., the reach length of interest);
- a depth scale, Y, (e.g., the mean flow depth);
- a velocity scale, U, (e.g., the mean flow velocity or a wave speed);
- a time scale, T, (e.g., the duration of the event); and
- a slope scale, z, (e.g., the channel drop over the reach length).

The details of this scaling of the Saint Venant equations are described by Hicks and Steffler (1990). The conservation of mass scales down to:

$$\frac{L}{UT}+1=0 \qquad [5]$$

Therefore, if $\frac{L}{UT} << 1$ then a steady flow approximation is reasonable. This case would exist for a rainfall flood having a very large time scale compared to the length scale. For an ice jam release situation, the time scale is small compared to the large length scale thus making this an unsteady flow situation.

A scaling analysis on equation [4], the conservation of momentum equation, results in the following formulation for unsteady flow where $\frac{L}{UT} \sim 1$:

$$\underbrace{1 + 1}_{\text{Acceleration Forces}} + \underbrace{\frac{1}{Fr^2}}_{\text{Pressure Forces}} = \underbrace{\frac{gz}{U^2} - \frac{L}{100Y}}_{\text{Friction Forces}} \qquad [6]$$

where Fr is the Froude number, defined as:

$$F_r = \frac{U}{\sqrt{gY}} \qquad [7]$$

If F_r is small, as occurs in subcritical flow, the pressure term will be big compared to the other terms. The opposite will occur for supercritical flow, with a large F_r. If $F_r = 1$ (critical flow), all terms are important. This occurs, for example, at waterfalls or hydraulic jump locations.

A propagating surface wave can be described as kinematic, diffusive or dynamic. Each of these flow approximations depend upon which terms are most significant in the scaled version of the Saint Venant equations [5] and [6]. These flow approximations are discussed in detail in the following sections.

2.1.1 Kinematic Wave Approximation

This type of wave approximation applies to cases where a steep channel reach (large F_r) and/or a long reach length exists. Frictional effects dominate and the acceleration and pressure forces can be neglected, reducing the Saint Venant equations to:

$$\frac{\partial y}{\partial t}+\frac{\partial Vy}{\partial x}=0 \qquad [3]$$

and,

$$S_o = S_f \qquad [8]$$

Applying Chezy's equation to [8],

$$V = C_* \sqrt{gRS_f} = C_* \sqrt{gRS_0} \qquad [9]$$

where C_* is the non-dimensional Chezy coefficient. By assuming a wide rectangular channel such that the hydraulic radius, R, can be approximated by the depth of flow, y, equation [9] becomes,

$$V = C_* \sqrt{gyS_o} \qquad [10]$$

Then V is only a function of y when the bed slope, S_o, is constant. Multiply V by y to get:

$$Vy = y^{3/2} C_* \sqrt{gS_o} \qquad [11]$$

then find,

$$\frac{\partial Vy}{\partial y} = \frac{\partial}{\partial y}\left(y^{3/2} C.\sqrt{gS_o} \right) = \frac{3}{2} C.\sqrt{gyS_o} = \frac{3}{2} V \qquad [12]$$

Therefore,

$$\frac{\partial Vy}{\partial x} = \frac{3}{2} V \frac{\partial y}{\partial x} \qquad [13]$$

Combining this with the continuity equation (mass conservation) results in the Kinematic Wave Equation:

$$\frac{\partial y}{\partial t} + \frac{3}{2} V \frac{\partial y}{\partial x} = 0 \qquad [14]$$

where the speed of propagation of the kinematic wave is $\frac{3}{2}V$. A more general form of this equation is,

$$\frac{\partial y}{\partial t} + \alpha V \frac{\partial y}{\partial x} = 0 \qquad [15]$$

where α is $^3/_2$ when the friction slope is calculated based on Chezy's equation, and α is $^5/_3$ when it is calculated based on Manning's equation.

Equation [15] is a convection equation, which neglects attenuation effects and assumes that the depth of flow, *y*, remains constant as the wave travels downstream. Each constant depth propagates at a speed which is dependent upon this depth (Hicks and Steffler, 1990). Consequently, the kinematic wave front steepens as it propagates downstream, and this approximate solution eventually breaks down (Hicks and Steffler, 1990).

2.1.2 Diffusive Wave Approximation

This is a more sophisticated flow approximation, which takes into consideration not only frictional forces, but also pressure forces. The Saint Venant equations are then approximated by:

$$\frac{\partial y}{\partial t}+\frac{\partial Vy}{\partial x}=0 \qquad [3]$$

and,

$$\frac{\partial y}{\partial x}=S_o-S_f=S_o-\frac{V^2}{ygC_*^2} \qquad [16]$$

where Chezy's equation is applied to calculate the friction slope, S_f, and it is again assumed that R can be approximated by y (wide channel assumption). The velocity, V, is now dependant on both y and on the slope, $\frac{\partial y}{\partial x}$. For a constant bed slope, S_o,

$$\frac{\partial^2 y}{\partial x^2}=\frac{-2V}{ygC_*^2}\frac{\partial V}{\partial x}+\frac{V^2}{y^2gC_*^2}\frac{\partial y}{\partial x} \qquad [17]$$

This can be rearranged to become,

$$\frac{\partial y}{\partial x}=\frac{ygC_*^2}{2V}\frac{\partial^2 y}{\partial x^2}+\frac{V}{2y}\frac{\partial y}{\partial x} \qquad [18]$$

Combining [18] with the continuity equation [3] results in the Diffusive Wave Equation:

$$\frac{\partial y}{\partial t}+V\frac{\partial y}{\partial x}-\frac{y^2gC_*^2}{2V}\frac{\partial^2 y}{\partial x^2}+\frac{V}{2}\frac{\partial y}{\partial x}=0 \qquad [19]$$

or a more general form of,

$$\frac{\partial y}{\partial t} + \alpha V \frac{\partial y}{\partial x} = D \frac{\partial^2 y}{\partial x^2} \qquad [20]$$

where D is the diffusive term of,

$$D = \frac{y^2 g C_*^2}{2V} \qquad [21]$$

and α is defined the same as in the kinematic wave approximation: $^3/_2$ when using Chezy's equation, and $^5/_3$ when using Manning's equation.

Equation [20] is an advection-diffusion equation, meaning that these diffusive waves attenuate as they propagate downstream, at a rate defined by this diffusive term, D. In this case, it can be shown that V is a function of both the depth and the slope of the water surface (Hicks and Steffler, 1990). As a result, a looped rating curve exists with larger velocities on the rising limb of the wave (steep wave front) than on the falling limb (as the water surface slope is flatter on the back of the wave). Also, the peak water level does not coincide with the peak discharge (Henderson, 1966).

Kinematic and diffusive waves are often grouped under the common heading of 'bulk wave' since they both involve a single wave disturbance propagating in the downstream direction at a wave speed of αV (Henderson, 1966).

2.1.3 Dynamic Wave Approximation

All waves to some extent are dynamic in nature, in that all of the terms and associated forces in the Saint Venant equations play a role. These full equations are repeated below:

$$\frac{\partial y}{\partial t}+\frac{\partial Vy}{\partial x}=0 \qquad [3]$$

and,

$$\frac{\partial V}{\partial t}+V\frac{\partial V}{\partial x}+g\frac{\partial y}{\partial x}=g\left(S_o-S_f\right) \qquad [4]$$

The celerity of a small wave disturbance is,

$$c=\sqrt{gy} \qquad [22]$$

such that,

$$y=\frac{c^2}{g} \qquad [23]$$

Differentiating equation [23] gives,

$$dy=\frac{2c}{g}dc \qquad [24]$$

which substituted into the continuity equation [3] results in,

$$\frac{2c}{g}\frac{\partial c}{\partial t}+\frac{c^2}{g}\frac{\partial V}{\partial x}+\frac{2c}{g}V\frac{\partial c}{\partial x}=0 \qquad [25]$$

Then dividing by c/g gives,

$$\frac{\partial 2c}{\partial t}+c\frac{\partial V}{\partial x}+2V\frac{\partial c}{\partial x}=0 \qquad [26]$$

Now substitute [24] into [4] to get,

$$\frac{\partial V}{\partial t}+V\frac{\partial V}{\partial x}+2c\frac{\partial c}{\partial x}=g(S_o-S_f) \qquad [27]$$

If the mass and momentum equations are added, equations [26] and [27] respectively, the following results:

$$\frac{\partial}{\partial t}(V+2c)+(V+c)\frac{\partial}{\partial x}(V+2c)=g(S_o-S_f) \qquad [28]$$

And by subtracting the mass and momentum equations, [26] and [27] respectively, it is found that:

$$\frac{\partial}{\partial t}(V-2c)+(V-c)\frac{\partial}{\partial x}(V-2c)=g(S_o-S_f) \qquad [29]$$

Equations [28] and [29] are known as the 'characteristic equations' with characteristic wave velocities of *(V+c)* and *(V-c)*. Therefore, the fully dynamic Saint Venant equations have two waves at two propagating celerities. A progressive wave propagates at a celerity of *(V+c)* in the downstream direction. Whereas as regressive wave propagates at a celerity of *(V-c)*. The regressive wave moves in the upstream direction in a subcritical flow and downstream in a supercritical flow.

The dynamic wave approximation considers friction forces to be negligible compared to acceleration and pressure forces. In this case, the characteristic equations reduce to:

$$\frac{\partial}{\partial t}(V+2c)+(V+c)\frac{\partial}{\partial x}(V+2c)=0 \qquad [30]$$

and,

$$\frac{\partial}{\partial t}(V-2c)+(V-c)\frac{\partial}{\partial x}(V-2c)=0 \qquad [31]$$

These equations are applicable for only very short reach lengths, over which friction forces can reasonably be assumed to be negligible. In the practical application, it is unknown what distance it will take for friction forces to become significant. Therefore, the full dynamic equations should be used for routing dynamic waves, rather than relying on the approximate equations (Hicks and Steffler, 1990).

2.2 APPLICATION TO ICE JAM RELEASE EVENTS

Henderson and Gerard (1981) conducted the first theoretical study of the water level and velocity changes from ice jam failure, applying the dynamic wave approximation (classic dam break theory) to the problem. Using an implicit finite difference scheme to solve the full Saint Venant equations, Beltaos and Krishnappan (1982) modeled the same event including consideration of friction and channel slope effects. The full dynamic Saint Venant equations were again utilized in the hydraulic modeling efforts of Hicks *et al.* (1997). These simulations used a more comprehensive set of field measurements from an event on the Saint John River in New Brunswick as validation data for model result comparison. Rectangular cross section approximations were used along the length of the study reach, and again ice effects on the surge propagation were neglected. Further analysis using this same field data was performed by Blackburn and Hicks (2003) but using actual cross section geometry. Blackburn and Hicks (2003) also looked at increased resistance effects, possibly due to ice, for the initial onset of jam release.

The continued question of the effect of an ice cover and/or ice within a jam on surge propagation was studied by Jasek (2003). Jasek looked at the mechanics of the ice cover for both the unimpeded and impeded ice jam scenario. These observations should be kept in mind when analyzing modeled results (Chapter 5).

2.2.1 Theoretical Analysis Using the Dynamic Wave Approximation

Henderson and Gerard (1981) performed a preliminary theoretical study of the rapid changes in water level and velocity as a result of the formation, failure, and reformation of ice jams. The failure process was compared to that of a classic dam break scenario using the dynamic wave approximation (friction forces considered negligible) reproduced below:

$$\frac{\partial y}{\partial t}+\frac{\partial Vy}{\partial x}=0 \qquad [3]$$

and,

$$\frac{\partial V}{\partial t}+V\frac{\partial V}{\partial x}+g\frac{\partial y}{\partial x}=0 \qquad [32]$$

At the instant of ice jam release, there is an increase in the energy across the length of the jam. Since the two terms in the continuity equation [3] must still equal zero, the commonly reported observation that there is an immediate increase in velocity without any increase in depth appears to be a reasonable phenomenon.

After the instant of ice jam release, a positive (progressive) surge propagates downstream and a negative (regressive) wave propagates upstream. As shown in Figure 2-1, these two waves are separated by a uniform flow section, in which the depth is y_1. The height of the surge (y_1-y_0), where y_0 is the depth downstream of the surge, is never more than 0.5 of the original drop in water level across the ice jam, (y_2-y_0). The equations governing the surge as determined by Henderson and Gerard (1981) are:

$$c(y_1-y_0)=V_1y_1-V_0y_0 \qquad [33]$$

and,

$$\frac{(c-V_0)^2}{gy_0} = \frac{1}{2}\frac{y_1}{y_0}\left(\frac{y_1}{y_0}+1\right) \qquad [34]$$

By neglecting the effects of slope and friction, the surge is unable to attenuate which is not realistic. Therefore, the above equations are only valid for a short time after the release occurs.

At the time of Henderson and Gerard's (1981) study, the attenuation effects due to friction were considered too complex to analyze. Therefore a more indirect method of attenuation was considered, where the negative wave encounters a backwater curve upstream of the ice jam. This encounter was believed to create another negative wave that would travel downstream, eventually overtaking the surge. The depth and velocity of this second negative wave would interact with those of the surge thus reducing its height and celerity. They argued that the surge would continue to attenuate as successive negative waves overtook the surge. Analysis of this attenuation theory showed the degree of subsidence to increase with an increase in bed slope. Whereas the subsidence associated with normal flood waves is very small at a high slope.

Beltaos (1995) extended Henderson and Gerard's (1981) analysis to quantify the effect of these reflected negative waves on the celerity of the propagating surge, obtaining:

$$V_s \approx V_o + \sqrt{(1+0.4m_o)(1+0.2m_o)gy_o} \qquad [35]$$

where m_o is the relative backwater of the jam, defined as:

$$m_o = \frac{y_2 - y_o}{y_o} \qquad [36]$$

According to Henderson and Gerard (1981), 'typical' values of m_o for ice jam releases events would be about 0.5 to 1, and would result in surge wave celerities of

$V_s \approx V_o + 1.15\sqrt{gy_o}$ to $V_s \approx V_o + 1.30\sqrt{gy_o}$. Interestingly, this seems to contradict the logic described by Henderson and Gerard (1981) in that the surge celerity is increased by these negative waves.

Henderson and Gerard applied this theory to field measurements on the Athabasca River obtained by Doyle and Andres (1979) during the 1979 breakup event. The depth behind the surge matched well, but a fully developed backwater curve had not yet formed behind the ice jam. Therefore the attenuation would have been larger than predicted by the theory. There was a large discrepancy between the theoretical and measured surge celerities of 11 m/s and 4 m/s respectively. This discrepancy was believed to be a result of ice resistance, which would also cause an increase in height and possibly reduce the amount of attenuation due to negative wave reflection. Henderson and Gerard recommended further studies on the effect of resistance on surge attenuation. It was also suggested that more field data be obtained.

2.2.2 Hydraulic Modeling Using the Full Saint Venant Equations

As previously mentioned, the dynamic wave approximation does not allow for attenuation of an ice jam release surge. Although this approximation may apply at the immediate instant of jam release, the distance of travel beyond which friction forces become significant is unknown, and very case specific. Therefore, considering all of the terms in the Saint Venant equations is the best method for modeling the propagation of surge events. As the full dynamic equations cannot be solved analytically, a numerical method must be used to obtain a solution.

Using an implicit finite difference scheme to solve the Saint Venant equations, Beltaos and Krishnappan (1982) modeled Doyle and Andres' (1979) event on the Athabasca River, including consideration of friction and channel slope effects, and again (like Henderson and Gerard) assuming rectangular channel geometry and neglecting ice effects. Their model had difficulties matching the shape of the observed water level

hydrograph. A major limitation to their study was a lack of adequate field data with which to assess the model.

Using a superior set of data from a 1993 ice jam release which occurred on the Saint John River, NB, Hicks *et al.* (1997) investigated the value of using a shock-capturing numerical scheme for this dynamic problem and also explored the need to consider actual channel geometry. Using a non-Windows® version of the University of Alberta's River1-D model, known then as the cdg-1D model, Hicks *et al.* (1997) analyzed a release event which occurred in April 1993 on the Saint John River, NB. This finite element model employs the *characteristic-dissipative-Galerkin* (CDG) finite element scheme (Hicks and Steffler, 1990). Field data available from this ice jam release event was obtained by Beltaos *et al.* (1994) and included the following:

1. channel geometry;
2. ice jam profile;
3. stage hydrograph obtained during the release event, at a location approximately 5 km downstream of the original jam toe; and
4. hourly streamflow data on the Saint John River and four major tributaries along the study reach.

Hicks *et al.* (1997) assumed a rectangular channel approximation, but did account for varying widths and that the ice within the jam provided no resistance to flow. Ice present in the channel downstream of the jam was also neglected. Modeled results were compared to the measured hydrograph located about 5 km downstream of the jam. The model accurately reproduced the surge propagation celerity over this short reach, but the simulated peak stage was found to be about 1 m too high. It was believed that this difference in stage might be due to peak attenuation effects resulting from the remnant ice observed downstream of the ice jam prior to release, or as a result of using approximate geometry to describe the channel shape. The limited data available was again a significant constraint particularly as few details were known about the remnant ice. It was recommended that future field measurements should ideally include: ice extent and thickness data both upstream and downstream of the ice jam; details of the stage

hydrograph before during and after passage of the surge; and, more hydrographs capturing the propagation of the wave over a longer reach.

The simulated discharge hydrograph provided some interesting observations. The discharge profile initially consisted of two peaks, which eventually combined as the stored water became mobilized. Also interesting to note was that the peak discharge measured just upstream of the ice jam toe propagated upstream, while the surge front propagated downstream. Thirdly, the simulated results showed a rapid increase in discharge with little change in the water level at the initial onset of release, as has been observed in the field (Henderson and Gerard, 1981).

Blackburn and Hicks (2003) reanalyzed the same Saint John River ice jam release event using natural channel geometry rather than the rectangular approximation. They used the University of Alberta's cdg1-Dn model, an extended version of the cdg1-D finite element model, adapted to consider natural channel cross sections based on the following form of the Saint Venant equations:

$$\frac{\partial A}{\partial t}+\frac{\partial Q}{\partial t}=0 \qquad [37]$$

and,

$$\frac{\partial Q}{\partial t}+\frac{\partial\left(\beta Q^2/A\right)}{\partial x}+gA\frac{\partial H}{\partial x}+gAS_f=0 \qquad [38]$$

where,

β = the momentum flux correction coefficient; and

H = the stage (elevation of water surface above a specified datum).

Blackburn and Hicks (2003) conducted three model runs. Run 1 involved an instantaneous release of the ice jam with ice effects neglected. This was the same model run performed by Hicks *et al.* (1997), and thus facilitated an assessment of the importance of using natural channel geometry. The resulting peak water level decreased by about 0.5 m (as compared to the results using a rectangular channel approximation) but the surge celerity was unchanged. Therefore, actual channel geometry was deemed important for forecasting the peak water level, but not essential to capture the celerity. The results also suggested that ice effects were not essential. However, the recession portion of the stage hydrograph did not accurately represent what was measured and it was suspected that it could possibly be due to the resistance effects of remnant ice in the receiving channel.

The second model run analyzed the sensitivity of results to Manning's n. It was thought that increasing Manning's n in the receiving channel would approximate resistance from remnant ice and/or resistance between moving ice and the channel bank. The results showed an overall increase in stage, and most notably an improved agreement with the recession limb of the stage hydrograph as compared to the measured one (location about 5 km downstream of the released jam's toe). Results also showed a decrease in the peak discharge, but no significant effect on surge celerity.

Run 3 introduced an increased resistance along the length of the ice jam for the first 15 minutes. This was an attempt to simulate a delayed mobilization of the jam as compared to an instantaneous release in Run 1. 15 minutes was selected based on the computed time for the regressive wave to propagate upstream through the ice jam in Run 1. The only significant effects on the computed results observed in Run 3 were in the discharge hydrograph immediately downstream of the jam toe. A minor oscillation with its peak discharge at about 5000 m^3/s occurred before reaching a maximum peak of about 8000 m^3/s.

From these modeled results, requirements for future field data were assessed. Blackburn and Hicks (2003) recommended measuring stage hydrographs at numerous

points upstream and downstream of the ice jam toe. It was also suggested that stage data be obtained before and after the release event to capture a larger scope of the wave shape.

Both Hicks *et al.* (1997) and Blackburn and Hicks (2003) have shown that the one-dimensional hydraulic model River1-D (previous version known as cdg-1D) using the full Saint Venant equations is reasonably successful in modeling ice jam release events. However, the relative importance of ice resistance effects is still questionable. The main requirement for further study is a more complete data set involving numerous stage hydrographs along the study reach and observations of the ice cover.

2.2.3 Mechanics of the Ice Cover for Ice Jam Release Events

Jasek (2003) studied the mechanics of ice covers and/or ice floes within an ice jam for unimpeded and impeded ice runs. An unimpeded ice run has an open water condition downstream, whereas an impeded ice run involves the interaction of the ice run with a downstream ice cover. Jasek (2003) describes both types of ice runs in terms of a dimensionless ratio known as "jam lengths" where,

$$\frac{D_s}{D_j} = \frac{\text{distance traveled}}{\text{length of jam before release}} \qquad [39]$$

Jasek (2003) documented water level and ice concentration (100% ice concentration has no open water areas visible on the surface) for four unimpeded ice jam release events on the Porcupine and Yukon Rivers in the Yukon Territory. Comparison showed that after the ice run traveled a short distance of approximately one jam length, the majority of the ice concentration was on the rising limb of the stage hydrograph. Very soon after the water level started to rise, the ice concentration rose and fell rapidly. By the time the ice run had propagated 7.5 and 8.1 jam lengths, the water level had started to rise long before the ice arrived, but the majority of the ice concentration was still on the rising limb, though near the crest of the stage hydrograph. By the time the ice run had propagated about 26 jam lengths, the majority of ice concentration was still near

the crest of the stage hydrograph but on the falling limb. Further comparison of data obtained where the ice run propagated 7.5 and 8.1 jam lengths had shown that other variables are important such as ice jam thickness, volume of the ice jam, base flow, bed slope, and width of the channel.

Jasek (2003) described the early stages of unimpeded ice runs as involving moving multi-layered rubble (MMLR). He suggested that this MMLR is unable to spread out due to the confining banks with resulting confining stresses and bank shear causing the peak water level to propagate at a slower speed. As ice pieces accelerate away from the toe of the ice run, the length of MMLR decreases. At the point where MMLR ceases to occur, confining stresses are removed and the surface ice concentration falls below 100% with the majority of ice still traveling with the peak water level (Jasek, 2003).

Jasek (2003) also reported that continued wave propagation without MMLR, shows ice to lag behind the crest of the wave. Ice pieces tend to be drawn to the outside of a channel bend rubbing against the bank. This friction slows the ice, causing it to lag behind the crest. Ice rubbing along the banks also slows the momentum of the water. Therefore, the wave propagation is slowed and travels with the ice concentration peak. More work in this area was recommended (Jasek, 2003).

Quantitative data was obtained by Indian and Northern Affairs Canada for an ice jam release that occurred on May 3 to 4, 1995, on the Porcupine River (Jasek, 2003). Data included aerial observations of ice concentration at various times, as well as stage measurements 7 km and 130 km downstream of the release location. Observations showed the front of the surge to travel much faster than the ice, with the peak water level celerity increasing from 1.4 m/s to 2.2 m/s at different points of ice concentration. This increasing celerity was believed to be due to decreasing confining stresses, contribution of tributary inflows, and increases in slope and channel width. MMLR was observed to travel 3 jam lengths before the ice concentration fell below 100%. These field observations disagree with the laboratory results of Wong *et al.* (1985) discussed earlier,

who concluded that rubble in the jam release had little effect. Perhaps the experimental jams being shorter and held in place by gates could not reproduce the same friction effects experienced in the field.

Jasek (2003) also looked at the ice mechanics involved in an impeded ice run. In this case, new downstream ice is broken and incorporated into the moving ice pack. The transition between moving fragmented ice and a stationary downstream solid ice sheet is known as a breaking front.

Jasek (2003) noted that two types of breaking fronts have been observed: rubble front and sheet front. A rubble front tends to occur where an ice sheet is confined and thus not able to be set in motion. Instead, the ice sheet is broken into smaller ice pieces that combine with the moving ice floes. This type of front tends to occur in thin or weak ice areas, when a surge approaches rapidly. Sheet fronts tend to occur where there is space for large sheet ice movement. For example, when the stage increases significantly before the arrival of the breaking front, open water areas are created allowing for sheet ice movement. The celerity of a sheet front has been observed to be highly variable and depends on the width of the river. The sheet front tends to slow down in areas with a narrower width and areas of increasing water levels (Jasek, 2003).

Jasek (2003) suggests that breaking fronts most likely alternate between rubble and sheet fronts. Observations on numerous rivers suggest that channel slope may determine whether the breaking front is of rubble or sheet type, with rubble fronts tending to occur on more gentle slopes, and sheet fronts more common on steeper river slopes (Jasek, 2003).

This study by Jasek (2003) supports the importance of considering the effects of an ice cover on ice jam release surge propagation. Variations in ice resistance occur whether an ice run is unimpeded or impeded. Surge speed is also affected by the type of impeded breaking front experienced or the transition between the two: rubble and sheet

fronts. Analysis in Chapter 5 of both the modeled and measured hydrographs on the Athabasca River will keep these observations of ice resistance effects in mind.

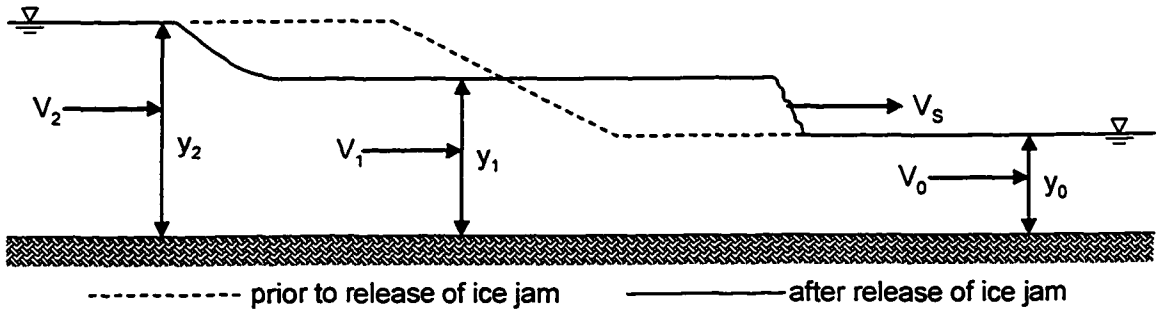

Figure 2-1. Water level profile of surge formation due to the release of an ice jam (adapted from Henderson and Gerard, 1981).

3 SUMMARY OF HISTORICAL EVENTS

3.1 INTRODUCTION

The town of Athabasca is approximately 400 km upstream of Fort McMurray, and it is suspected that propagating waves from breakup at Athabasca typically initiate the onset of breakup at Fort McMurray. Figure 3-1 shows the Athabasca River between the town of Athabasca and the city of Fort McMurray. The corresponding bed profile is shown in Figure 3-2, along with the name and location of some major inflow tributaries and rapid sections. The bed of the Athabasca River between the two communities is fairly steep, particularly for about 200 km upstream of Fort McMurray, which contains numerous rapids or bed discontinuities. Many of these rapids sections are in the order of a few meters high, as shown in Figures 3-3 and 3-4, and during breakup are accessible only by helicopter. It is along this reach that breakup is characterized by numerous ice jams that form and release in a cascade of failures that typically progresses downstream. This has been consistently observed by University of Alberta investigators over the last six years, and is also documented in the historical records.

The river bed flattens noticeably at Fort McMurray downstream of the MacEwan Bridge near the confluence with the Clearwater River, and surges of ice and water from upstream often become arrested in this location. Numerous bars and islands in the channel downstream of Fort McMurray tend to exacerbate this effect.

Researchers from the Alberta Research Council (ARC) installed a staff gauge network along the Athabasca River near Fort McMurray in the early 1980's, in order to facilitate the measurement of water levels associated with ice jams and ice runs. These staff gauges allowed for indirect ice level measurements by taking photographs from a helicopter. The elevations of these staff gauges were initially determined by Alberta Environment (AE) by tying them to the Geodetic Survey of Canada. As later discussed, historical observations of breakup events ceased after 1990, and therefore this staff gauge network was neglected. In 1998, a University of Alberta (UA) field team relocated and

repaired this staff gauge network for the purpose of this study. These gauged sites become monitoring locations as discussed in Chapter 4.

Figure 3-5 shows the location of some of these staff gauges along the reach of the Athabasca River between Crooked Rapids (G150) and just downstream of the Water Survey of Canada (WSC) gauge site (G55). It should be noted that the numbering system of these stations does not refer to the actual distance between stations; they merely denote their position relative to other stations. Some sites have the letter G before the station number (ie. G140, G130), which means a staff gauge is located at this site for reference measurement in a photograph. Stations without a G (ie. 100), are accessible by road and therefore do not require a staff gauge, since surveys can easily be done to attain ice and water levels at any time.

Breakup events along the Athabasca River near the city of Fort McMurray have been documented for more than 100 years. From 1977 to 1990, the majority of breakup events documented by ARC involved the co-operation with AE, Alberta Transportation, and the Department of Civil and Environmental Engineering at the UA. This documentation primarily consisted of a description of the events and conditions leading up to river ice breakup as well as a description of the breakup event itself.

Since this study looks at the propagation of surge waves resulting from ice jam release events, documentation of events that initiated in the upstream portion of the reach is desirable in order to capture this propagation. According to the documentation of historical ice jam release events, ice jams tend to form and release in three areas:

1. upstream of the study reach from Long Rapids extending past Grande Rapids,
2. near Crooked Rapids (the upstream end of the study reach), and
3. at Mountain Rapids (near the middle of the study reach, approximately 12 km upstream of the MacEwan Bridge).

Ice jams also tend to form within or downstream of Fort McMurray, but since the ice jam release monitoring network was installed upstream of the city, those events were not considered here.

This chapter provides a brief description of the historical events where an ice jam release event was documented, as well as the jam release measurements obtained. These measurements typically consist of the arrival time of the peak water level or breaking front at certain locations, which facilitate calculation of the celerity of the surge or ice run. Also, water level measurements, when available, allow the magnitude of the wave to be determined. The magnitude of the wave refers to the change in water level from before the event occurred to the peak water level as the wave passed. When reference is made to the *study reach*, the channel between Crooked Rapids and Fort McMurray is being considered.

Since this study is only concerned with ice jam release surges, only data from the historical documentation pertinent to this objective are discussed. If the reader is interested in a more comprehensive description of historical breakup events at this site, please refer to Robichaud (2003). Also, analyses using this historical data were carried out by Friesenhan (2004), including a detailed analysis of all documented stationary ice jams at Fort McMurray.

3.2 DOCUMENTED ICE JAM RELEASE EVENTS

Reports compiled by ARC and their collaborators are available for breakup events from 1977 to 1990. Ice jam release events that propagated along the Athabasca River and provided valuable data fell into one of three categories depending on the origin of the release location. The first category pertains to a release location upstream of Crooked Rapids, and is known as Type 1. The second category, Type 2, has an ice jam toe that released near Crooked Rapids at the upstream end of the study reach. A release near the center of the study reach, at Mountain Rapids, is classified as Type 3. The following table summarizes the types of release events documented in the ARC reports.

Table 3-1. Summary of documented ice jam release events on the Athabasca River.

Year	Type 1	Type 2	Type 3	Source
1977		■	□	ARC
1978		■		ARC/AE
1979			■	ARC/AE
1980				
1981				
1982	■			AE
1983				
1984	■		■	ARC/AE
1985	■		■	ARC/AE
1986				ARC
1987		■		ARC
1988	■			AE
1989				
1990	■			THE

Table 3-1 shows the amount and type of historical data available, with solid squares indicating events documented in the historical record (actual or presumed) and open squares indicating suspected events, deduced based on reconsideration of all available data in the light of current knowledge. No reports or data documenting breakup were available for the years that are shaded. All quantitative observations were stopped after 1990, with the report source in 1990 being Trillium Engineering and Hydrographs Inc. (TEH). Multiple types of ice runs can occur in any given year (i.e., 1984), which reflects the tendency for a cascade of release events all the way down from the town of Athabasca. It is highly probable that multiple events occurred in all years, so what was reported historically is only a small part of the big picture.

3.2.1 Breakup 1977 (Doyle, 1977)

Breakup at the town of Athabasca occurred on April 12 sending an estimated 2.5 m wave downstream. At this time, an ice jam had formed in the upstream portion of

the study reach. The ice jam was believed to have an original position in the area of Crooked Rapids (Type 2) due to the 8 m thick shear walls upstream of Little Cascade Rapids observed after breakup at Fort McMurray. Ice conditions prior to breakup along the remainder of the study reach were not documented.

On April 14 at 06:50, a wave with an estimated height of 5 m was observed at the MacEwan Bridge and was observed to be *"tossing ice blocks into air as it passed at an estimated velocity of 5 – 6 m/s"* according to eyewitness accounts (Doyle, 1977). Documentation also mentioned that ice floes and pieces of broken ice with sizes as large as 10 to 15 m in diameter arrived at the MacEwan Bridge 5 minutes after the arrival of the wave, suggesting the ice lagged behind the wave peak.

Based on the height of the shear walls documented upstream of Little Cascade Rapids, Doyle (1977) presumed that an ice jam had formed and failed upstream of Little Cascade Rapids, *"probably in the area of Crooked Rapids"*. This assumption was based on the fact that the flood wave seemed *"little attenuated"* when it reached McEwan Bridge; however, it is important to note that this event and report predate any theoretical analysis in the literature. It now seems unrealistic to assume that an ice jam release surge would propagate over such a great distance (approximately 40 km) without attenuating. Given the magnitude of the wave at MacEwan Bridge was more than half the height of the shear walls documented upstream of Little Cascade Rapids, the theory of Henderson and Gerard (1981) suggests that it is more likely that the ice jam reformed upstream of the city (e.g., at Mountain Rapids) and then released subsequently. Therefore, it has been classified as a Type 3.

As mentioned in the 1977 report, *"when the rush of water and ice hit the wide, flat, shallow reach of river downstream of the bridges it lost much of its momentum and failed to move the ice cover at the head of Poplar Island."* This flowing ice downstream of the MacEwan Bridge, moving at an estimated celerity of 1.5 m/s, impacted a fractured ice cover upstream of Poplar Island (8.8 km downstream of MacEwan Bridge) and became arrested. A 22.8 km long ice jam was formed that later released on April 15.

Table 3-2 shows the arrival times based on the estimated wave celerity as well as the magnitude observed at the MacEwan Bridge.

Table 3-2. Arrival time, celerity and magnitude of Type 3 ice run on April 14, 1977.

Toe Location	Station (km)	Time (hh:mm)	Celerity (m/s)	Magnitude (m)
80 MacEwan Bridge	294.9	06:50	5 to 6	5
Poplar Island	286.1	08:28	1.5	

3.2.2 Breakup 1978 (Doyle and Andres, 1978)

Visual observations of ice conditions were documented prior to breakup in 1978. A reconnaissance flight taken on March 20 found rough ice downstream of Fort McMurray, due to freeze-up jams, as well as open water within Mountain Rapids. It was observed that Mountain Rapids had actually been open throughout the winter season, resulting in large amounts of frazil production. This frazil was believed to have caused thicker ice accumulations downstream of this open water area.

By April 7, melt water and overflow were observed around the islands downstream of the Clearwater River confluence, and open water leads were present at Crooked Rapids. Open leads were seen downstream of the mouth of the Clearwater River by April 10. Therefore, the ice cover along the study reach was fairly deteriorated prior to breakup, with possibly thicker ice accumulations around the MacEwan Bridge. Breakup at the town of Athabasca was reported to have occurred on the evening of April 13, which sent an estimated 1 m high wave downstream. At that time, a 4 km long ice jam was poised upstream of Crooked Rapids, which resulted in a Type 2 breakup event.

The ice jam at Crooked Rapids released on April 19 at 11:00. Within 30 minutes, the leading edge of the resulting ice run passed Little Cascade Rapids. At 14:15 the ice run halted at Cascade Rapids, but released almost immediately with estimated celerity ranging from 3 to 6 m/s. However, an average celerity of about 2.8 m/s was observed in

the final 3 km of travel, upstream of the MacEwan Bridge. A 0.5 m wave passed the MacEwan Bridge at 16:40, but by 20:00, a 22 km long ice jam had formed with its toe at the MacEwan Bridge and head 0.6 km downstream of station 133. This jam remained in place until April 26. These events are summarized in Table 3-3.

Table 3-3. Arrival time, celerity and magnitude of Type 2 ice run on April 19, 1978.

Toe Location	Station (km)	Time (hh:mm)	Celerity (m/s)	Magnitude (m)
3 km u/s Crooked R.	335.8	11:00		
Little Cascade Rapids	325.8	11:30	5.6	
Cascade Rapids	322.8	14:15	0.3	
80 MacEwan Bridge	294.9	16:40	3.2	0.5

A flight was taken on April 25, the day before the ice jam poised at MacEwan Bridge released, and 30 km long shear walls were found far upstream of the study reach between Rapides du Joli Fou and the Pelican River. These shear walls were 5.5 to 6 m high; 2 to 3 m higher than the shear walls along the rest of the banks. It was presumed that this was the location of an ice jam that released around noon on April 18, prior to the release at Crooked Rapids on April 19 (Doyle and Andres, 1978). That is, it was presumed that the impact of this jam release caused Crooked Rapids to let go.

3.2.3 Breakup 1979 (Doyle and Andres, 1979)

An ice jam was positioned just downstream of Mountain Rapids prior to breakup in 1979. Many areas of the downstream channel contained an intact ice cover and these were described as having a rough surface as a result of freeze-up, especially downstream of the MacEwan Bridge. Ice thickness measurements taken on April 21 near the MacEwan Bridge ranged from 0.75 to 1.43 m, where the average was approximately normal for that time of the year. Breakup at the town of Athabasca occurred on April 24 without a noticeable rise in stage.

On April 28, the ice jam previously mentioned was 8 km long, with its toe 4 km downstream of Mountain Rapids. This ice jam failed (Type 3) at 19:30 on April 28,

passing the MacEwan Bridge at approximately 20:20. A water level increase of 2.8 m was measured at the MacEwan Bridge over the course of 20 minutes. This event is summarized in Table 3-4.

Table 3-4. Arrival time, celerity and magnitude of Type 3 ice run on April 28, 1979.

Toe Location	Station (km)	Time (hh:mm)	Celerity (m/s)	Magnitude (m)
4km d/s Mountain R.	303.2	19:30		
80 MacEwan Bridge	294.9	20:20	2.8	2.8

The ice continued to run until 22:35, when a new jam formed with its toe 16 km downstream of the MacEwan Bridge (major jam). The water level at the MacEwan Bridge continued to rise due to the backwater effects of this newly formed jam. On the morning of April 29, the head of this jam was 2 km downstream of Mountain Rapids making it approximately 25 km long. There were several open water areas throughout the jam, as it was not very densely packed. A second jam (minor jam) had also formed, with its toe 28 km downstream of the MacEwan Bridge. This minor jam was initially 9 km in length, but consolidated to 6 km. Measurements taken at the MacEwan Bridge showed a 4.2 m drop in water level from 01:00 to 07:00 on May 4 when the major jam released. These observations show the cascading effect of ice jam release events along the Athabasca River.

3.2.4 Breakup 1982 (Rickert and Quazi, 1982)

Breakup at the town of Athabasca occurred on April 24 between 15:30 and 18:00, with breakup at Fort McMurray following on April 26. A reconnaissance flight on the morning of April 26 reported the leading edge of an ice run at Long Rapids at 08:57. From this flight it was observed that from Long Rapids downstream to Cascade Rapids there was open water, and from Cascade Rapids to upstream of Mountain Rapids there was a consolidated ice cover. A competent ice cover extended downstream from Mountain Rapids to past the city of Fort McMurray.

The leading edge of this ice run reached Cascade Rapids at 12:00, the competent ice cover at Mountain Rapids by 13:30, and the MacEwan Bridge by 16:40. As this ice run traveled between Long Rapids and the MacEwan Bridge, temporary stalling was frequently observed but released almost immediately. The ice run jammed between the MacEwan Bridge and the Clearwater River confluence, but released at 20:30. Between 20:30 and 20:55, the entire left side of the channel from the MacEwan Bridge to the confluence released with an estimated celerity of 3.5 to 4.5 m/s. Shear walls observed along the banks at Poplar Island (approximately 9 km downstream of the MacEwan Bridge) suggest temporary jamming sometime after 20:55. Table 3-5 outlines the arrival time of the leading edge of the ice run as well as the calculated wave celerity. Peak magnitudes were not measured and thus magnitude attenuation cannot be determined for 1982.

Table 3-5. Arrival time and celerity of Type 1 ice run on April 26, 1982.

Toe Location	Station (km)	Time (hh:mm)	Celerity (m/s)
d/s Long Rapids	341.0	08:57	
just u/s Crooked R.	334.0	09:50	2.2
just d/s Crooked R.	331.6	10:16	1.5
0.6 km d/s G135	319.2	11:34	2.6
1.1 km d/s stn 133	316.4	12:00	1.8
132	314.2	12:24	1.5
1.4 km u/s G120	309.4	13:30	1.2
w/in Mountain Rapids	306.6	14:26	0.8
0.3 km d/s G110	303.0	15:04	1.6
80 MacEwan Bridge	294.9	16:40	1.4
70 Clearwater	292.9	20:30	0.1
0.6 km u/s 57 WSC	289.8	20:55	2.1

3.2.5 Breakup 1984 (Andres and Rickert, 1984)

Breakup in 1984 involved two ice jam release events along the study reach. The first initiated upstream of the study reach (Type 1), that reformed a jam just downstream of Moberly Rapids at the mouth of the Horse River. The second event was the release of this jam at the Horse River (Type 3), that traveled through Fort McMurray without

rejamming. Ice conditions along the study reach at the time of these release events were not documented, but most of the ice around Fort McMurray had already melted in place.

On April 10, the trailing edge of the first ice run was observed at Grande Rapids with the leading edge at Middle Rapids at 17:50, Long Rapids at 18:00, and at Rock Rapids at 19:00. This ice run continued with an average celerity of 2.6 m/s before jamming below the mouth of the Horse River at 22:40. Table 3-6 summarizes the location and time of the observed leading edge as it propagated downstream. Estimated water levels were not able to be obtained and thus no comparison can be made of magnitude attenuation.

Table 3-6. Arrival time and celerity of Type 1 ice run on April 10, 1984.

Toe Location	Station (km)	Time (hh:mm)	Celerity (m/s)
Middle Rapids	349.4	17:50	
Long Rapids	344.6	18:00	8.0
Rock Rapids	330.6	19:00	3.9
mouth of Horse River	296.1	22:40	2.6

The ice jam at Horse River released on April 11 at 00:26, as summarized in Table 3-7. A water level increase of 2.2 m was measured at the MacEwan Bridge at 00:30, and an increase of 2.5 m at 02:00 at the WSC gauge. Measurements from the shear walls taken after the ice jam released, suggested that the toe of the ice jam was approximately 0.8 km upstream of the MacEwan Bridge and extended 9.4 km upstream just before reaching Mountain Rapids.

Table 3-7. Arrival time, celerity and magnitude of Type 3 ice run on April 11, 1984.

Toe Location	Station (km)	Time (hh:mm)	Celerity (m/s)	Magnitude (m)
mouth of Horse River	296.1	00:26		
80 MacEwan Bridge	294.9	00:30	5.0	2.2
57 WSC Gauge	289.2	02:00	1.1	2.5

3.2.6 Breakup 1985 (Andres and Rickert, 1985)

Breakup in the study reach in 1985 was characterized by numerous ice runs that progressed along the Athabasca River. On April 13 a 3 km long ice jam was observed with it toe located at Long Rapids, approximately 12 km upstream of Crooked Rapids. Intact, but deteriorated ice extended downstream from the toe to Fort McMurray. By the time the observation flight was conducted on April 14, there was a continuous ice run extending from Brule Rapids (54 km upstream of Crooked Rapids) to Cascade Rapid (11 km downstream). The length (65 km) and extent of this ice run suggests that the small Long Rapids ice jam was taken out by a large ice run coming from a released jam further upstream. Andres and Rickert (1985) estimate the average celerity of that surge at 3.9 m/s between the House River and Cascade Rapids.

The ice run eventually stalled at Mountain Rapids on April 14 forming an 18 km long jam. Andres and Rickert (1985) documented an average celerity of the surge of 5.2 m/s[1] between Cascade and Mountain Rapids. It is interesting to note that a water level peak was noted at the WSC gauge at 14:00 suggesting that although the ice stopped at Mountain Rapids, not all of the water did. This water wave propagated under the intact ice cover at a speed of 1.9 m/s. Unfortunately, the WSC gauge failed during passage of this wave, so the full magnitude was not documented. However it is known that it was at least 0.18 m high.

A reconnaissance flight on April 17 identified ice jams between Stony River and Rapides du Joli Fou (far upstream of the study reach), which would have prevented any more upstream ice from reaching the Mountain Rapids jam. Consequently, this ice jam deteriorated in place for a few days before releasing some time after 20:00 April 18.

[1] Surge celerity was originally estimated to be 3.5 m/s, but calculations of documented arrival times found a celerity of 5.2 m/s.

Table 3-8. Arrival time and celerity of Type 1 ice run on April 14, 1985.

Toe Location	Station (km)	Time (hh:mm)	Celerity (m/s)	Magnitude (m)
Cascade Rapids	322.8	10:30		
Mountain Rapids	307.2	11:20	5.2	
57 WSC Gauge	289.2	14:00	1.9	0.18+

The gauge at station 57 malfunctioned so the magnitude is likely larger than 0.18 m.

The intact ice upstream of the MacEwan Bridge, and downstream of the Mountain Rapids jam, started to break on the morning April 18. This ice released at about 20:00 on April 18, resulting in a 2 m increase in water level at the MacEwan Bridge as a small ice run passed at 22:00. The WSC gauge downstream of Fort McMurray was not operational from April 14 to April 19; therefore no stage or discharge data was available. This Type 3 release event is summarized in Table 3-9.

Table 3-9. Arrival time, celerity and magnitude of Type 3 ice run on April 18, 1985.

Toe Location	Station (km)	Time (hh:mm)	Celerity (m/s)	Magnitude (m)
Mountain Rapids	307.2	20:00		
80 MacEwan Bridge	294.9	22:00	1.7	2

3.2.7 Breakup 1986 (Andres, 1988)

Breakup was documented in 1986, but was entirely thermal in nature. No significant ice runs were observed.

3.2.8 Breakup 1987 (Malcovish, Andres and Mostert, 1988; Winhold, 1988)

Breakup was observed to commence at the town of Athabasca at 14:00 on April 15, with an ice run commencing at 16:00. The water level peaked at 18:00 with the wave height being 1.2 m, based on WSC gauge record. A reconnaissance flight taken on April 15 found three short ice runs, each about 3 km long, between Grande Rapids and Cascade Rapids.

Another flight on April 16, reported a 6 to 7 km long ice jam in place at 09:30 with its toe at Cascade Rapids. Two ice runs were observed, a light ice run at Crooked Rapids and a heavier run further upstream. It was suspected that this heavier run was due to the wave associated with breakup at the town of Athabasca the previous day. A solid ice cover extended downstream from Cascade Rapids to Fort McMurray.

The ice jam at Cascade Rapids released (Type 2) within minutes of being reported as summarized in Table 3-10. At the MacEwan Bridge a gradual 2 m rise in water level was recorded over a 30 minute period, prior to the ice run arriving at 16:00 with a wave peak magnitude of about 4.6 m. The ice run jammed between the right bank and the second bridge pier at 16:35, and also jammed on the left side of the island just downstream of the MacEwan Bridge by 16:52. The jamming slowly proceeded along the river but halted downstream of Poplar Island by about 19:00. This jam released on the afternoon of April 17.

Table 3-10. Arrival time, celerity and magnitude of Type 2 ice run on April 16, 1987.

Toe Location	Station (km)	Time (hh:mm)	Celerity (m/s)	Magnitude (m)
Cascade Rapids	322.8	09:30		
Moberly Rapids	296.6	15:45	1.2	
90 Water Intake 1	296.55	16:04	0.04	4.4
80 MacEwan Bridge	294.9	17:15	0.4	4.6
75 MacIsland	294.2	17:30	0.8	4.3
57 WSC Gauge	289.2	18:00	2.8	

3.2.9 Breakup 1988 (Rickert and Quazi, 1988)

The Athabasca River broke up on April 10, following a 2 day snowstorm in the basin. Until that time, breakup had been progressing thermally. Only a 0.5 m rise in water level accompanied breakup there. An ice run originating from upstream of Grande Rapids, that had been missed during an observational flight on April 15, propagated through Fort McMurray on April 16. This surge caused a 3.5 m increase in water level at

the MacEwan Bridge, and created an ice jam with its toe at Poplar Island and its head just downstream of Mountain Rapids. Contradicting peak water levels of 243.5 and 244.5 m were measured at the Clearwater confluence (station 70), but this does not give a measure of magnitude, only a measure of stage.

Table 3-11. Arrival time, celerity and magnitude of Type 1 ice run on April 16, 1988.

Toe Location	Station (km)	Time (hh:mm)	Celerity (m/s)	Magnitude (m)
Moberly Rapids	296.6	15:00		
90 Water Intake 1	296.55	15:35	0.02	
80 MacEwan Bridge	294.9	16:00	1.1	3.5
Poplar Island	285.6	21:30	0.5	

3.2.10 Breakup 1990 (Van Der Vinne, 1994)

Ice conditions prior to breakup along the Athabasca River were not documented for the event in 1990. However, a large ice run was recorded traveling from Grande Rapids, past the MacEwan Bridge, and on to the Muskeg River (approximately 50 km downstream of the MacEwan Bridge) on April 20. This might possibly be attributable to ice breakup at the town of Athabasca, where a 0.4 m water level increase was documented at the gauge on the previous day (peak at 18:00 on April 19). This ice run propagated, apparently without jamming along the entire river section monitored, and continued to flow freely beyond the Muskeg River.

Arrival time of the leading edge of the Type 1 ice run was obtained at 10 locations between Grande Rapids and the Muskeg River, over a distance of about 180 km. The leading edge of the ice run was observed at Grande Rapids at 13:15 on April 20, and at Crooked Rapids by 22:15 that same day. It then continued downstream, arriving at the MacEwan Bridge by 01:15 on April 21. Wave peak magnitude measurements were obtained at 8 of the 10 locations enabling magnitude attenuation to be assessed. These measurements are summarized in Table 3-12.

Table 3-12. Arrival time, celerity and magnitude of Type 1 ice run on April 20-21, 1990.

Toe Location	Station (km)	Time (hh:mm)	Celerity (m/s)	Magnitude (m)
Grande Rapids	427	20/04/1990 13:15		
G140 Crooked Rapids	332.8	20/04/1990 22:15	2.9	1.3
Little Fisheries River	298.7	21/04/1990 00:45	3.8	3.6
90 Water Intake 1	296.55	21/04/1990 01:00	2.4	2.6
80 MacEwan Bridge	294.9	21/04/1990 01:05	5.5	2.5
70 Clearwater	293.2	21/04/1990 01:19	2.0	2.2
57 WSC Gauge	289.2	21/04/1990 01:49	3.2	
G35 Sawmill	279.3	21/04/1990 02:22	5.0	1.3
Suncor Site	265.6	21/04/1990 03:10	4.8	1.2
Muskeg River	244.7	21/04/1990 05:20	2.7	1.8

3.3 DISCUSSION OF HISTORICAL DATA

Of the ARC reports from 1977 to 1990, ice jam release events were documented for 9 of these 14 years. Since breakup along the Athabasca River between Athabasca and Fort McMurray covers a distance of about 400 km, the documented events discussed are only a snapshot of what may have occurred. Although the documentation is limited to only 9 years of historical ice jam release events, a pattern has already been found of the various locations ice jams tend to form and release. These are classified as Type 1 where ice jams release upstream of Crooked Rapids, Type 2 near Crooked Rapids, and Type 3 near Mountain Rapids.

All of the documented years provide evidence of a cascading effect of ice jams along the Athabasca River, except for the events in 1990. A reformation of an ice jam was reported at the MacEwan Bridge for the years of 1978, 1982 and 1987. Jamming was also documented downstream of the MacEwan Bridge, most commonly around the area of Poplar Island, as discussed in the 1977, 1979, 1982, and 1987 reports. A great example of multiple ice jam release events was in 1984. An ice jam was initially in place upstream of the study reach, but upon release, it reformed into an ice jam at the Horse River. This ice jam at the Horse River then released about 2 hours later, sending a surge through Fort McMurray. Observations for both of these release events in 1984 were

documented. Another interesting year was 1985, where a jam was positioned far upstream of the study reach at Rapides du Joli Fou, and a second jam close to Fort McMurray at Mountain Rapids. The release event measurements were not of either of these ice jams, but of the ice cover between Mountain Rapids and the MacEwan Bridge that broke up and created a small ice run. This historical documentation shows the frequency of ice jam release events and the likelihood of multiple release events in any given year, thus making this site ideal for the study of the propagation of surge waves resulting from ice jam failure.

Valuable quantitative data has been obtained from this historical documentation. Measurements of arrival time of the peak water level or breaking front provide an idea of the celerity that these surge waves have. Accompanying some of these time measurements, are observations of the peak wave magnitude (the difference in water level from before the wave arrives to the peak water level attained). Some documented years provide estimated measurements of the toe location of the ice jam and its corresponding length. For events that initiated upstream of the study reach, measurements of ice jam location and length were difficult to obtain. A summary of these findings are in Table 3-13, where *No. Time Meas.* and *No. Mag. Meas.* refers to the number of locations along the Athabasca River that arrival times and peak wave magnitudes were measured, respectively.

Table 3-13. Summary of historical data obtained from ARC reports.

Year	No. Time Meas.	No. Mag. Meas.	Ice Jam Toe Location	Ice Jam Length	Comments
1977	2	1	Crooked Rapids		8 m thick shears walls d/s of jam
1978	4	1	u/s Crooked Rapids	4 km	
1979	2	1	d/s Mountain Rapids	8 km	
1982	12	0			initiated u/s of Crooked Rapids
1984	4	3			initiated u/s of Crooked Rapids
1984	3	2	Horse River	9.4 km	
1985	3	2	Long Rapids	3 km	
1985	2	1			not a fully developed ice jam
1987	6	3	Cascade Rapids	7 km	
1988	4	1	u/s Grande Rapids		
1990	10	8			initiated u/s of Crooked Rapids

The above table shows the amount of data available for analysis. Most events had measurements of surge or breaking front arrival times at an average of about 4 sites. This is a relatively small amount of data to study the propagation of surge waves; therefore more measurement locations are desired. Events of 1982 and 1990 are an exception, with 12 and 10 arrival time measurements respectively. The peak wave magnitude measurements are even more lacking, with an average of only 2 measurements along the surge path. Again, 1990 is an exception with 8 measurement locations. This lack of magnitude data prevents the magnitude attenuation to be studied as numerous data points are required. Of all the documented events, no magnitude measurements were obtained at the ice jam release location. Although the historical data presented in this chapter is invaluable for preliminary ice jam release analysis, it is limited in its applicability to study the propagation of ice jam release surge events.

Due to the dangerous nature of ice jam release events, water level measurements are difficult to obtain. Therefore, it is desirable to find a set of equipment to obtain these water levels. Ideally, this equipment should be able to be used in a remote area, such as the reach between Crooked Rapids and Mountain Rapids, and would not require human manipulation thus being self-sufficient. A full stage hydrograph of the surge is advantageous, rather than just the peak water levels, to study the entire shape of the surge wave.

Another area that could require more data collection is information on the ice conditions prior to breakup. If the mechanics of the ice cover are to be studied, as earlier described according to Jasek (2003), the ice cover downstream of the ice jam would be required. This could at least classify an ice jam as either unimpeded or impeded. Measurements of not only the time of the peak water level, but of the first instant of increasing water levels and the arrival of the rubble ice cover would aid in analysis. With this data, a comparison could be made of the ice front or maximum ice concentration in relation to the peak water level. Coupled with the distance the surge and ice had traveled, further comparisons could be made with Jasek's observations (2003).

Data of the ice conditions within the ice jam would also aid in studying the propagation of an ice jam release surge, but possibly the ice cover mechanics as well. By knowing the location of the toe of the ice jam and the length of the ice jam, a better understanding of the corresponding downstream water levels could be attained. The ice thickness within the ice jam, a very difficult measurement to obtain, would greatly enhance the knowledge of the shear volume contained within the ice jam. It would also provide an initial condition for computer modeling purposes.

Overall, this historical data provides a precious insight to the behaviour of a surge resulting from an ice jam release. The change in surge celerity can be assessed as it propagates downstream, but magnitude attenuation is lacking in quality data. A data set involving stage hydrographs at numerous locations along the river is required. The documentation shows a high frequency of ice jam release events with multiple events occurring in most years. Therefore, the Athabasca River near Fort McMurray is an ideal location to implement a program to obtain this more developed data set.

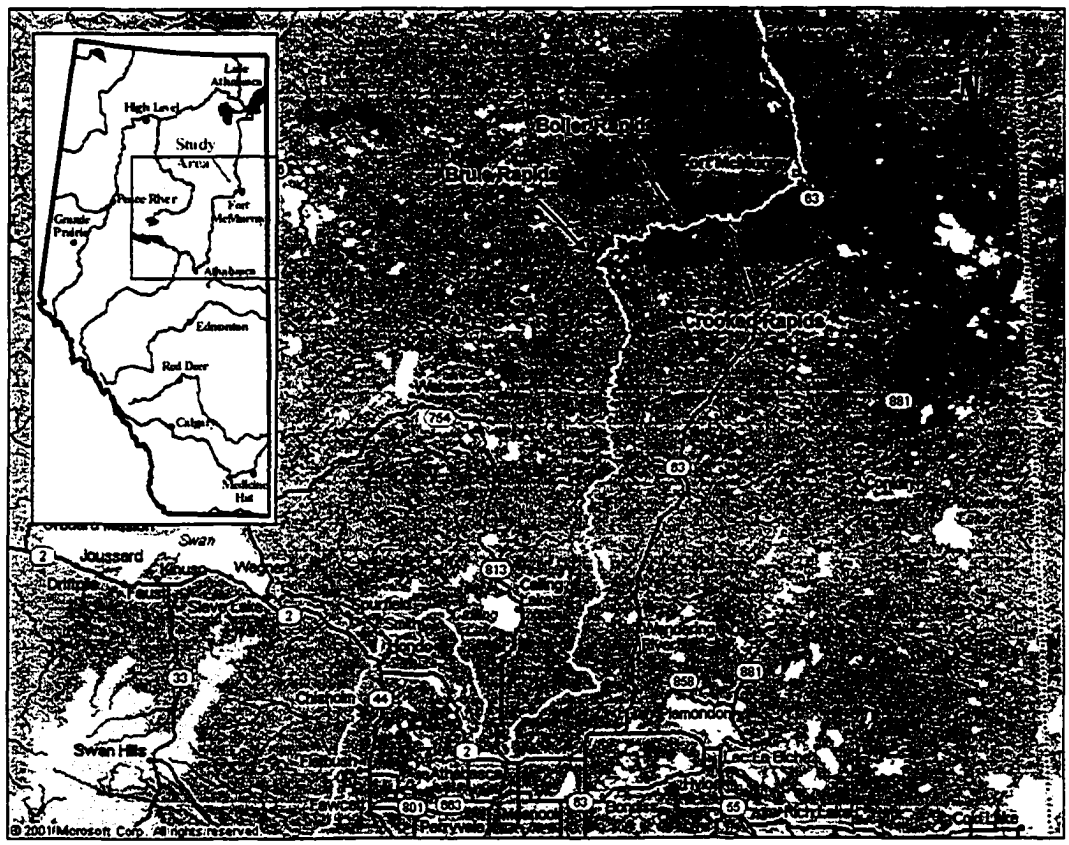

Figure 3-1. Athabasca River extending from Athabasca to Fort McMurray.

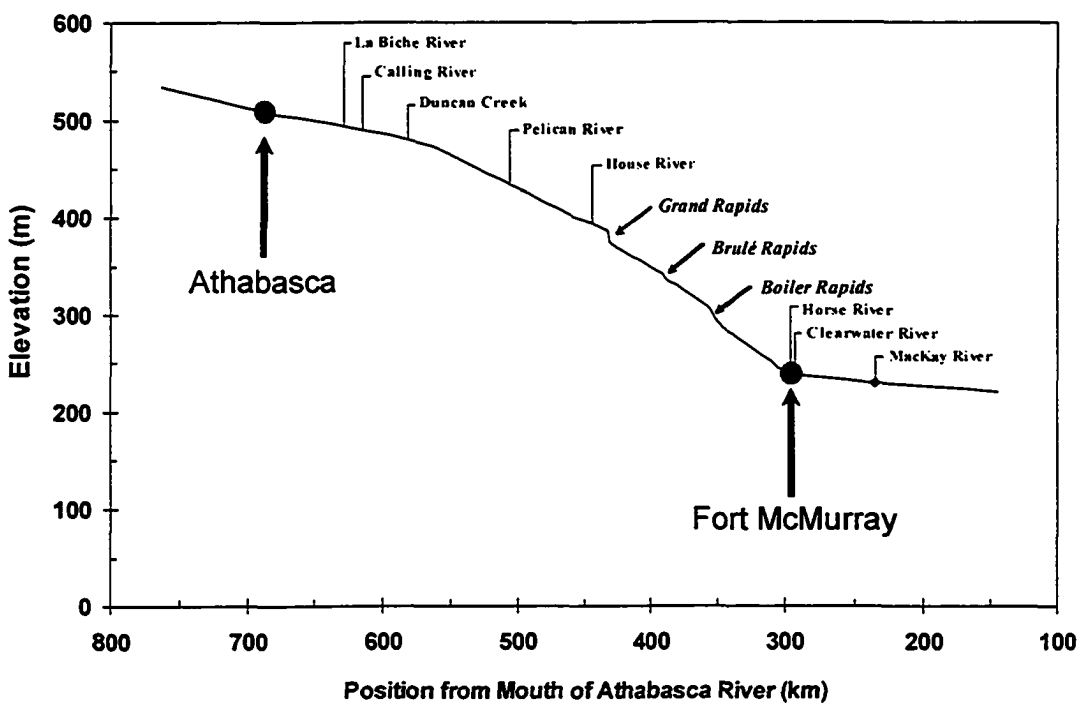

Figure 3-2. Bed profile for the Athabasca River.

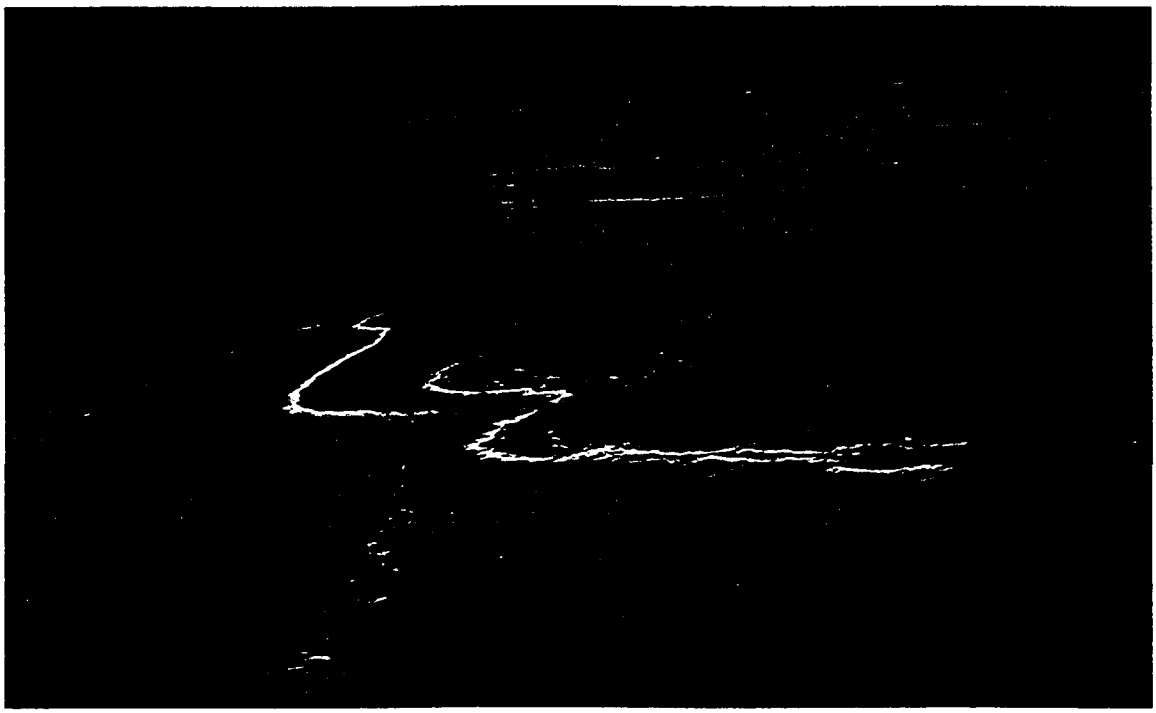

Figure 3-3. Bed discontinuity along the study reach of the Athabasca River.

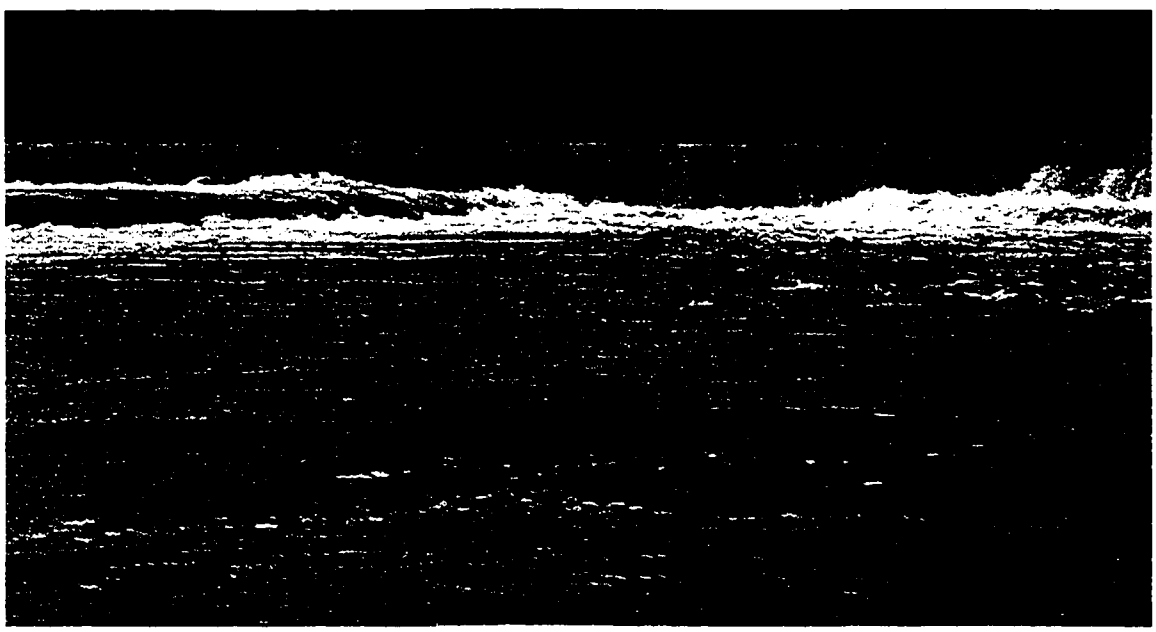

Figure 3-4. Close up view of flow over a bed discontinuity on the Athabasca River.

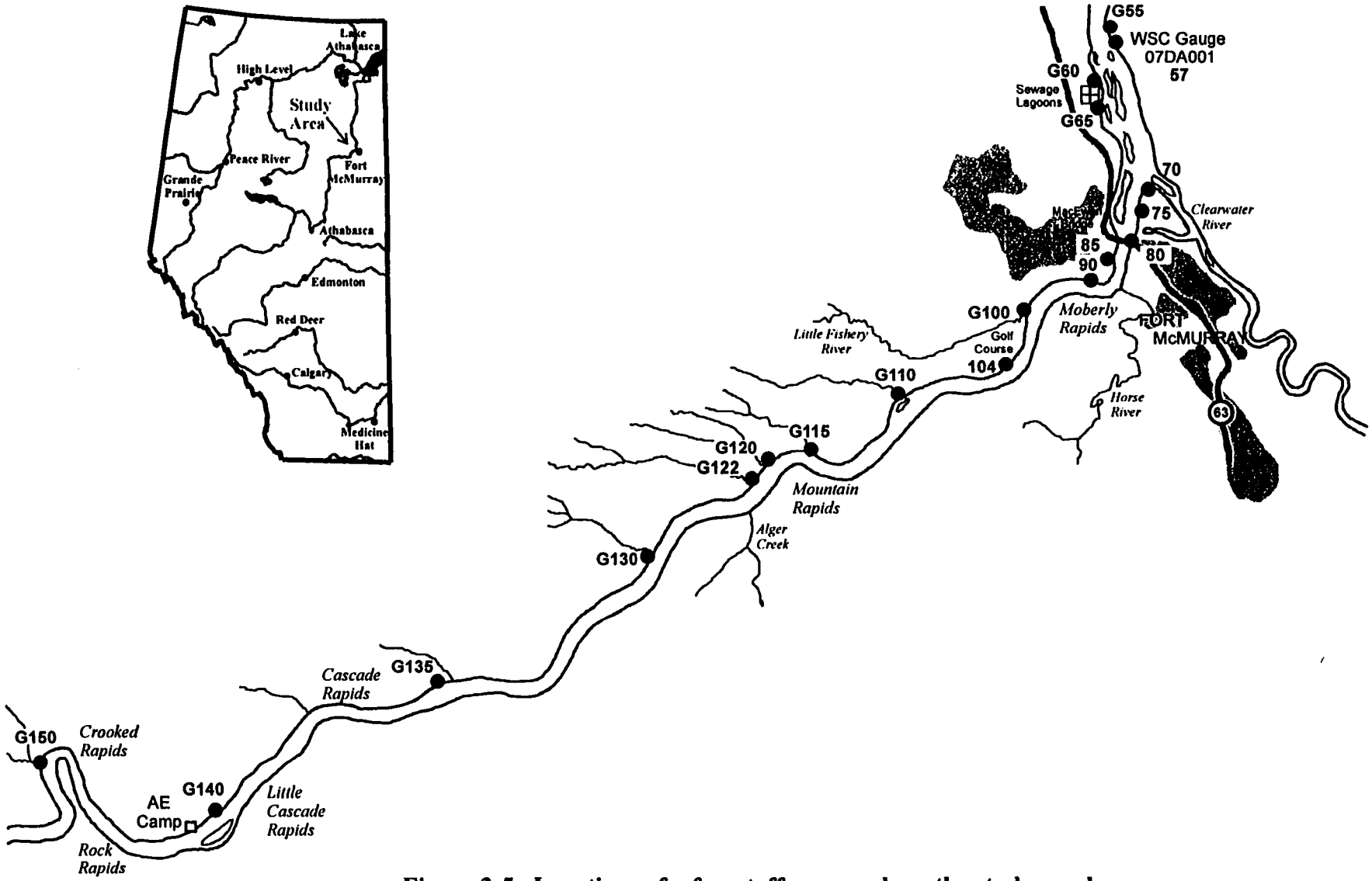

Figure 3-5. Locations of a few staff gauges along the study reach.

4 FIELD STUDY

Clearly ice jam release surges frequently propagate along the Athabasca River reach between Crooked Rapids and the city of Fort McMurray, making it an excellent location to study such events. However, upon investigating the historical record it became apparent that the available historical data at this site is quite limited. Measurements not only of surge arrival time, but of water levels throughout the entire passage of the surge, are essential to study the propagation of surge waves resulting from ice jam release events. Therefore, for this study, a monitoring network was implemented along this reach in an attempt to obtain detailed measurements of propagating surges. Preliminary components were installed by University of Alberta (UA) field staff in advance of the 2001 breakup, and the network was expanded and improved in the following years (2002-2004).

The details of this remote monitoring network and the data obtained will be discussed in this chapter. The monitoring network was successful in measuring the passage of surges in 2001, 2002 and 2003. However, breakup in 2004 was an uncommonly thermal process where most of the ice melted in place, consequently no surges occurred.

Complementary data, collected during the period of operation of the remote network, are also described in this chapter. For example, during breakup, water level measurements within the city limits and aerial observations of ice conditions were taken by Regional Municipality of Wood Buffalo (RMWB) and Alberta Environment (AE), respectively. For the years considered in this monitoring study, UA participated in these measurements. Water level profiles were taken at accessible stations around the city in the period leading up to breakup, as well as during the passage of surges, where possible. UA also collaborated with AE in conducting daily observational flights during breakup, to assess the deterioration of the ice cover and to observe any ice jams in place.

4.1 REMOTE MONITORING NETWORK - FIELD INSTRUMENTATION

Since this reach of the Athabasca River is remote and is only accessible by helicopter during the breakup season, the measurement equipment used in the remote network had to be both robust and self-powered. The equipment had to be able to run throughout the breakup season without manual assistance, and it had to be able to communicate with monitoring staff to provide warning if significant events were occurring. The instrumentation employed for each remote monitoring station typically included the following four components:

1. a pressure sensor,
2. a data acquisition device (data-logger),
3. a communication system, and
4. a self contained power system.

Various types of pressure sensors were used to measure water levels, each described in detail below. These measurements were stored for download using a data-logger, which was also responsible for controlling the frequency of water level measurements. At the interactive (communicating) stations, this data could be accessed on a real-time basis using cellular phone technology. For non-communicating stations, the data-logger had to be retrieved and downloaded manually. Solar panels and batteries were used to power each station. Details of each component are discussed below.

4.1.1 Pressure Sensors

Automated water level measurements were taken using submersible pressure sensors. The basic premise of this approach is that the depth of water above the sensor is proportional to the pressure measured. This approach assumes a hydrostatic pressure distribution within the flow, as validated by accompanying manual measurements on numerous occasions. Most apparent is a comparison of manual measurements by AE at station G140 for breakup 2002 (discussed later and shown in Figure 4-18), where the most dynamic data was measured. If a hydrostatic pressure distribution is valid at G140, then it must be valid elsewhere. Pressure transducers also require calibration in the lab,

prior to field deployment, to determine the instrument's unique relationship between measured voltage and actual pressure.

There are basically two types of submersible pressure sensors applicable in this situation: vented and un-vented. In the case of a vented pressure probe, the sensor (located under the water) is vented to the atmosphere using a length of hollow tubing, which runs up on to the bank out of the water. The vent provides the instrument with a reference to atmospheric pressure, eliminating the effect of atmospheric pressure variations on the measured water pressure data. This is convenient from the perspective of data analysis, and atmospheric pressure data is not needed. However, the venting tube is expensive, which limits the practical length that can be employed, and it is vulnerable to damage and/or water submersion of the orifice during ice runs.

Un-vented pressure sensors are more robust in that they do not require the venting tube. Instead, they measure the total pressure which is a combination of barometric pressure (in air) and hydraulic pressure (in water). To get an accurate measure of water depth, only the hydraulic pressure should be considered. Therefore, a correction must be made to the data by subtracting the barometric pressure from the total pressure. At the beginning of this study, a meteorological station was set up in Fort McMurray to measure numerous meteorological variables, including barometric pressure. Data from Environment Canada was also available at stations in the surrounding area. These barometric pressure measurements did not show a significant variation over the period of surge propagation past each station. That is, the air pressure did vary, but so slowly that it was essentially constant over the period of travel of a surge past each sensor. Since the actual water level elevation was not critical and only the change in water level during the surge passage was required, the effect of barometric pressure was considered negligible.

The instrument accuracy of these pressure sensors is fairly high (maximum error of about ~1 cm over the range of depths measured). However, practically speaking, it is impossible to measure the water levels associated with large ice runs in shallow flows to that level of accuracy. A conservative estimate of the error would probably be

approximately ± 10 to 15 cm^2. This is actually much better than manual measurements (i.e., those taken by conventional surveying using a rod and level) because of the inaccuracy required in estimating the actual water level in that approach. For example, an ice run 2 m thick with a typical specific weight of about 0.9 times that of water, would be running with the top of ice averaging 20 cm above the actual water level. Since the water level cannot be directly measured in such a situation, the actual water level variation must be estimated from the top of ice level. Taking into account the large sizes of ice floes typically seen, and the random orientation of these ice floes, surveyed water levels during ice runs likely have an error in the order of ±50 cm.

4.1.2 Data Control, Storage and Acquisition

Data-loggers were employed to store the data collected by the pressure sensors, to control the frequency of water level measurements, and to facilitate communications (for downloading data and sending out alarms). Two manufacturers' data-loggers were employed in this study: Campbell Scientific's CR510®, and Optimum Instrument's DataDolphin-3000®. In general, it was found that the former was considerably more flexible, in terms of programmable capabilities; however, a considerable time investment in learning the programming language was necessary to take advantage of this. Optimum's DataDolphin was considerably easier to use, with the distinct advantage of employing a user-friendly window interface for control programming. Both types of data-logger had alarm capabilities when used with a communications system.

Water level measurements were taken throughout the freeze-up, winter and breakup periods. Sampling intervals were 30 minutes in winter, but this was increased to measure water levels every 5 minutes during breakup, in order to adequately capture the details of passing surges. Both types of data-loggers were programmed to use transducer calibration information directly to convert the sensor signal to cm of water depth. At the time of each measurement, in addition to the sampled water level, the Campbell data-

[2] Personal communication, F. Hicks, Nov. 2004

loggers stored the maximum and minimum water levels for the preceding 30 minutes. Battery voltage was also monitored by both types of data-logger.

4.1.3 Communications Systems

A number of the remote monitoring stations were interactive, using cellular communications technology to facilitate real-time monitoring as well as data downloading. These communication systems were also used to take advantage of the alarm capabilities of the data-loggers, allowing them to signal an alarm when a sudden increase in water level was measured, or when a failure of the pressure sensor signal was detected.

Two types of cellular communications were used. A conventional analog cell phone (3W) was connected to the Campbell data-loggers using a custom modem. For the Optimum data-loggers, Cellular Digital Packet Data (CDPD) communications technology was employed. This technology uses the digital band of the conventional cellular network (the component that records and transmits user data, such as call duration, for billing). Data was transmitted from the data-logger through an IP (internet protocol) modem connected to a 3W CDPD compatible radio. This allowed the DataDolphin loggers to be accessed directly through the internet.

Both systems employed 12 element, 11dB Yagi® antennas perched on top of 30 to 40 foot aluminum towers. Each of these towers was stabilized using three guy wires anchored at the ground using reinforcing steel bars (rebars) and a turning buckle. Typical tower setups are shown in Figures 4-1 and 4-2.

4.1.4 Power Systems and Power Management

Since the monitoring stations were in remote locations, each station had to be self-sufficient in terms of its power supply. Those stations employing communications technology were especially demanding of power and for these, a 75W solar panel equipped with 6A solar controller was used to maintain the charge in a 12V battery.

Power management was necessary to ensure the battery did not discharge below a minimum recovery threshold. This was achieved by limiting the timing and duration of accessibility for downloading data.

The Campbell data-loggers, which were accessed by dialing in to an analog cell phone, were programmed to receive incoming calls only during the first 15 minutes of each hour from 09:00 to 17:00 MST. This facilitated data download throughout the majority of the daylight hours. Additional batteries and much larger solar panels would have been required to extend communications into the night; however, the cost was prohibitive. Instead, the alarm capabilities of the data-logger were employed to facilitate data download during actual surge propagation events (day or night). Specifically, the data-loggers were programmed to call out if the water level had increased by 10 cm within the previous 30 minutes, and to stay on (ready to receive incoming calls) for the next 30 minutes. In this way, data could be downloaded at any time of day, if surge events were occurring.

The Campbell data-loggers were also programmed to repeat the alarm call two additional times on 5 minute intervals, to ensure the alarm was actually received. This was deemed necessary for two reasons: first, most of the towers were on the fringe of the cell phone network and so signal performance was occasionally poor; and second, the dial-out contact number was also a cell phone, which might temporarily be in a poor reception zone when being called with an alarm.

The alarm sequence on the Campbell data-loggers was set to repeat any time the water level had increased by 10 cm within the previous 30 minutes. With data being collected on 5 minute intervals, this led to a continuous string of outgoing calls during the passage of a surge. The only way to stop this from occurring was to upload an alternate version of the data-logger control program (one without alarms) immediately upon receiving an alarm call. Then later, once that surge had passed, the alarm version of the program would have to be re-loaded to be ready for the next surge event. This was a very cumbersome process, particularly given the size of the control program and the poor

quality of the cell phone connection at most sites. Often only part of the program could be uploaded before the connection was lost, necessitating multiple retries. Given that this would always be occurring during a time when a surge event was also happening, it was an extremely inconvenient necessity.

Power management for the Optimium DataDolphin data-loggers was somewhat simpler, as the CDPD communications were digital and thus less demanding of power. These data-loggers could be accessed for downloading at any time through the daylight hours, and for 30 minutes following an alarm after dark. These data-loggers had a simpler alarm capability than the Campbell data-loggers, in that they could only send an alarm when the measured water level passed a specified threshold. Alarm notification was also communicated in a different way, because of the CDPD communications technology used. These alarms were actually routed through the internet to Optimium's server, which would then send out email messages to a user-specified list of addresses. A cell phone equipped with text-messaging capability was then used to provide immediate notification of that email's arrival. This system required the user to access Optimium's server through the internet to confirm receipt of the alarm before any subsequent alarms could be sent. However, resetting the alarm threshold with a new (usually higher) value was extremely simple and quick, involving just changing one entry in the data-logger access software.

4.1.5 Other Equipment and Methods Used

Another type of water level measurement device used in this study was an instrument known as a Levelogger® (also know as a Diver®). This is a device which combines an un-vented submersible pressure sensor, a submersible data-logger, and a power source (a small battery). Leveloggers have no communications capability; they must be retrieved from the water and connected to a computer to access the data. Originally intended for well logging applications, these devices can be programmed to start and stop on any prescribed date, and to collect water levels on any desired interval. For example, although these devices were typically deployed before river freeze-up, they

could be programmed to activate the following spring and had sufficient memory to store 55 days of water level data taken at 5 minute intervals.

Leveloggers come precalibrated, but the standard pressure conversion charts used for calibration are based on a specific weight of water at 4°C. To increase the accuracy of the readings for our application, all conversion multipliers and offsets were changed for a specific weight of water at 0°C in order to represent the situation at breakup and freeze-up (0°C). The altitude of the water level at the measurement location is also required for a Levelogger to partially compensate for atmospheric pressure, and can range between 3000 m above and 300 m below sea level. The readings are then automatically adjusted, where 0.1 cm of water column is associated with each meter of altitude difference using an *M series* type (metric). A reference point must be established in order to process the collected readings by using the distance between the initial water level and the reference point elevation. Typically, a TBM located in close proximity to the Levelogger was used as the reference point. Again, since it was the relative change in water level during surge passage which was of interest, rather than absolute water levels, these adjustments were not critical to data accuracy.

Another type of device used in this study was a trip wire, which employed the alarm capabilities of the data-loggers. An early version of this wire setup (used in 2003) involved extending a length of wire onto the ice cover prior to breakup, and freezing it in place. When the ice cover started to move, it would pull the wire out of the data-logger causing the alarm to signal. As it turned out, this approach had two disadvantages. First, having the wire physically pull out of the data-logger was undesirable because of the potential for physical or electrical damage to the system. Second, the wire was so delicate that even minor ice movements (e.g., due to thermal expansion and cracking) would trip the alarm. AE field staff came up with a better design in 2004 in which a rope was tied to a piece of wood and placed far out on to the ice cover (Figure 4-3). On the bank, the rope was connected to the wires leading to the data-logger. As shown in Figure 4-4 the connection was arranged so that the pull on the rope as the ice moved would simply open the electrical connection, rather than ripping the wire right out of the data-

logger. This allowed the trip wire to be reset multiple times. These trip wires were very useful to track event speeds and to provide warning of incoming ice runs, particularly in locations where pressure sensors were not feasible.

Although most of the trip wires were used at the Campbell and DataDolphin data-logger sites, in one instance a trip wire was set up at the AE water quality monitoring station at Grande Rapids (approximately 100 km upstream of Crooked Rapids). Communications for this trip wire were facilitated through the GOES satellite, the system used by AE for telemetry to most water level and water quality recording stations. This provided updated information every 3 hours, which was quite adequate given the large distance between Grande Rapids and the study reach.

4.1.6 Issues with Daylight Savings Time

Unfortunately, the switch in April to Daylight Savings Time (DST) from Mountain Daylight Time (MST) moves the time 1 hour ahead of MST right in the middle of the breakup observation season. Both the Campbell data-loggers and the Leveloggers operate in a fixed mode, and continued recording in MST throughout the breakup period. This required manual adjustment of the data which, when forgotten, was often a source of error when viewing data real-time during the breakup period. This was inconvenient, but turned out to be far better than the system employed with the DataDolphins. Those data-loggers actually switch over to DST automatically the first time they are accessed after DST comes into use, not at the time MST/DST change-over actually occurs. The problem with this approach is that the record can be hard to interpret and correct afterwards. The data-logger has no option to leave it on MST or to do the switch-over at the actual time it is supposed to happen.

This project covers several years of operation of the automated remote network and associated manual measurements and observations. In the following sections, for each year, the equipment configuration for the remote stations is discussed, followed by a

description of breakup in terms of the occurrence of ice jam release surges, and finally a summary of the data obtained.

4.2 BREAKUP 2001

This was the first year that automated monitoring stations were installed and therefore, in order to evaluate the best possible instrumentation and configuration, only part of the network was set up.

4.2.1 Setup 2001

Three monitoring stations were installed prior to freeze-up in 2000, in preparation for breakup in 2001. These were located at stations G120, G130 and G135 as can be seen in Figure 4-5. Each site was equipped with a vented pressure transducer, connected to a Campbell data-logger communicating via an analog cellular phone.

The typical setup involved is shown in Figures 4-6 to 4-8. The pressure sensor was placed inside a steel pipe and fixed in place using a steel plate. This pipe was then bolted to a concrete pad that was placed into the water and anchored using a steel cable. Since it was unknown how the vented pressure transducers would perform on the first year of monitoring, Leveloggers were placed alongside the vented pressure transducers to collect backup data. The Leveloggers were also encased in the steel pipe and bolted on the concrete block as shown in Figure 4-9.

Due to its high cost (~$3/ft), the vent tube/transmission line from the vented pressure sensor was only approximately 30 m (100 ft) in length. About 70 ft (~20m) of the line extended from the water's edge to the pressure transducer in the water (in order to get it into water as deep as possible), leaving only about 30 ft (~10m) of length to run up the bank. However, the data-logger and communications tower had to be located several hundred feet up on to the bank in order to be safely above break-up ice runs. Therefore the venting tube/transmission line had to be terminated on a junction box on the bank, and a communications cable extended from this junction box to carry the signal up the bank walls to the data-logger and communication tower. The junction box and

vent/transmission cable were protected inside of steel pipes. The steel anchor cable ran alongside the transmission line, past the junction box, and up to the tower where it was wrapped around a large tree.

Initially, all of the data-loggers were programmed with alarms, triggered to set off when the water level increased by 10 cm in 30 minutes. However, as the ice cover formed in the early winter months, the alarm was being set off continuously. Therefore, a new program was installed that did not set off an alarm, which was to be used just during the winter months. The alarm program was re-installed just prior to breakup during a field trip in March 2001.

Communications with station G120 ceased in late February, 2001. During a field trip, the tower was found leaning against a tree and one of the guy wires was broken. This broken guy wire was likely due to a moose, since numerous tracks were found around the tower location. The tower was straightened and communication was re-instated.

Unfortunately, none of the vented pressure transducer systems survived the rigors of breakup ice runs. However, the Leveloggers were successful in capturing data throughout the breakup period. As it turns out, the Levelogger units for G130 and G135 were accidentally switched during installation, therefore appropriate altitude corrections were required after the data was downloaded.

4.2.2 Event Description

On April 25, the day before breakup occurred, the channel was opening up downstream of the MacEwan Bridge, and the intact ice cover upstream of the MacEwan Bridge showed evidence of thermal deterioration (Figure 4-10). Aerial observations summarized in Figure 4-12 shows intact ice was also in place upstream at station G100, with an ice run forming an ice jam just upstream of G110. The running ice contributing

to this ice jam extended upstream to station G135. There were localized sections of both intact ice and jamming in the upper reach from station G135 to Crooked Rapids.

At 18:55 on April 26 the AE observers, stationed about 1 km upstream of G140, noted the commencement of breakup. They documented an estimated increase in water level of about 1.0 m with the associated ice run continuing for 2.5 hours. After passage of this event, most of the reach was left with open water with some remnant ice present along the bends and islands, as shown in Figures 4-11 and 4-13. Upstream of the MacEwan Bridge, shear walls were clearly visible with ice thicknesses ranging from 0.5 to 1.0 m.

4.2.3 Measured Data

At the time of breakup in the spring of 2001, none of the un-vented pressure transducers were operational. One station was frozen into the ice during freeze-up. Another station was recording very low water levels, thus it was suspected to be frozen into the ice. Field observations found a large aufeis deposit, which is characterized by multiple layers of ice forming on top of a previous ice cover. This type of accumulation tends to form at the mouth of inflowing tributaries or from ground water springs through the banks of the river. A spring was located upstream of the station and therefore, it is likely that the pressure transducer was frozen into the ice. All three of the vented pressure transducers retrieved in July 2001 had damage to the probes that could not be repaired. Water found in the junction box located on the river bank was also responsible for erroneous results.

Although the vented pressure transducers were destroyed, the Leveloggers were successful in measuring the event. The ice map in Figure 4-13 shows the stage hydrographs obtained at stations G120, G130, and G135, along with the arrival time and magnitude of the peak water level (referenced to the water level prior to the event). A more detailed look at the stage hydrographs is provided in Figure 4-14. Table 4-1 provides a summary of the surge peak characteristics as it traveled downstream. Such

dramatic and rapid increases in water level leave little doubt that this was an ice jam release surge event.

Table 4-1. Arrival time, celerity and magnitude of ice run on April 26, 2001.

Toe Location	Station (km)	Time (hh:mm)	Celerity (m/s)	Magnitude (m)
G135	319.8	19:39		1.21
G130	312.3	20:39	2.08	1.31
G120	308.0	20:34	14.33	1.01

4.3 BREAKUP 2002

The equipment setup in 2002 was the most extensive, with five communicating stations, three recording stations, two manual measurement stations, and one automated station.

4.3.1 Setup 2002

After the poor performance of the vented pressure transducers during breakup in 2001, it was decided that un-vented pressure transducers should be employed in subsequent years. The Leveloggers had performed extremely well, but it was desirable to have a system with real-time communications capability. This was made possible by the discovery of a suitable communications wire being used in the mining industry for borehole logging. This steel cable, capable of withstanding 10,000 lb of tension, encases transmission wires thus enabling it to be used for both anchoring and communications. Although normally sold in reels of more than a thousand meters at a cost of several dollars per foot, remnant pieces 100-300 m in length were available for about $1/ft. This cable was connected to the un-vented pressure sensors which were again encased in a steel pipe and attached to a concrete pad in the same manner as the vented pressure transducers in the previous year.

Two additional remote monitoring stations were installed in the fall of 2001, in preparation for the 2002 breakup season. These new stations, one located upstream and

one downstream of the previous stations, used DataDolphin data-loggers and CDPD communications. The equipment from station G120 (installed in 2001) was moved upstream to G122 in order to avoid the aufeis problem which had encased the sensor in ice the previous year. Figure 4-15 shows the locations of these five communicating stations at 104 (new), G122 (relocated), G130, G135 and G140 (new).

The new communications tower at G140 had to be placed near the top of the valley wall, several hundred meters above river level, in order to be able to access the cell phone system. The transmission cable was then run from the tower, down the valley wall to the middle of the river channel, a total distance of several hundred meters. During breakup, both of the new communicating stations were programmed with a threshold water level condition to send out an email alarm through Optimum's alarm server. These worked excellently, notifying observers in Edmonton and Fort McMurrray of the passage of a major surge.

The Leveloggers that had been used as backup systems in 2001 were relocated to provide three new recording (non-communicating) stations, in order to obtain intermediate stage hydrographs between the five communicating stations. One recording station was placed about 2 km upstream of G130, and became known as station 132. Another Levelogger was placed about 2 km downstream of G135, and was known as station 133. The third Levelogger was located just upstream of the power lines near station G110, and was referred to as station 112. These sites are also shown in Figure 4-15.

The Leveloggers were encased in a perforated pipe and bolted to a concrete pad. A mooring cable was attached to the concrete pad for retrieval in the spring, but also to act as an anchor as the other end was tied around a tree. Once again, although they were installed prior to freeze-up, the Leveloggers were programmed to activate in late March and measure water levels every 5 minutes throughout the breakup period.

Each year during breakup, AE stations two ice observers at a camp on the river bank about 1 km upstream of the station G140. These observers record manual water level measurements throughout the breakup period as well as provide records of visual observations including ice cover texture, and/or any movement of the ice cover. The measurements and observations from AE were used as a comparison with the data measured by UA's remote station at G140.

Accompanying these monitoring stations were measurements within the city limits. RMWB provided manual measurements at station 90 at the water intake near Moberly Rapids, and at the Clearwater confluence, known as station 70. Automated water level measurements by WSC were also obtained just downstream of Fort McMurray at station 57.

4.3.2 Event Description

The majority of the study reach was showing signs of deterioration on April 26 prior to breakup. Open leads and small ice runs were occurring along the darkening ice surface, the most advanced deterioration being downstream of the MacEwan Bridge and within the rapid sections upstream of Fort McMurray. Ice conditions along the reach prior to breakup are shown in Figure 4-16. Also on April 26, a 17 km long ice jam with its toe approximately 10 km upstream of Crooked Rapids, near Long Rapids, was seen during the observational flight. Shear walls could be seen extending upstream from Long Rapids beyond Boiler Rapids, a distance of about 8 km.

In the late evening of April 26, this 17 km long ice jam released sending a surge of ice and water downstream. AE observers, stationed at the camp just upstream of G140, manually measured water levels and recorded visual observations. According to their records, the water level increased dramatically within about 15 minutes.

The surge propagated down through the study reach all the way to Mountain Rapids, coming to an abrupt halt at station 104, and forming a new 8 km long ice jam.

Gravel bars were created at the toe of this jam, possibly indicating grounding at the toe as the ice run arrested. These gravel bars buried and destroyed the sensor at station 104. Figure 4-17 shows the newly formed ice jam with its toe at station 104 inhibited by a downstream intact ice cover.

4.3.3 Measured Data

The pressure sensor at G122 did not survive the winter, again due to aufeis problems, and it was decided to discontinue this station in future years. The pressure sensors at the communicating stations G130, G135 and G140 survived breakup and measured a number of waves passing, including the large surge propagation event. The sensor at the new station 104 was successful in measuring part of this same wave. Of the three Leveloggers, the one at station 112 ended up within an ice jam and was lost, the one at station 133 was found pushed up on the bank, and the one at station 132 was successful in measuring throughout breakup.

In all, stage hydrographs were obtained from 7 of the 11 stations installed or manned during breakup. These hydrographs are shown in Figure 4-17 along with the peak wave arrival time and magnitude (the difference between the peak water level and the water level before the wave arrived). The peak arrival time at station 132 is shown as an approximate value since the measurement time of this Levelogger was not synchronized with the other stations. A more detailed stage hydrograph at G140 is shown in Figure 4-18. From this figure, a 4.4 m rise in water level can be seen in just 15 minutes.

Measurements from AE observers provide invaluable data as to what was actually occurring during the breakup process. These measurements also provide a stage hydrograph for comparison with measurements at the communicating station at G140. Based on the AE station log and data in Figure 4-18, the Long Rapids ice jam was believed to have formed a new ice jam at Crooked Rapids just upstream of G140 before re-releasing. This explains the smaller wave measured before the large surge arrived.

The photograph inset in Figure 4-18, courtesy of AE, provides a look at the shear walls left behind after the passage of this wave. It was believed that the sensor at G140 shifted to a deeper position after the peak of the wave was attained as supported by manual water level measurements from AE. Figure 4-18 shows the correction made to the data as a result of this shift in position.

The surge then came to an abrupt halt at station 104 where a new, 8 km long, ice jam was formed. Although the sensor at station 104 was eventually destroyed during this event, it was operational long enough to be able to capture the peak of this wave as it continued propagating underneath of the competent ice cover downstream of the ice jam. More detailed stage hydrographs at all of the stations that successfully measured this event are shown in Figure 4-19, with a summary of the peak wave measurements in Table 4-2. Photographs of the toe of the ice jam at station 104 are shown in Figures 4-20 and 4-21.

Table 4-2. Arrival time, celerity and magnitude of ice run on April 27, 2002.

Toe Location	Station (km)	Time (hh:mm)	Celerity (m/s)	Magnitude (m)
G140 Crooked Rapids	327.0	1:51		4.06
G135	319.8	2:20	4.14	2.02
132	314.2			1.83
G130	312.3	3:00	3.13	1.67
104	300.3	4:16	2.63	1.05
90 Water Intake 1	296.55	6:10	0.55	1.39
57 WSC Gauge	289.2	9:30	0.61	0.64

According to open channel hydraulics theory (Henderson and Gerard, 1981) the re-formation of a jam results in a positive surge propagating upstream from the new jam location, as well as a negative surge traveling downstream. Evidence of a positive surge propagating upstream in response to the ice jam formation at station 104 was looked for, but was not evident in the water level records at the upstream stations. Likely, this wave would have attenuated substantially during passage under the 8 km ice jam and along the channel to the next upstream monitoring station, G130 (12 km upstream).

Numerous smaller release events were subsequently documented along the study reach (Figure 4-22) due to the dynamic nature of breakup on this river. Two waves with magnitudes of approximately 30 cm each passed through the ice jam at station 104 without affecting its position, but a third wave of about 50 cm caused the ice jam to release. As a result, an ice run was observed within the city of Fort McMurray extending over a duration of about 2 hours. The surge was quite attenuated by the time it reached Fort McMurray (only about 1 m high) and was not measured.

Although the pressure sensors at G130, G135 and G140 survived breakup, over the ensuing months one by one they stopped working. It was suspected that the sensors became clogged with sediment during the spring and summer runoff events. As a consequence more expensive sediment resistant pressure sensors were used afterward.

4.4 BREAKUP 2003

No Leveloggers were installed in preparation for breakup 2003. However, communication stations were still in place at G130, G135 and G140 and trip wires were installed at stations 104 and G140.

4.4.1 Setup 2003

The equipment setup for breakup in 2003 is summarized in Figure 4-23. Due to funding limitations, pressure transducers could not be installed in the fall of 2002. Instead, un-vented pressure transducers were deployed through the ice cover at stations G130, G135 and G140 during the first week of April, 2003. No pressure transducer was placed at station 104 since further analysis of the historical record confirmed this to be a typical ice jam toe location (as experienced in 2002). Automated water level measurements were taken every 5 minutes, with the same output and alarming specifications used in 2002. Analog cellular communications were still being used at stations G130 and G135, and digital CDPD was again being used at stations 104 and G140.

In 2003, stations 104 and G140 were equipped with a trip wire system. Simple electrical wires were hooked up to the second precision input on the data-logger with the other end frozen into the ice cover. When this wire was pulled out of the data-logger due to a shift in the ice cover, an alarm would be triggered. Unfortunately, the wire at G140 was connected to the wrong input connection and did not work throughout the breakup season. The trip wire at 104 had one false alarm after a minor ice movement; it was reset and later successfully notified field staff of an incoming ice run.

Manual water level measurements were taken by RMWB within city limits at station 75, known as MacDonald Island, just upstream of the Clearwater confluence and at station 90 at the water intake near Moberly Rapids. Automated water level measurements were made available from WSC, taken from station 57 just downstream of Fort McMurray. No Leveloggers were installed for breakup 2003.

4.4.2 Event Description

The ice cover downstream of the MacEwan Bridge started to show signs of thermal deterioration by April 15. Also at this time, there were open leads present at rapid sections upstream of Fort McMurray as well as border flow. These conditions changed very little until an ice run was observed on April 21 by AE staff stationed upstream of station G140. The ice run started at 08:15 with water levels rising by about 3 m in 25 minutes. This ice run continued to pass G140 for about 45 minutes. By 15:15, a 10 km long ice jam had formed at Mountain Rapids, about 10 km upstream of Fort McMurray as depicted in Figure 4-24.

The next day at 08:00, April 22, the Mountain Rapids ice jam was still in place and water levels were decreasing in Fort McMurray. This was likely due to water being stored within the ice jam itself. At 12:30, the length of this jam had increased to about 12 to 15 km. The daily observational flight found an ice run upstream of Crooked Rapids, which was expected (based on observed speed) to impact the Mountain Rapids ice jam at about 16:00.

4.4.3 Measured Data

AE staff monitoring the river from their station just upstream of G140 reported the ice run arrival at 15:00 and measured a 2 m rise in water level. This ice run hit the head of the ice jam and caused it to release. The resulting surge traveled through the city as summarized by Table 4-3. The WSC gauge broke down part way through this event but captured a wave magnitude of 0.163 m. However, this is not necessarily the maximum water level experienced at station 57 during this surge event since the gauge had not yet peaked at the time of the failure.

Table 4-3. Arrival time, celerity and magnitude of ice run on April 22, 2003.

Toe Location	Station (km)	Time (hh:mm)	Celerity (m/s)	Magnitude (m)
90 Water Intake 1	296.55	18:45		4.29
75 MacIsland	294.2	19:15	1.31	3.15
57 WSC Gauge	289.2	20:00	1.85	0.163+

The gauge at station 57 malfunctioned so the magnitude is likely larger than 0.163 m.

High water marks were measured along the banks within the city limits after the release of this ice jam. These high water marks vary between 2.9 m and 3.9 m, thus lending some credibility to the magnitudes measured during the event of 4.29 m and 3.15 m at stations 90 and 75, respectively. These high water marks are summarized below in Table 4-4.

Table 4-4. High water marks measured after the ice jam release event of 2003.

Toe Location	Station (km)	Magnitude (m)
G100	298.9	3.92
90 Water Intake 1	296.55	3.73
85 Water Intake 2	295.45	3.88
80 MacEwan Bridge	294.9	2.89
70 Clearwater Confl.	293.2	3.26

Aerial observations were not made of the study reach after the release of this ice jam. Therefore, a map is not available to show the remnant ice conditions. Full stage

hydrographs are not available as the manual measurements were taken at large intervals, and the automated station at 57 discontinued during this event. Since the toe of the ice jam was downstream of the communicating stations at G130, G135 and G140, these stations did not provide valuable data on this release event.

4.5 BREAKUP 2004

4.5.1 Setup 2004

The equipment set in place prior to breakup in 2004 is shown in Figure 4-25. Communicating stations using un-vented pressure transducers, mounted in cylindrical concrete filled pipes, were installed prior to freeze-up in the fall of 2003 at stations G130, G135 and G140. However, due to errors during installation, G130 did not record any data. Station G140 worked initially, but measurements ceased after freeze-up. A field trip by AE during the early winter months found that station G130 was hooked up incorrectly, and as a result the pressure sensor was destroyed. The sensor at G140 was found along the edge of the channel, likely pushed out by the ice during freeze-up (likely attributable to the cylindrical shape of the anchor). The wires were severed and this pressure sensor was also destroyed. Therefore, the only data that could be observed on a real-time basis during breakup 2004 was from station G135. This station was still programmed to signal the cell phone three times during significant events, as in previous years.

Since water level measurements were only being obtained at station G135, trip wires were installed at stations 104, G130, and G140, as well as at Grande Rapids (which is located approximately 100 km upstream of Crooked Rapids). These trip wires, installed using the rope and wire design described earlier, were all effective in contacting the field team during all ice movements. Additional water level measurements came from RMWB at stations 70, 80 and 90, as well as from WSC at station 57. A Levelogger was installed in the Clearwater River just upstream of the Athabasca River confluence, at Clearwater Island. This recording station was to provide valuable water level

information if an ice jam was to block the confluence, forcing the water to back up the Clearwater River and flood downtown Fort McMurray.

Since ice jam release events had originated from stationary jams at Mountain Rapids in two of the previous three years, preparations were made to measure an ice jam profile in this remote area. TBMs were installed on April 8, 2004 at 5 new locations between stations 104 and G115. At each of these TBM locations a permanent staff gauge was installed at the top of the bank (above maximum ice level), and two to three temporary staff gauges were installed at lower levels towards the water's edge. These staff gauges and TBM's were all tied in to the Geodetic Survey of Canada datum using Global Positioning Systems (GPS) and a total station. The intent was that, if an ice jam formed in this area, the profile could be measured using photographs referencing these staff gauges from the safety of a helicopter.

4.5.2 Event Description

Breakup in 2004 was uncharacteristically thermal in nature. Therefore, no ice jam formation or release events were measured. Due to the thermal processes observed, only a very small accumulation formed near Mountain Rapids which was below all but one of the temporary staff gauges. As a result, most should be in place for the 2005 breakup season. In the fall of 2004, an attempt was made to retrieve the Levelogger at Clearwater Island; however, it was found to be lodged under water and could not be extricated.

4.6 SUMMARY AND EQUIPMENT LEGACY

Ice jam release events are highly dynamic in nature, and obtaining measurements of such events is difficult and dangerous. By installing a remote monitoring network with communicating capabilities, detailed measurements of ice jam release events were obtained. The most notable of events measured is for breakup 2002, with seven stage hydrographs spanning about 40 km. Since the ice jam released close to the most

upstream station, the propagation of this surge wave was captured. This is likely the largest event measured of this kind and it is quite astonishing that the equipment survived the passage of this large ice run.

Due to the debatable question of the importance of an ice cover to the propagation of a surge, it would have been beneficial to get a more detailed measurement of the ice surface prior to breakup. However, these measurements are virtually impossible to obtain when the ice cover is highly deteriorated, and the possibility of an ice release event is unknown and likely. Yet, aerial observations have provided a large amount of insight to the ice surface conditions as summarized in the ice maps previously discussed.

It would also be beneficial to know the ice jam profile. An attempt was made in 2004 by installing a temporary staff gauge network in the area of Mountain Rapids. Ice jams have been frequently observed in this rapid section, thus making it an ideal site for the staff gauge network. Unfortunately, the breakup events of 2004 were uncharacteristically thermal. As a result, no ice jam profile nor ice jam release events were measured in 2004.

Although 2004 marked the end of this experimental program, it was desirable to continue to maintain, and even upgrade the remote network, not only to obtain additional surge data for research purposes but also because it serves as an effective early warning system for the people of Fort McMurray. Fortunately, Alberta Environment has recognized this value and have taken over maintaining and operating the system. Preparations for 2005 include the replacement of station G140 with a fully operational provincial water level gauging station with GOES satellite communications, installation of a pressure sensor at Grande Rapids also communicating on the GOES system, and un-vented pressure sensors at stations G130 and G135 (the latter being intact from the previous year thanks to a sediment resistant sensor). Trip wires will be installed at all of these stations, as well as at station 104, in late winter 2005.

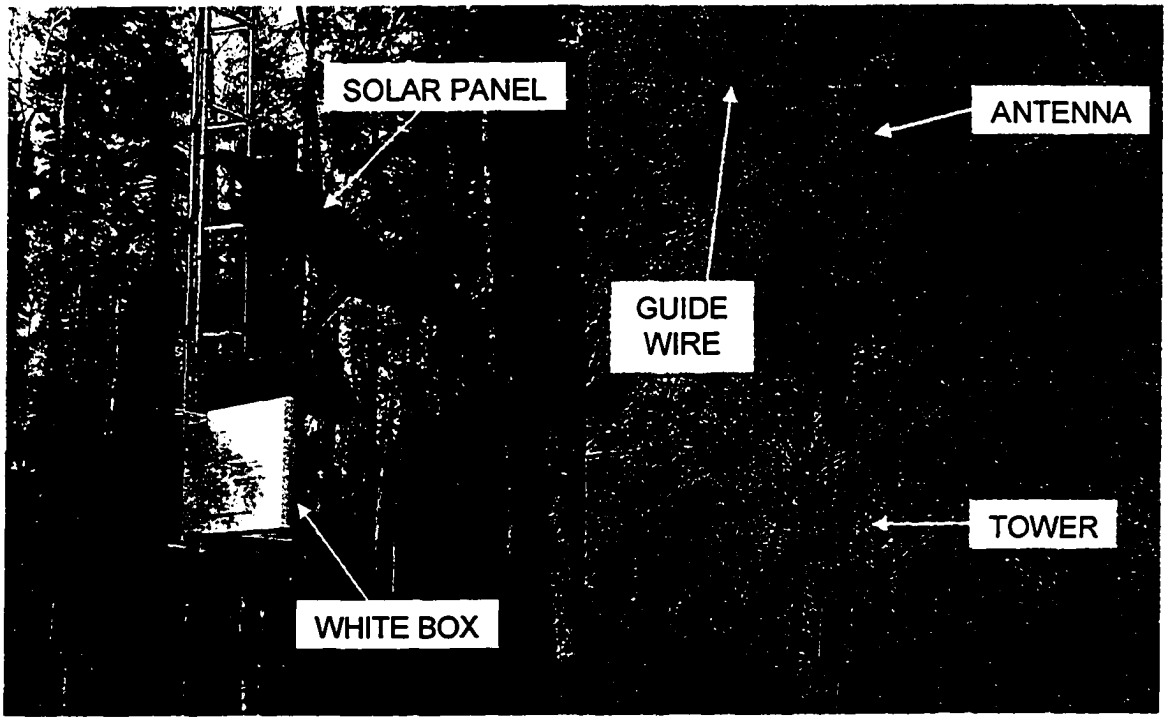

Figure 4-1. Typical setup of communication towers.

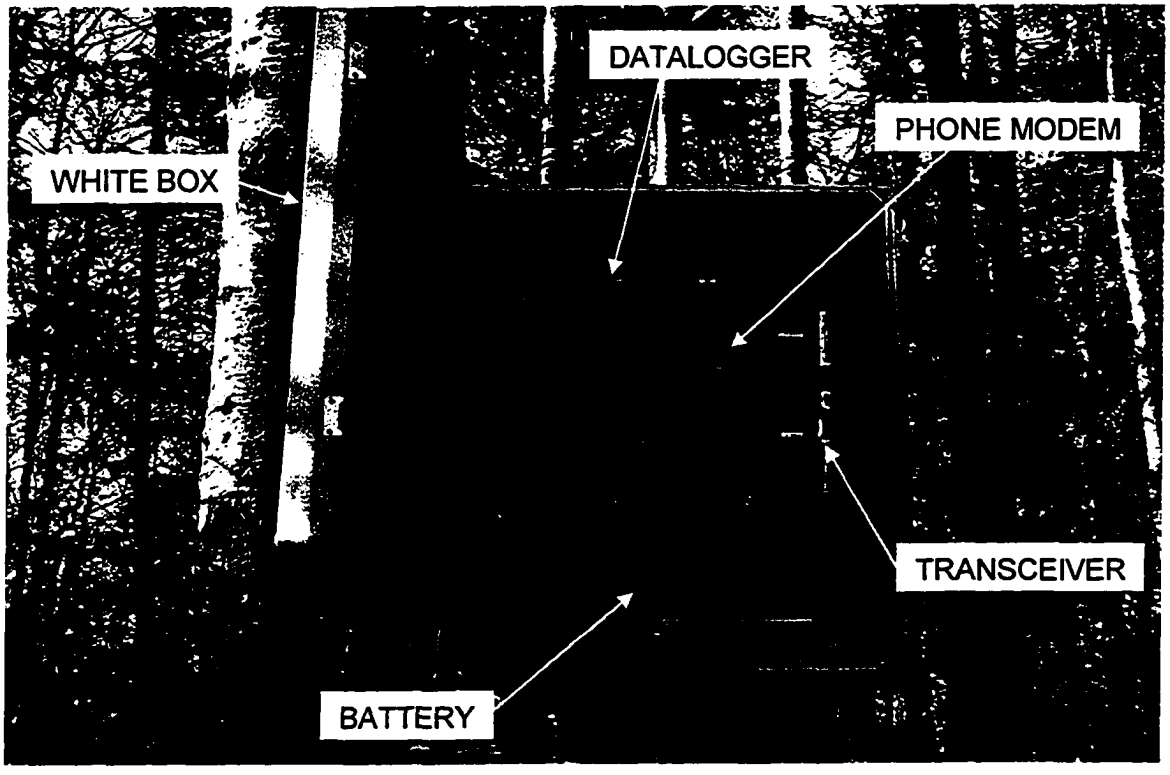

Figure 4-2. Equipment encased in weather proof housing (white box).

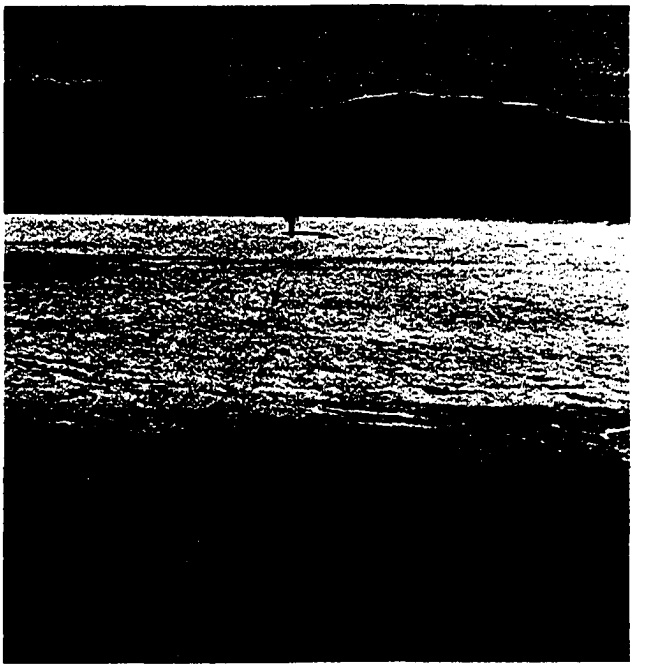

Figure 4-3. Example trip wire set-up. Rope is tied to a branch that is set out on the ice cover.

Figure 4-4. Example trip wire connection. The wires are connected with an easily breakable screw connection. When the rope pulls, this connection is broken, triggering the data-logger alarm. However, the wires remain connected to the data-logger. Consequently it can easily be reset.

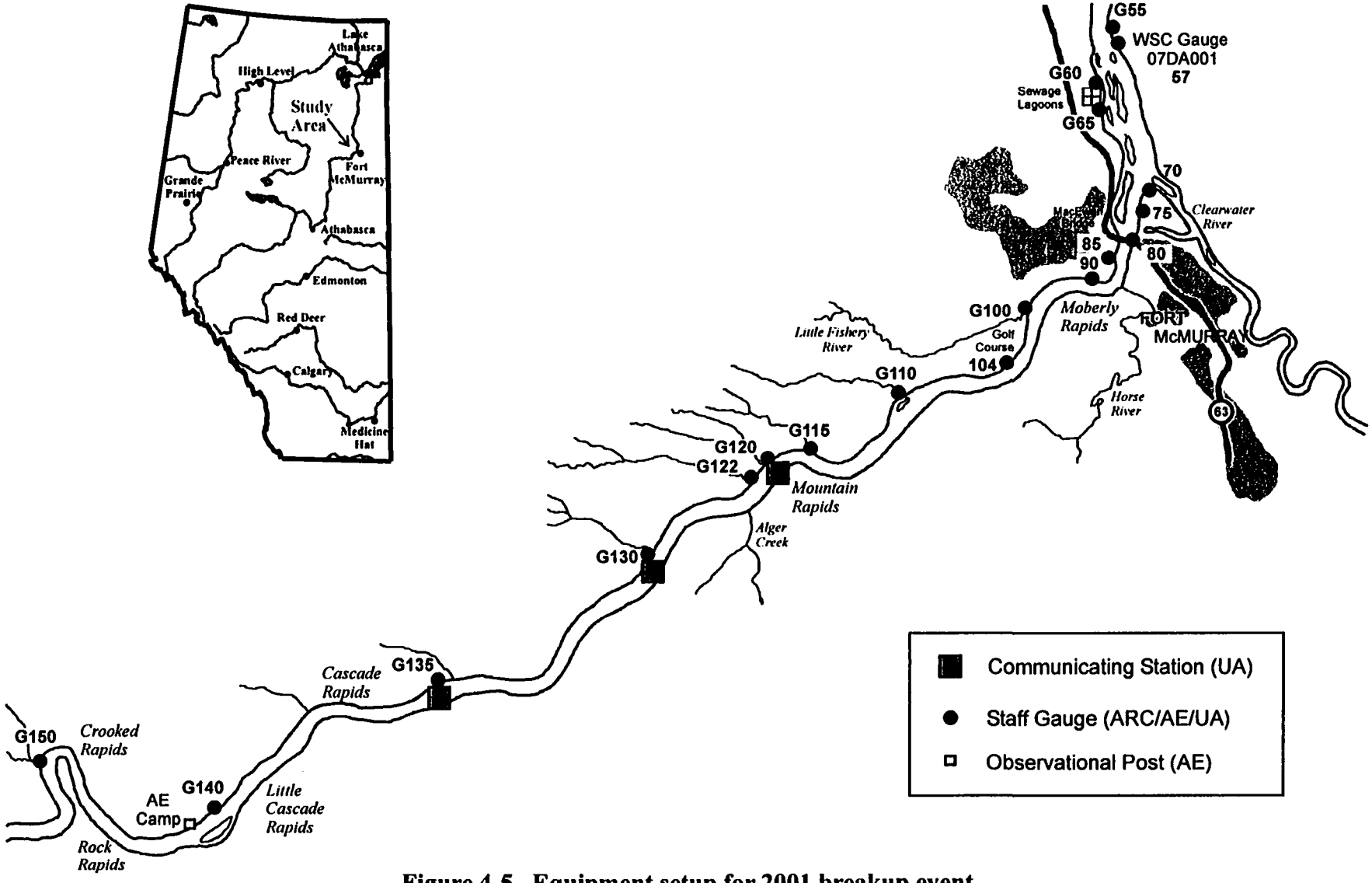

Figure 4-5. Equipment setup for 2001 breakup event.

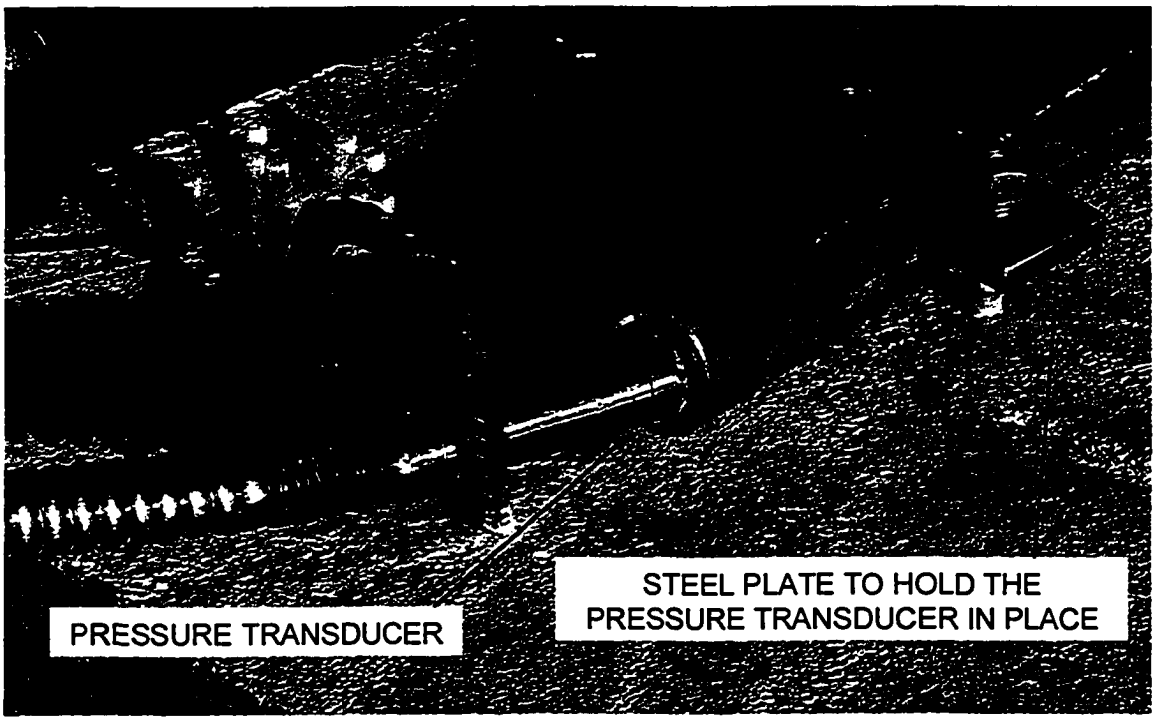

Figure 4-6. Pressure transducer encased in a steel pipe and bolted to a concrete pad.

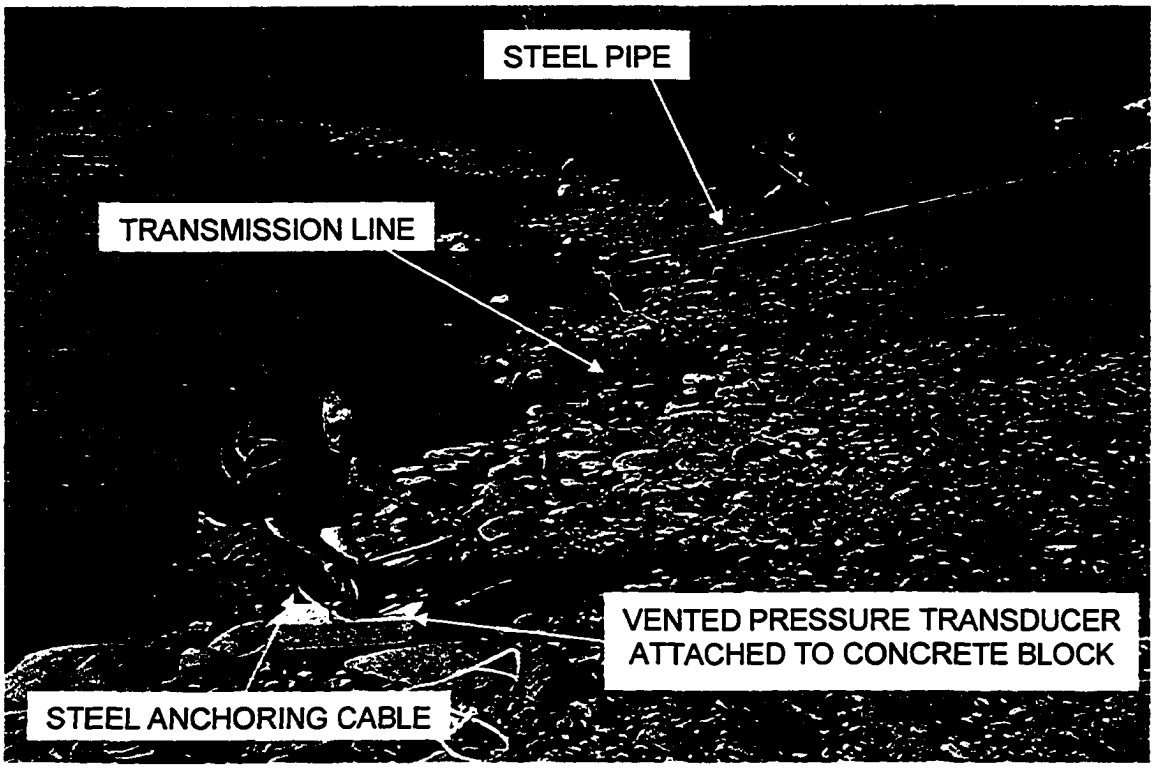

Figure 4-7. Setup of vented pressure transducer.

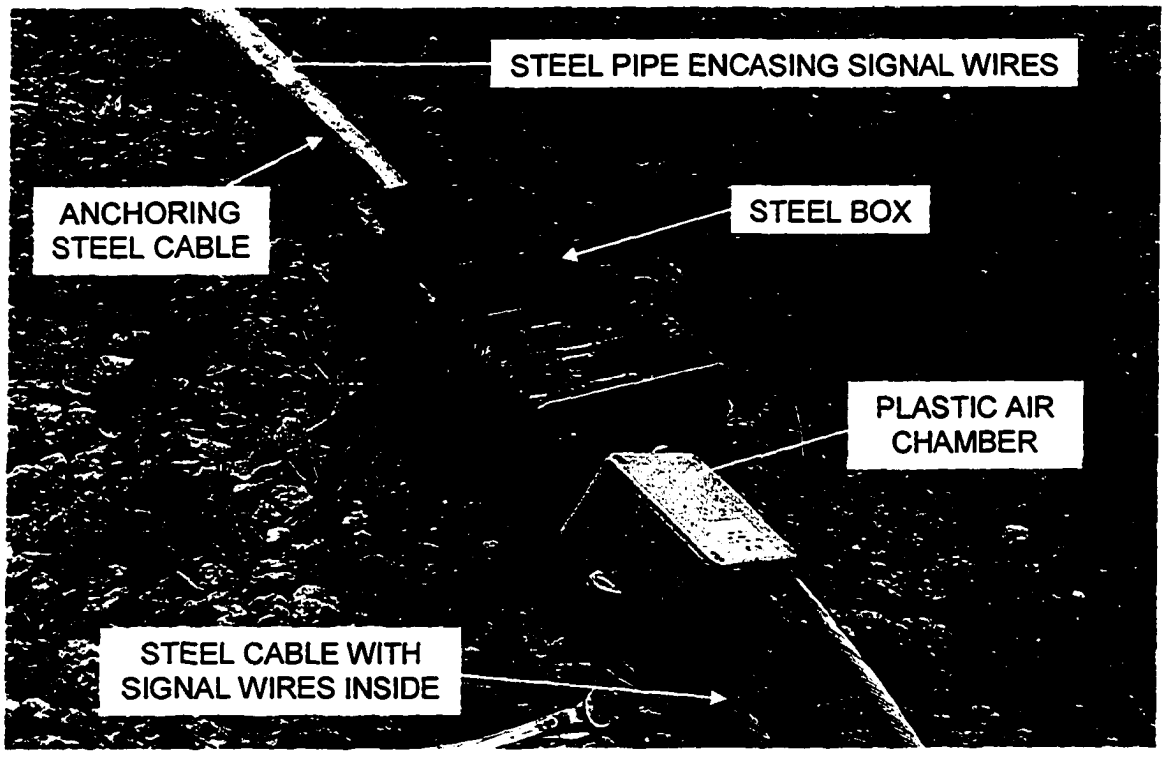

Figure 4-8. Vented end of pressure transducer encased in a steel box.

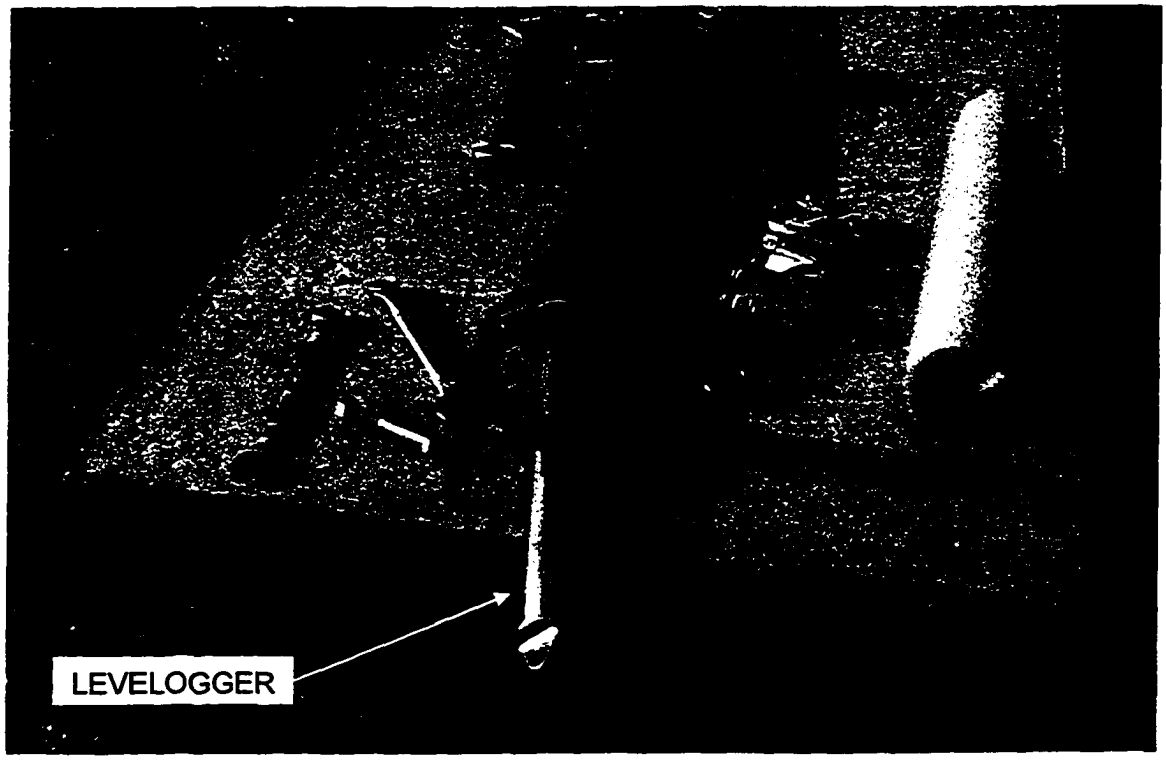

Figure 4-9. Levelogger encased in a steel pipe and bolted to a concrete pad.

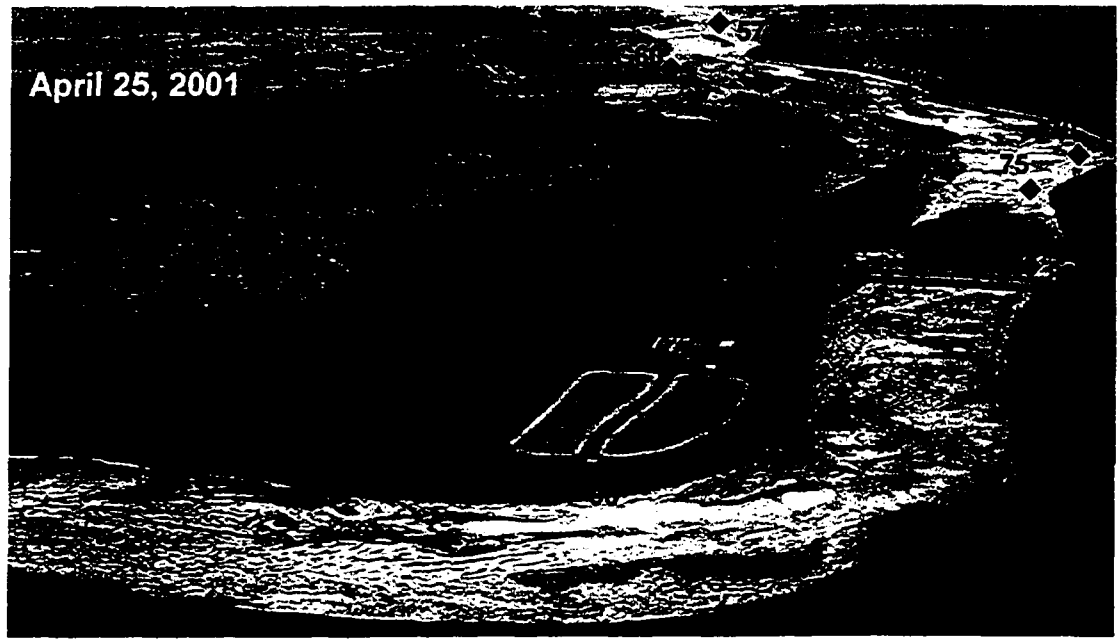

Figure 4-10. Aerial view showing a patchy and thin ice cover across the entire length of the reach upstream of the MacEwan Bridge and open water downstream of the MacEwan Bridge on April 25, 2001.

Figure 4-11. Aerial view showing a distinct open water section with ice consolidation on the left bank upstream of the MacEwan Bridge and on the right bank of the bend on April 26, 2001 after the jam release event.

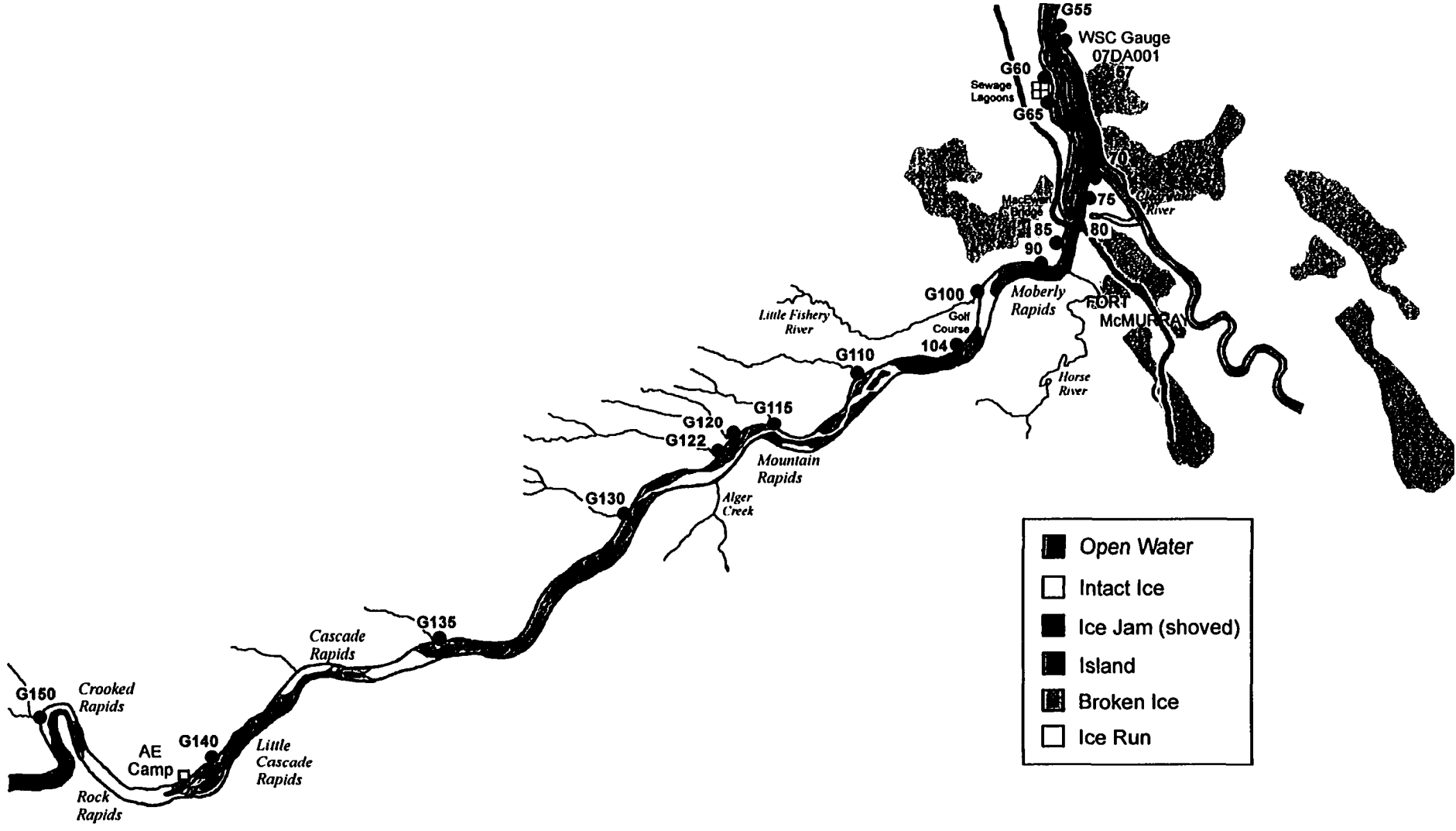

Figure 4-12. Ice conditions on April 25, 2001 prior to surge event.

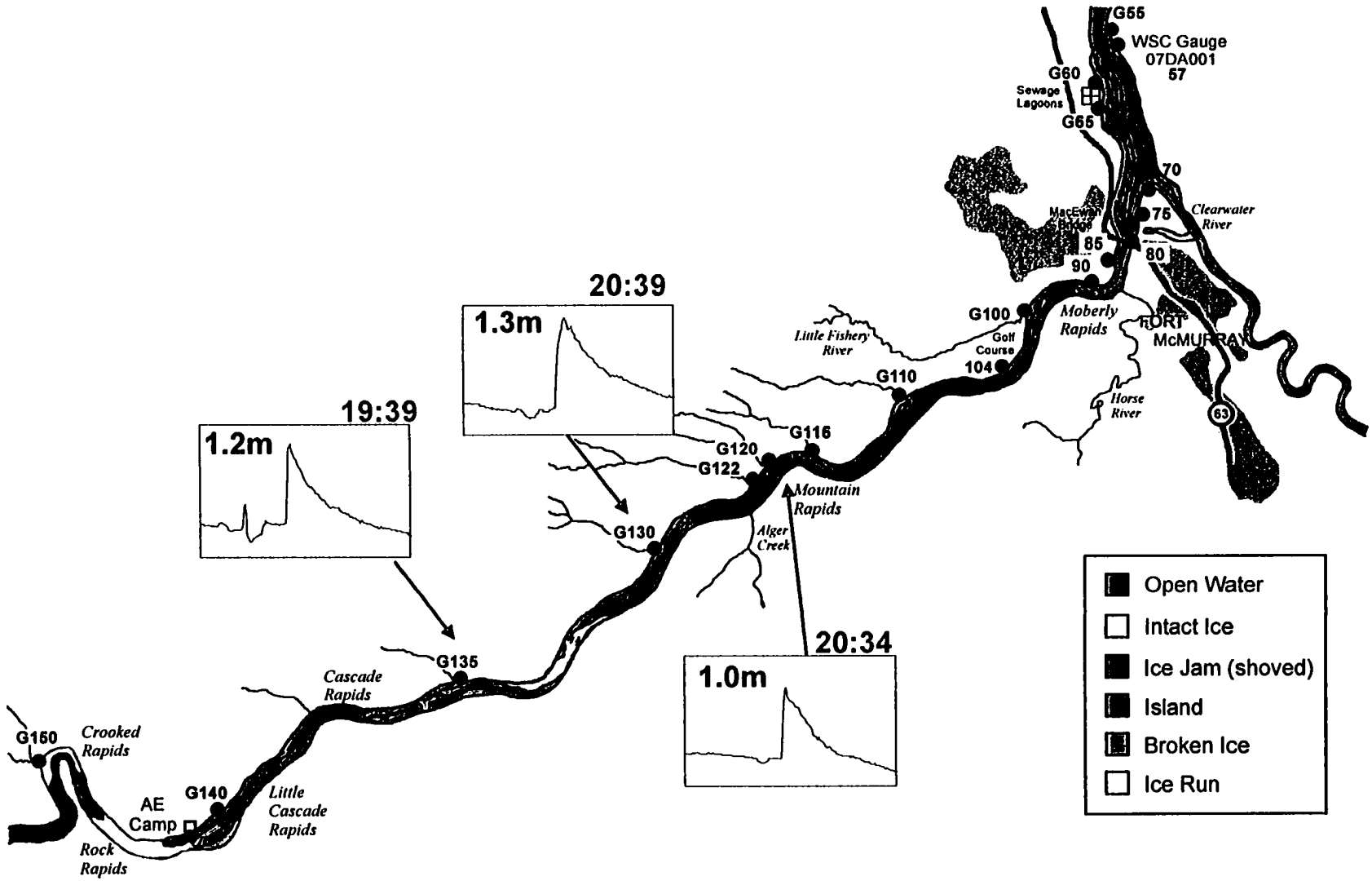

Figure 4-13. Ice conditions after surge event on April 26, 2001 and measured stage hydrographs during the surge event.

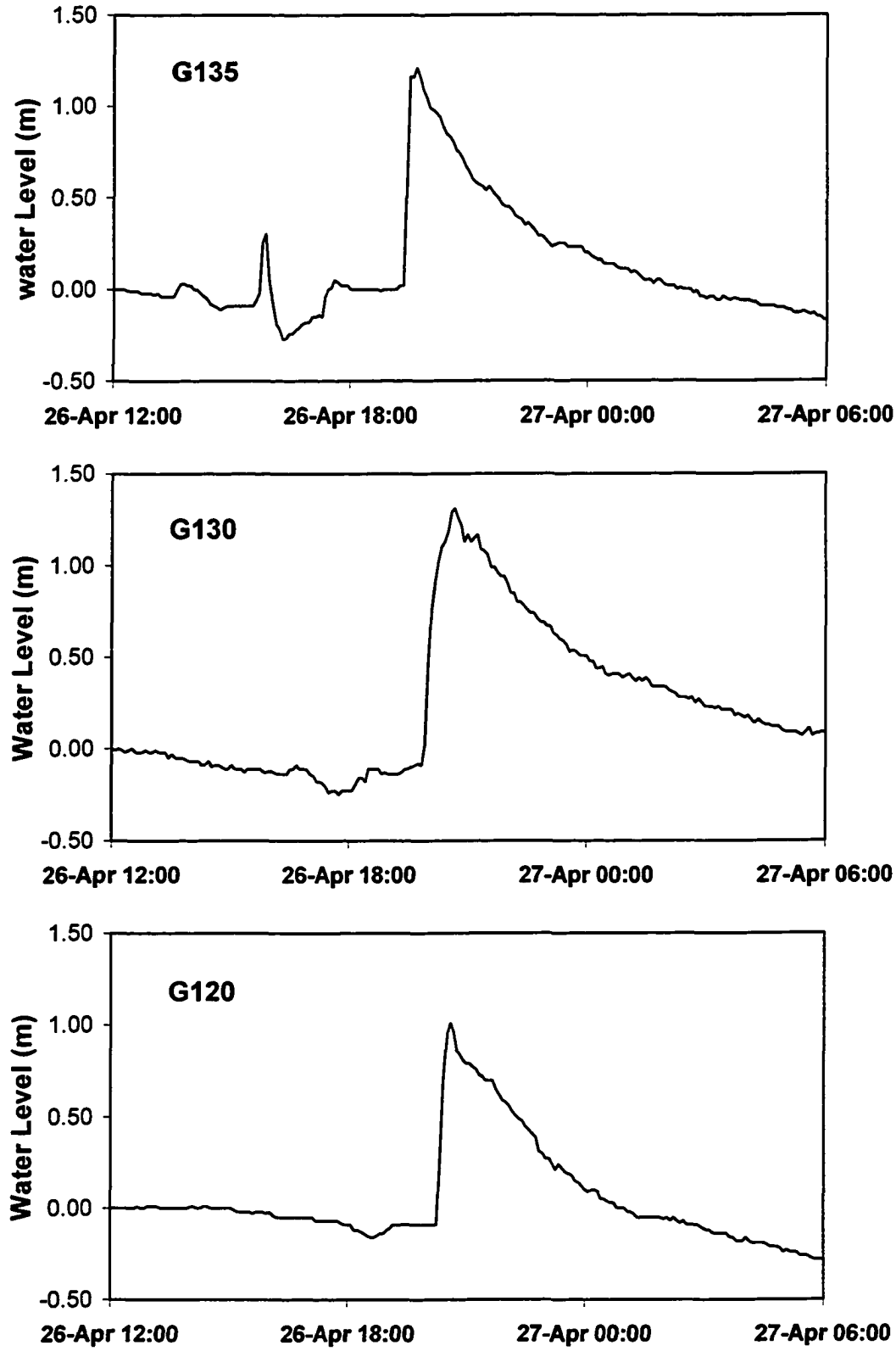

Figure 4-14. Water level hydrographs at remote stations G120, G130 and G135 during ice jam release event, 2001.

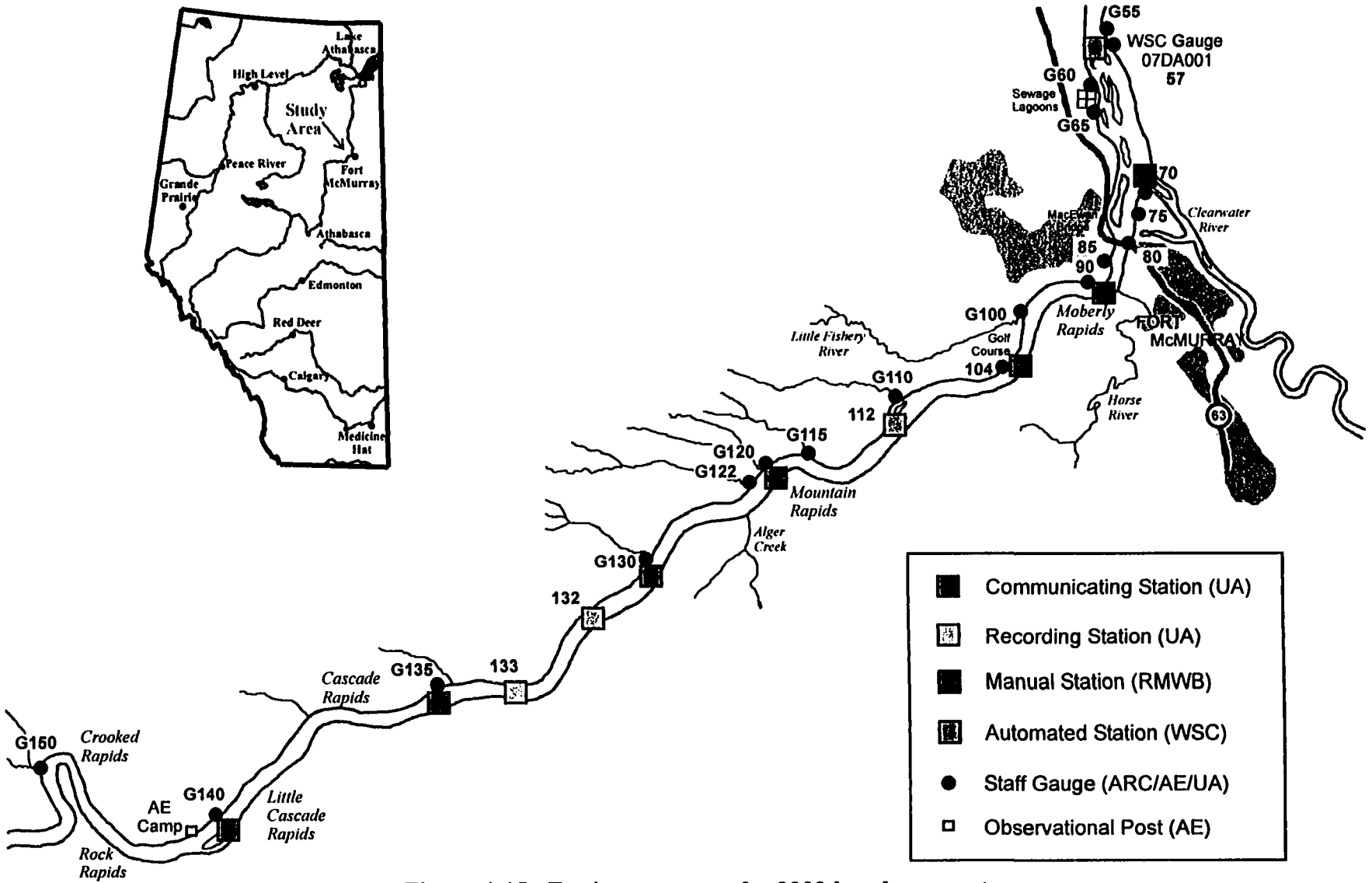

Figure 4-15. Equipment setup for 2002 breakup event.

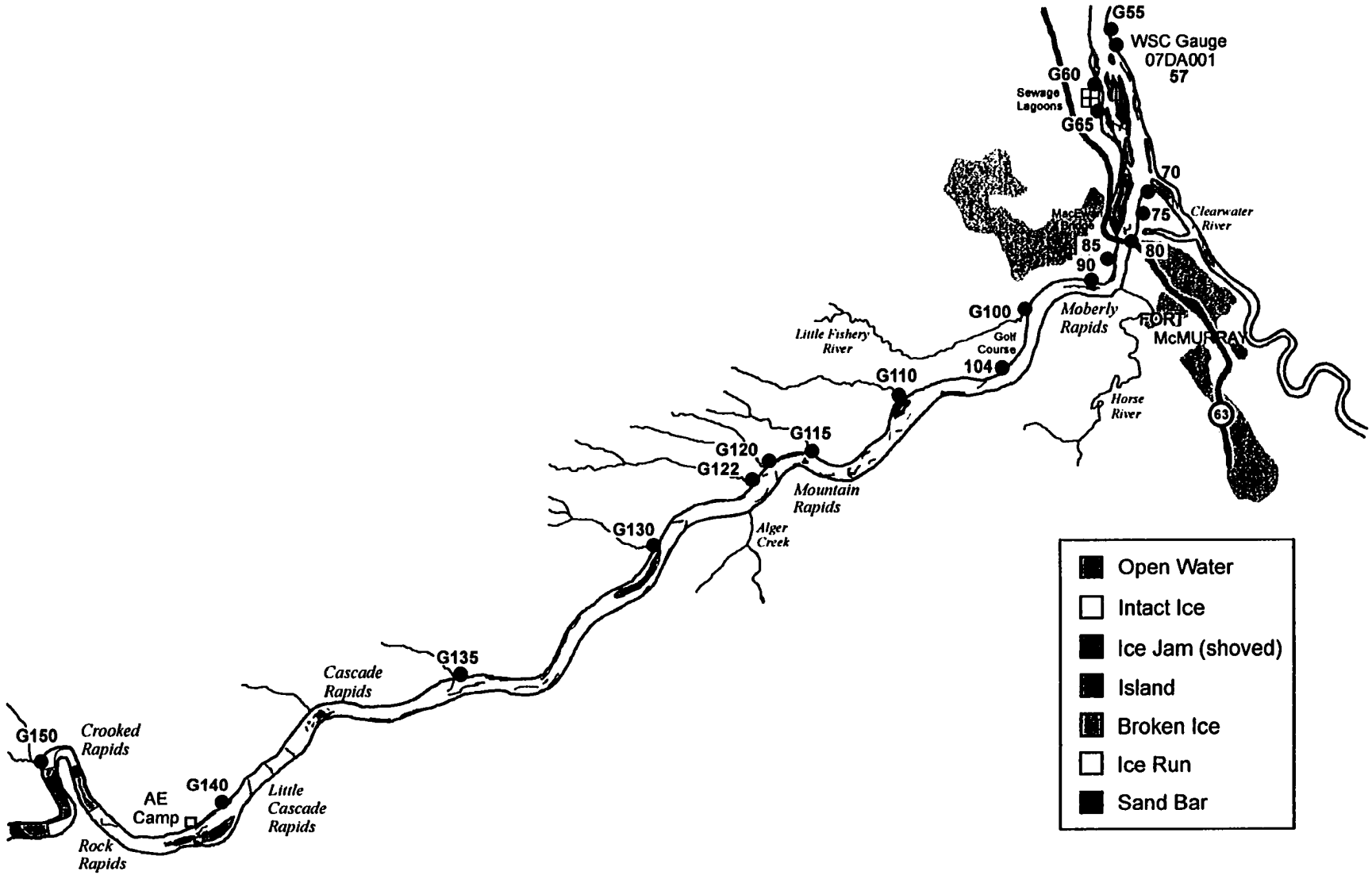

Figure 4-16. Ice conditions on April 26, 2002 prior to surge event.

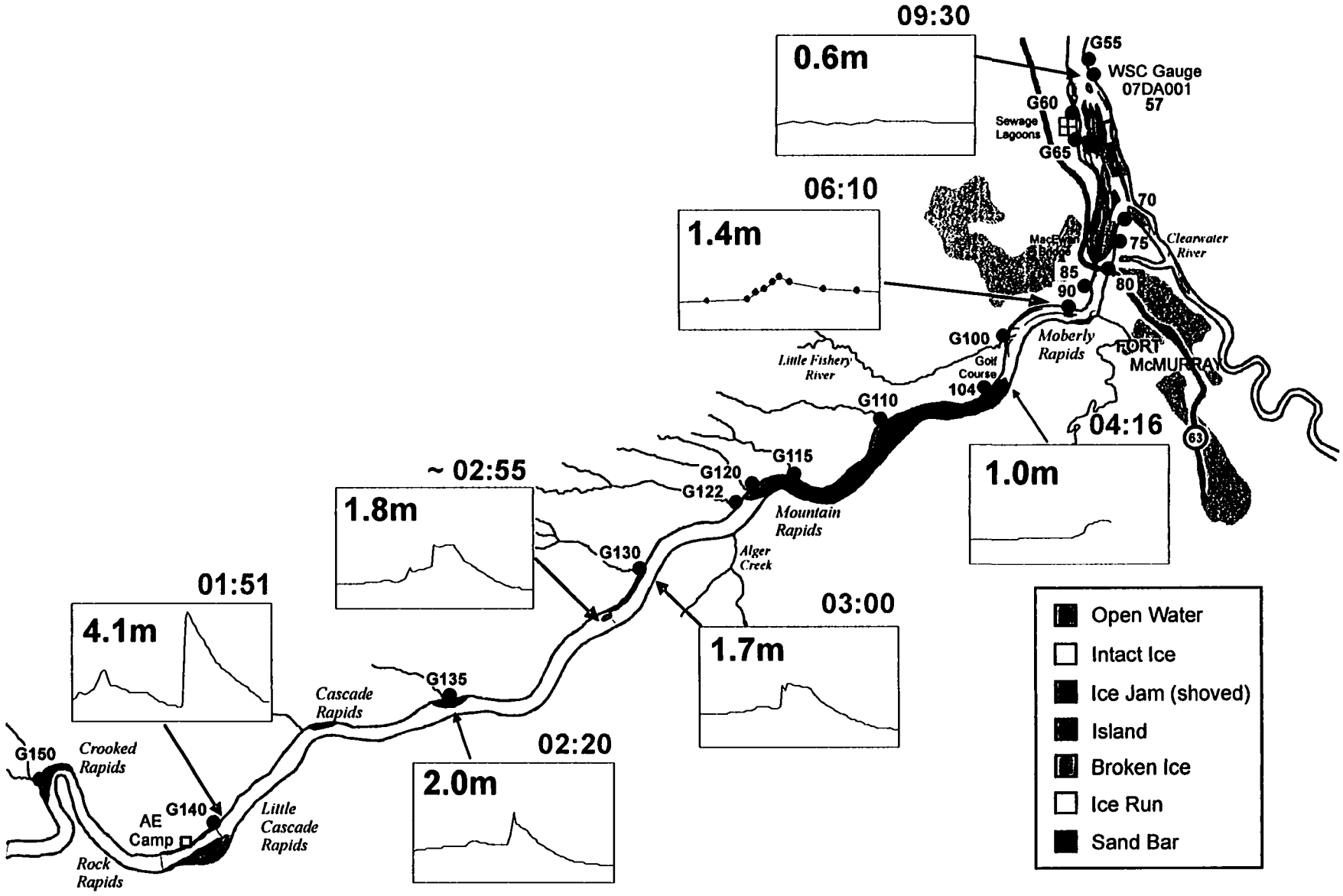

Figure 4-17. Ice jam configuration on April 27, 2002 and measured stage hydrographs during the surge event.

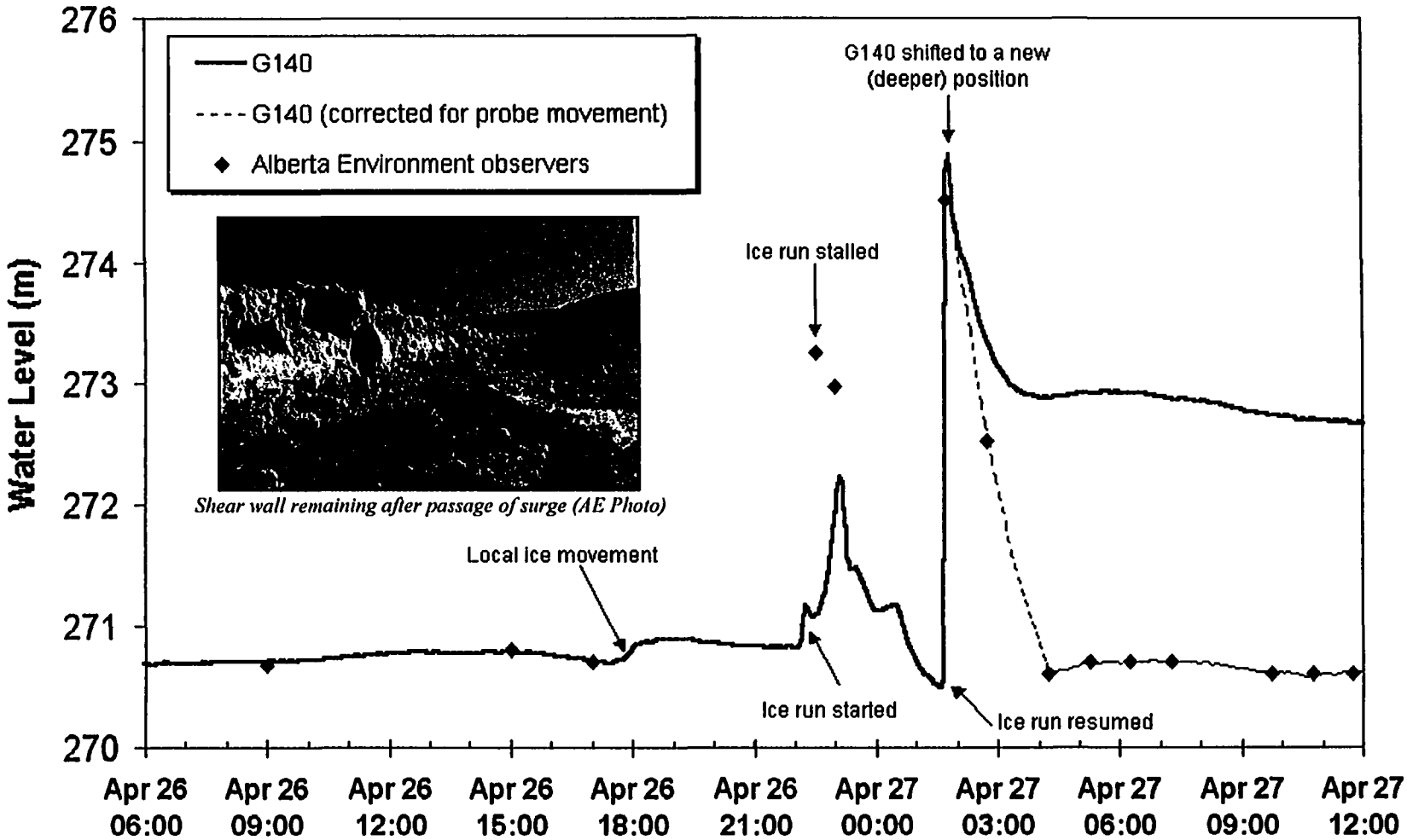

Figure 4-18. 4.4 m high surge measured at G140 during ice jam release surge event, 2002.
(comments are from the Alberta Environment Monitoring station records)

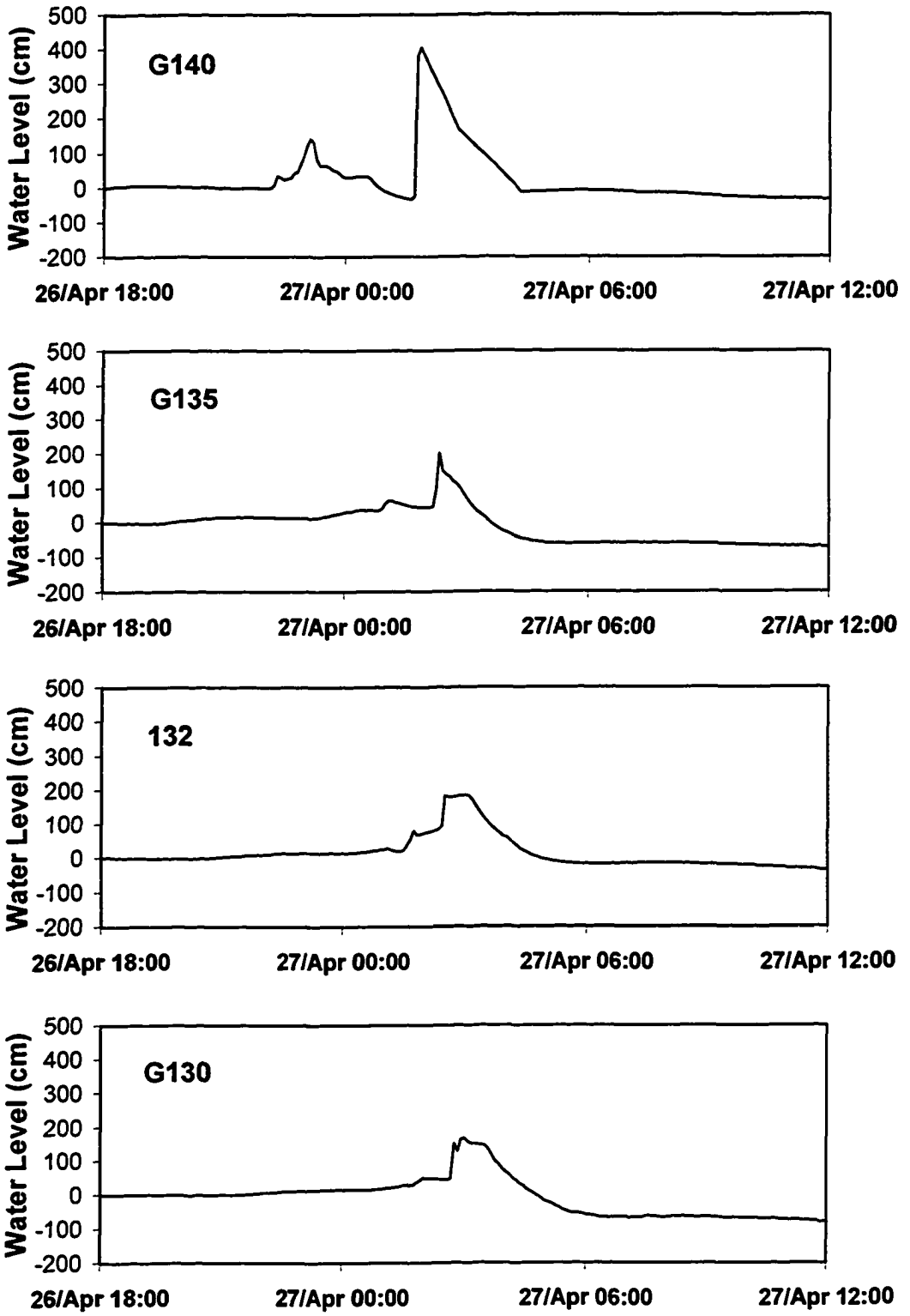

Figure 4-19. Water level hydrographs measured at remote stations G130 to G140 during ice jam release event, 2002.

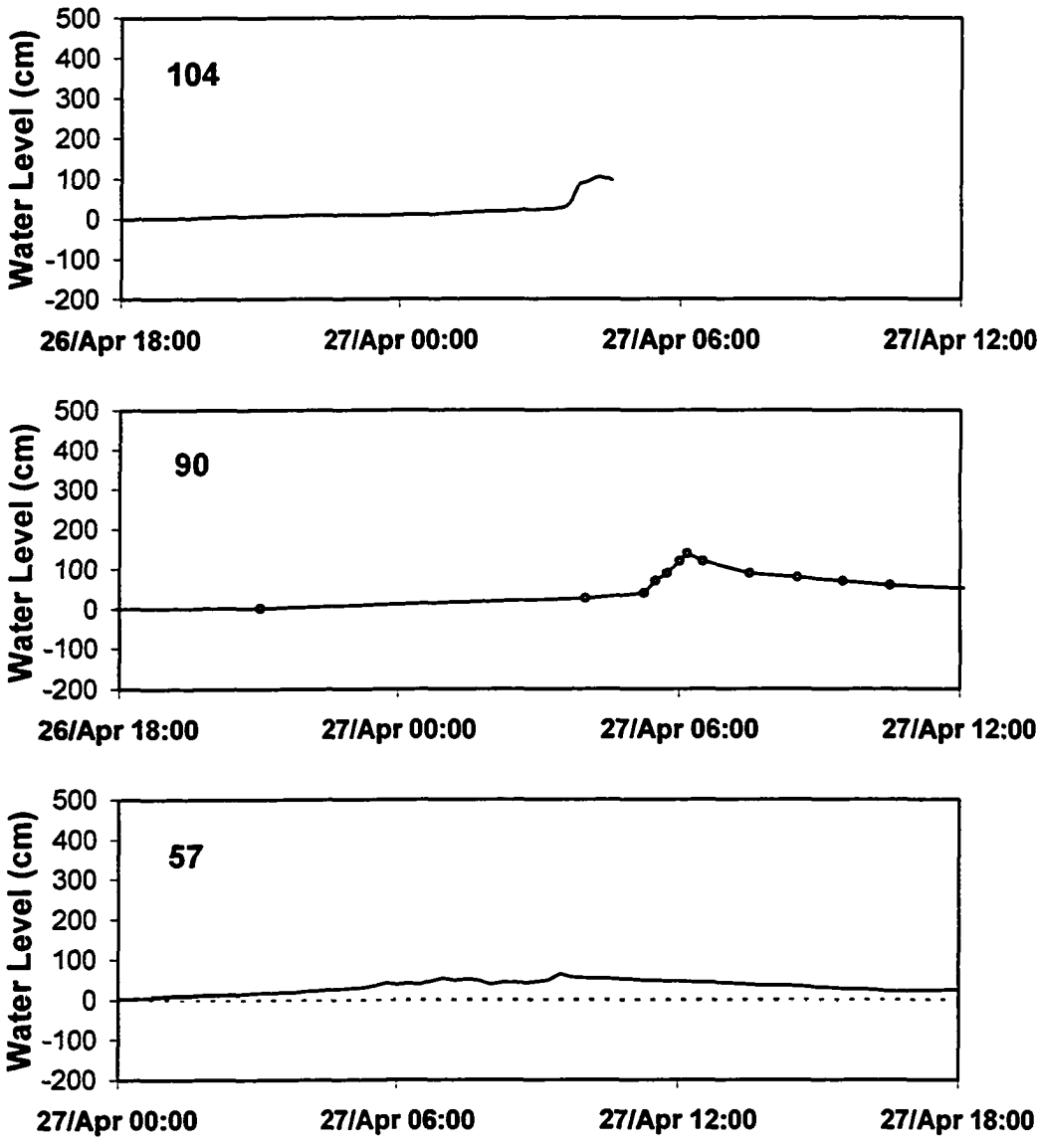

Figure 4-19 Continued. Water level hydrographs at remote station 57 to 104 during ice jam release event, 2002.

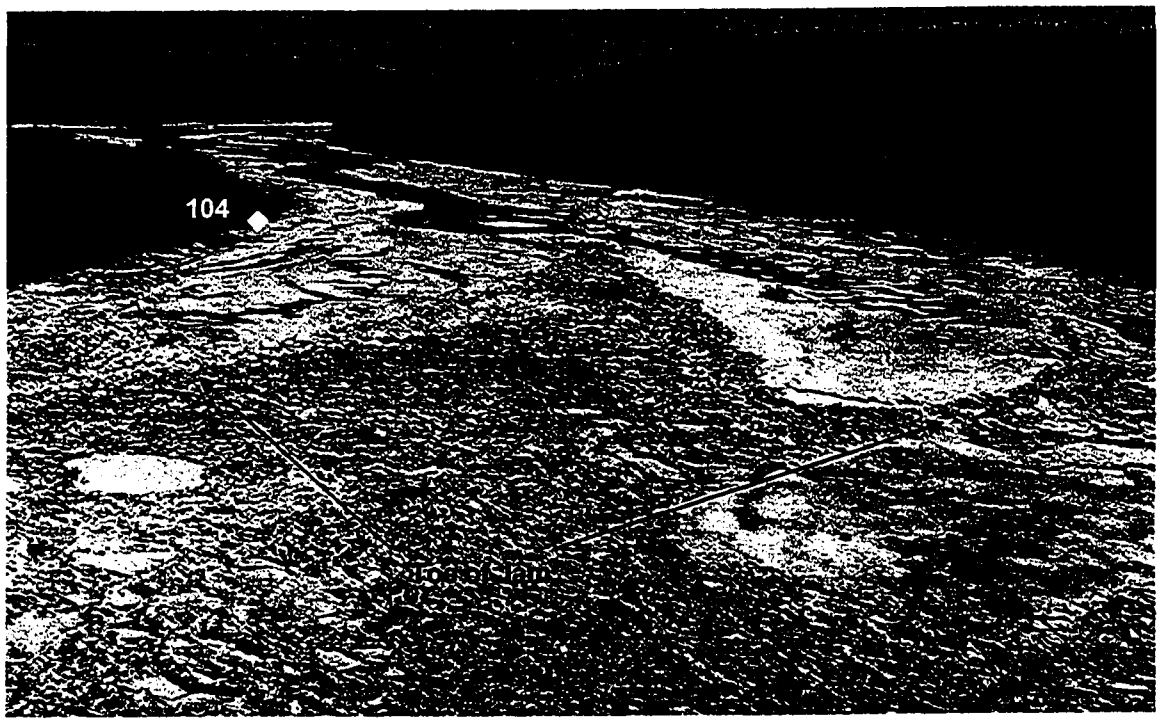

Figure 4-20. Photograph looking downstream towards station 104 showing the toe of the ice jam on April 27, 2002.

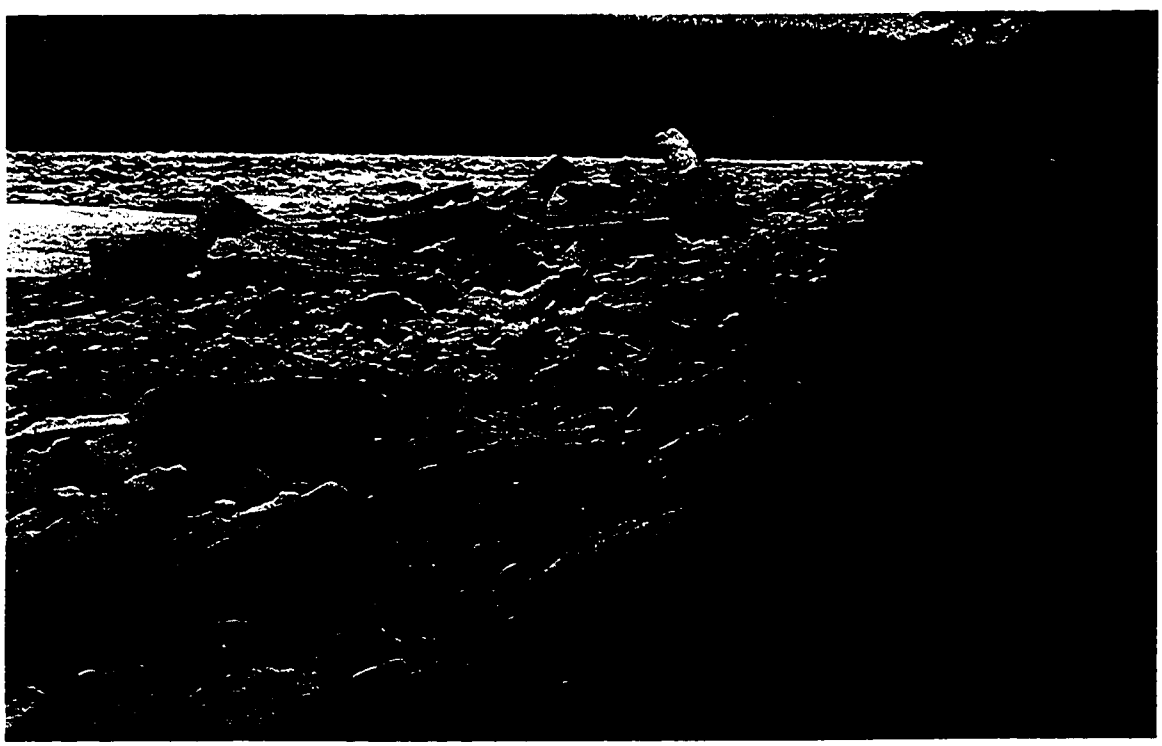

Figure 4-21. Photograph taken April 27, 2002 looking upstream showing ice floes at station 104 (toe of jam).

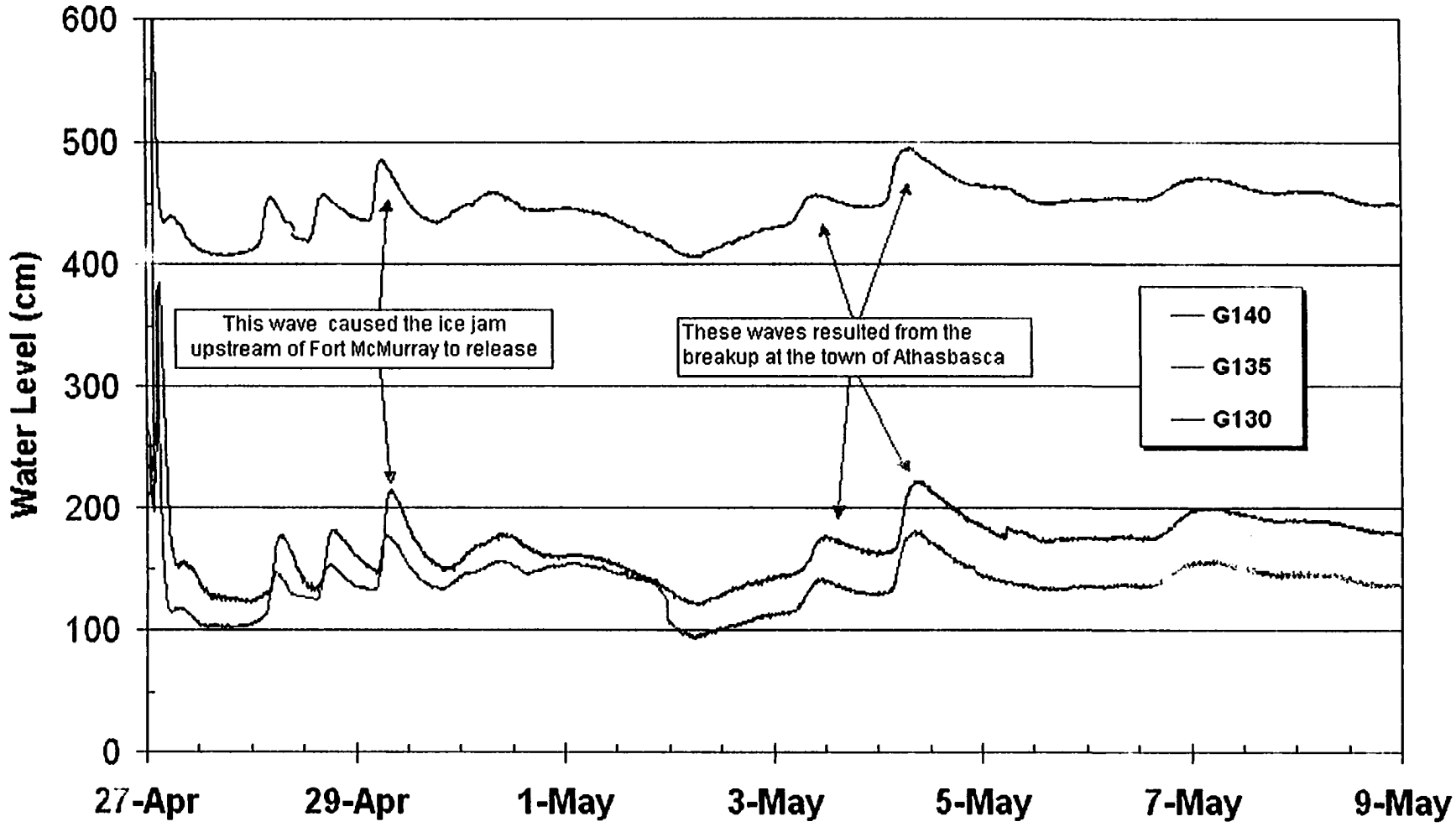

Figure 4-22. Smaller surges measured along the Athabasca River study reach after April 27, 2002.

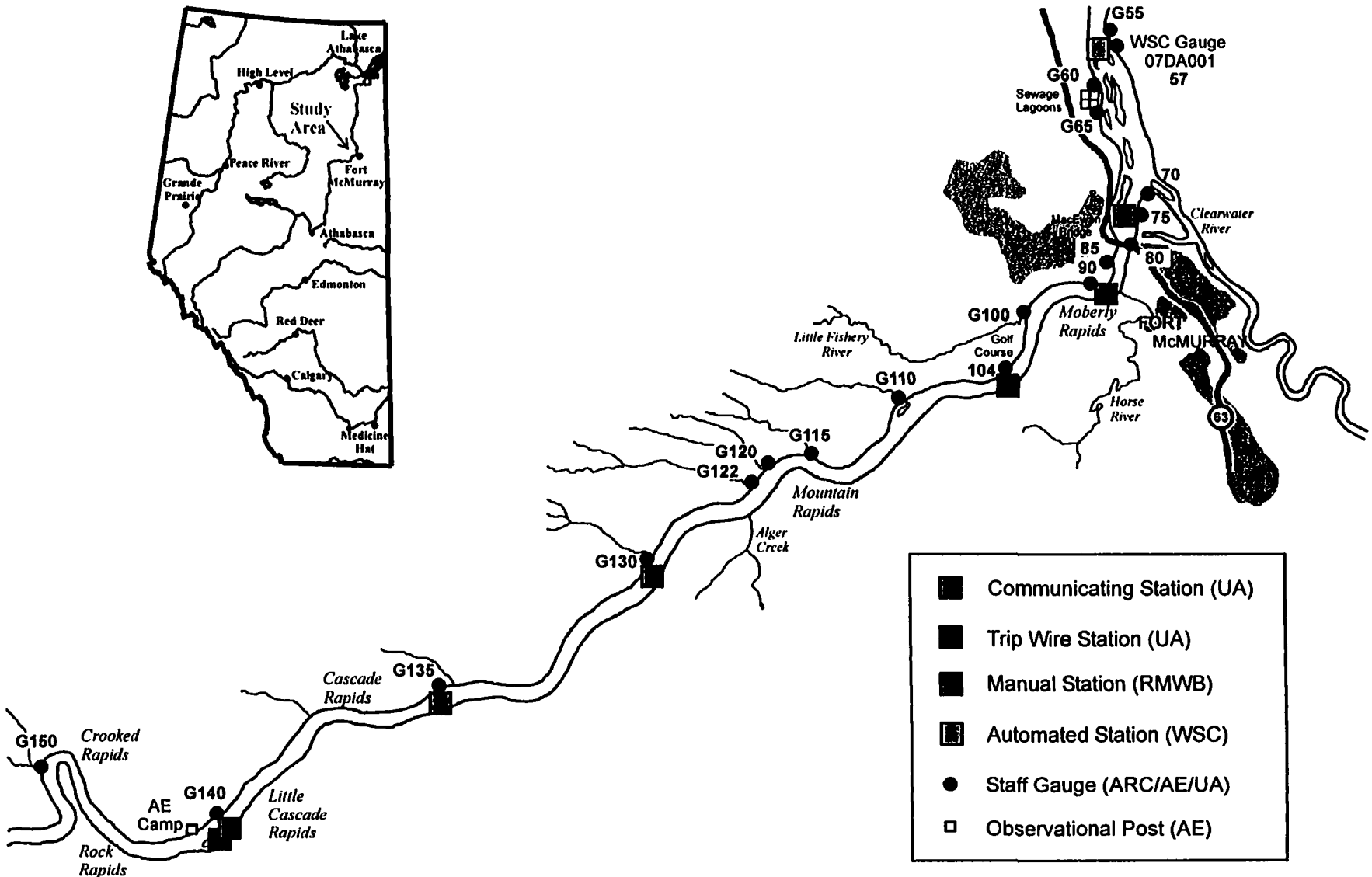

Figure 4-23. Equipment setup for 2003 breakup event.

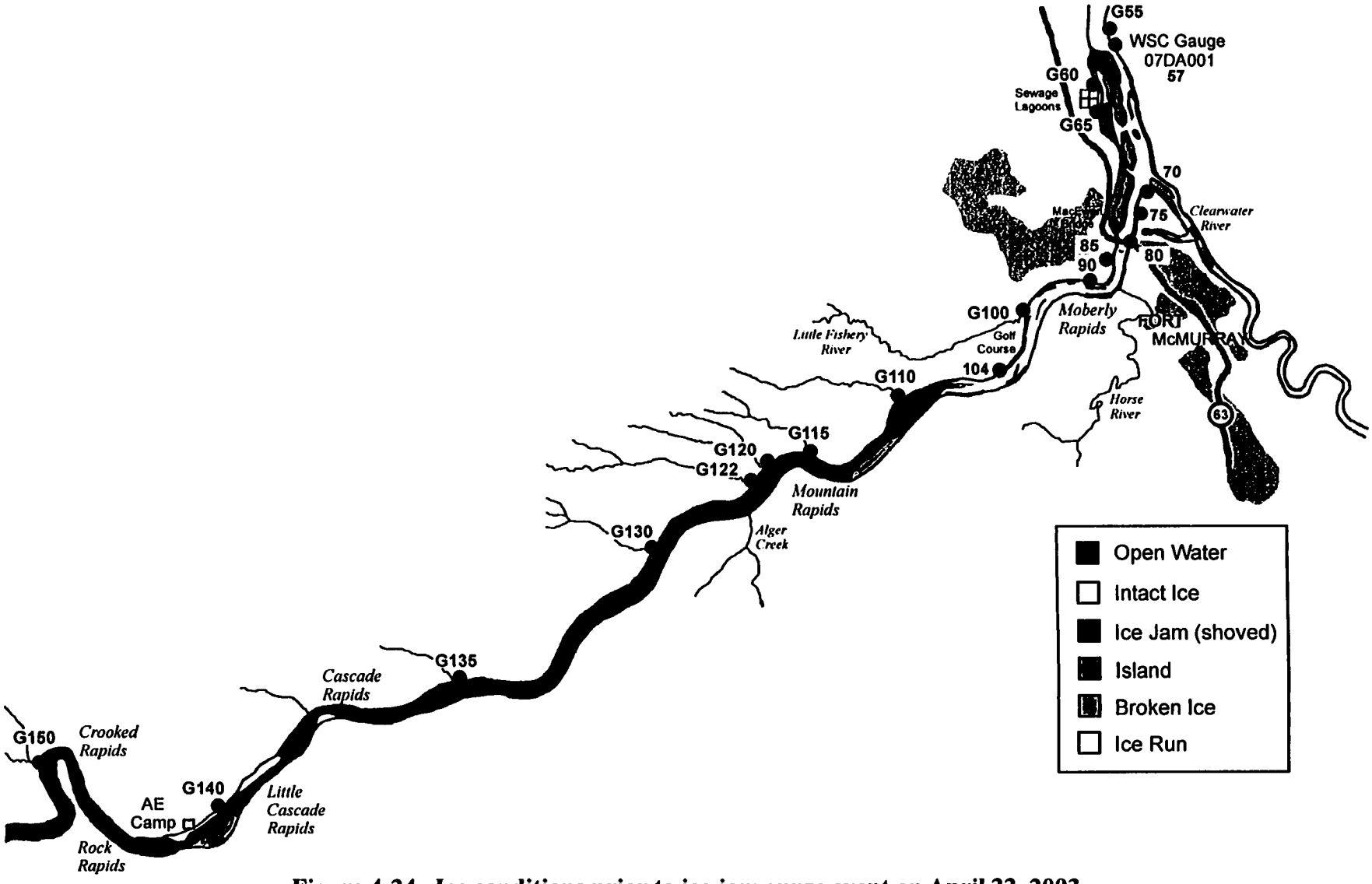

Figure 4-24. Ice conditions prior to ice jam surge event on April 22, 2003.

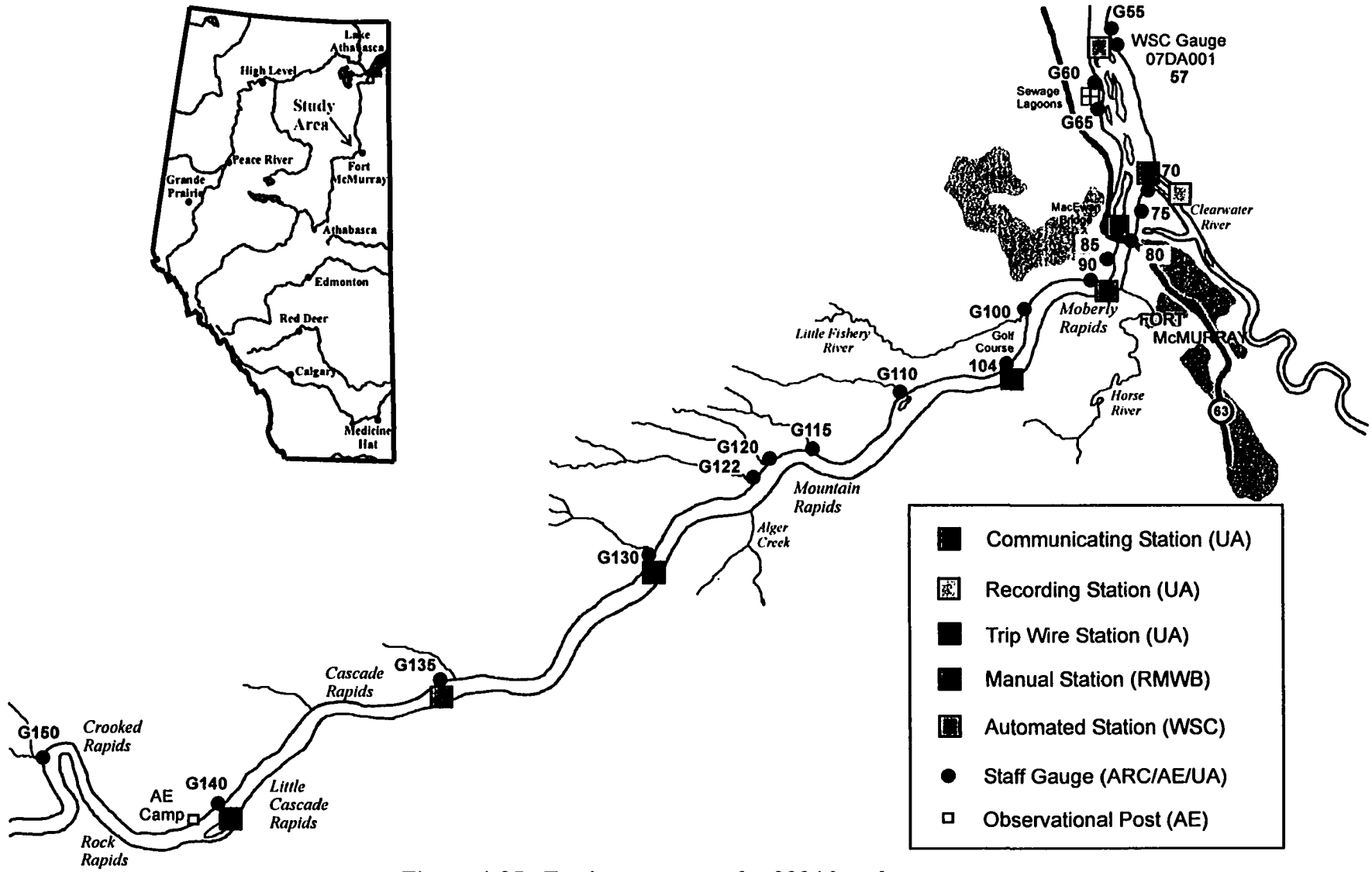

Figure 4-25. Equipment setup for 2004 breakup event.

5 ANALYSIS OF DOCUMENTED SURGE PROPAGATION EVENTS

The previous chapters have presented the data available to study surge waves resulting from ice jam release events on the Athabasca River. This data included historical documentation, as well as measured data from the remote monitoring network installed for this study. This chapter provides a comparison between these documented events with the objective of looking for patterns in the data. The most complete set of data, the 2002 event, is then used as a test case to determine if a dynamic open channel flow model is appropriate to model ice jam release events. The importance of an ice cover on surge propagation is also assessed. The modeling program River1-D is used for analysis.

5.1 COMPARISON BETWEEN ALL DOCUMENTED EVENTS

Surge propagation resulting from the release of ice jams have been documented by ARC between the years of 1977 and 1990. Measurements of both peak arrival time and magnitude were summarized for each of these years in Chapter 3 of this thesis. Additional documentation based on data collected by UA field teams has been presented for the breakup years of 2001, 2002 and 2003 in the previous chapter. This section provides a comparison of results between all documented years in terms of peak arrival time and magnitude attenuation.

As previously mentioned, ice jam release events along the Athabasca River can be classified as one of three types, specifically:

- Type 1: ice jams that release upstream of Crooked Rapids;
- Type 2: ice jams that release near Crooked Rapids at the upstream end of the study reach; and
- Type 3: ice jams that release near the middle of the study reach at Mountain Rapids.

This classification system was applied to the historical events between 1977 and 1990 as summarized in Table 3-1. According to the event descriptions for the more recent release events documented for this study: 2001 was a Type 1 event, 2002 was a Type 2 event, and 2003 was a Type 3 event. The following analysis will be separated into these three category types.

Jasek (2003), as discussed in Chapter 2, provides some interpretations of surge propagation behaviour as affected by an ice cover. These interpretations came from numerous field observations. When considering the distribution of ice traveling on an ice jam release surge, Jasek found that the majority of the ice concentration was on the rising limb of the stage hydrograph for about the first 'jam length', where a jam length was classified as the distance traveled by the surge divided by the length of the jam before the release. He found that after one jam length of travel, the majority of the ice concentration would fall towards the crest of the wave, and eventually, to the falling limb of the stage hydrograph. Therefore, one would expect the largest amount of resistance from the ice within the ice jam to be experienced in the first few kilometers of propagation.

Jasek (2003) also discussed the variability in surge celerity resulting from different ice concentrations present in the receiving channel downstream of the toe of the released ice jam, known as an impeded ice run. He found the largest amount of variation in surge celerity occurred when a sheet front was observed, as the speed of the breaking front seems to depend on the width of the river. Sections of a river with a narrower width tend to have less open water areas and thus the speed of the sheet front slows down. Less variation in surge celerity was observed for a rubble breaking front. Since breaking fronts typically tend to alternate between sheet fronts and rubble fronts, changes in propagation speed can be expected during these occurrences. These observations are considered in the following analysis.

It is important to note that for dynamic events of this type, some of the variability in surge speed can be attributed to measurement errors. This error can be particularly significant when determining celerity over a short distance, since even slight errors in

time can translate in to large errors in surge celerity in this case. This is most apparent when considering surge celerities between stations within the area of Fort McMurray, as they are in such close proximity to each other. Consequently, the trend in celerity over a reach should be considered as well as the individual values. Conversely, when the points used to determine surge celerity are quite far apart, the resulting value is clearly an average that may be considerably lower than the actual values just downstream of the release location, especially if the ice run stalled in the intermediate reach. Another source of variability is the possible inconsistency in defining surge arrival at a location. Specifically, it is unknown if historical observations were documenting the arrival of the leading edge of an ice run, the breaking front of an ice cover, or the peak water level attained. For those events measured as part of this study (2001 to 2003), surge celerity refers to the rate of travel of the measured peak water level.

5.1.1 Type 1 Ice Jam Release Events

Breakup in 1982, 1984, 1985, 1988, 1990 and 2001 involved ice jam release events that initiated upstream of Crooked Rapids. The leading edge of the resulting ice run in 1982 was observed at Long Rapids, approximately 12 km upstream of Crooked Rapids. In 1984, the leading edge of an ice run was observed at Middle Rapids, 17 km upstream of Crooked Rapids. Both of these events had their trailing edge at Grande Rapids with ice run lengths of 80 km and 75 km, respectively. In 1985, a large ice run approximately 65 km in length caused a 3 km long ice jam to release. This small ice jam had its toe at Long Rapids. Originating about 92.2 km upstream of Crooked Rapids near Grande Rapids, the 1988 ice run propagated through the study reach before forming a jam downstream of Fort McMurray. The leading edge of the 1990 event was unknown, but the trailing edge was also at Grande Rapids. The ice jam that released in 2001 was not observed prior to release. However, documentation from aerial observations suggest that the ice jam released upstream of Crooked Rapids.

The surge wave celerities, based on arrival times as summarized in previous chapters, are shown in Figure 5-1 for the years in which a Type 1 event occurred. Figure

5-2 shows the corresponding wave peak magnitudes, which are unavailable for 1982 and 1984. In both figures the river profile is shown at the top, to facilitate interpretation. Overall, as would be expected, a decrease in celerity can be seen as the surges propagate downstream. However it is interesting to note that, at some locations, surge celerity actually increases in the downstream direction. This implies that the ice run stalled, possibly re-jamming at least briefly (Henderson and Gerard, 1981). For example, in 1982 the celerity increased from 0.14 to 2.07 m/s within the area of Fort McMurray. It was reported that temporary jamming was observed at numerous locations throughout breakup in 1982, possibly explaining this increase in surge wave celerity.

Another likely example of an ice run stalling temporarily occurred in 1990. In fact it appears to have happened at least three times, despite the fact that this ice run was documented as proceeding past Fort McMurray without stopping. As seen in Figures 5-1 and 5-2 (and Table 3-12), between Crooked Rapids and the Little Fisheries River (in the vicinity of Mountain Rapids just upstream of station 90), the surge celerity increased from 2.9 to 3.8 m/s and the peak magnitude increased by 2.25 m. The most likely explanation for this is that the ice run arrested somewhere between these two observation points, temporarily re-jamming, before re-releasing along this length of the study reach. Consequently this event should be classified as also being a Type 3 event.

Downstream of the Little Fisheries River the surge magnitude then decreased considerably over the next 5.5 km, as would be expected just downstream of an ice jam release location. However, the wave celerity increased substantially between the Water Intake and the MacEwan Bridge (from 1.4 to 5.5 m/s). This may be an anomalous value resulting from a time synchronization error, as these two stations are quite close together (about 1.5 km apart).

The surge celerity increased again, this time from 3.2 to 5.0 m/s, within the reach downstream of the Clearwater River confluence (from station 57 to G35, over a distance of 10 km). This was not a single anomalous value; a celerity of 4.76 m/s was documented over the next 14 km. The river slope flattens out noticeably in this reach downstream of

the Clearwater River confluence, so channel slope is unlikely as an explanation, but the river does exhibit an anabranching planform pattern with numerous bars and islands. Consequently, the most feasible explanation for the increase in surge celerity in this reach is that the ice run congested briefly among the island in this reach and then re-released almost immediately. Further downstream, as seen in Figure 4-2 and Table 3-12, the wave peak magnitude increased, suggesting the occurrence of a third, less significant, stall of the ice run.

A very large increase in surge wave celerity from 2.08 m/s (G135 to G130) to 14.33 m/s (G130 to G120) was documented by the remote monitoring network in 2001 (Levelogger data). This latter value is likely erroneous given its extreme magnitude, as it is unlikely that such a large surge wave celerity would result from a temporary jamming and re-release scenario. More likely the extraordinary wave celerity reflects, at least in part, an error in synchronizing the time between the Leveloggers at these two stations (as they are relatively close to each other). The magnitudes measured in 2001 also suggest a temporary arrest of the ice run resulting in re-jamming, as the magnitude increased slightly between stations G135 and G130. This may be evidence of a typical stalling point, which implies it is related to channel geometry rather than a variation in the ice cover conditions. One possibility is the bend between these two stations tends to slow down, or even stall, the progression of ice runs. The large surge velocity downstream of G130, although likely imprecise, supports this interpretation. At the least, the reach between G135 and G130 is worth observing during ice runs in future years.

5.1.2 Type 2 Ice Jam Release Events

Breakup events in 1977, 1978, 1987 and 2002 are believed to have involved the release of ice jams initially poised within ±10 km of Crooked Rapids, at the upstream end of the study reach. The surge wave celerities, based on arrival times or celerities documented in the field, as summarized in previous chapters, are shown in Figure 5-3 for the years in which a Type 2 event occurred. Figure 5-4 shows the available corresponding wave peak magnitudes.

Limited data is available for the 1977 release but, as discussed in Chapter 3, all evidence points to the strong likelihood that this ice run arrested at Mountain Rapids before re-releasing as a Type 3 event. No data is available for the Type 3 component of the 1977 ice run, and this is especially unfortunate since this breakup resulted in the most severe flood event at Fort McMurray in the past 27 years.

Ice jam lengths of 4, 7, and 17 km were involved in 1978, 1987 and 2002, respectively, as described in the previous chapters. As shown in Figure 5-3, an overall decreasing trend in surge celerity in the downstream direction is again evident. Although it appears that a wider range of values are seen across the study reach as compared to Type 1 events, it is important to remember that limited data was available in most cases. When surge speeds are calculated using widely spaced locations, the resulting value only represents an average wave celerity (i.e., they underestimated the surge celerity just downstream of the release point).

Some accelerations in surge celerity in the downstream direction again suggest temporary stalling of some ice runs. For example, as discussed in Chapter 3, in 1978 the ice run was documented to have stalled and re-jammed briefly at Cascade Rapids, a relatively tight bend in the river just downstream of station G140. This resulted in a localized lower average surge celerity of 0.3 m/s. Wave celerities of 3 to 6 m/s were reported downstream of Cascade Rapids after this new accumulation released, with the overall average surge celerity between Cascade Rapids and Fort McMurray documented at 3.2 m/s. An average celerity of about 2.8 m/s was observed in the final 3 km of travel, upstream of the MacEwan Bridge. The ice run stalled just upstream of the MacEwan Bridge (station 80) creating a new 22 km long ice jam with its toe at the bridge. A 0.5 m high wave was measured at the MacEwan Bridge, which was unfortunately the only wave peak magnitude documented that year.

For the 1987 event, the surge celerity of 1.11 m/s documented in the upper reach appears low, but it should be remembered that there are no observation points within this 30 km reach, and therefore it is not known if the run stalled at any point downstream of

Cascade Rapids. Clearly the ice run did stall in the vicinity of Mountain Rapids, as evidenced by the local reduction in surge speed and corresponding increase in peak magnitude.

Breakup 2002 is the year the UA remote monitoring network measured a 4.4 m high surge passing G140. The event propagated down the channel, arresting at Mountain Rapids to form a new, 8 km long, ice jam with its toe at station 104. Measurements show that a wave escaped from the newly formed ice jam and continued to propagate underneath of an intact ice cover (similar to the 1987 event). Figure 5-3 shows a definite change in overall surge propagation celerity occurring right at station 104. This much smaller wave celerity downstream of station 104 is understandable since a lot of the surge's mass and momentum would have been lost to the formation of the new ice jam.

The trend seen in the magnitude of the surge wave peak for 2002 involved a significant decrease in magnitude within the first 10 km of propagation, but a slower and more consistent rate of decrease for the remainder of the reach. It is believed that this drastic decrease in magnitude in the initial phase of travel was due to resistance effects of ice. As discussed by Jasek (2003), when an ice jam first releases ice floes will be initially concentrated ahead of the peak of the surge wave, potentially creating a large resistance to the flow. As the wave propagates downstream, bank resistance slows the ice pack, such that the ice floes start to lag behind the peak, riding on the falling limb of the wave. As a consequence, less resistance to the wave peak propagation would be expected as it progresses downstream. The more consistent rate of attenuation from station G135 to 57 was expected since the resistance to the surge comes from the channel geometry and bed resistance characteristics as well as any ice present prior to the commencement of the release event. The ice cover before this event occurred was fairly deteriorated along the study reach, and would provide little resistance to the surge as compared to the resistance offered by the rough ice accumulation at the instant of the release.

It is interesting to note the increase in peak magnitude between stations 104 and 90 for breakup in 2002. This section of the reach is immediately downstream of the toe

of the newly formed jam and the wave was propagating underneath an intact ice cover. This increase in magnitude is possibly due to the geometry in this section of the reach (including any staging up that might occur due to the velocity reduction under the intact ice cover) or it might be a result of error in the manual measurements taken at station 90. Analysis of this portion of the reach is studied further in following sections.

5.1.3 Type 3 Ice Jam Release Events

Another common location for ice jams to form is within the vicinity of Mountain Rapids. These Type 3 ice jam release events were documented in 1977, 1979, 1984, 1985, 2002 and 2003. The available surge wave celerities, based on arrival times or speed documented in the field, as summarized in previous chapters, are shown in Figure 5-5 for the years in which a Type 3 event occurred. Figure 5-6 shows the available corresponding wave peak magnitudes. Unfortunately, the small Type 3 event in 2002 was not measured.

The events for 1979, 1984 and 2003 had ice jam toe locations downstream of Mountain Rapids at 4 km, 11 km and 2.5 km, respectively. The 1985 event was the only one to have the toe of the ice jam right at Mountain Rapids. Observations of the 1977 event found wave magnitudes at the MacEwan Bridge to be more than half the height of the shear walls upstream of Little Cascade Rapids, suggesting that an ice jam reformed in the vicinity of Mountain Rapids. The details of each of these events were described in previous chapters. Figure 5-5 shows that very similar average surge wave celerities of approximately 2 m/s were experienced for each year. A fairly high value of 5 m/s was observed just downstream of the toe in 1984, but this decreased to about 1 m/s by the time the surge reached the MacEwan Bridge. The toe of the 1984 ice jam was documented to have the furthest downstream location. Therefore, it is reasonable to expect higher values of surge celerity upon arrival at the MacEwan Bridge due to the shorter travel distance. The large decrease in surge celerity experienced after the MacEwan Bridge could be attributed to congestion among the bridge piers and/or around the islands downstream.

The data from the 1979 event was used by Henderson and Gerard (1981) to assess the applicability of the classic dam break scenario to an ice jam release situation. Their theoretical calculations predicted a surge wave celerity of approximately 11 m/s to occur at the MacEwan Bridge. This theoretical value is much larger than the value observed in the field of about 3 or 4 m/s (Doyle and Andres, 1979). Henderson and Gerard attributed this discrepancy in surge celerity to ice effects slowing the propagation of the surge wave.

As shown in Figure 5-6, the historical events of 1979, 1984, 1985 and 1990 all show peak magnitudes between 2 and 3 m. However, the 2003 event shows peak magnitudes between 3 and 4 m in the same area. Accompanying the peak magnitude values for 2003 are measured high water marks. These high water marks were taken shortly after the event and show fairly good agreement with the peak magnitudes observed. The peak magnitude at station 57 (WSC gauge) appears low in 2003 compared to 1984, but the WSC record shows a drop in water level of over 2 m on the evening of April 22, 2003, after which the water level remains constant throughout the following day.

As discussed earlier, little information is available for 1977, other than it is suspected that the documented ice run must have arrested just upstream of Fort Murray and then re-released to have produced the surge celerity of 5 to 6 m/s and peak magnitude of 5 m observed at the MacEwan Bridge. Given the magnitude of the 2003 wave of about 3 m, and the moderate size of that Mountain Rapids ice jam, it is not difficult to conceive that the 1977 event was caused by a Type 3 release from a large jam poised at Mountain Rapids.

5.1.4 Summary

Upon comparing the surge wave celerity of each of the years documented, no obvious trend can be seen between the three types of events. Overall, fairly similar values of surge celerity can be seen, but there is variability with increasing and

decreasing celerity as the surge propagates. Therefore, there are definitely more factors influencing surge propagation celerity than just the distance traveled and the size of the surge. These factors could include the geometry of the channel, surface ice conditions in the receiving channel, the interaction of ice and water within the ice jam as explained by Jasek (2003), and, it appears most significant, temporary jamming and re-release. Therefore, ice appears to be an important factor in the behaviour of ice jam release events.

Documentation is lacking in terms of the magnitude of the peak of the surge wave for many of the historical events. The values available for comparison show a large amount of variability with no obvious trend. With very few values of peak magnitude over a significant distance of the study reach, magnitude attenuation cannot really be assessed in great detail. However, the 2002 event provides an excellent dataset showing a significant decrease in peak magnitude in the first 10 km of travel. This initial drastic decrease immediately downstream of an ice jam release location is also shown in the 1990 data. This supports the observations of Jasek (2003).

Although the historical data provides some insight to the behaviour of surge waves resulting from ice jam release events, the relatively inaccurate measurements do not allow for in-depth analysis. The remote monitoring network that obtained measurements for the 2002 release event provides an excellent dataset of both the surge celerity and peak magnitude. Therefore, the 2002 event data will be further analyzed using computer modeling as discussed in the next section.

5.2 RIVER1-D MODELING OF 2002 EVENT

Previous studies of ice jam release events are inconclusive in regards to the effect ice has on surge propagation. Two experimental studies discussed in a previous chapter had conflicting conclusions as to this question of the importance of ice. Wong *et al.* (1985) set up an experiment using polyethylene blocks to simulate the ice within an ice jam. These blocks were obstructed using a retaining gate, which was then lifted suddenly to simulate an ice jam release situation. They found that the moving ice had very little effect on the passage of the surge. An experimental study by Khan *et al.* (2000) used similar polyethylene blocks to simulate not only the ice within the jam, but also considered the effect of an ice cover in the downstream receiving channel. The celerity of the surge was found to decrease under the effects of an ice cover. The magnitude of the surge peak increased as a result of an ice cover, with even larger magnitudes at higher degrees of ice concentration. It is unknown if these ice effects were due to the ice within the ice jam, the ice in the receiving channel, or a combination of both. Since laboratory experiments are limited by the constraints of the equipment, such as length of the flume, analysis of full surge propagation was unattainable. Field observations have also been made by Jasek (2003), where ice within the ice jam and ice in the downstream channel was believed to affect surge propagation. Further discussion of Jasek's findings were discussed in Chapter 2.

In order to advance the knowledge of surge propagation resulting from ice jam release events, models of dynamic open channel flow have been used. However in the past, due to limited data, it was inconclusive as to how well this modeling approach had performed. Documentation by Beltaos *et al.* (1994) of the 1993 event on the Saint John River, NB, includes information of channel geometry, ice jam profile, and a partial stage hydrograph as the surge passed a point 5 km downstream of the toe of the released ice jam. However, a hydropower facility was located further downstream of the release location and so additional propagation data could not be obtained to evaluate attenuation effects. This data was modeled by Hicks *et al.* (1997) with the University of Alberta's cdg-1D model using approximate (rectangular) channel geometry. The celerity of the

surge was adequately modeled, but not stage. It was suggested that this might be attributable to the use of the rectangular channel approximation or to the effects of remnant ice in the channel downstream of the released ice jam. Further modeling efforts by Blackburn and Hicks (2003) using actual channel geometry were again successful in modeling the celerity of the surge. Actual channel geometry was found to improve the modeled peak water level, but the recession portion of the stage hydrograph could not be reproduced. Again, it was suspected that this might be attributed to the effects ice, either within the propagating surge, in the receiving channel, or both.

A two-dimensional ice dynamic model was used by Liu and Shen (2004) to study the effects of an ice cover on surge propagation. The same data for the 1993 event on the Saint John River was used, but the channel was approximated by rectangular cross sections due to imprecise field data. Ice was found to have a significant effect on both the stage and discharge hydrographs. Primarily, the effect was a change in the shape of the hydrographs. The peak stage was relatively unaffected, whereas the peak discharge was found to decrease. Although these results show an ice cover has an effect on surge propagation, there is no verification data for these results to be compared against. Therefore, the modeling in this study of the 2002 event on the Athabasca River will assess the importance of an ice cover on surge propagation, and the adequacy of using a one-dimensional dynamic open channel flow model. A comparison will be made with the field data measured by the remote monitoring network to verify the results.

5.2.1 Model Description

Hydrologic models have been used in the past for flood routing studies; they are attractive from a data requirement perspective (streamflow hydrographs as input only). Although they consider conservation of mass deterministically, they consider momentum effects only empirically. Therefore, these models only provide discharge hydrographs at the gauge stations used in calibration. Additionally, these models cannot properly analyze dynamic events, such as ice jam releases. Hydraulic models, on the other hand, are deterministic, considering conservation of both mass and momentum as a basis, and

thus require physical data including not only streamflow data, but channel geometry and channel resistance characteristics (Hicks, 1996). A major benefit of hydraulic modeling is that the output includes stage or water level hydrographs at any point along the study reach, thus not just being limited to gauge stations. Consequently, hydraulic models solving the full dynamic equations can be used to model ice jam release surge events provided that ice effects are handled adequately.

The hydraulic model River1-D Version 1.00 was used in this analysis. River1-D is a public domain model developed at the University of Alberta which solves the Saint Venant equations of one-dimensional unsteady open channel flow for the conservation of mass and momentum. It is the updated (Windows ®) version of the cdg-1D model employed by Hicks *et al.* (1997) and Blackburn and Hicks (2003). These equations, assuming rectangular channel geometry, are shown below (presented and discussed earlier in Chapter 2).

$$\frac{\partial A}{\partial t}+\frac{\partial Q}{\partial x}=0 \qquad [1]$$

and,

$$\frac{\partial Q}{\partial t}+\frac{\partial (Q^2/A)}{\partial x}+\frac{\partial}{\partial x}\left(\frac{gAy}{2}\right)-\frac{gAy}{2B}\frac{dB}{dx}=gA\left(S_o-S_f\right) \qquad [2]$$

In the River1-D model, these equations are solved using the *characteristic-dissipative-Galerkin* (CDG) finite element scheme as developed by Hicks and Steffler (1990). The two extremes of a surge are dynamic and diffusive waves. However, the typical situation is the transition between these two. The CDG scheme is able to handle these transitional flows without resorting to the flow approximations discussed in Chapter 2. A reach characterized by ranging slopes, as seen along the Athabasca River, can create areas of subcritical and supercritical flows. Other numerical methods (e.g., finite

difference methods) require these sub-reaches to be subdivided and handled separately, but the CDG finite element scheme is able to solve both of these regimes simultaneously.

5.2.2 Input Geometry

River1-D requires two input files to run the model: a geometry file and a boundary condition file. The geometry file contains data describing the river at each computational node along the study reach. The boundary condition file provides the time dependent inflow data to allow the model to run an unsteady flow simulation. An optional third input file allows an ice covered condition to be modeled. Each of these files and their corresponding required data is described in detail in this section.

The geometry file requires data for every node along the river reach. For the Athabasca River, stations (in km) have been assigned using an origin located at the mouth of Lake Athabasca and increasing in the upstream direction. For the model of the study reach, nodes were spaced at a 1 km interval in the reach from 0 km to approximately 265 km, as this downstream section was only required to prevent reflective waves or backwater effects from the downstream boundary. From 265 km to the maximum upstream limit of 400 km, a node spacing of 50 m was used. This value was chosen to adequately resolve the shape of the steep waves being modeled and also because it adequately described locations of TBMs, measurement stations, surveyed cross sections, rapid sections, and other important locations. A list of the river stationing for some of these important locations is in Table 5-1.

Table 5-1. Athabasca River stationing for important locations.

Station Name	Location (km)
*Town of Athabasca	679
**Pelican River	511
*Pelican Rapids	496
*Stony Rapids	492
*Rapides du Joli Fou	460
*Grande Rapids	425
*Little Grande Rapids	421
Brule Point	398
Brule Rapids	386.8
Boiler Rapids	353
Middle Rapids	349.4
Long Rapids	344.6
G150	333.7
Crooked Rapids	332.8
Rock Rapids	330.6
AE Camp	328
G140	327
Little Cascade Rapids	325.8
Cascade Rapids	322.8
G135	319.8
133	317.5
132	314.2
G130	312.3
G122	308.7
G120	308
Mountain Rapids	307.2
112	304.9
G110	303.3

Station Name	Location (km)
104	300.3
100	298.9
Little Fisheries River	298.7
Moberly Rapids	296.6
90 Water Intake 1	296.55
Horse River	296.1
85 Water Intake 2	295.45
80 MacEwan Bridge	294.9
75 MacIsland	294.2
70 Clearwater Confl.	293.2
G65	291.3
G60	290.2
57 WSC Gauge	289.2
G55	289
G50	287.5
Poplar Island	285.6
G45	283.6
G40	281.4
Stony Island	278
G35 Sawmill	278.3
G30	275.4
G25	274
Inglis Island	271
G15	270.4
G10	268.8
G5 Suncor Site	266.7
Muskeg River	244.7

** These station locations are from Alberta Environment measurements. All other station locations are from University of Alberta measurements.*

*** This station location is from historical reports by Alberta Research Council.*

River1-D Version 1.00 is capable of modeling rectangular, trapezoidal, and natural cross section data. At the time of this analysis, modifications were being made to the program's equation formulation to better handle natural cross sections. Since the Athabasca River can actually be characterized as a wide and shallow channel, rectangular cross sections adequately described the study reach. The program is now better able to handle natural cross sections, and thus future work could consist of modeling this same

event with the natural cross section data, should sufficient channel geometry data become available.

At each node, rectangular cross sections were described by the bed elevation and channel width. Where possible, the rectangular bed elevation was estimated using actual surveyed cross section data by calculating the average of the surveyed bed elevations between the two banks. Bed elevations for those nodes without an accompanying surveyed cross section (i.e. the majority of the nodes) were interpolated between nodes with actual surveyed cross sections. The river widths were measured between the two banks of the surveyed cross sections. These widths were then compared to the widths measured off of 1:50,000 National Topographic Series (NTS) maps, and were found to be very similar in most cases. Therefore, to be consistent along the entire reach, widths were obtained from NTS maps for all nodes.

Channel roughness is most commonly described using Manning's coefficient, n. The rougher a channel is, the larger the n value. This roughness coefficient is then used in Manning's equation to calculate flow of the channel (Chow, 1959), as shown below:

$$Q = \frac{AR^{2/3}S_f^{1/2}}{n} \qquad [40]$$

where R is the hydraulic radius, the ratio of the cross sectional area divided by the wetted perimeter (P):

$$R = \frac{A}{P} \qquad [41]$$

An ice cover increases the wetted perimeter to include the underside of the floating ice. On a wide and shallow river, such as the Athabacsa River, an ice cover effectively doubles the wetted perimeter. A composite Manning's coefficient, n_o, can be calculated for ice cover conditions using Sabenev's equation (Ashton, 1986):

$$n_o = \left(\frac{n_i^{3/2} + n_b^{3/2}}{2} \right)^{2/3} \quad [42]$$

where n_i is the Manning's coefficient for the underside of the ice cover, and n_b is the Manning's coefficient for the bed of the channel.

Another method to describe channel roughness involves using a roughness height, k, and Chezy's equation:

$$Q = AC_* \sqrt{gRS_f} \quad [43]$$

where C_* is the non-dimensional Chezy coefficient (Henderson, 1966). The Chezy coefficient is based on the log-law (Schlichting, 1979):

$$C_* = 5.75 \log\left(\frac{R}{k}\right) + 6.2 \quad [44]$$

where the constant 6.2 is used for open channel flow (Keulegan, 1938).

Friesenhan (2004) analyzed stationary ice jams in the vicinity of Fort McMurray using the U.S. Army Corps of Engineers' HEC-RAS model and obtained calibrated values of the Manning's roughness coefficients for the same reach of the Athabasca River as used in this study. Manning's roughness coefficient varies with depth, with decreased resistance typically experienced at larger water depths. This variation must be input manually, which is inconvenient when modeling unsteady flows. Therefore roughness height, k, is a more convenient and accurate means of quantifying the frictional resistance effects as a large surge wave passes.

For this study, the Manning's roughness coefficients determined by Friesenhan (2004) were converted to a roughness height using the Strickler equation (Henderson, 1966), where:

$$n = \frac{k^{1/6}}{8.41\sqrt{g}} \qquad [45]$$

A composite roughness height can be found using Sabenev's equation in the form of,

$$k_o = \left(\frac{k_i^4 + k_b^4}{2} \right)^{1/4} \qquad [46]$$

where k_i is the roughness height of the underside of the ice cover, and k_b is the roughness height of the bed of the channel. Table 5-2 provides Manning's roughness coefficient, n, and roughness height, k, values, but roughness height was used for all of the modeling unless otherwise specified.

Table 5-2. Bed roughness characteristics for the Athabasca River study reach.

From (km)	To (m)	Manning's n (dimensionless)	Roughness Ht., k (m)
0	296.55	0.030	0.24
296.6	300.4	0.020	0.02
300.45	319.4	0.030	0.24
319.45	400	0.035	0.61

0 km corresponds to the mouth of Lake Athabasca.

The final data requirements for the geometry input file includes specifying the initial stage and discharge conditions at each node. The type of output file, such as peak values or hydrographs at user specified nodes, is specified in the River1-D program menu. Output of stage and discharge hydrographs were specified at each monitoring station (G140, G135, 132, G130, 104, 90 and 57). The initial stage and discharge values

at each node are dependent on the various model runs performed. These initial conditions must exactly match the values in the boundary condition file at time zero.

The boundary condition file consists of an upstream and downstream boundary condition due to the subcritical flow experienced at each of the modeled boundaries along this portion of the Athabasca River. The upstream condition uses an inflow discharge hydrograph, whereas the downstream condition uses a stage hydrograph. The downstream water level is calculated assuming uniform flow, using the initial inflow discharge at the upstream boundary. This downstream water level remains the same value throughout the model run. This boundary is sufficiently far downstream such that the variation in this water level will have virtually no effect on the water levels experienced along the study reach.

River1-D also allows for lateral tributary inflow hydrographs, which are specified in the boundary condition input file. This capability was not utilized since there is little data available on these tributaries; however, they are known to be extremely small and, at this time of year, their contributions are negligible compared to the flow in the Athabasca River. Also, many of these tributaries were frozen to the bed during the breakup season thus contributing an even smaller fraction of flow to the Athabasca River.

An ice file can be used in the River1-D program and requires knowledge of the ice thickness and underside ice roughness for each node along the river reach. The thickness and roughness can vary from node to node, but remains the same value throughout the model run. Therefore, moving ice can not be modeled in this version of River1-D. Current work is being done to incorporate this process in future versions.

5.2.3 Model Application

The breakup events for 2002 can be separated into two parts. The first part of the event was the release of the 17 km long ice jam, initially poised upstream of G140, that propagated through the study reach. This ice run became arrested at station 104

impinging upon a downstream intact ice cover, where a new 8 km long ice jam formed. The second part of the event occurred when a wave escaped from the new ice jam and continued to propagate underneath of the intact ice cover. Both parts of this event were modeled using River1-D, and will be discussed in separate sections.

Modeling the Dynamic Release in the Upper Reach

This section will look at the first part of the 2002 event, where a surge propagated through the study reach as a result of an ice jam failure that initiated just upstream of G140. Three types of model runs were performed to analyze the propagation of the surge as it traveled along the study reach. These model runs are summarized in Table 5-3.

Table 5-3. Description of model runs performed to analyze the dynamic release in the upper reach.

Run 1	G140 set as upstream boundary. Uniform flow was assumed to calculate an inflow discharge hydrograph based on the observed stage hydrograph at this location.	
	Run 1a	Open water condition along entire study reach.
	Run 1b	Ice cover condition along entire study reach.
Run 2	G135 set as upstream boundary. Uniform flow was assumed to calculate an inflow discharge hydrograph based on the observed stage hydrograph at this location.	
	Run 2a	Open water condition along entire study reach.
	Run 2b	Ice cover condition along entire study reach.
Run 3	Used HEC-RAS to get a water level profile for a 17 km long ice jam with its toe at the AE Camp, just upstream of G140. This water level profile was then used as the initial condition in River1-D.	
	Run 3a	Open water condition along entire study reach.
	Run 3b	Ice cover condition along entire study reach.
	Run 3c	Open water condition along entire study reach using Manning's roughness coefficient, n.
Run 4	G140 set as upstream boundary. Use looped rating curve from Runs 3a and 3b to calculate inflow discharge hydrograph based on the observed stage hydrograph at this location.	
	Run 4a	Open water condition along entire study reach.
	Run 4b	Ice cover condition along entire study reach.

All model runs used roughness heights, k, to describe resistance characteristics unless otherwise stated.

Model Run Parameters

All of the model runs used the same parameters when modeling the 2002 event in the upper reach. A time step increment was selected using a Courant number, C, of 0.5 as defined by the equation,

$$C = \frac{V_S \Delta t}{\Delta x} \qquad [47]$$

where V_S is the velocity of the surge, Δt is the time step increment and Δx is the distance between the nodes (set at 50 m). Table 5-4 summarizes the time increments calculated for the measured surge velocities in the upper reach using equation [47]. It was unknown how the model would compare to the measured data. Therefore, a time increment of 2 seconds, or 0.0005 hours, was used to be conservative, since the CDG finite element method accuracy improves as Courant number decreases (Hicks and Steffler, 1990).

Table 5-4. Measured surge velocities and the corresponding time increments for a Courant number of 0.5.

Station		V_s	Δt
From	To	(m/s)	(s)
G140	G135	4.14	6.0
G135	G130	3.13	8.0
G130	104	2.63	9.5

An unsteady flow simulation requires as input, details of the initial conditions (stage and discharge) at every node. Discharge is simply the flow rate prior to the event (the carrier discharge). However, water levels at every node are not typically known. Rather than conducting a separate steady flow water level profile analysis to determine these values (e.g. using HEC-RAS), one can run River1-D, using the time stepping unsteady flow simulation to achieve the same objective. In this case a constant inflow discharge is specified (the carrier discharge) along with a guess of the initial water levels, and the model is run until a steady water level profile is achieved. The results at

intermediate time steps are not physically meaningful and thus not of interest, just the final steady state solution is needed to establish the initial conditions for the subsequent unsteady flow simulation. Consequently a lower convergence tolerance and/or fewer iterations per time step can be employed to help to speed up this preliminary model run. This steady run was set at a time step of 0.0005 hours with a maximum of 5 iterations per time step. Once a relatively steady state was achieved along the reach, a transient or unsteady run was performed. The unsteady run also had a time step of 0.0005 hours, but a maximum of 25 iterations per time step was used. The unsteady run had a total simulation duration of 13 hours, as this was the length of time the surge took to propagate through the study reach according to the field measurements.

The only run that did not follow these parameters was Run 3. This run was different because HEC-RAS was used to develop a water level profile within the modeled reach, to be the initial condition in River1-D. Therefore, the steady model run in River1-D was not required as a steady state profile had already been attained in HEC-RAS. The unsteady run still used a time increment of 0.0005 hours, a maximum of 25 iterations per time step, and a simulation duration of 13 hours.

Run 1

The first run method involved setting station G140 as the upstream boundary condition, since it was the most upstream monitoring station along the study reach for this event. With the measured water level hydrograph at station G140, a uniform flow calculation using Chezy's equation provided an estimate of the corresponding inflow discharge hydrograph. This hydrograph was then routed along the reach and was compared to the water level hydrographs measured at the other monitoring stations downstream.

There was an intact ice cover downstream of the ice jam prior to release. However, since the event occurred at night, it is not known whether the releasing jam propagated through a sheet front or a rubble front (with respect to Jasek's 2003 classification system). Since the model does not consider either explicitly, two sub-types

of model runs were performed; Run 1a assumed an open water condition throughout the receiving channel downstream of the released jam, and Run 1b assumed an intact ice covered condition along the entire length of the receiving reach. The intent was that these two extreme conditions would represent the upper and lover bounds of the possible physical behaviour, in terms of the ice resistance in the receiving channel. For Run 1b, the ice cover was set at a consistent ice thickness of 0.8 m with an underside roughness height of 0.00381 m (n_i = 0.015), corresponding to established conditions prior to the release.

Initial Conditions

In the geometry file, initial water level elevations and discharges were required at each node. These values were merely estimates, as the steady model run in River1-D is used to establish the initial conditions for the simulation.

The uniform flow calculation for Run 1a indicated an initial (carrier) discharge of about 910 m^3/s at G140 prior to ice jam release. This discharge was applied to all nodes for the steady flow analysis. The corresponding depth of 1.96 m at G140 was then added to the bed elevations at each node to obtain the first guess of the initial water level elevations. For Run 1b, a discharge of about 405 m^3/s was calculated. The same depth of 1.96 m was applied to all the nodes to obtain the first guess of the initial water level elevations for Run 1b.

Boundary Conditions

Although the study reach contains numerous rapid sections, the flow regime at each of the boundaries of the modeled reach of the Athabasca River is subcritical. Therefore, boundary conditions are required at both the upstream and downstream ends of the reach to accurately describe the flow regime. The upstream boundary condition consists of a discharge hydrograph with 5 minute increments, corresponding to the increment in the measured data, for a duration of 13 hours. The duration of this hydrograph had to be sufficient to allow the simulation to continue until the surge had propagated through the study reach. A uniform flow approximation using Chezy's

equation was applied to the measured data at G140 to obtain this inflow discharge hydrograph. As discussed earlier, the downstream boundary condition was set sufficiently far downstream to make it possible to simply assume the water level elevation remained the same throughout the model run.

Results

Stage hydrographs comparing the modeled and measured water levels are shown in Figure 5-7. These figures show the results of both the open water and ice covered conditions, Run 1a and 1b, respectively. As Figure 5-7 indicates, the specified inflow discharge hydrograph, which was based on a uniform flow assumption, produces modeled water level values at station G140 that match reasonably well with the measured values. However the peak magnitude is about 1 m too low in the model run, and the falling limb of the stage hydrograph is not quite as steep as was measured. As this modeled surge traveled downstream, the overall peak magnitudes along the reach match the measured water levels fairly well at stations G130 and 104, but to a lesser degree at stations G135 and 132.

As discussed earlier, the ice run associated with this particular release event arrested at station 104, forming a new ice jam. However, some water escaped downstream propagating through Fort McMurray under the intact ice cover. The modeled peak magnitudes at stations 90 and 57, shown in Figure 5-7, are significantly larger than those measured. This suggests that not all of the water in the wave continued on downstream, only part of it. Conceivably, the remainder was lost to storage in the re-forming jam. This was investigated further in Runs 4 and 5, as described later in a later section.

A comparison of the model output assuming open water and ice covered conditions in the receiving channel, shows the open water assumption to have better agreement in terms of the match to the observed celerity of the wave. The peak magnitudes for both cases (1a and 1b) are very similar along the length of the reach, except at station 104 where the modeled peak magnitude is about 0.5 m higher when an

ice cover is assumed in the receiving channel. The overall shape of the stage hydrograph appears flatter for the assumption of ice in the receiving channel, as the water level does not increase or recede as quickly as for the open water situation.

Considering the carrier discharge (i.e. conditions prior to arrival of the surge wave at each site), the simulation conducted assuming ice in the receiving channel appears to match the measured water level better for all stations except for stations 90 and 57. This is as expected, since all evidence points to ice covered conditions in the receiving channel prior to the release event. Again, the lack of agreement for stations 90 and 57, supports the earlier conclusion that not all of the water escaped past the reformed ice jam at Mountain Rapids.

As the modeled water levels start to increase upon the arrival of the surge (i.e. the rising limb of the stage hydrograph), the open water condition appears to be more applicable. This implies that the ice cover in the receiving channel (whether removed by a rubble or sheet front), seems to offer little resistance to the arriving surge. Note that, given that this ice run arrested creating a new jam, the rubble breaking front is indicated.

The uniform flow approximation used to obtain the inflow boundary condition at station G140 for Run 1, assumes a single valued rating curve (the relationship between water level and discharge). However dynamic events, such as the release event being studied here, should create a looped rating curve since water surface slope is then also a factor in the stage discharge relationship. An investigation of the degree of looping of the modeled stage-discharge relationship during passage of the event can thus give some insight as to the adequacy of the uniform flow approximation.

Figure 5-8 provides an idea of the dynamic nature of this event. The larger the loop in the rating curve, the more dynamic the event is. G140 shows a large loop in the rating curve, which tapers off a fair amount upon arriving at station G135. The size of the loop, and thus the dynamic nature of the event, decreases as the wave propagates downstream. The rating curve still appears to be fairly dynamic between stations 104 and

57, but this section of the river was not accurately modeled and thus may be appearing more dynamic than what actually occurred.

Some questionable occurrences in the low discharge areas of these looped rating curves, most predominantly seen at stations 104, 90 and 57 (Figure 5-8), occur before the arrival of the wave front. These extra little "loops" correspond to initial fluctuating water levels as observed in Figure 5-7, most apparent at stations 90 and 57. Flow is spatially varied along the study reach being higher at G140 than at the downstream stations. Therefore the recession in water level prior to surge arrival at stations 57 and 90, and to a lesser degree at station 104, shows this spatial variation in discharge. Although a steady model run was performed to account for this variation, accurate initial discharge and water level conditions at the downstream stations were not attained.

Run 2

The next simulation involved setting station G135 as the upstream boundary. A uniform flow approximation was again used to determine the inflow discharge hydrograph for the upstream boundary condition. The reason for setting G135 as the upstream boundary rather than G140 was to eliminate the first few kilometers of travel where a drastic decrease in peak magnitude occurred. This drastic decrease was discussed earlier according to the observations of Jasek (2003). By neglecting the events between stations G140 and G135, the more consistent rate of magnitude attenuation between G135 and 57 was able to be studied. An open water receiving channel condition was modeled in Run 2a, and Run 2b provided a comparison with propagation under an ice cover. The ice conditions were the same as the previous analysis method, with an ice thickness of 0.8 m and an underside ice roughness height of 0.00381 m ($n_i = 0.015$).

Initial Conditions

The initial conditions for Runs 2a and 2b follow the same approach as discussed for Runs 1a and 1b. The difference being that the upstream boundary, in this case, was at G135 rather than at G140. The open water carrier discharge (Run 2a) was found to be about 1730 m^3/s compared to a carrier discharge of 798 m^3/s for the ice covered condition

(Run 2b). Both runs had an initial depth of 2.23 m applied to all of the nodes, as the first guess for the steady flow simulation used to obtain the initial conditions for the unsteady flow run.

Boundary Conditions

Boundary conditions were again required both upstream and downstream, as in Run 1. Chezy's equation was applied to the measured stage hydrograph at G135 to obtain the discharge hydrograph, assuming uniform flow conditions. This discharge hydrograph was used as the upstream boundary condition for a simulation duration of 13 hours. A time increment of 5 minutes was used to resolve the discharge hydrograph, which corresponds to the increment in the measured data. The downstream boundary condition was again a constant water level.

Results

The modeled results for Runs 2a and 2b are shown in Figure 5-9. A result for stations 57 and 90 are not shown as this portion of propagation is studied separately in future sections. As Figure 5-9 indicates, the specified inflow discharge hydrograph, which was based on a uniform flow assumption, produces modeled water level values at station G135 that match reasonably well with the measured values. However, the peak magnitude is approximately 0.25 m less than the measured peak and the falling limb of the modeled stage hydrograph appears about 0.25 m high. As this modeled surge wave propagates along the study reach, its celerity appears to match the observed data better than in Run 1, but overall the water levels are too low. At station 132, the closest station to the upstream boundary, model results show fairly good agreement with water levels before and after the surge, but the modeled peak magnitude is low. Upon reaching station G130, the entire modeled surge is significantly low compared to the observed data.

Comparing the modeling results for open water versus ice covered conditions in the receiving channel, the open water assumption again provides a better match to the observed celerity of the surge. The peak magnitudes of open water and ice cover are very

similar for both cases, from G135 to G130. However, the peak magnitude computed for the case of the ice covered receiving channel is larger at station 104.

Assuming open water conditions in the receiving channel also creates a reasonably good match to the measured shape of the stage hydrographs, although low in overall water level (e.g. see results at station 132). Clearly, as mentioned for Run 1, it is more representative to assume the presence of an ice cover in the receiving channel prior to wave arrival, given the observations to that effect. However, when considering the propagation of the surge, which almost certainly involved a rubble breaking front, it seems that assuming open water in the receiving channel is the better approximation.

By setting G135 as the upstream boundary rather than G140, a better match is observed for wave celerity, but the overall water levels and peak magnitudes are much too low. Comparing the looped rating curves for Run 1 (Figure 5-8) and Run 2 (Figure 5-10), the dynamic nature of the modeled waves in Run 2 are much less than in Run 1. However the modeled results are still fairly dynamic in the upper portion of the reach.

Run 3

Due to the dynamic nature of ice jam release events, a uniform flow approximation of the inflowing discharges seems inappropriate. Therefore, an attempt was made to more realistically model the release of this 17 km long ice jam poised upstream of the study reach. Since the ice jam occurred at night, in a remote reach, with no vertical survey control, it's profile and associated backwater conditions are unknown. Therefore, the ice jam profile was estimated by performing an ice jam profile calculation using the one-dimensional steady flow program HEC-RAS, developed by the US Army Corps of Engineers. This ice jam profile was then input into River1-D and an unsteady flow simulation was conducted. Since such a profile is 'unstable', in that the model has no ice to hold back the water, the result is the release of the water in a classic dam break fashion.

Three scenarios were considered, Runs 3a and Run 3b assumed open water and ice cover in the receiving channel, respectively (as in earlier runs). Run 3c was the same as Run 3a (involving open water conditions in the receiving channel) but employed Manning's n rather than the roughness height, k, to describe channel resistance (Table 5-2). This run was performed to analyze the difference in modeled water levels for Chezy's versus Manning's equation when used to model the friction slope.

The HEC-RAS model was set up with the same channel geometry as was used in River1-D, and an ice jam of 17 km length was placed with its toe 1 km upstream of station G140 (the location of the AE observational camp). This choice of ice jam length and position was based on the comments and measurements of the AE observers, as discussed in the previous chapter. An ice jam underside ice roughness of $n_i = 0.11$ was assumed, based on ice jam calibrations performed by Freisenhan (2004) for historical events in Fort McMurray. This roughness value remained fixed throughout the model run. The minimum ice thickness within the ice jam (a required input for the model) was determined using an iterative approach by matching the modeled stage hydrograph in River1-D to the measured water levels at G140. The best match was obtained for a minimum ice thickness of 4 m for open water in the receiving channel (Run 3a), and 6 m for an ice covered condition downstream of the ice jam (Run 3b). Ice within the jam was constricted to remain in the main channel as not to spread onto the banks. The ice cover in Run 3b had a thickness of 0.8 m and an underside ice roughness height of 0.0038 m ($n_i = 0.015$), as in earlier runs. Default values of the remaining ice jam parameters were used, as summarized in the following table. More information on these default parameters can be found in the HEC-RAS manuals (Brunner, 2002).

Table 5-5. Default ice jam parameters in HEC-RAS.

Parameter	Default Value
Specific Gravity	0.916
Friction Angle	45°
Porosity	0
Stress K1 Ratio	0.33
Ice Cohesion	0
Maximum Velocity	1.524 m/s

Initial Conditions

Carrier discharges were calculated for each model run based on the assumption considered (open water or ice covered receiving channel) and the measured water levels along the reach after the release event occurred. For Run 3a and 3c (open water) a carrier discharge of 850 m^3/s was used, while for Run 3c (ice cover) a carriage discharge of 200 m^3/s resulted. Carrier discharges were also calculated based on water levels prior to surge arrived, but the modeled results appeared too high.

The steady water level profiles determined by HEC-RAS, including the ice jam profile, were used as the initial condition for the unsteady flow simulation in River1-D. Two profiles resulted, as seen in Figure 5-11 and 5-12, one for each of the carrier discharges discussed above.

Boundary Conditions

The same carrier discharges used in the HEC-RAS profile calculations were then used to model the passage of the released wave along the study reach. Specifically, the inflow to the ice jam was kept constant at the prescribed carrier discharge, and the unsteady flow in the simulations was entirely due to the release of the water stored in the ice jam (as represented by the ice jam and backwater profiles). This run was simulated for a duration of 13 hours to ensure propagation of the surge through the study reach.

For this case, the upstream boundary was set at a distance of 400 km upstream of the mouth of the Athabasca River. This distance was necessary to be able to capture the full backwater curve upstream of the ice jam as computed in the HEC-RAS analysis. The most downstream node was the same as in all other runs, and was sufficiently far downstream of the study reach so as to allow the use of a constant water level for the boundary condition.

Results

The modeled results are shown in Figure 5-13. Looking first at the most upstream station, G140, which was located 1 km downstream of the toe of the jam, it is

seen that the steep rising limb of the computed water level hydrograph matches the measured data quite well, except for about the last meter before reaching its peak. The peak magnitude for both the open water and ice covered runs match the data well, but the peak arrives too late. The peak is characterized by a smooth curve upon starting its decent, but the measured stage hydrograph had a much sharper peak which River1-D thus far has been unable to model. The falling limb of the stage hydrograph is similar in shape to that measured, but occurs too late.

As the surge propagates further downstream, the water level before and after the surge match relatively well, but the computed peak magnitudes are way too high. The celerity of the surge is modeled fairly well upon arriving at station 104, particularly for the assumption of open water in the receiving channel. Overall, these simulations show acceptable wave celerity performance, but the ice jam profile is likely too large.

In general, as before, the assumption of intact ice remaining in the receiving channel results in higher water levels and peak magnitudes along the entire study reach, and is also characterized by a slower wave celerity compared to the open water assumption. As seen in Run 1 (with G140 as the upstream boundary), the water levels computed assuming an ice cover match better prior to surge arrival (which makes sense based on the observations), but the assumption of open water in the receiving channel produces slightly better celerity and wave peak magnitudes as the surge propagates. .

Run 3c was performed to compare the effects of using Manning's equation instead of Chezy's equation to quantify the friction slope. Even though Manning's n values are more commonly understood and utilized, as discussed earlier roughness heights are more applicable as large waves and associated large water depths are experienced. As the depth of water increases, the amount of resistance from the river bed decreases. This is not reflected when using a constant Manning's n value; therefore roughness heights appear to be more applicable for unsteady flow simulations.

A comparison of results for Runs 3a and 3c in Figure 5-14, show that higher peak magnitudes and faster surge celerities result when using Manning's equation. The rising and falling limbs of the stage hydrograph obtained using Manning's equation are steeper, but overall, the hydrograph shape computed using roughness height appears to be more representative of the measured data. Surge celerity is slightly better matched using Manning's equation, but the surge peak appears to experience more realistic attenuation when Chezy's equation is used. Overall, the use of Chezy's equation rather than Manning's n appears to be the better option for surge wave propagation analyses.

The rating curves (Figures 5-15) show much larger loops, meaning a more dynamic event, as compared to Run 1. Higher discharges are also indicated compared to the Run 1, which is to be expected, given the over prediction of water levels in Run 3.

For this run, it was possible to obtain the computed water level and discharge profiles near the toe of the ice jam, at various times. These profiles, shown in Figures 5-16 to 5-19 for Run 3a, indicate that within the first minute of release, the discharge at the toe of the ice jam has already increased from about 1000 to 10,000 m^3/s (Figure 5-19), but the water level has barely risen (Figure 5-17). This may explain the dramatic increases in velocity in open water areas downstream of ice jams observed immediately prior to jam release (as originally pointed out by Henderson and Gerard, 1981). The discharge profile shows numerous oscillations before arriving at the peak discharge near the ice jam toe. It is not until about 15 minutes that these oscillations combine into one wave as the stored water is mobilized (Blackburn and Hicks, 2003). The peak discharge at 0.5 minutes appears right at the toe of the ice jam, but successive time increments see lower peak discharge values that propagate upstream of the jam toe. This result is similar to the observations by Blackburn and Hicks (2003), where the peak discharge moved upstream during the initial period following the ice jam release, while the surge itself propagates downstream. To validate these observations, water level hydrographs upstream of the ice jam toe would be valuable, but extremely difficult to obtain.

Run 4

Although Run 3 made the most physical sense for modeling ice jam release events, by creating a water level profile that includes the position of the ice jam prior to release, the modeled stage hydrographs were much too large compared to the measured values. Much of this discrepancy can be attributed to the lack of knowledge of the positioning and geometry of the ice jam. However, Run 3 did match the measured stage hydrograph at G140, located 1 km downstream from the release location. The looped rating curves at G140 for Runs 3a and 3b were used to create an inflow discharge hydrograph for Runs 4a and 4b by setting G140 as the upstream boundary. As in other modeling runs, an open water condition (Run 4a) and an ice covered condition (Run 4b) was performed. An ice thickness of 0.8 m with an underside ice roughness height of 0.00381 m ($n_i = 0.015$) was used for Run 4b.

Initial Conditions

Water level and discharge is required at each node for the initial condition, which are adjusted by a steady model run. For the open water scenario (Run 4a) a discharge of 962 m^3/s corresponded to the initial water level according to the looped rating curve for Run 3a. Unfortunately, the looped rating curve for Run 3b did not extend to the initial measured water level. Chezy's equation, which assumes uniform flow, was therefore applied to the first two values of the measured stage hydrograph to obtain the initial inflow discharge values for Run 4b. The discharge for Run 4b at time zero was specified as 885 m^3/s. Both scenarios applied a depth of 1.93 m to all nodes to calculate the initial water level.

Boundary Conditions

The subcritical flow regime experienced at the boundaries of the study reach requires both upstream and downstream boundary conditions. For the upstream boundary, the looped rating curves from Runs 3a and 3b were applied to the measured stage hydrograph at G140 to develop inflow discharge hydrographs for Runs 4a and 4b. A time increment of 5 minutes was used to resolve the discharge hydrograph (corresponding to the time increment in the measured data), which was modeled for a

duration of 13 hours. The downstream boundary condition was set at a constant water level as specified in the other model runs.

Using a uniform flow assumption (Run 1) involves a single valued rating curve, but a looped rating curve accounts for a more rapid increase in discharge on the rising limb of the discharge hydrograph. Little difference is seen when comparing the looped rating curves for Runs 1 and 3, but Run 3a does show a higher rate of increase in discharge and a larger peak discharge by about 500 m^3/s as compared to Run 1a. Therefore Run 4 was performed to assess the difference in using a uniform flow assumption or a looped rating curve at the upstream boundary.

Results

The modeled results between stations G140 and 104 are shown in Figure 5-20. Overall, Run 4 appears to be very similar to the results of Run 1. The peak water level at G140 for Run 4 is slightly higher than that of Run 1; however the peak water levels at the other stations are slightly lower for Run 4a (open water).

Comparing the open water (a) and ice covered conditions (b), the open water condition again appears to be the more adequate match to the measured data. As seen in other model runs, the ice covered condition appears to be a better match prior to the arrival of the surge. The looped rating curves for Run 4a (Figure 5-21) are also very similar to Run 1a (Figure 5-8).

Since very little difference is seen between Run 1 (uniform flow assumption) and Run 4 (looped rating curve from Run 3), assuming uniform flow to attain an inflow discharge hydrograph at the upstream boundary appears to be an adequate assumption for modeling purposes. The validity of this assumption could change as more information on the geometry and release processes of ice jams become available.

Discussion

Figure 5-22 compares the computed discharge hydrographs at station G140 for Runs 1 and 3 assuming open water (a) and ice covered (b) conditions in the receiving channel. A peak discharge between 7500 and 8000 m^3/s was computed for the open water case. For the case of an ice covered receiving channel, the peak discharge is lower at about 6500 m^3/s. These values are enormous when compared to the estimated carrier discharge prior to the release of about 1000 m^3/s, and show just how large these events can be.

Equations [35] and [36] in Chapter 2 describe the effects of reflected negative waves on the celerity of the propagating surge (Beltaos, 1995; Henderson and Gerard, 1981). The relative backwater of the ice jam, m_o, is dependant on the change in depth across the toe of the ice jam. According to Hendrson and Gerard (1981), 'typical' values of m_o for ice jam release events are considered to be about 0.5 to 1. This corresponds to V_S of 6.1 m/s and 6.7 m/s, respectively, calculating V_s at G140 with a depth of 2.05 m and a discharge of 850 m^3/s, prior to surge arrival. The water level profile for the ice jam in Run 3a is shown in Figure 5-23. The change in depth across the toe of the ice jam is approximately 7.8 m resulting in a m_o value of 3.8 and V_S of 10.4 m/s, as calculated using the same assumption for m_o of 0.5 and 1.

The dynamic wave approximation of the Saint Venant equations, as discussed in Chapter 2, describes the speed of a surge just downstream of the toe of a released ice jam to be much faster than the mean channel flow velocity by an amount of $\sqrt{gy}$ (where g is gravitational acceleration and y is the wave height). Using a mean channel velocity of 0.92 m/s, assuming the same depth of 2.05 m and discharge of 850 m^3/s, and a height of surge, or peak magnitude, of 4.06 m at G140, the celerity of the surge can be approximated as 7.2 m/s.

Figure 5-24 provides a comparison of surge celerity between Runs 1a, 2a, 3a and 4a (conducted assuming open water conditions in the receiving channel). These model results are compared to the measured values as well as the theoretical surge celerities just

described. All model runs show fairly good agreement with the observed surge celerity between stations G140 and 104. Again, the theoretical value greatly over-predicts the measured surge celerity, as was observed by Henderson and Gerard (1981) when they analyzed the 1979 data from Doyle and Andres (1979). The dynamic wave approximation of the Saint Venant equations also over-predicts surge celerity. Henderson and Gerard (1981) attributed the discrepancy to ice effects; however, the River1-D model does not consider these explicitly and yet does an excellent job of modeling the wave celerity. Consequently, it appears that channel friction is playing a dominant role here (considered in this model but not by Henderson and Gerard (1981) in their classic dam break analysis). Since a different process is occurring between station 57 and 104 as explored in futures sections, surge celerity along this reach is not shown in Figure 5-24.

Peak magnitudes calculated for Runs 1a, 2a, 3a and 4a are compared to the measured peak magnitudes in Figure 5-25. Run 1a, where G140 was set as the upstream boundary and uniform flow was assumed, provides the best match to the measured data, although Run 4a is very similar. Setting G135 as the upstream boundary in Run 2a results in overall peak magnitudes being too low by about 1 m. Run 3a, using HEC-RAS to create an initial water level profile, resulted in a fairly good match of peak magnitude at G140, but the remaining values are 1 m to 2 m too high. Using a water level profile as in Run 3a makes more practical sense for modeling surge propagation events. However, without details of the actual ice jam profile, this approach does not seem viable.

As seen in Figure 5-25, the large decrease in peak magnitude observed over the first 10 kilometers of travel, between G140 and G135, was not accurately modeled. This drastic initial decrease has been explained by complex ice cover behaviour (Jasek, 2003) and thus, likely, improved consideration of the ice cover and water interaction is required in the model to improve this result.

Each of the model runs discussed above compared the computational solution assuming open water in the receiving channel (no ice resistance effects) and assuming an

ice covered condition persisted in the receiving channel. The intent was that these two extremes would bracket the range of actual physical behavior. For Runs 1, 2 and 4 there was no major difference in water level or peak magnitude of the calculated surge between these two extremes, although a flatter wave shape was consistently observed for the case where an ice covered condition was assumed in the receiving channel. Run 3 resulted in more significant differences between the two assumed receiving channel conditions. Water levels and peak magnitudes of the surge were larger, and a smaller surge celerity was observed along the entire study reach when an ice covered condition was assumed in the receiving channel. Overall, these two extremes were not found to bracket the actual conditions, which means that effects of the ice within the ice run itself are likely significant and will have to be considered before improved results can be obtained.

One of the components of the Saint Venant equations solved using River1-D is conservation of mass. Measured stage hydrographs for the open water condition were converted to discharge hydrographs by applying a uniform flow approximation (Chezy's equation). By taking the area underneath the discharge hydrograph, the volumes of the surge was calculated to be 29.3×10^6 m^3, 14.9×10^6 m^3, 20.2×10^6 m^3 and 28.8×10^6 m^3 at stations G140, G135, 132 and G130, respectively. The fact that these volume calculations do not match perfectly, as mass must be conserved, additional evidence is provided that the ice jam stalled along the study reach.

Modeling the Wave Propagation under the Intact Ice Cover

The second part of the 2002 release event involved the propagation of the wave that released from the newly formed ice jam at station 104. This ice jam extended to a length of 8 km with its toe most likely partially grounded (Figure 5-26). This was evidenced by the fact that large gravel bars were visible at the toe site, once open water conditions were restored after the breakup season, as seen in Figure 27.

As discussed in the previous chapter, the wave was measured at stations 90 and 57 as it propagated underneath the intact ice cover. As model Run 1 illustrated, clearly not all of the water in the surge wave made it down past the new jam toe. Therefore, it is

interesting to examine what proportion of the water actually did escape and the numerical model can help with that assessment. Two types of model runs were performed on the sub-reach downstream of station 104, as summarized in Table 5-6.

Table 5-6. Description of model runs performed to analyze the wave propagation under the intact ice cover.

Run 5	104 set as upstream boundary. Uniform flow was assumed to calculate an inflow discharge hydrograph based on the observed stage hydrograph at this location.	
	Run 5a	Varying underside ice roughness.
	Run 5b	Varying ice thickness.
Run 6	Match stage hydrographs at stations 90 and 57 to determine the wave shape that likely released from the ice jam formation at station 104.	

Model runs 5 and 6 involve an intact ice cover along the entire study reach.
All model runs used roughness heights, k, to describe resistance characteristics unless otherwise stated.

Model Parameters

As mentioned in the Model Parameters section for the event in the upper reach, all model runs, including Runs 5 and 6, used a time increment of 2 seconds, or 0.0005 hours. This value ensured a Courant numberless than 0.5 was achieved. This time step of 2 seconds was used for both the steady and unsteady parts of the model run, using the same number of maximum iterations per time step as previously described, 5 and 25 respectively. The only difference between the analysis in this lower reach compared to the upper reach, is that the total duration for Run 6 was extended to 30 hours to capture the entire falling limb of the wave at station 57.

Run 5

In Run 5 a uniform flow approximation was used to determine an inflow discharge hydrograph for the upstream boundary condition at station 104. As the measured data at station 104 only extended to just past the peak, a dimensionless comparison with the hydrograph shape at station 90 was used to approximate the falling limb of the hydrograph at station 104. A downstream ice thickness of 0.6 m was used,

based on measurements obtained by RMWB within the area of Fort McMurray on March 6, 2002. An ice underside roughness of k_i = 0.0038 m (corresponding to an n_i = 0.015) was used, as in previous ice covered model runs. To better match the measured water levels at stations 90 and 57, various ice thickness (Run 5a) and ice underside roughness (Run 5b) values were investigated.

Initial Conditions

Chezy's equation was used to calculate the discharge hydrograph at the upstream boundary for all of the various ice thickness, t_i, and underside roughness, k_i, values modeled. A summary of the initial conditions for each model run is summarized in Table 5-7. The discharge in this table is for station 104 at time zero. The corresponding depth, ΔH, was applied to all other nodes to obtain an initial water level profile.

Table 5-7. Initial conditions for Run 2 using various ice thickness and underside roughness values.

	t_i (m)	k_i (m)	Q (m^3/s)	ΔH (m)
Run 5a	0.6	0.00381	777	2.138
	0.6	0.244	535	2.128
	0.6	15.6	197	1.733
Run 5b	0.2	0.244	737	2.093
	0.4	0.244	633	2.111
	0.6	0.244	535	2.128
	0.8	0.244	445	2.146
	1.2	0.244	284	2.181

Boundary Conditions

As in model Runs 1 and 2, the upstream boundary condition consisted of a discharge hydrograph calculated using a uniform flow approximation applied to the measured water level data at this upstream boundary (in this case at station 104). Since the measured data ceased just after the peak water level was attained, the falling limb of the wave at 104 was approximated using a non-dimensional comparison with the

measured wave form at station 90. A stage hydrograph was used as the downstream boundary condition, with the estimated stage remaining constant throughout the model run (as in earlier runs, this downstream boundary was set well downstream of the reach of interest).

Results

The results of the model run with an ice thickness of 0.6 m and an ice roughness height of 0.0038 m, created a wave that was much too high, in terms of water level, and that was traveling too fast. Therefore, additional model runs were performed varying the roughness height of the underside of the ice surface, k_i. The results for a roughness height of 0.0038 m (n_i = 0.015), 0.244 m (n_i = 0.030) and 15.6 m (n_i = 0.060) are shown in Figure 5-28.

Compared to the hydrograph shape obtained using a roughness height of 0.0038 m, a larger roughness height lowers the peak magnitude by flattening the shape of the hydrograph. An increased ice roughness height also slows the celerity of the propagating wave. The results in Figure 5-28 show the roughness height of 15.6 m as the best model results; however this large of a roughness height is not reasonable. Also, the overall water levels before and after the wave is still too high. Possibly the most realistic roughness height in this area would be 0.244 m, which was used when analyzing different ice thicknesses in Run 5b.

A roughness height of 0.244 m might appear high for the underside of an ice cover, but various stages in ice deterioration can cause the underside of the ice to become fairly rough. Ice ripples that form on the underside of an ice cover can cause this level of roughness. Carey (1966) obtained observations of such ripples on the St. Croix River in Wisconsin. Of the twelve measurements obtained, the average wave length was 19.8 cm, the wave amplitude was 2.1 cm, and the resulting Manning's n was approximated to be between 0.010 and 0.028. Similar measurements were made on May 3, 1992, of ice ripples on the Mackenzie River at Fort Providence, NWT, as seen in the photograph of Figure 5-29. The wave length was about 18 cm to 20 cm, the wave amplitude was 8 cm,

and resulted in a calibrated roughness of n_i = 0.030. The photograph in Figure 5-30 shows evidence of ice ripples along the study reach on the Athabasca River, which appear similar to those on the Mackenzie River. This photograph was taken on April 19, 1985. Due to past measurements on the St. Croix River and the Mackenzie River, an ice underside roughness height of 0.244 m (n_i = 0.030) is considered realistic and was thus used in further analyses in this section.

Although an ice thickness of approximately 0.6 m was measured prior to the release event, ice thicknesses of 0.2 m, 0.4 m, 0.6 m, 0.8 m and 1.2 m were all modeled and results are plotted for comparison in Figure 5-31. Significant changes in water level can be observed prior to the arrival of the wave at stations 57 and 90. Although a steady model run was performed, the spatial variation in discharge along the study reach was not able to be attained. This further suggests that a much smaller discharge released underneath of the ice cover after the new ice jam formed at station 104. Neglecting this and focusing on the actual wave propagation, it is seen that the magnitude and celerity of the modeled waves change little with varying ice thickness. Interestingly, the smallest ice thickness of 0.2 m gives the highest peak magnitude at station 90, but the lowest at station 57. This could largely be due to the fluctuations associated with developing the initial water level conditions, as most apparent at station 57. Although the variation in wave celerity is small, the thicker ice condition does slow the propagation of the wave.

By varying both ice roughness and ice thickness, a realistic combination of ice characteristics was not obtained to match the measured waves at stations 90 and 57. The results from Figures 5-28 and 5-31 suggest then, that the assumption of a uniform flow rating curve is not realistic. Clearly the arresting of the ice run and re-formation of the jam are highly dynamic processes and so this is not surprising. With these results and those from Run 1, it is clear that it is unlikely that all of the water in the surge passed downstream. Consequently, Run 6 was devised to attempt to quantify approximately what proportion of the water actually escaped downstream.

Run 6

As discussed above, the purpose of Run 6 was to attempt to quantify how much of the original surge actually propagated downstream of the newly formed ice jam at station 104. This was achieved by trial and error, essentially trying different inflow hydrograph shapes and sizes at station 104 and routing them downstream under the intact ice cover, to see if they matched the observed water levels at the downstream stations.

Initial Conditions

Since Run 5b showed the thickness of an ice cover had very little effect on the overall shape of the modeled hydrograph, a thickness of 0.6 m (as measured by RMWB) was used in Run 6. An ice underside roughness of 0.244 m (n_i = 0.030) was selected as the most likely for a deteriorated ice cover. This roughness value is in line with what was reported for ice ripples on the St. Croix River and the Mackenzie River, as previously discussed. The final shape of the new inflow hydrograph resulted in an initial discharge of 170 m^3/s with a corresponding depth of 1.34 m. This depth was applied to all of the nodes as a first guess of the initial conditions.

Boundary Conditions

The initial shape of the estimated inflow hydrograph at station 104 was achieved by adjusting the measured water levels and then using Chezy's equation to estimate the associated discharges (a simple uniform flow assumption). Since the measured stage hydrograph at station 104 was incomplete, its full shape had to be approximated. A triangular shape was first tried, and this shape was then further refined until computed water levels matched the observed values at station 90, and to a lesser degree, station 57. Not only did this require adjustment to the water level magnitudes at station 104, but also their timing. The resulting stage hydrograph, which had a 5 minute time interval and a total duration of 30 hours, is shown as the 'adjusted data' in Figure 5-23. As in earlier model runs, the downstream boundary condition consisted of a specified constant water level, set well downstream of the reach of interest.

Results

Based on this trial and error procedure, an inflow hydrograph was developed at station 104 which produced a reasonably good match to the observed water levels at station 90, downstream. The computed water levels from this run are presented in Figure 5-32 for station 104, 90 and 57 At station 104 the computed water levels based on this inflow hydrograph (shown as 'River1-D'), are relatively close to the values derived with Chezy's equation assuming uniform flow (shown as the 'adjusted data'). As mentioned, the match is very good at station 90, except for some small variations on the falling limb of the hydrograph. From these results, it could be interpreted that a short pulse of water escaped under the intact ice cover about 1.3 hours after the ice jam arrested at 104.

The water level actually matches quite well at station 57 also, especially compared to all previous runs attempted, particularly in terms of the wave speed, which seems reasonably well approximated by the model. The measured hydrograph was slightly higher overall by about 0.1 m to 0.2 m, and was flatter with a less steep rising limb than the computed hydrograph here. The shapes of the computed and measured falling limbs compare reasonably well. Increasing the roughness between stations 90 and 57 would cause the hydrograph to flatten, but would also delay the peak timing, when the celerity is already reasonably matched. Increasing the ice thickness may raise the overall water level, but aerial observations described in Chapter 4 showed the ice cover between stations 90 and 57 to be more deteriorated with some open water areas as compared to the more solid ice cover between stations 104 and 90. Therefore, using a thicker ice cover between stations 90 and 57 to increase the overall water level is physically unrealistic. Most likely, the rectangular channel geometry approximation would account for this difference, and so the first thing to explore would be the effect on results when using natural channel geometry.

Figure 5-33 shows the corresponding computed discharge hydrographs at the three stations for Run 6. The maximum discharge is substantially less than the discharge measured in the upper portion of the study reach. To evaluate just how realistic this deduced inflow hydrograph at station 104 was, conservation of mass was evaluated by

determining the volume of water in the wave by calculating the area underneath of the modeled discharge hydrograph. The mass of the new wave must be conserved in comparison to the waves at stations 90 and 57. The volumes at stations 90 and 57 are 10.9×10^6 m^3 and 10.3×10^6 m^3, respectively. The volume at station 104 was calculated to be 10.7×10^6 m^3, which matches the volumes at 90 and 57 within about 6%. These volumes are significantly lower than those calculated at stations G140, G135, 132 and G130 as 29.3×10^6 m^3, 14.9×10^6 m^3, 20.2×10^6 m^3 and 28.8×10^6 m^3, respectively. Therefore, the larger volumes experienced upstream are likely being stored within the newly formed ice jam poised at station 104 and releasing only about 10×10^6 m^3 underneath of the ice cover.

Looped rating curves were also analyzed for this deduced inflow hydrograph at station 104, as shown in Figure 5-34. Compared to the looped rating curves of the other analysis methods discussed (all curves being plotted on the same scale), the overall discharges are drastically smaller but still show a loop, meaning the wave is partially dynamic in nature. According to wave approximations of the Saint Venant equations discussed in Chapter 2, the diffusive wave speed (dominated by friction forces) is about 1.5 times the mean channel flow velocity. Based on a discharge of 170 m^3/s determined from Run 6, a diffusive wave speed of 0.25 m/s, 0.24 m/s and 0.22 m/s correspond to stations 104, 90 and 57, respectively. Measured wave speeds of 0.55 m/s and 0.61 m/s between stations 104 and 90 and between 90 and 57, are larger than the diffusive wave speeds but are still fairly diffusive in nature.

Discussion

Since Runs 1, 2, 3 and 4 were unable to reproduce the measured hydrographs at stations 90 and 57, just this lower section of the reach was analyzed. Run 5 used a uniform flow approximation with the measured stage hydrograph at station 104 as the upstream boundary condition. However, the modeled waves at stations 90 and 57 were found to be propagating too fast with water levels that were much too high.

Additional model runs were performing using the same upstream boundary condition, but varying the ice underside roughness and ice thickness. Three roughness heights were used to describe the underside of the ice surface. Results showed that increasing roughness flattened the hydrograph, decreasing both the peak magnitude and the celerity of wave propagation. However, the overall water levels still appeared much too high. A decrease in water level was anticipated by varying the ice thickness. Therefore, a range of ice thickness values between 0.2 m and 1.2 m was modeled. Results showed almost negligible change to the peak magnitude, but a slight decrease in the celerity of the wave was observed with increasing ice thickness. Although various effects of ice cover characteristics were observed, these modeling attempts were unsuccessful in capturing the wave measured at stations 90 and 57.

Run 6 was used to explore the possibility that the wave that released after the formation of the ice jam at station 104 was much smaller than a uniform flow approximation would suggest, attempting to deduce what the escaping wave actually looked like using trial and error. Modeled results showed the new wave form at station 104 to be a short pulse with a larger peak magnitude that released about 1.3 h after the ice run arrested. This new wave form appeared to match the celerity of the waves measured at stations 90 and 57. However, the overall magnitude of the computed hydrograph at station 57 was about 0.1 m to 0.2 m too low. In comparison to all other modeling attempts, this is fairly good match and is within the expected error associated with using approximate channel geometry.

To evaluate the consistency of the deduced discharge hydrograph escaping from the newly formed ice jam, conservation of mass was evaluated by determining the volume of water in the wave by calculating the area under the discharge hydrograph. These calculations showed much larger volumes in the upper reach, with only about 10×10^6 m^3 escaping underneath of the ice cover at 104. This decrease in volume downstream of the newly formed ice jam is likely due to the large volume of water stored within the new, 8 km long ice jam.

Summary

Five categories of model runs were conducted to analyze the surge wave that traveled along the Athabasca River during breakup 2002. The measured data at stations G140, G135, 132, G130, 104, 90 and 57 all provided invaluable data to study the movement and attenuation of this surge. Runs 1 to 4 explored various ways of modeling the dynamic surge released from the ice jam upstream near Crooked Rapids (upstream of station G140). Runs 5 and 6 were used to investigate the wave that escaped from the re-formed ice jam at Mountain Rapids (upstream of station 104).

The best results for modeling the initial surge came from Run 1, which involved setting station G140 as the upstream boundary and using uniform flow to calculate an inflow discharge hydrograph from the measured water level data. Run 4 was incredibly similar to Run 1, which used the looped rating curve from Run 3 to create the inflow discharge hydrograph at G140 based on the measured stage hydrograph. Therefore, using a uniform flow approximation, which does not seem theoretically applicable, appears adequate for modeling purposes with the current available data.

All other runs provided additional insight to the nature of this event. By setting station G135 as the upstream boundary (Run 2), a better surge celerity was obtained but with lower water levels, suggesting that ice effects become less important as the surge propagates further. In Run 3, HEC-RAS allowed for an initial water level profile to be created that theoretically seemed to represent the event more accurately, but the model was not able to match the attenuation of such a dramatic event. This illustrates the importance of measuring the actual profile of the ice jam before release, something that was not possible in this case due to the remote location (and lack of vertical survey control) as well as the time of occurrence (at night). These analyses also provided a comparison of results assuming open water versus ice covered conditions in the receiving channel, which were expected to envelop the full range of behaviour. However, they did not, suggesting that the effects of ice within the ice run are equally or more important. Also, the effects of calculating the friction slope using Manning's versus Chezy's equation were evaluated. Results supported the use of roughness height as a better option

for surge wave propagation, since the decreasing amount of resistance associated with increasing water levels can automatically be accounted for in the latter case.

Runs 5 and 6, analyzing the downstream section from stations 104 to 57, provided evidence that the discharges deduced using a uniform flow assumption with the measured hydrograph at station 104, do not necessarily describe the wave that continued to propagate underneath of the intact ice cover downstream. By matching water level hydrographs at downstream stations, a possible discharge hydrograph emanating from the newly formed jam was deduced. Wave volume calculations showed a drastic decrease in volume between the upper and lower portions of the study reach. This is likely attributable to the water and ice stored within the ice jam that formed at station 104.

Modeling of the 2002 measured surge wave provides an idea of the shear size of such events. The discharge at the peak of the wave at station G140 (near the toe of the released ice jam) was modeled to be between 7500 m^3/s and 8000 m^3/s for an open water condition, which understandably explains the past destruction resulting from similar events. Not only has the celerity of the surge been accurately modeled, but the shape of the wave including the peak magnitude has been somewhat captured. From this research, it has been found just how complex an ice jam release event is. The next phase of research should study the processes of the ice cover in the receiving channel and the progression of the ice within the ice jam to further understand the propagation of such surge waves.

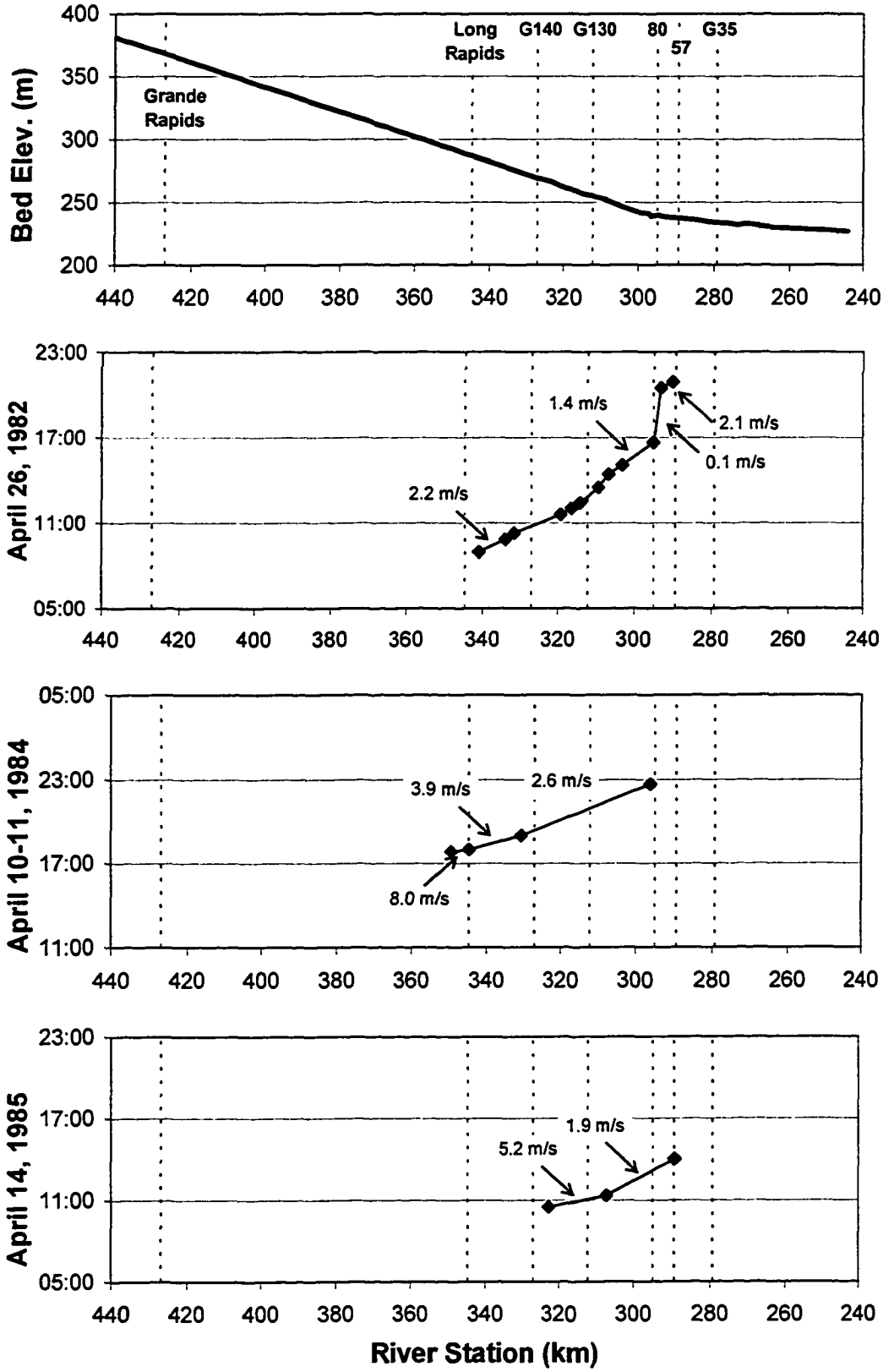

Figure 5-1. Wave celerity of Type 1 ice jam release events.

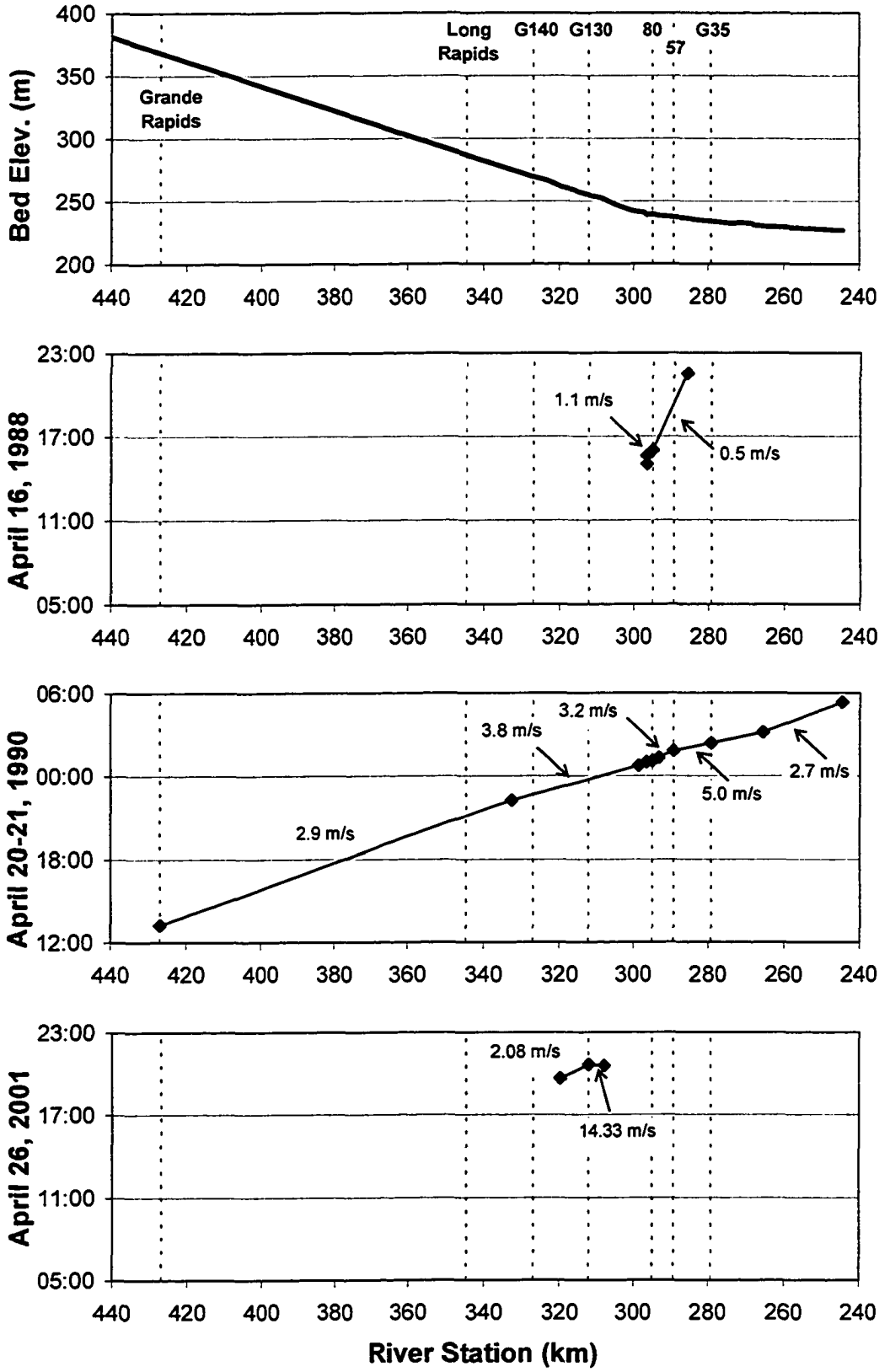

Figure 5-1 Continued. Wave celerity of Type 1 ice jam release events.

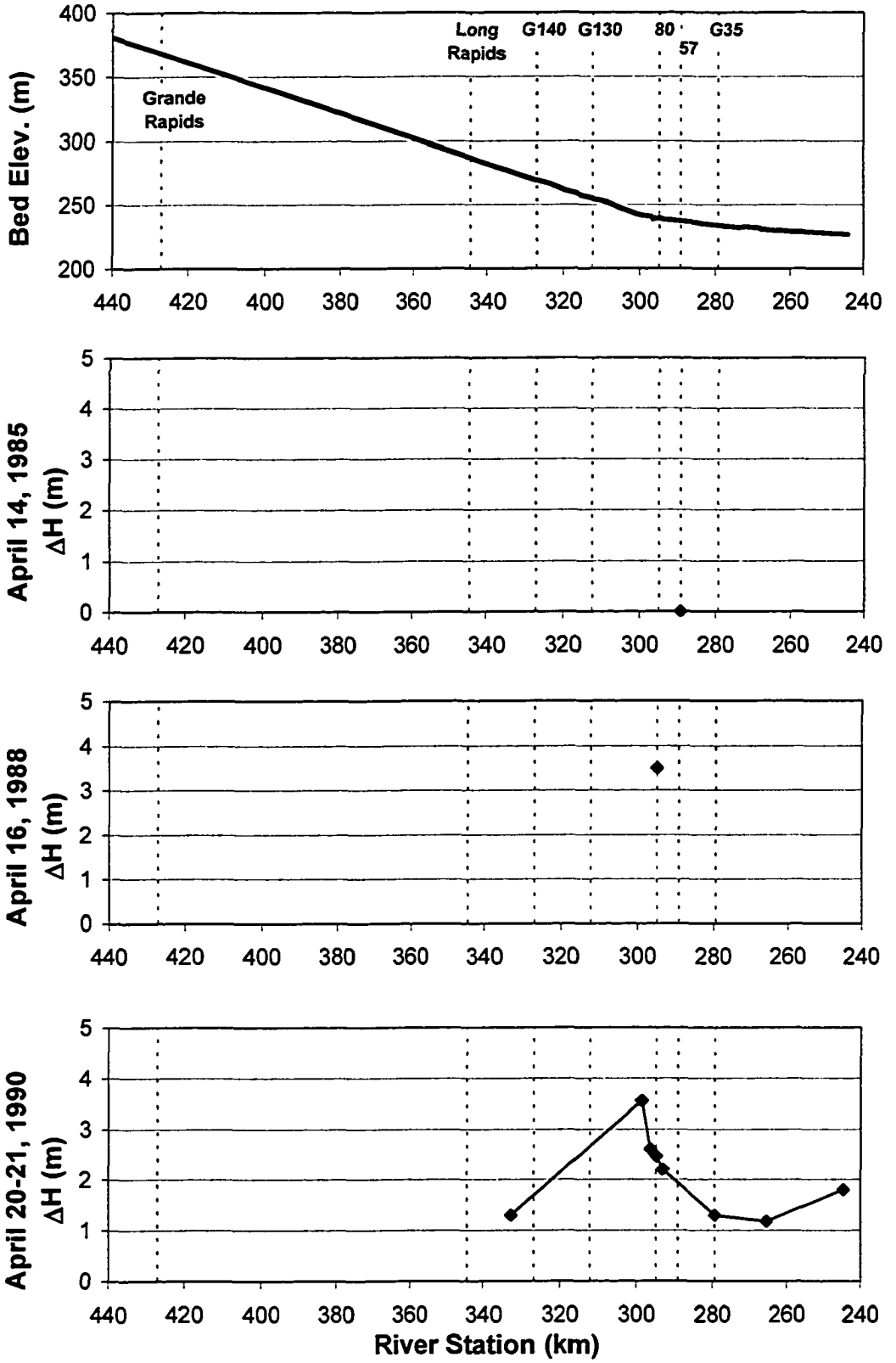

Figure 5-2. Magnitude attenuation of Type 1 ice jam release events.

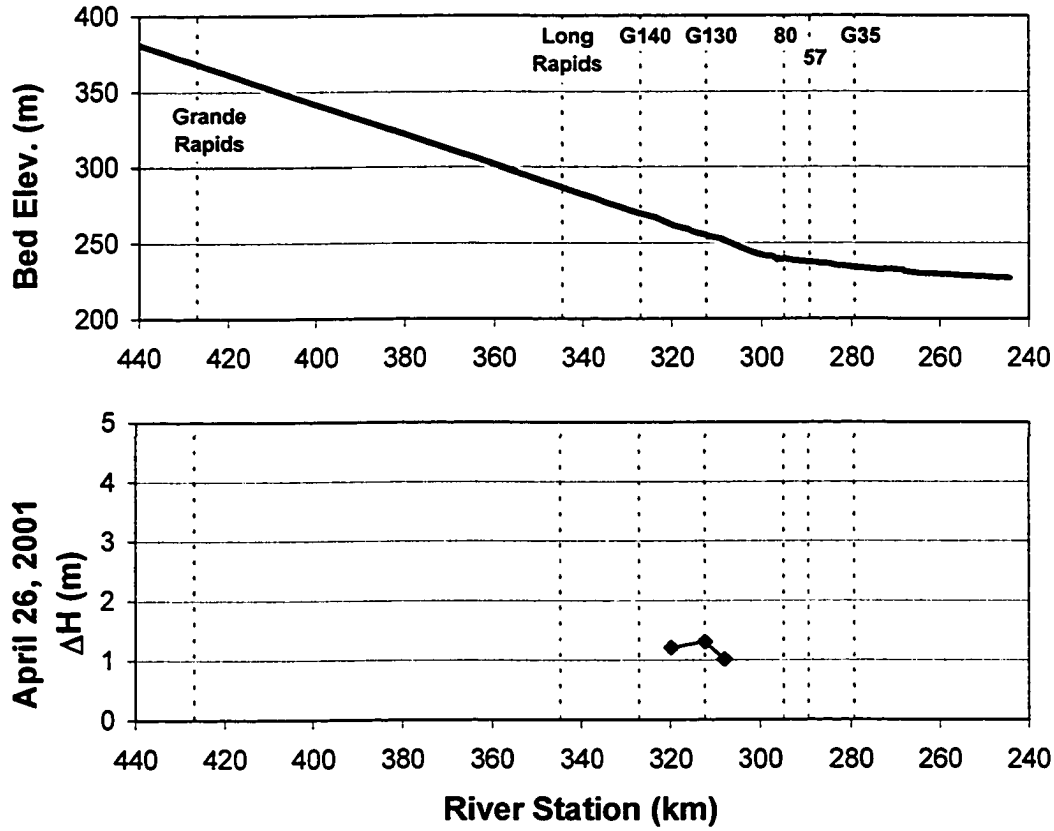

Figure 5-2 Continued. Magnitude attenuation of Type 1 ice jam release events.

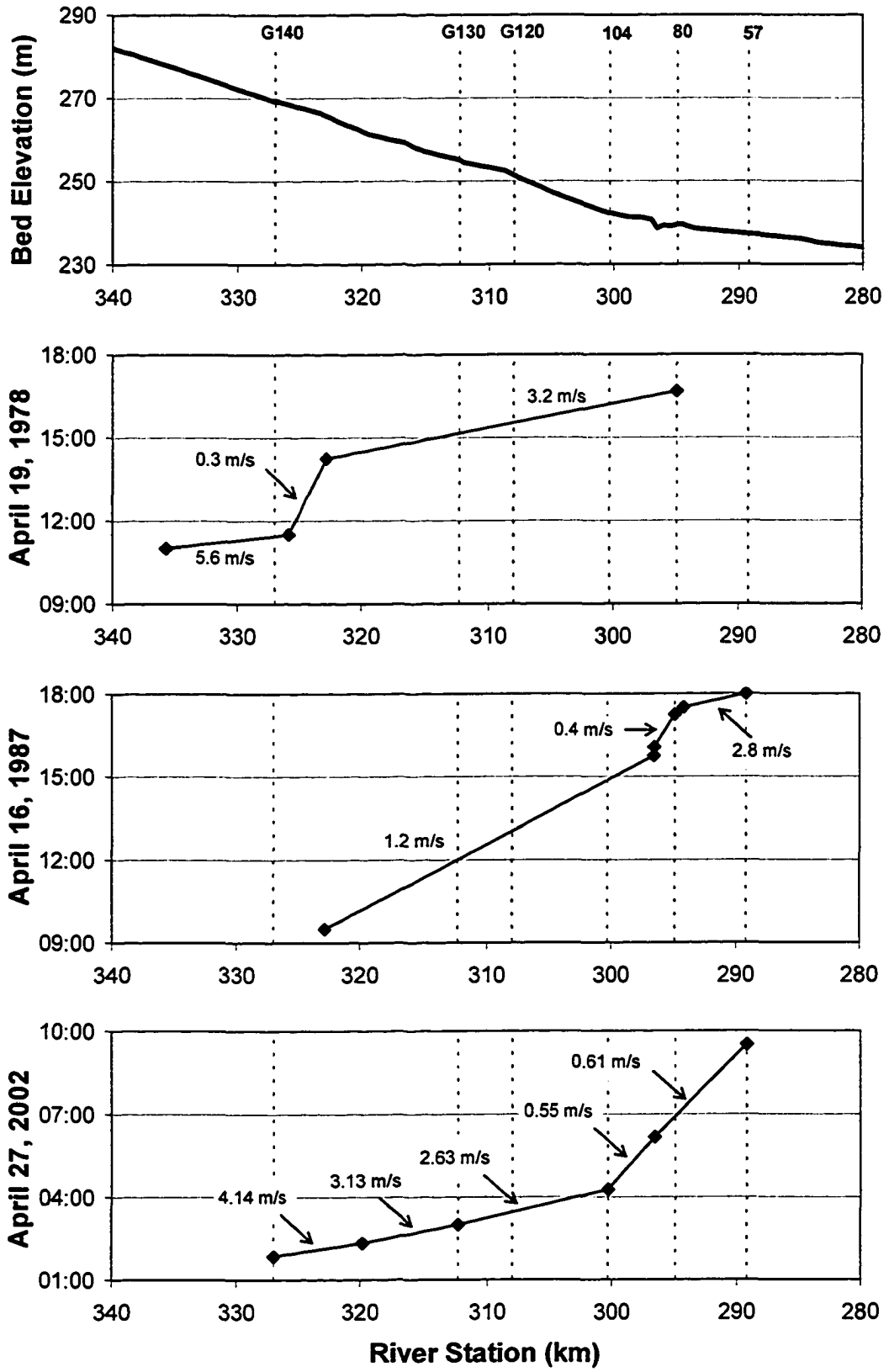

Figure 5-3. Wave celerity of Type 2 ice jam release events.

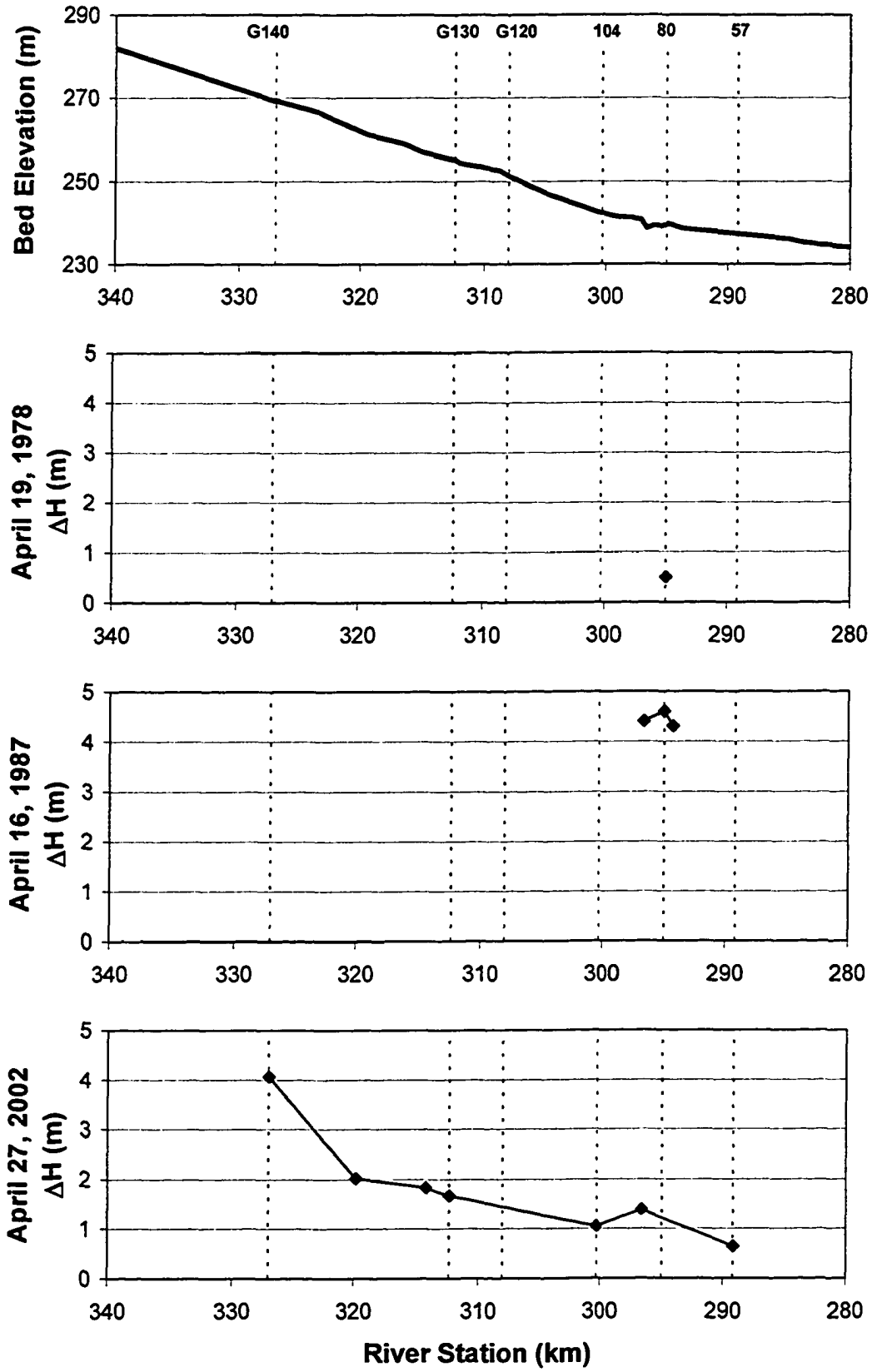

Figure 5-4. Magnitude attenuation of Type 2 ice jam release events.

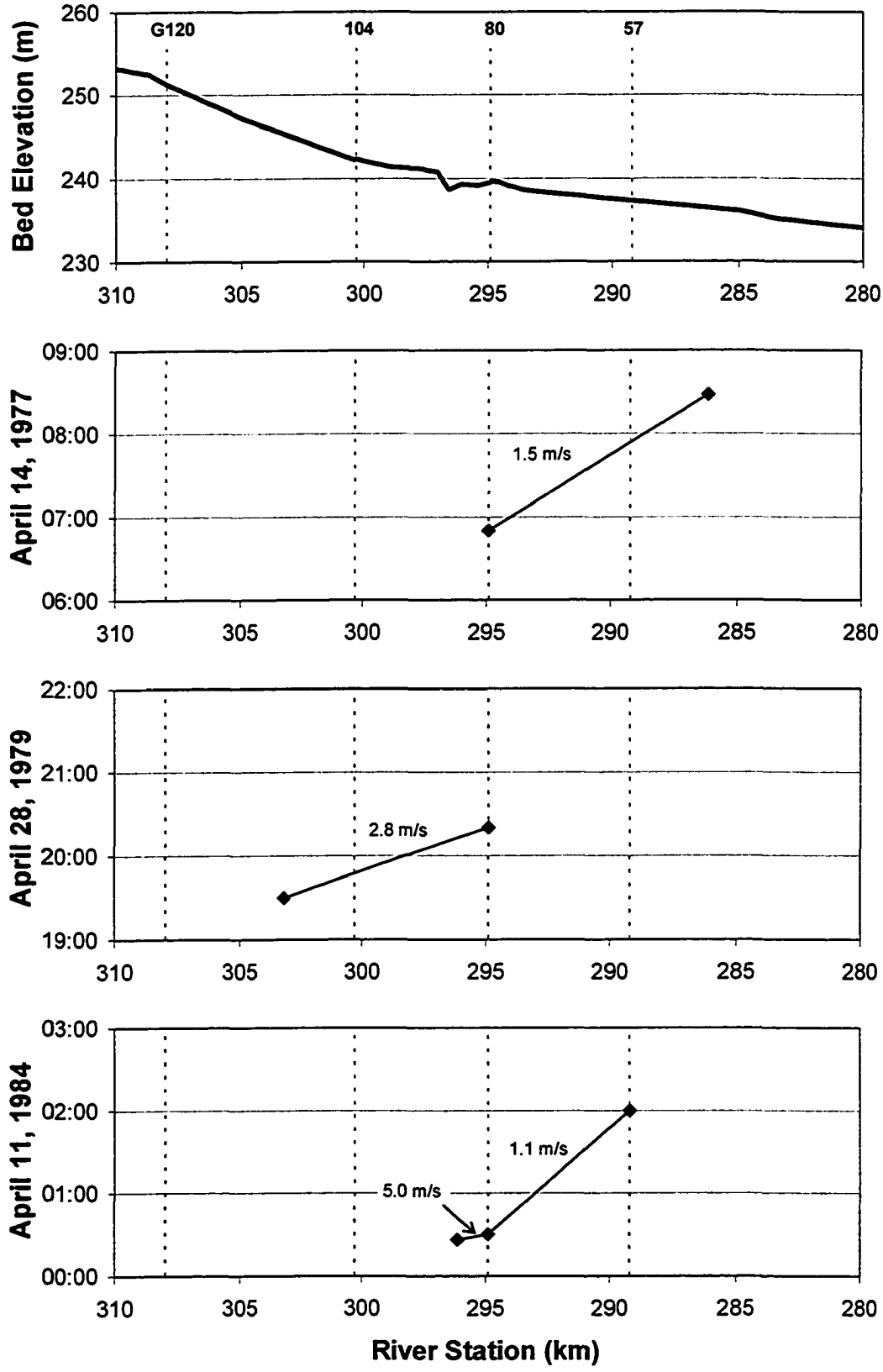

Figure 5-5. Wave celerity of Type 3 ice jam release events.

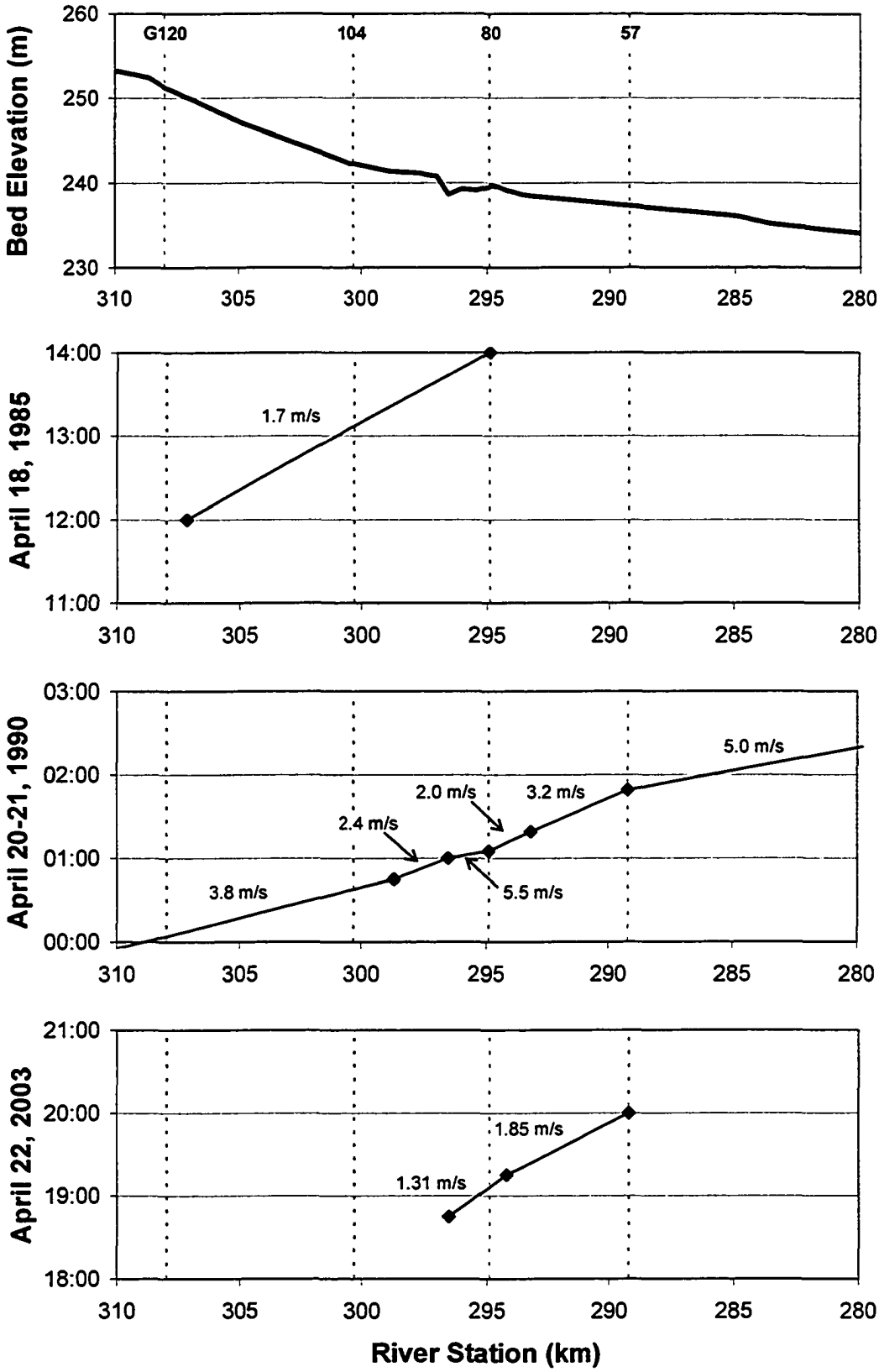

Figure 5-5 Continued. Wave celerity of Type 3 ice jam release events.

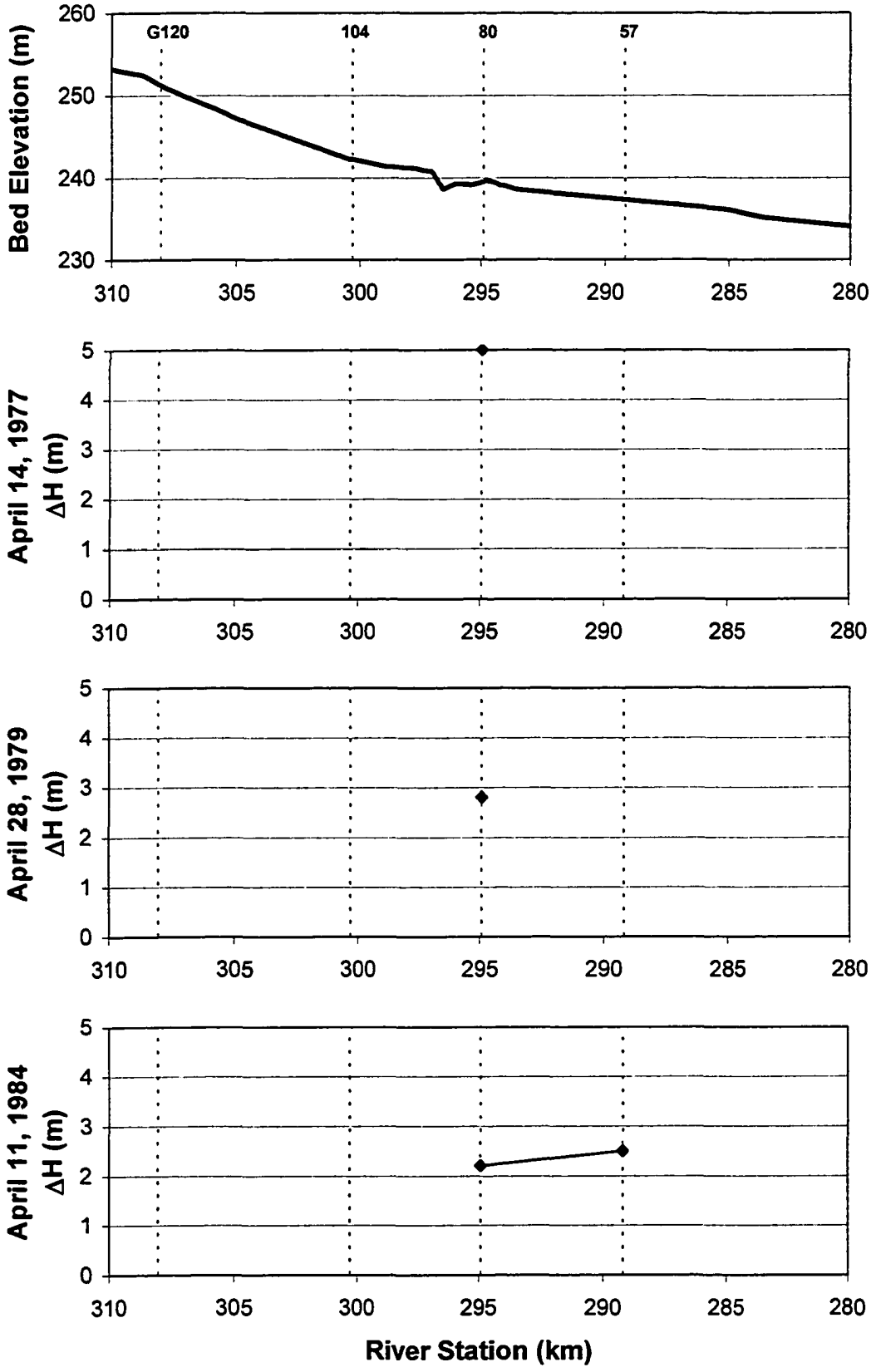

Figure 5-6. Magnitude attenuation of Type 3 ice jam release events.

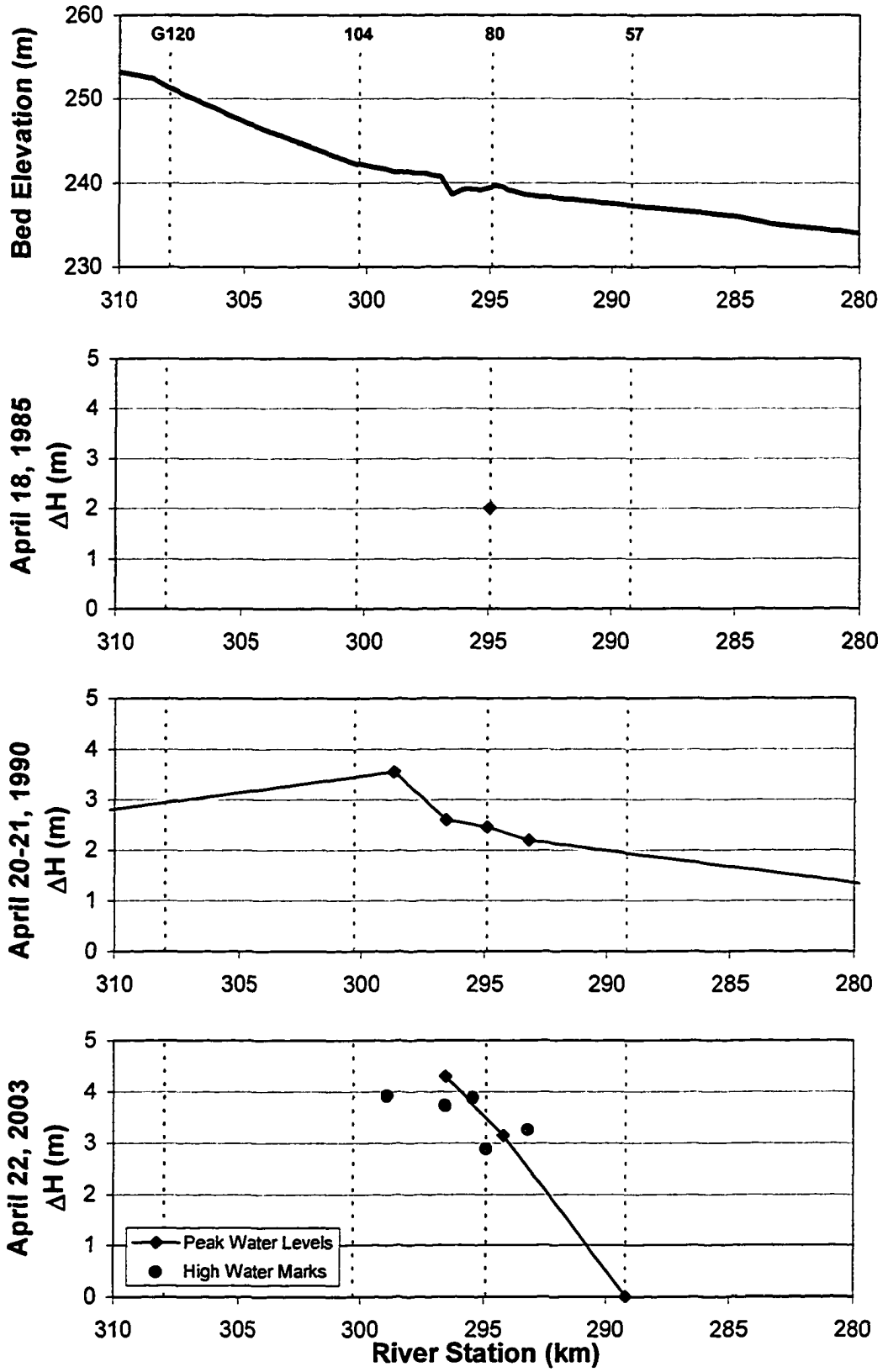

Figure 5-6 Continued. Magnitude attenuation of Type 3 ice jam release events.

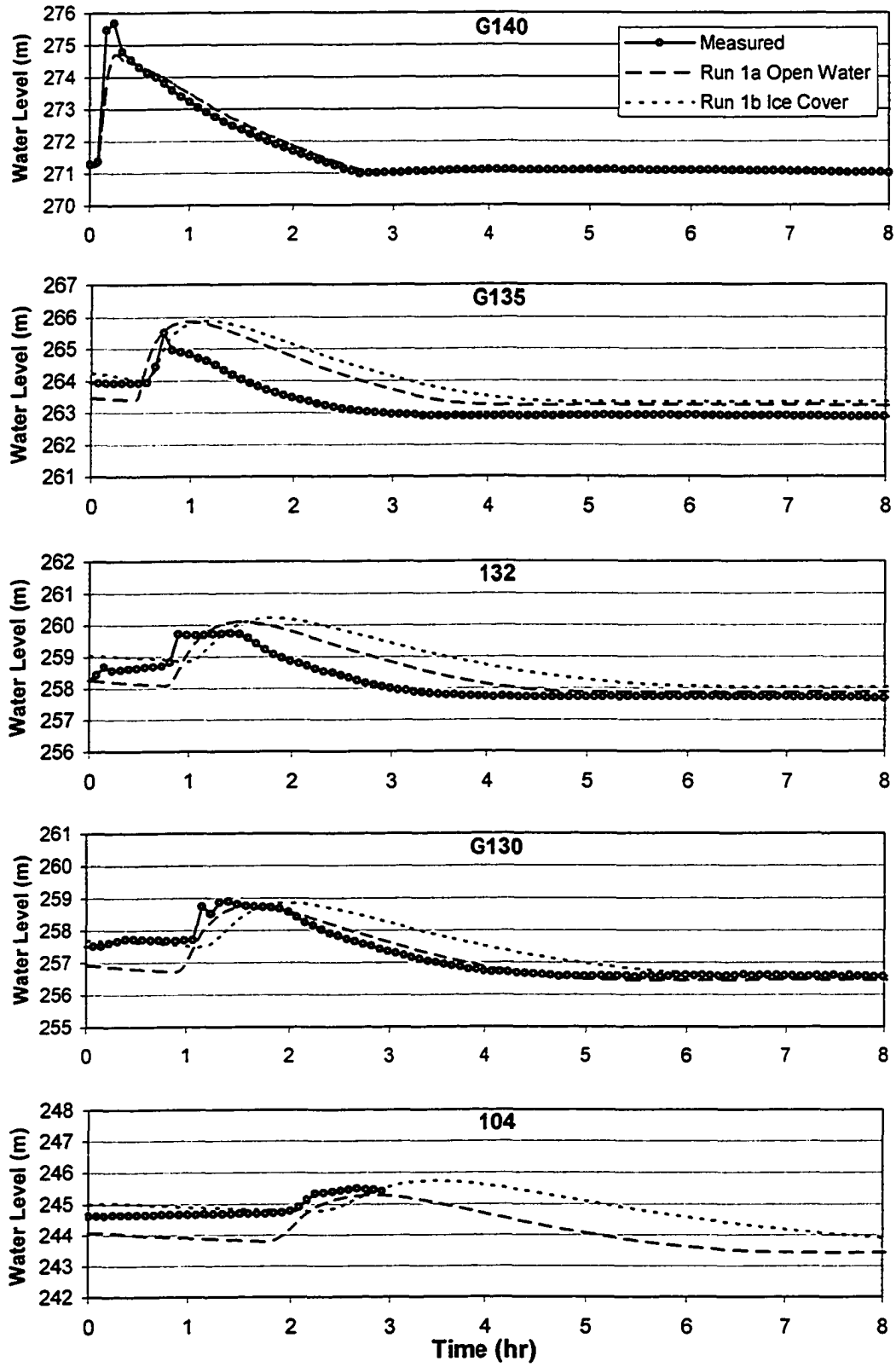

Figure 5-7. Water levels in upper portion of the study reach for Run 1.

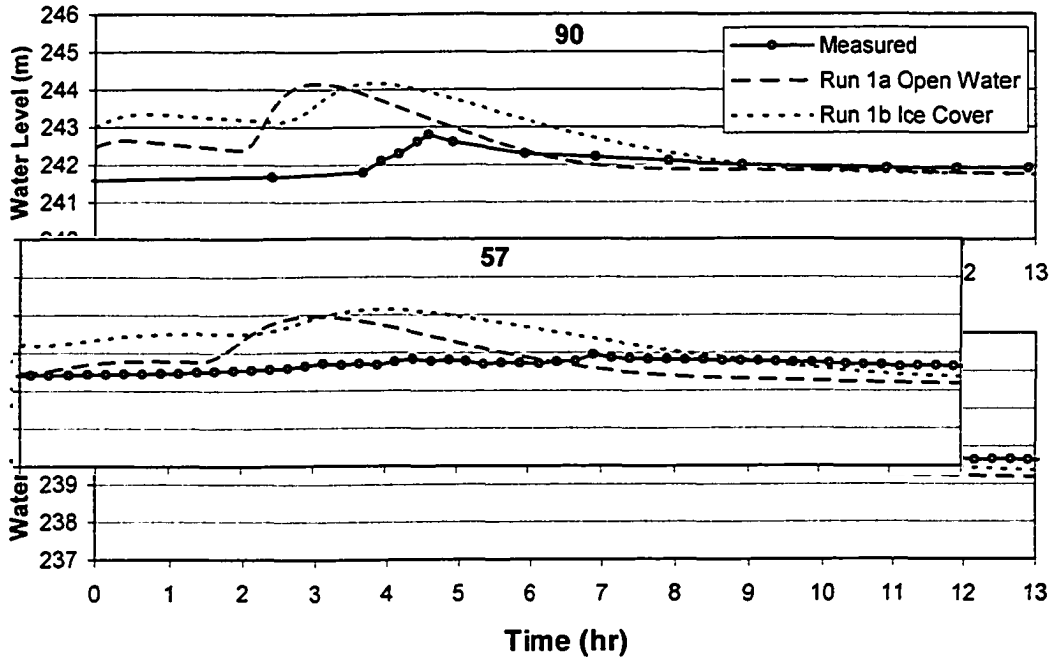

Figure 5-7 Continued. Water levels in lower portion of the study reach for Run 1.

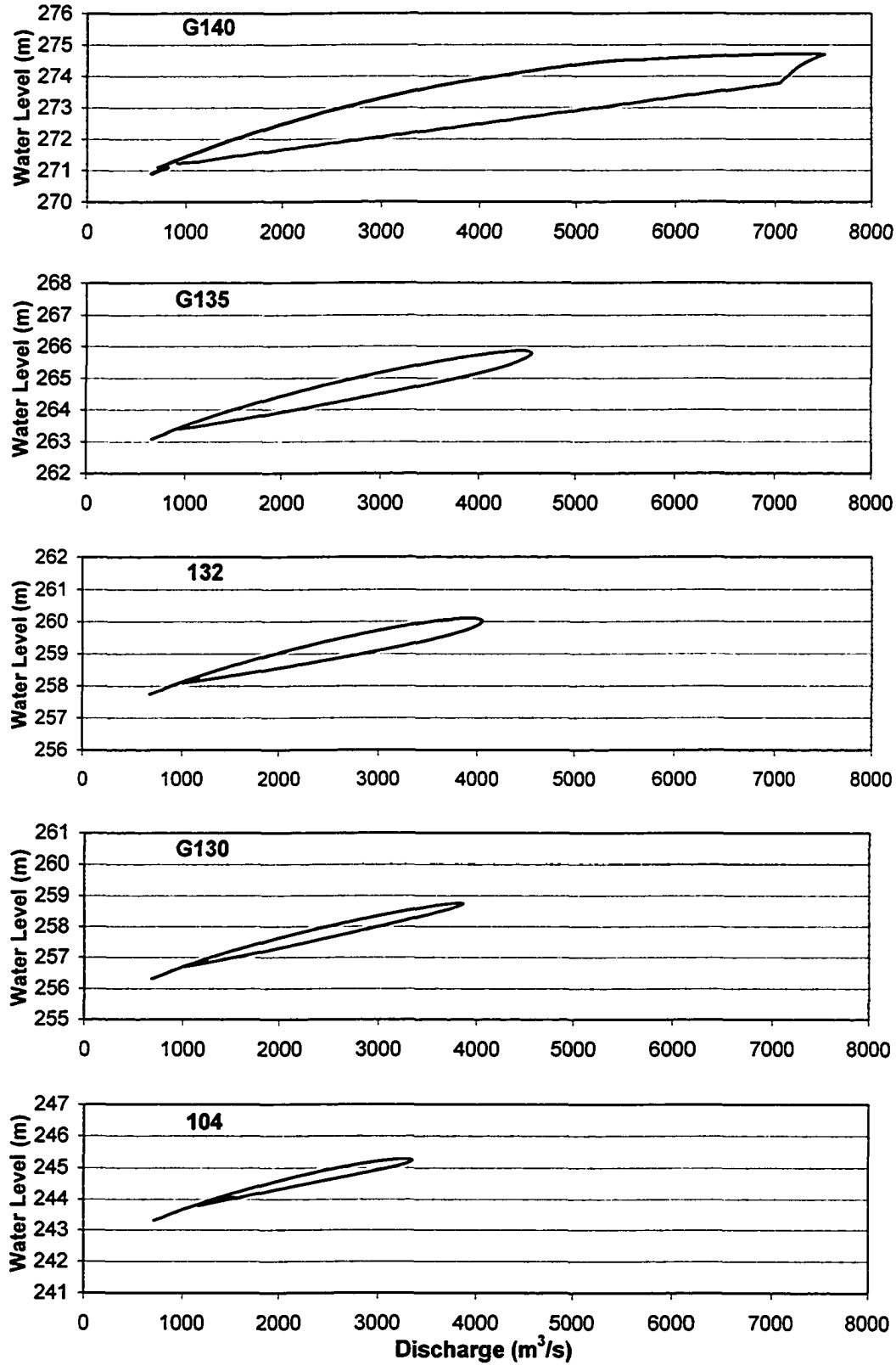

Figure 5-8. Looped rating curves in upper portion of the study reach for Run 1a.

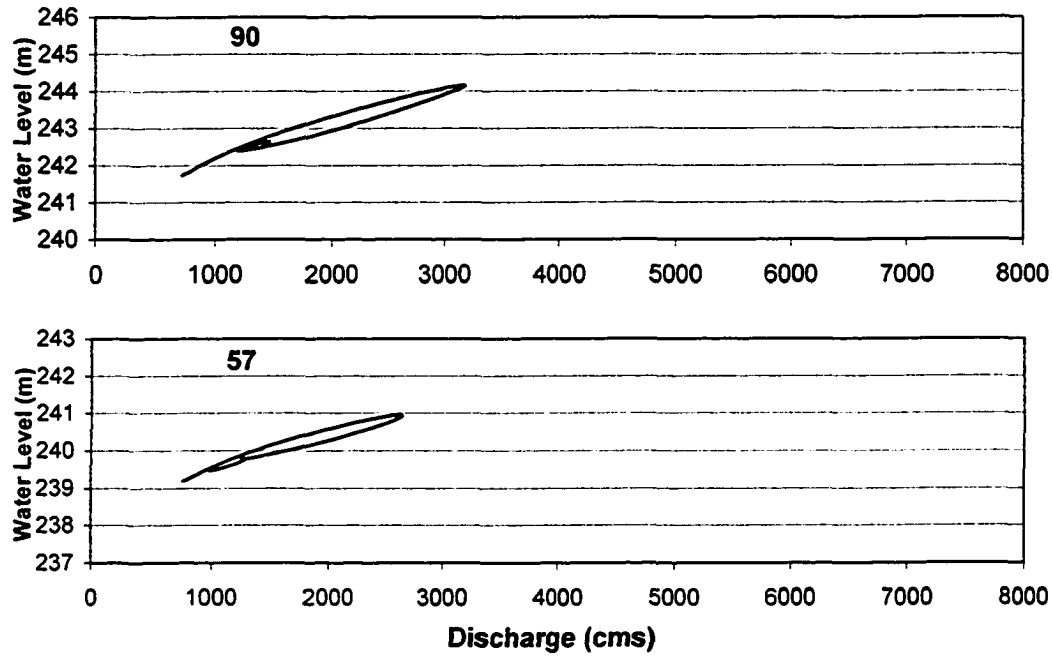

Figure 5-8 Continued. Looped rating curves in lower portion of the study reach for Run 1a.

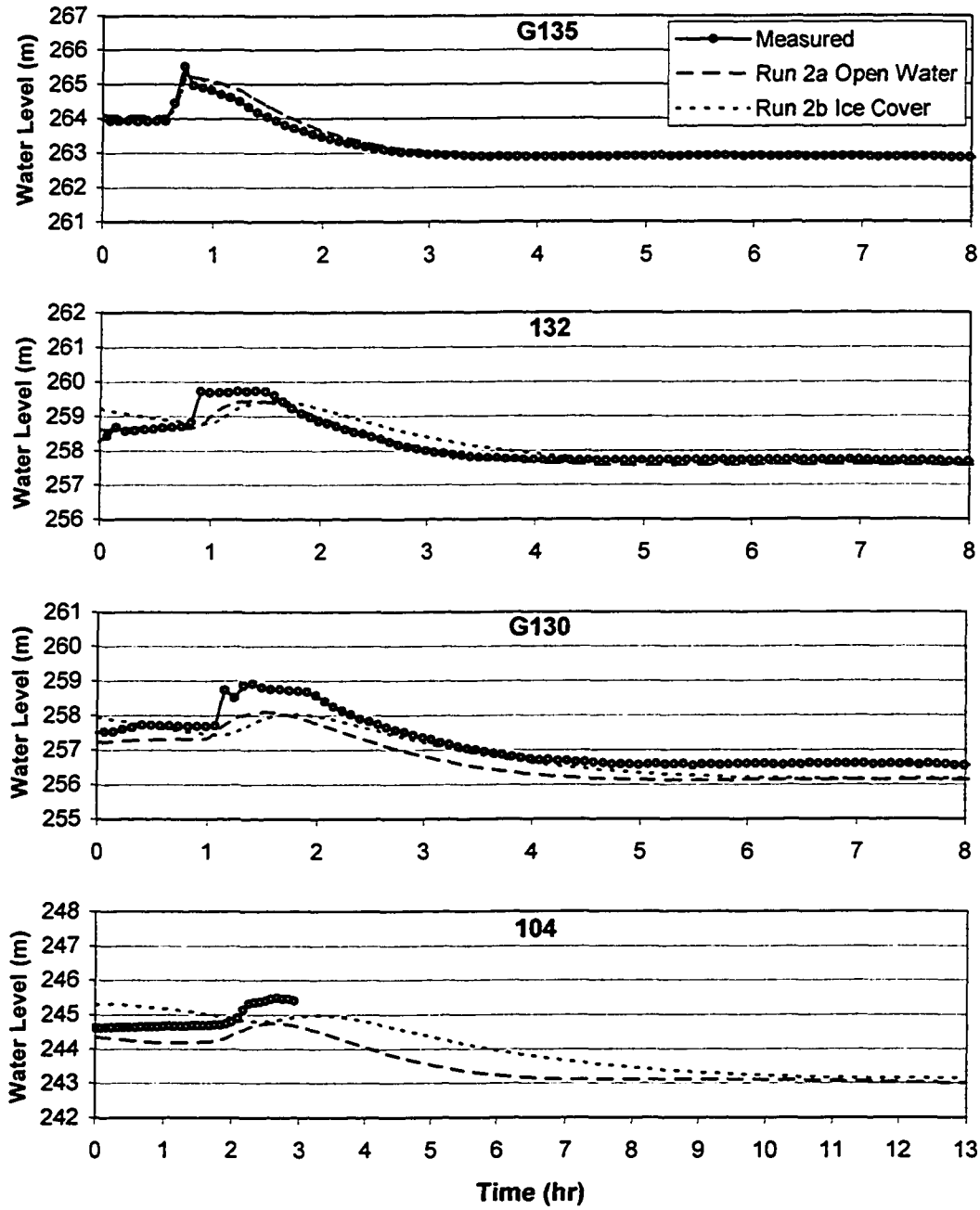

Figure 5-9. Water levels in upper portion of the study reach for Run 2.

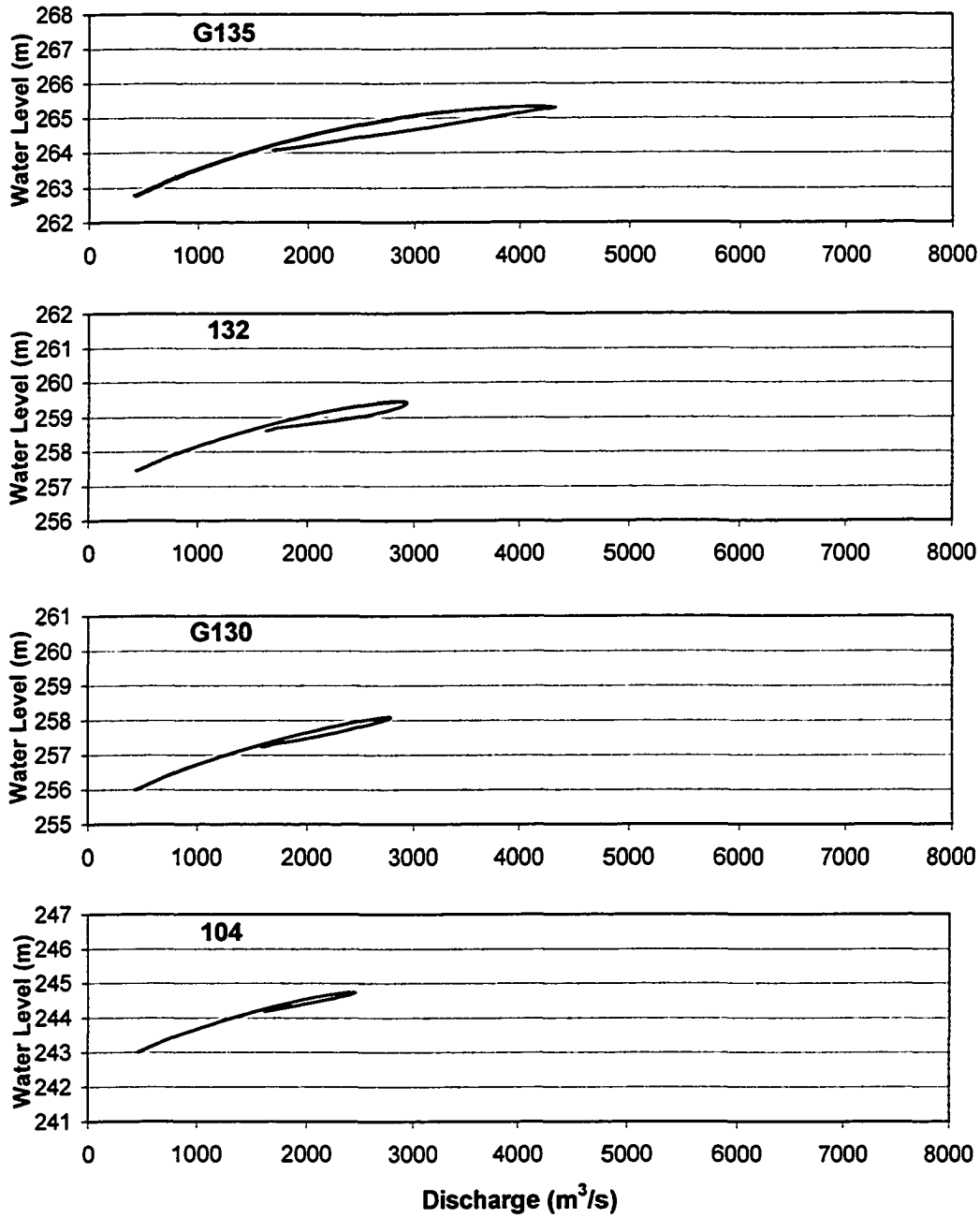

Figure 5-10. Looped rating curves in upper portion of the study reach for Run 2a.

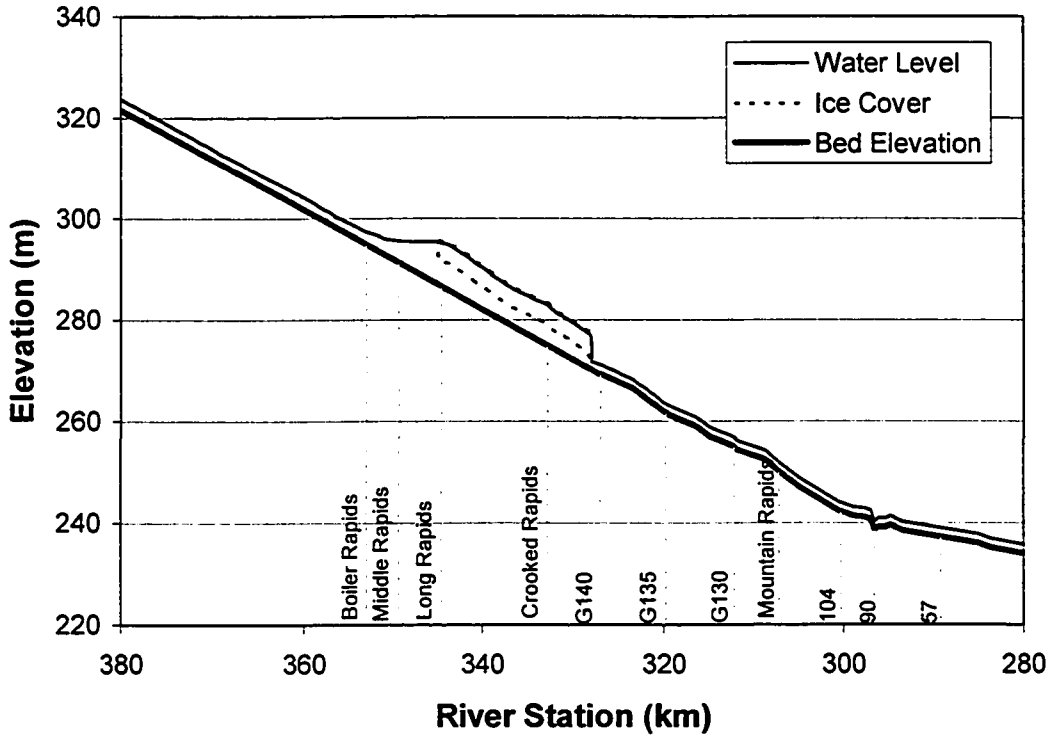

Figure 5-11. Water level profile for Run 3a developed using HEC-RAS.

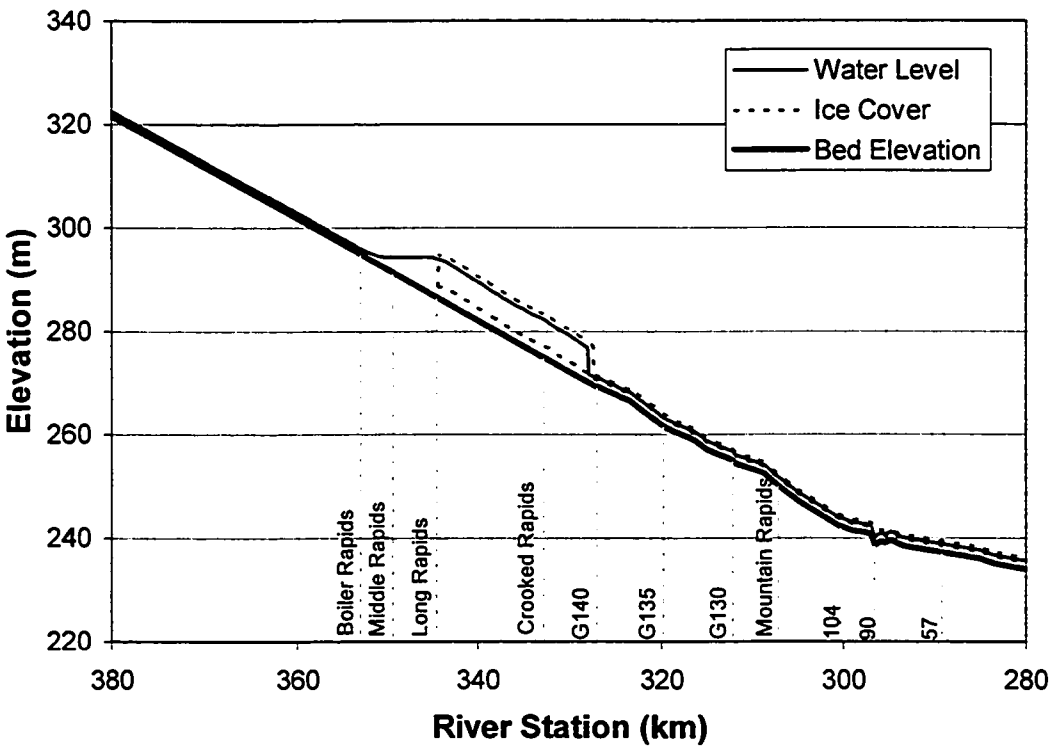

Figure 5-12. Water level profile for Run 3b developed using HEC-RAS.

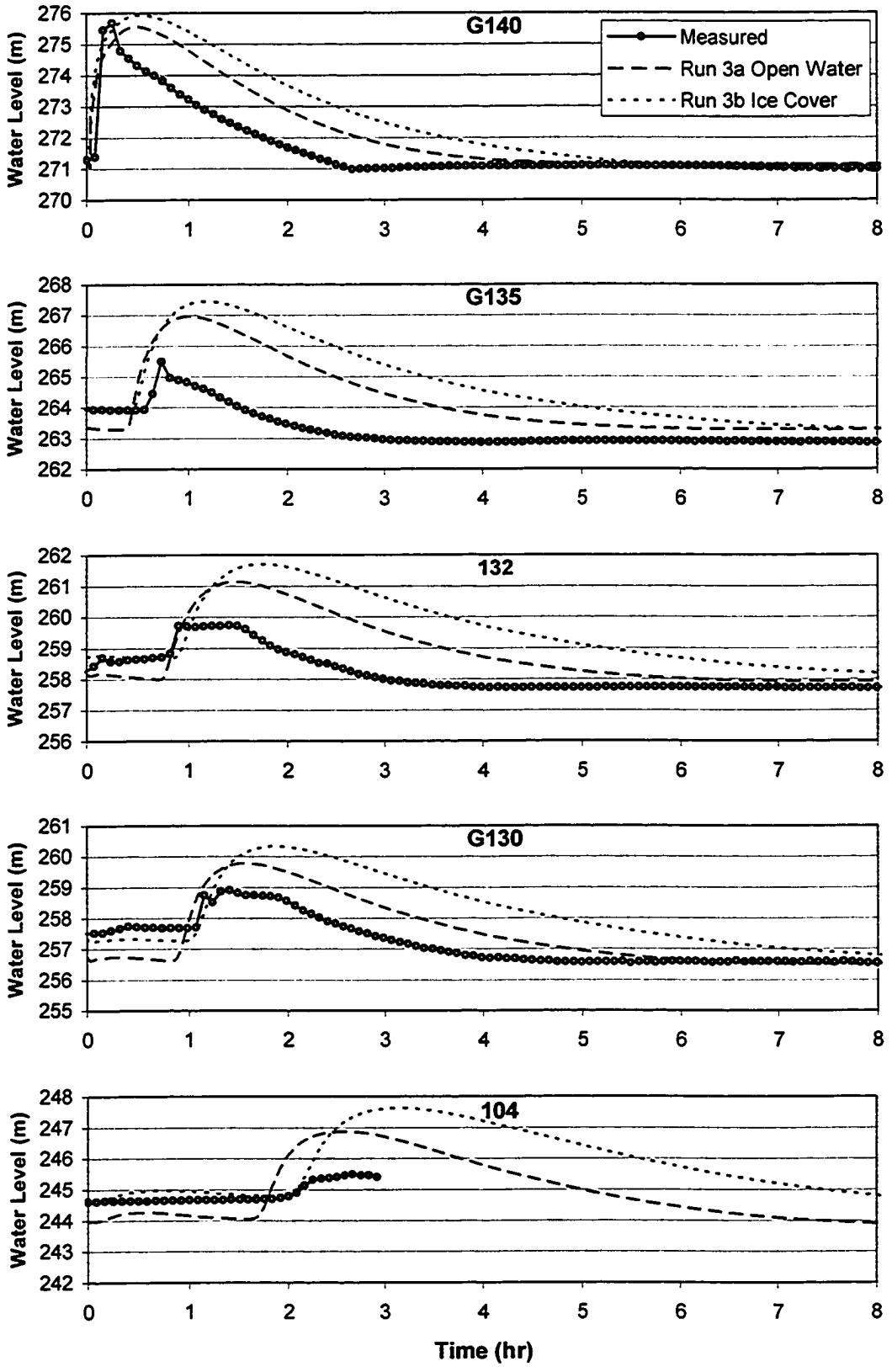

Figure 5-13. Water levels in upper portion of the study reach for Runs 3a and 3b.

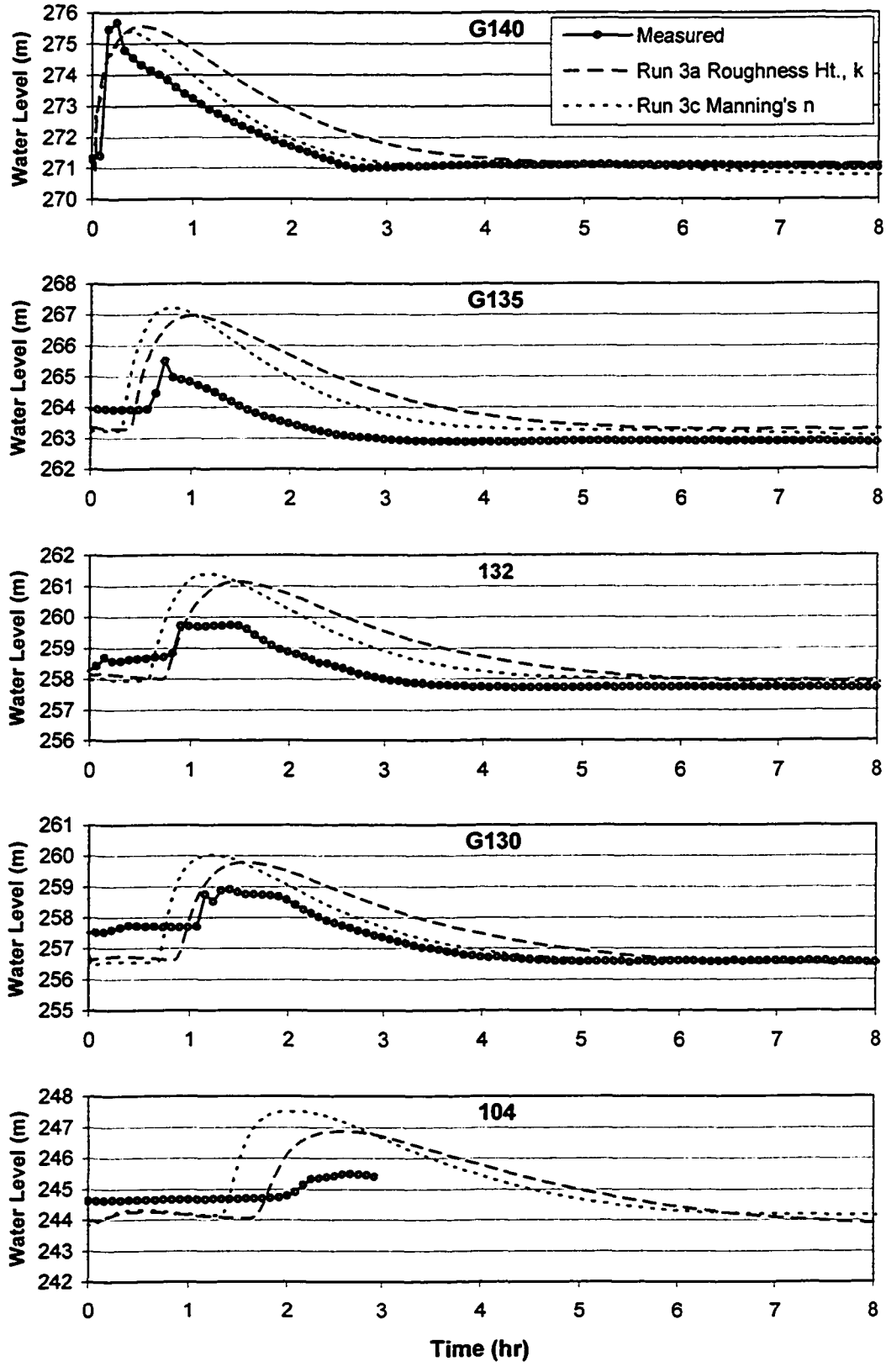

Figure 5-14. Water levels in upper portion of the study reach for Runs 3a and 3c.

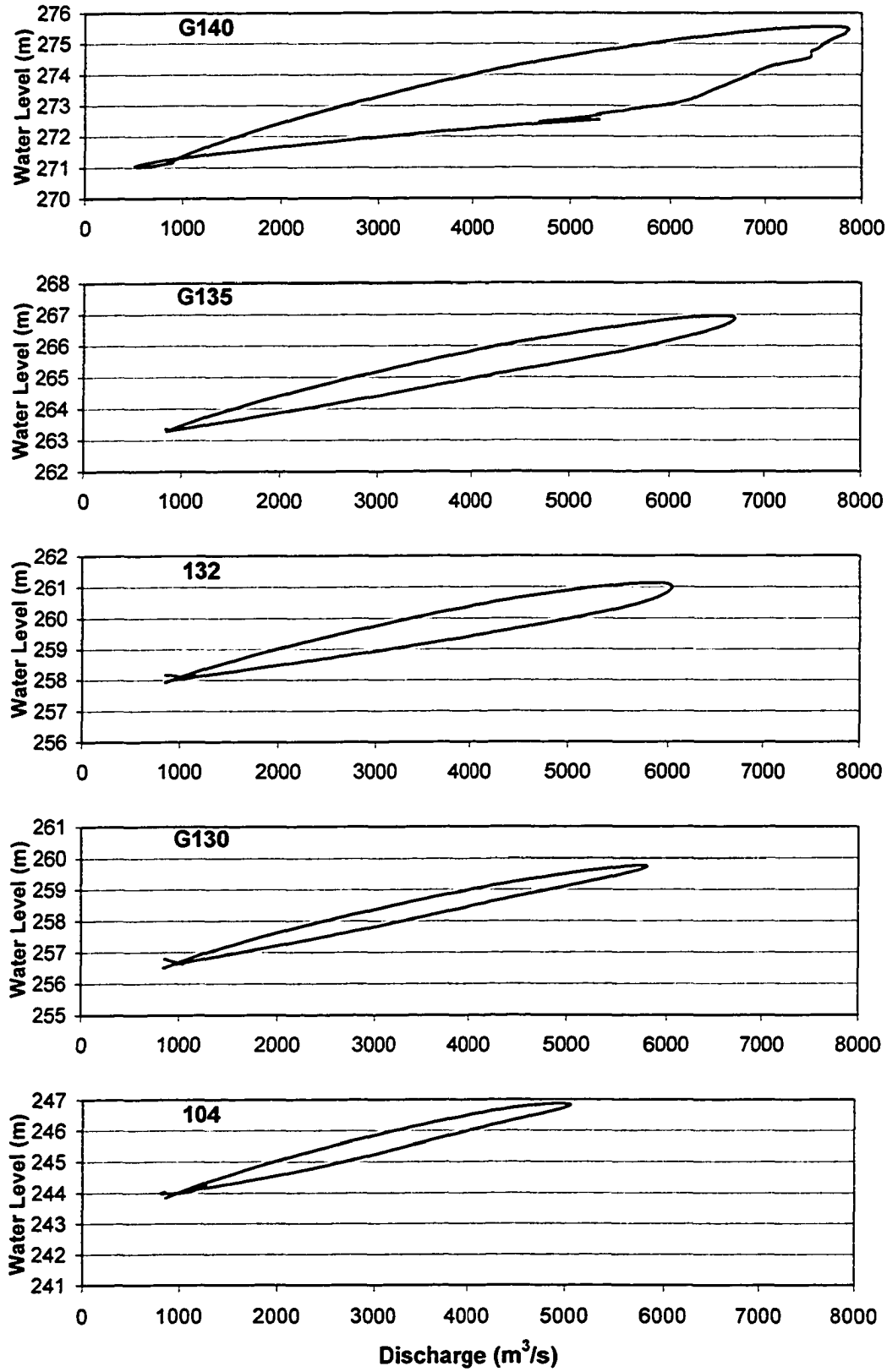

Figure 5-15. Looped rating curves in upper portion of the study reach for Run 3a.

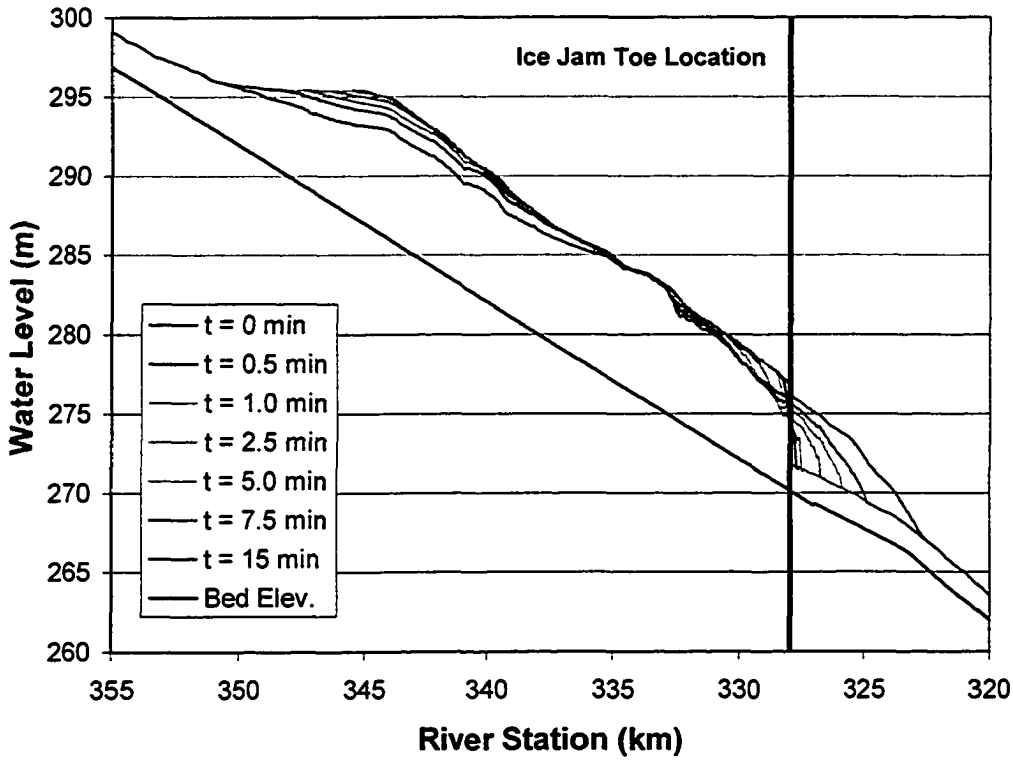

Figure 5-16. Water level profile for Run 3a with the ice jam toe at AE Camp.

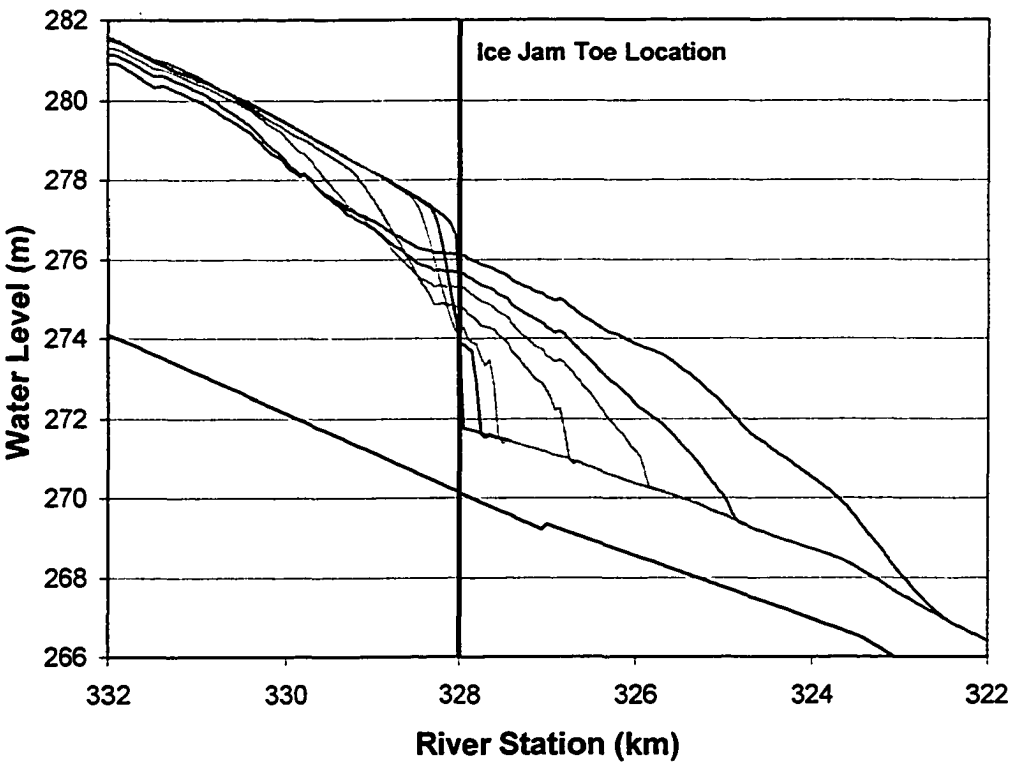

Figure 5-17. Up close view of water level profile at jam toe for Run 3a.

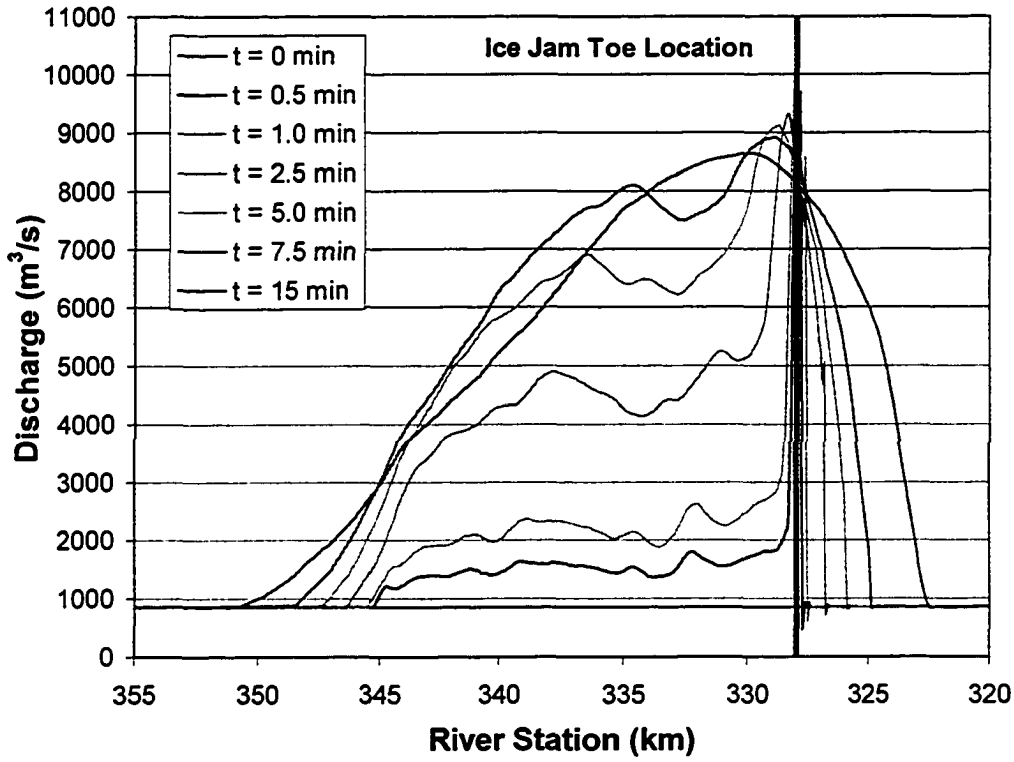

Figure 5-18. Discharge profile for Run 3a with the ice jam toe at AE Camp.

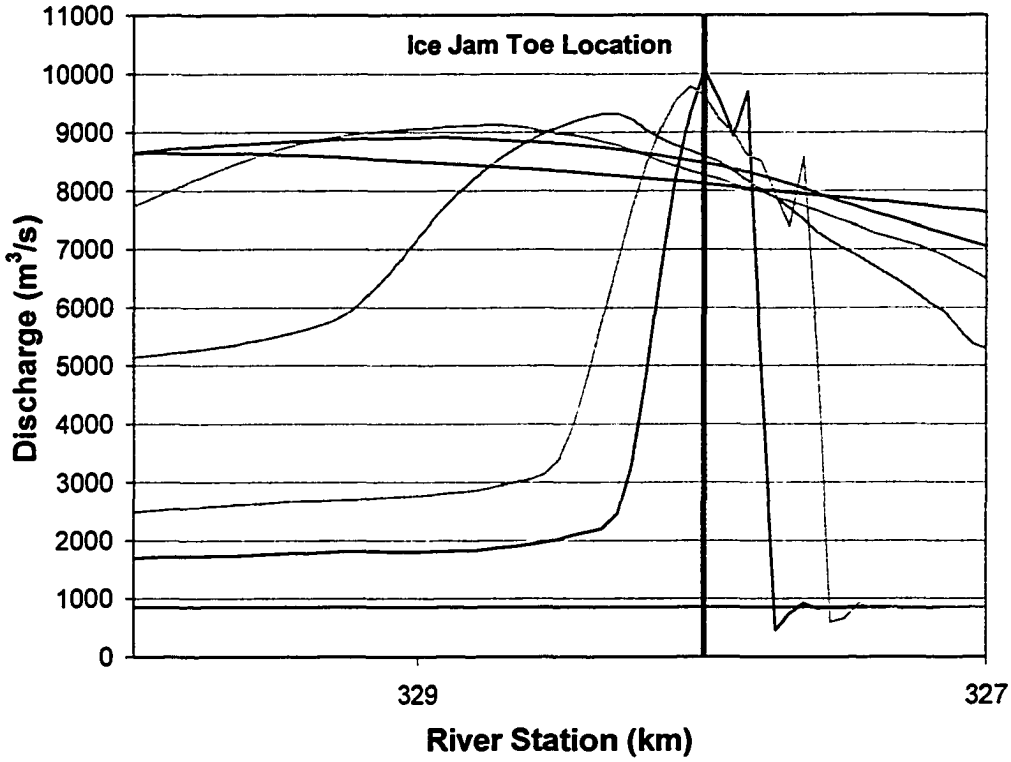

Figure 5-19. Up close view of discharge profile at the jam toe for Run 3a.

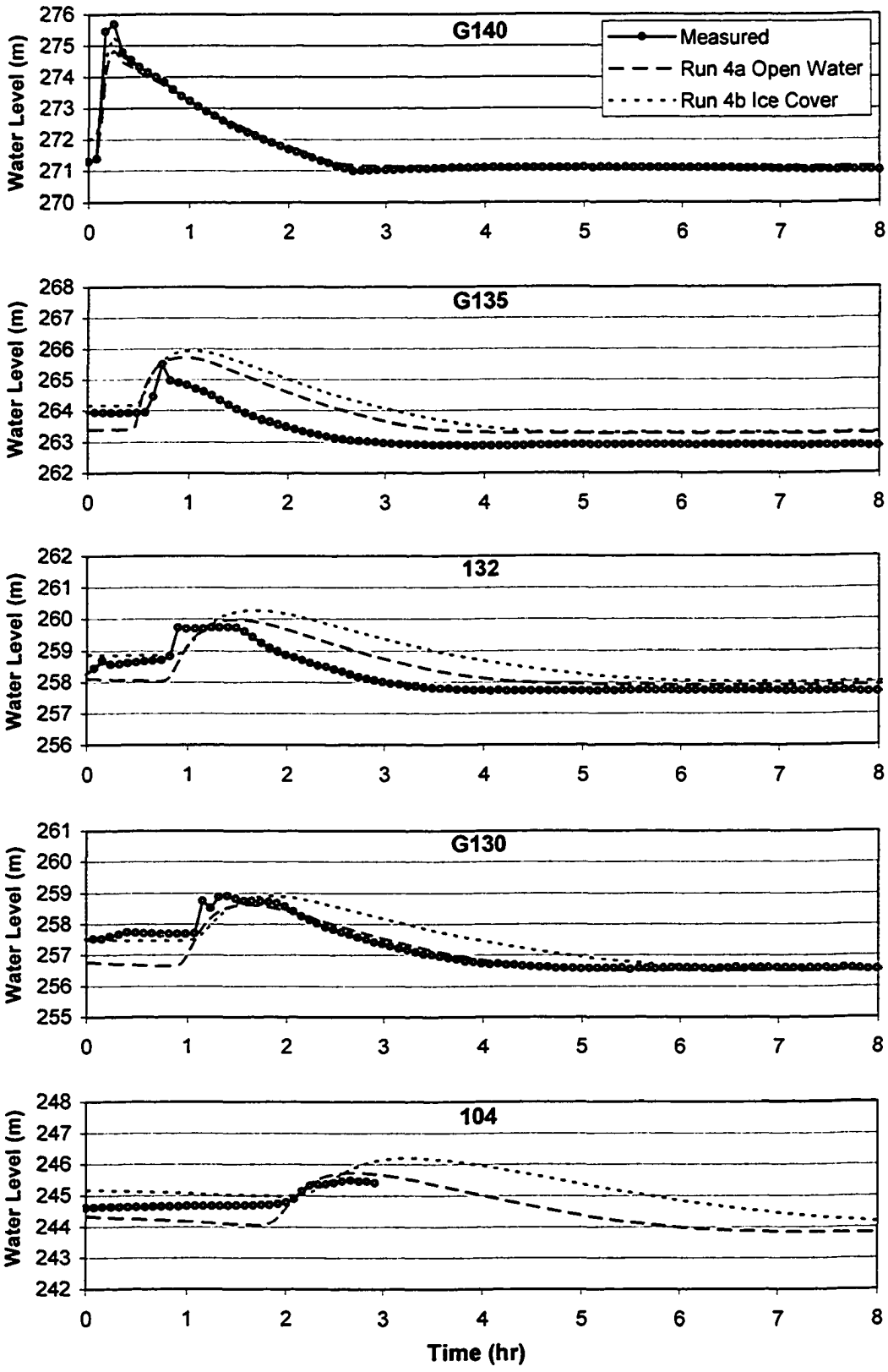

Figure 5-20. Water levels in upper portion of the study reach for Run 4.

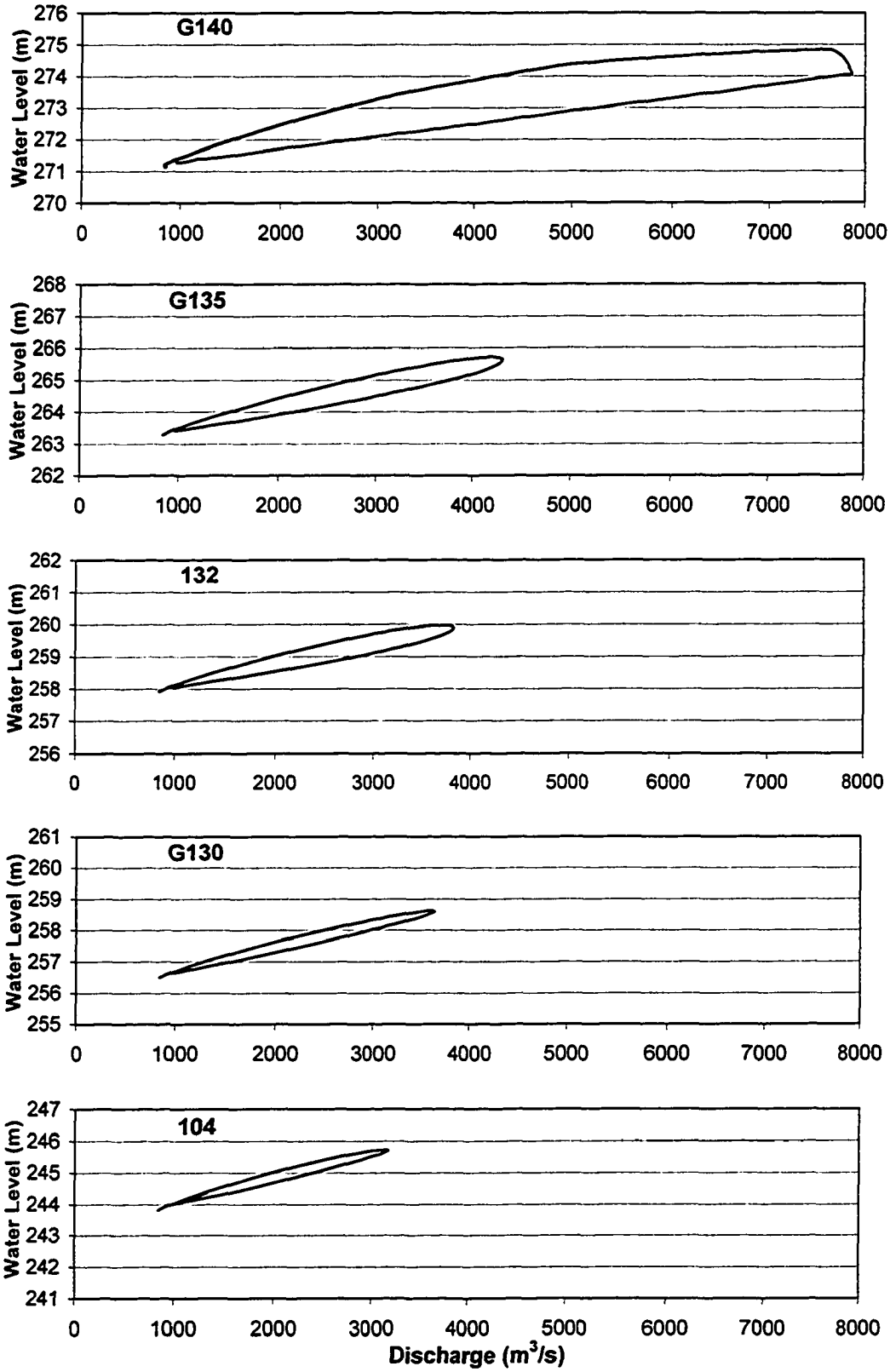

Figure 5-21. Looped rating curves in upper portion of the study reach for Run 4a.

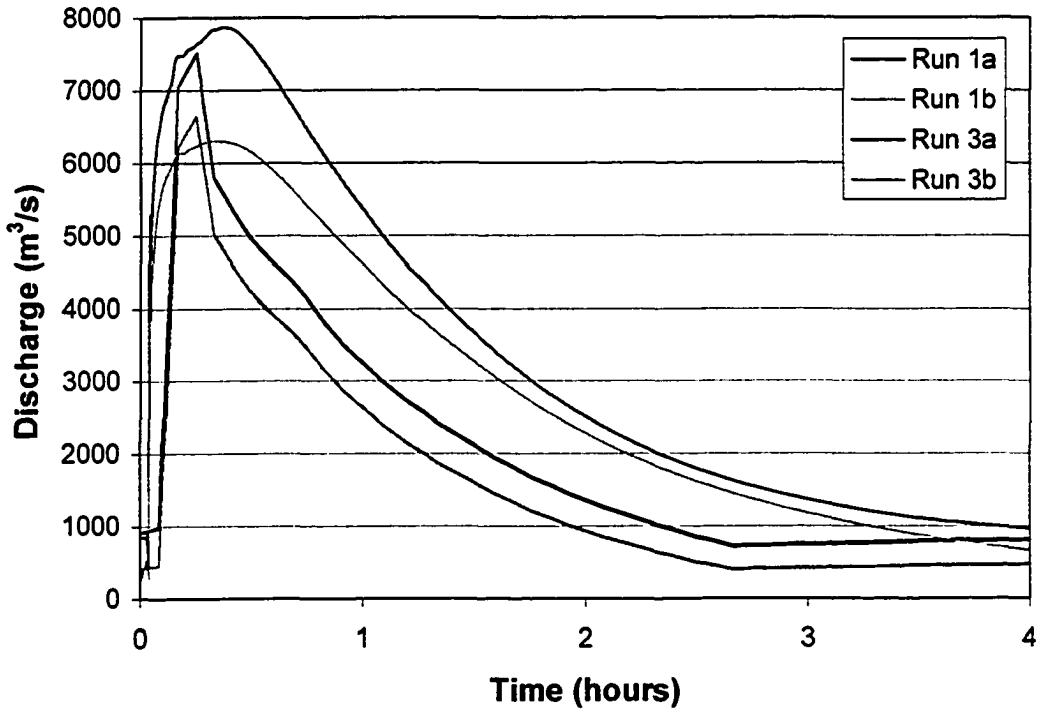

Figure 5-22. Modeled discharge hydrographs at station G140.

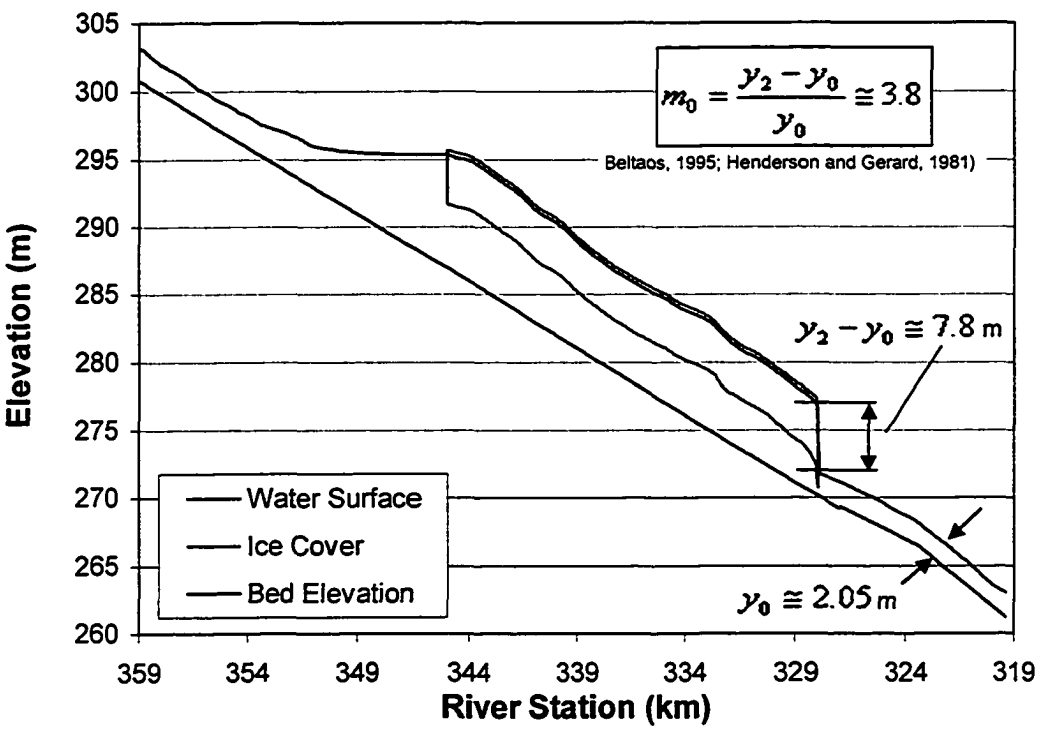

Figure 5-23. Approximate m_0 value for Run 3a ice jam profile.

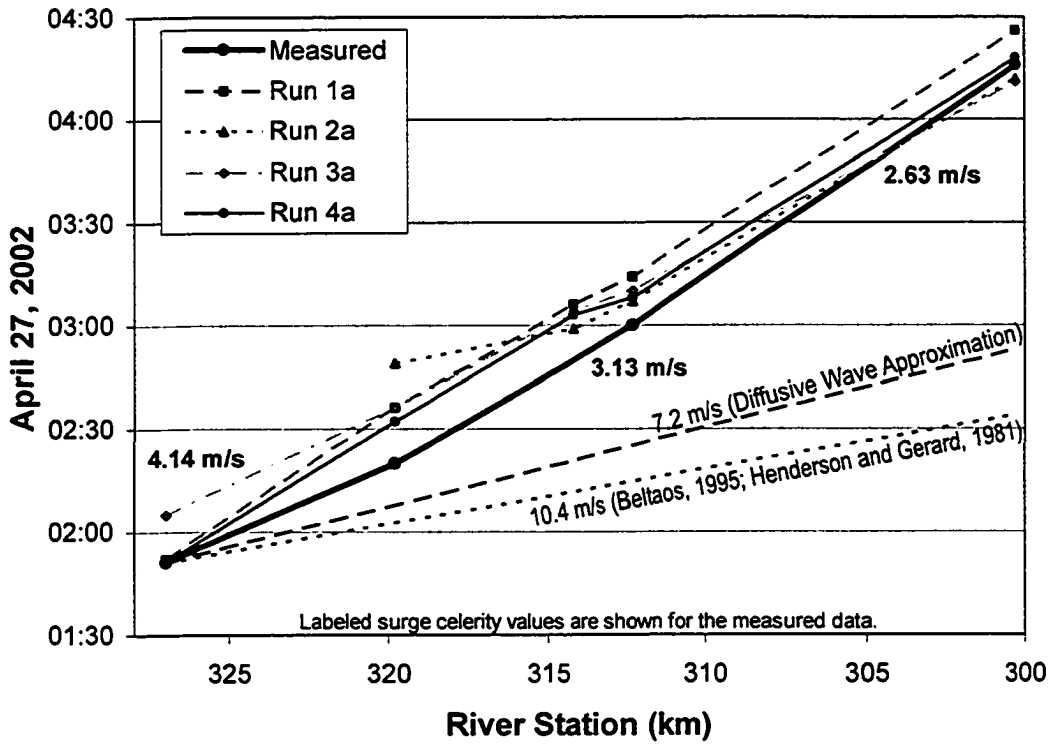

Figure 5-24. Celerity of surge for model runs with an open water condition.

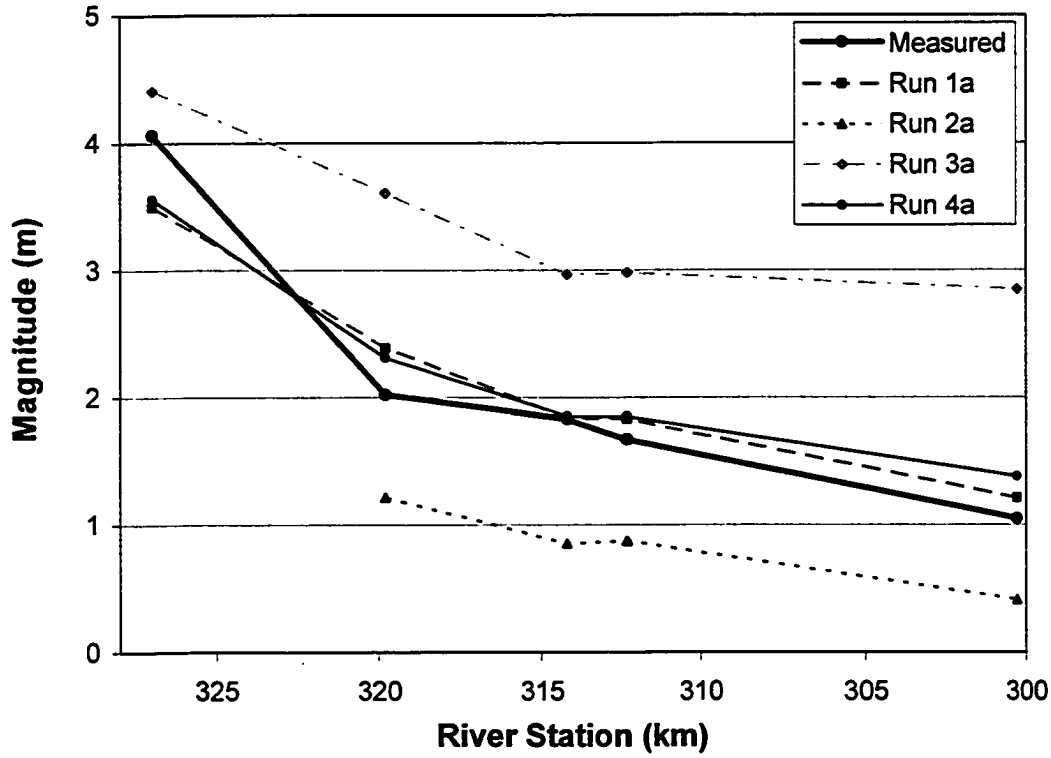

Figure 5-25. Peak magnitude of surge for model runs with an open water condition.

Figure 5-26. Toe of newly formed ice jam near station 104.

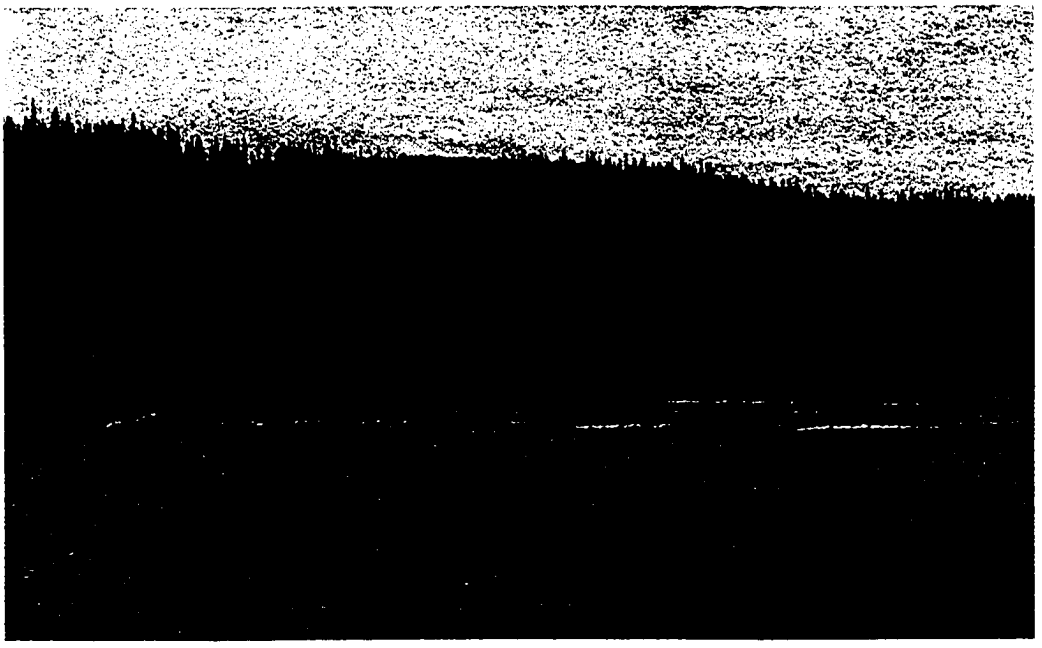

Figure 5-27. Gravel bars left behind from the formation of the ice jam near station 104.

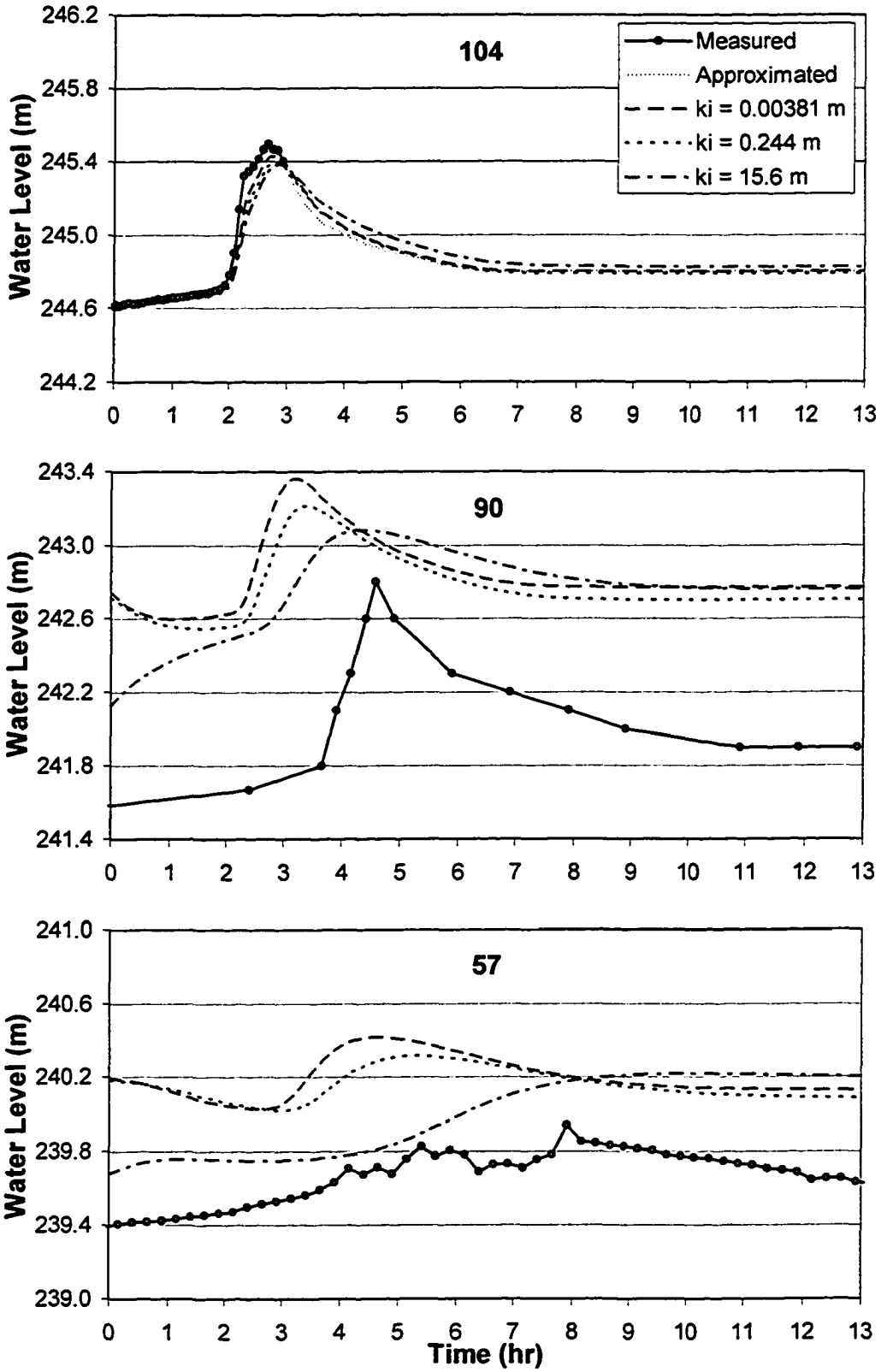

Figure 5-28. Water levels in lower portion of the study reach for Run 5a with an ice thickness of 0.6 m and varying ice underside roughness heights.

Figure 5-29. Photograph of ripples found on the underside of the ice cover along the Mackenzie River on May 3, 1992.

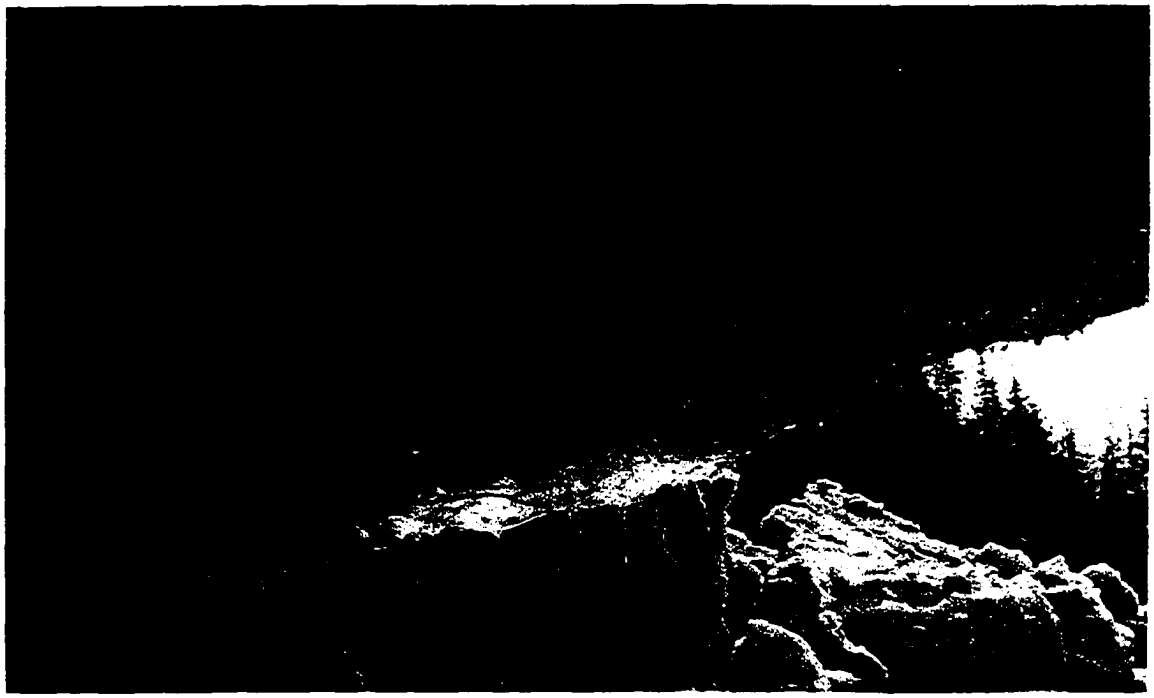

Figure 5-30. Photograph showing evidence of ripples on the underside of the ice cover along the Athabasca River on April 19, 1985.

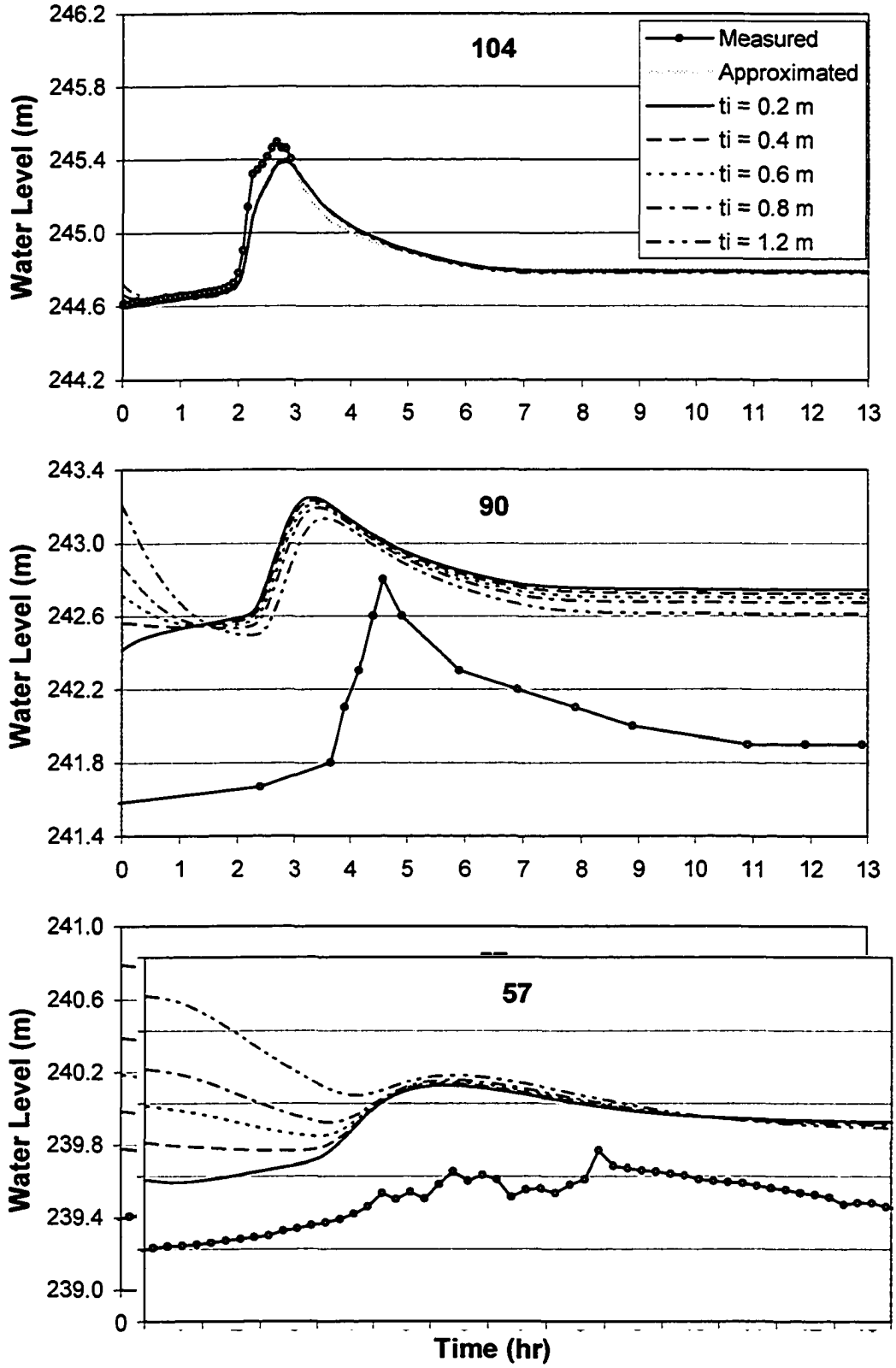

Figure 5-31. Water levels in lower portion of the study reach for Run 5b with an ice underside roughness of ki = 0.244 m and varying ice thicknesses.

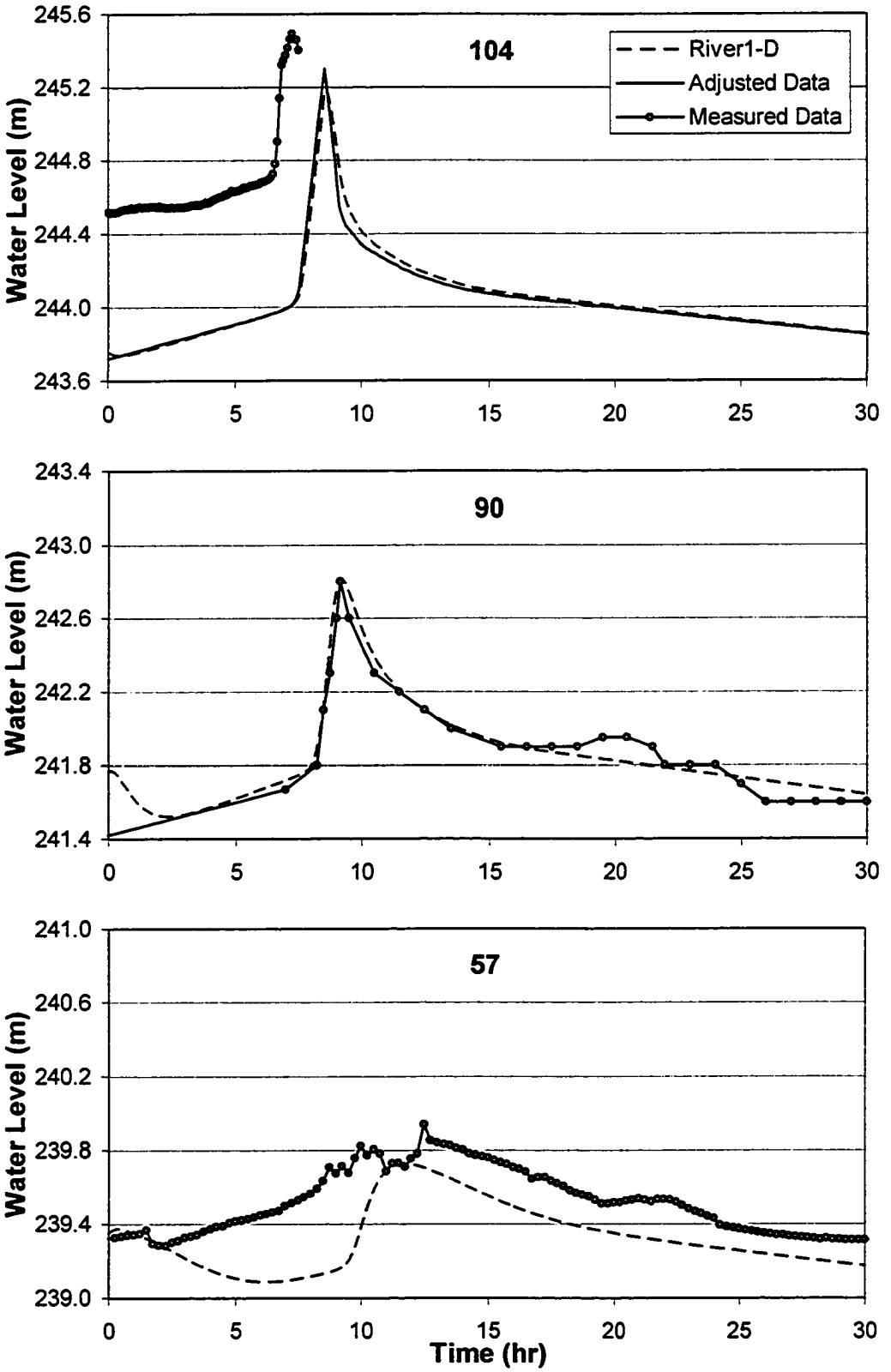

Figure 5-32. Water levels in the lower portion of the study reach for Run 6 with an ice thickness of 0.6 m and roughness height of 0.244 m (ni = 0.03).

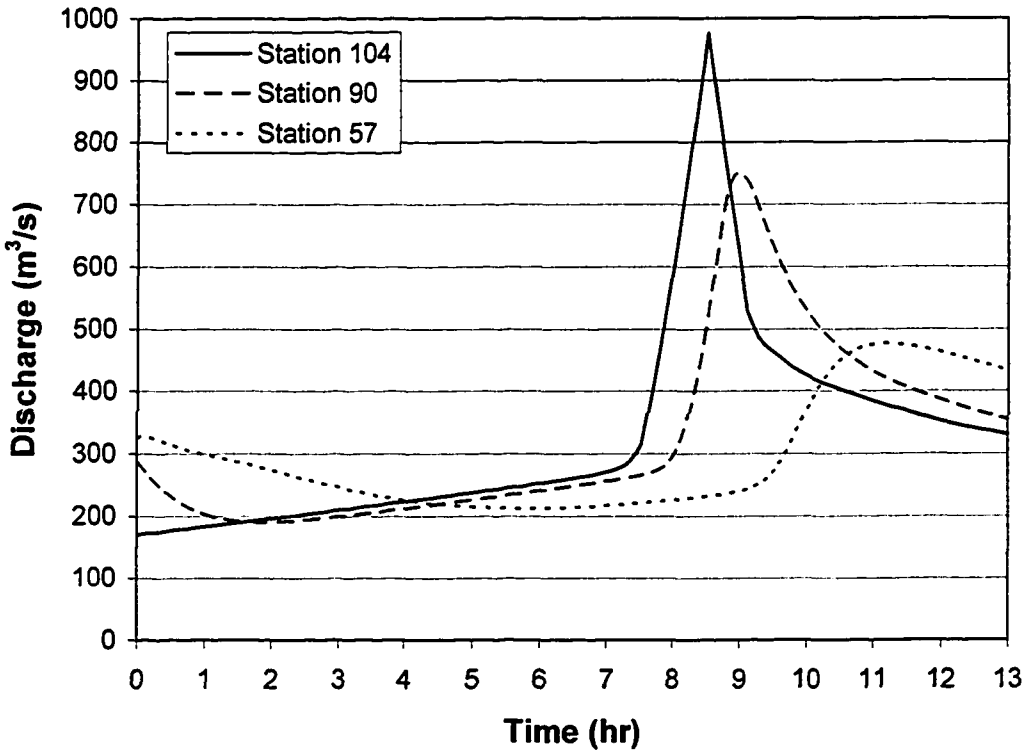

Figure 5-33. Discharge hydrographs for Run 6.

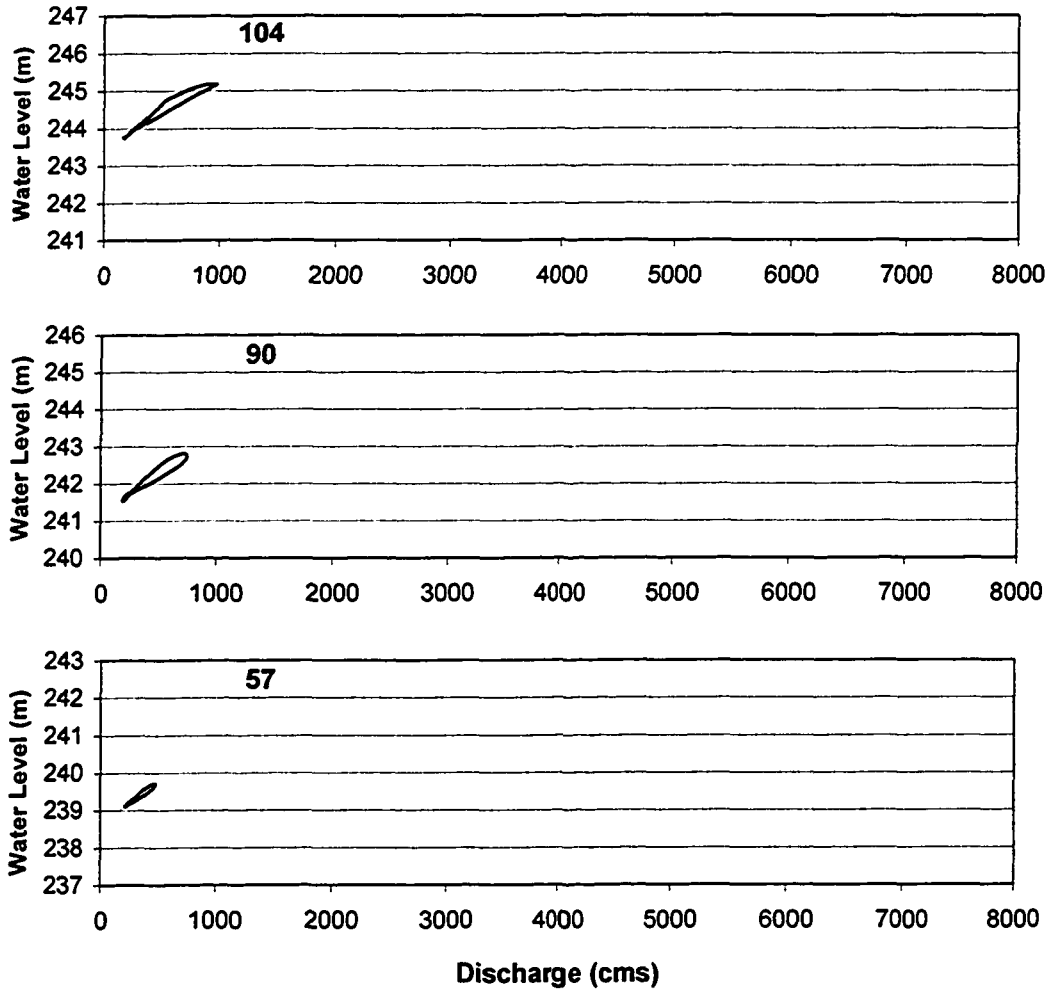

Figure 5-34. Looped rating curves in lower portion of the study reach for Run 6 under ice covered conditions.

6 SUMMARY AND RECOMMENDATIONS

The most dangerous type of ice-related flooding is a result of an ice jam release event. The associated increases in water level and discharge occur quickly, giving downstream communities little time to react. Badgar, NF, experienced such an event in 2003 where a 2 m high surge flooded the town. Severe flooding due to ice jams have occurred on numerous occasions along the Hay River, NWT. Documentation along the Athabasca River shows a high frequency of ice jam release events with flooding experienced in Fort McMurray on some occasions. The most dramatic flooding event in Fort McMurray was recorded by the Hudson's Bay Company in 1875, where the water was estimated to have risen 60 feet in only half an hour. Being able to predict these rapid water level increases would aid in the purpose of flood forecasting and could save lives.

Past studies have tried to analyze ice jam release events, both analytically and numerically, using laboratory and field data. The main outstanding question appeared to be whether the ice from the jam has any significant effect on the propagation surge. A laboratory study by Wong *et al.* (1985) found that ice within the jam did not have a significant effect on surge propagation. However, the laboratory study by Khan *et al.* (2000) showed the celerity and the height of the surge to be affected both by the ice within the jam, as well as an ice cover in the downstream receiving channel. Jasek (2003) conducted qualitative studies of the effect of ice on propagating surges in the field. He found that the celerity of an ice jam release surge was affected by ice conditions, the extent of which depending upon whether it was an unimpeded or impeded ice run. He found that the celerity was also affected by the type of breaking front for the case of an impeded ice run, and observed that the ice within the jam would contribute the largest amount of resistance within the first jam length of propagation distance.

Analytical and numerical solutions of the full dynamic equations, and approximations (as discussed in Chapter 2), have also been used to address the question of how ice from the jam affects the propagating surge. Using a rectangular channel

approximation, an analytical solution of the classic dam break equations (neglecting ice, channel slope and friction) by Henderson and Gerard (1981) for the 1979 event along the Athabasca River, over-predicted the celerity of the surge substantially. They concluded that this was due to the effects of ice. Numerical solution of the full dynamic equations by Hicks *et al.* (1997) and Blackburn and Hicks (2003) for the 1993 event on the Saint John River, NB, adequately modeled the celerity of the surge (disproving that earlier conclusion). However, their models could not accurately reproduce the peak water levels or the shape of the surge hydrograph. Use of natural channel geometry was found to improve results, but it was concluded that the effects of an ice cover were likely still important to accurately modeling the peak magnitude attenuation. Additional modeling by Liu and Shen (2003) showed that an ice cover slows the release process and thus they concluded that ice cannot be neglected. However, Liu and Shen did not have field data to verify their findings.

In summary, results of laboratory and numerical modeling attempts have been inconclusive in determining to the importance of an ice cover on surge propagation. However, one clear result of all of these earlier studies was that more data on ice jam release events was needed to resolve the issue. Since historical documentation was available for numerous ice jam release events along the Athabasca River, AB, this site was selected for this study, with the following specific objectives in mind:

1. to collate and analyze all of the historically documented ice jam release surge events at the study site;
2. to identify the inadequacies in that data and attempt to get more and better scientific data;
3. to use that data to assess the importance of ice on the nature of the propagating surge.

Ice jam release events have been documented along the study reach, between Crooked Rapids and the WSC gauge just downstream of Fort McMurray, between the years of 1977 and 1990. The documentation of these historical ice jam release events

show three typical areas of release location: Type 1 initiates upstream of Crooked Rapids, Type 2 initiates near Crooked Rapids, and Type 3 initiates near Mountain Rapids.

Analysis of the celerity and peak magnitude attenuation characteristics of these historical events indicated no obvious trends, but similar overall celerity values were documented. Some situations were observed where surge celerity drastically increased or even decreased. This shows that there are numerous factors influencing surge propagation celerity besides just the size of the surge and the distance traveled. Some factors could include: the geometry of the channel, surface ice conditions in the receiving channel, as well as the interaction of ice and water within the released ice jam as explained by Jasek (2003), and/or temporary jamming and re-release. Less comparable results were found for surge peak magnitude. Most events only had a couple of magnitude measurements; therefore magnitude attenuation could not be analyzed for the historical events.

Although these historical events provide valuable data to observe overall behaviour of surge waves, measurements describing the propagation of surge events over a significant distance were needed to understand the true nature of surge propagation. In order to capture the entire shape of a surge hydrograph at various locations along an extensive reach, a remote monitoring network was installed by UA in the fall of 2001, and events were measured in 2002 and 2003. (Breakup in 2004 was entirely thermal and so no events were measured). Most exciting was the 4.4 m high surge measured in 2002, which was documented at 7 sites as it propagated over a 40 km reach. This data allowed for both the surge peak celerity and the magnitude attenuation to be assessed. The River1-D model was applied to this event to further analyze the propagation of surge waves and to investigate the effects of ice on the propagating surge. Based on a series of runs the following conclusions were noted regarding the modeling of ice jam release events:

1. Using a uniform flow rating curve with the stage hydrograph measured at the toe of the releasing jam to estimate the inflow boundary condition, produced model

results in good agreement with surge celerity and a reasonable match for the surge peak magnitudes at most stations.

2. Using an ice jam profile estimated from a steady ice jam profile model (HEC-RAS) as the initial condition for the release event, produced model results with reasonable surge celerity, but which greatly overestimated both the volume of water in the wave and the peak magnitudes. This can most likely be attributed to error in the estimated length of the initial ice jam, which had likely melted (and shortened) between the time it was observed and the time it released. This stresses the need for knowledge of the original ice jam profile if the event is to be adequately modeled.
3. The drastic decrease in peak magnitude measured between G140 and G135 was not adequately modeled in any of the runs. Therefore, this phenomenon is likely attributed to the effect of ice within the ice jam, consistent with the qualitative observations of Jasek (2003) who found that ice effects were most pronounced as the surge propagated along the first x km, where x is the original length of the jam.
4. Assuming an ice cover in the downstream receiving channel produced a flatter hydrograph shape with a slower receding limb, as compared to assuming open water in the receiving channel. For all model runs it was found that the modeled peak discharge was lower for the ice covered condition, and also resulted in a slower surge celerity. However, these two extreme assumptions did not produce model results that bracketed the actual data. This again implies that the ice from the released jam has a significant effect on the propagating surge.

For the model simulations of the wave which escaped downstream past the reformed jam and propagated under the intact ice cover through Fort McMurray, it was found that:

1. Using a uniform flow approximation to create an inflow discharge hydrograph at the upstream boundary did not produce reasonable results (unlike the ice jam release case).

2. Varying ice underside roughness in the receiving channel resulted in a flattening of the modeled hydrographs, a decrease in the peak magnitude, and a decrease in the celerity of the modeled wave.
3. Varying ice thickness in the receiving channel had a negligible effect on the modeled peak magnitude and only slightly decreased the wave celerity.
4. By trial and error, the likely release hydrograph from the toe of the reformed jam was deduced. A volume calculation indicated that approximately $^1/_2$ to $^1/_3$ of the original wave was trapped in the reformed jam.

This study has contributed many valuable findings to the analysis of ice jam release events. Past studies have been inconclusive as to the importance of an ice cover on surge propagation. This study has undeniably shown that ice, both within the released ice jam and in the downstream receiving channel, is an important factor in predicting surge behaviour. It has also been shown that River1-D, a one-dimensional hydraulic model that solves the full Saint Venant equations for unsteady open channel flow using the CDG finite element scheme, is appropriate for highly dynamic events such as ice jam release surge waves. Modeled results were able to predict surge celerity, as well as a reasonable estimate of the corresponding water levels, despite not explicitly considering ice effects. Therefore this modeling effort is a potentially useful flood forecasting tool for the city of Fort McMurray.

Another major contribution of this study is the collection of new, comprehensive ice jam release event data providing an in-depth dataset of stage hydrographs spanning approximately 40 km, describing the surge propagation behaviour of the 2002 event. Water levels are available from before and after surge arrival depict the entire shape of the hydrograph at 7 stations as the surge passed. Aerial photographs capturing the ice surface conditions prior to ice jam release, as well as the new ice jam had formed just upstream of Fort McMurray, provide information on antecedent and resulting conditions. Channel geometry is also available, as are numerous documented historical release events which help to define the typical nature of breakup along the Athabasca River.

6.1 RECOMMENDATIONS

Since the effect of an ice cover has been deemed important, further studies should be done to quantify the extent of this effect. In terms of data, it would be valuable to obtain better measurements of an ice jam profile prior to its release, as well as additional stage hydrographs both along the length of the released jam and upstream to further analyze release behaviour. In terms of modeling, River1-D should be modified to handle moving ice from the released ice jam, and to simulate a breaking front through the ice in the downstream receiving channel.

7 REFERENCES

Andres, D.D. and Rickert, H.A. (1985). *Observations of the 1985 Breakup in the Athabasca River Basin Upstream of Fort McMurray, Alberta.* Alberta Research Council, Edmonton, AB, Report SWE 85/10.

Andres, D.D. and Rickert, H.A. (1985). *Observations of Breakup in the Athabasca River Basin Upstream of Fort McMurray, Alberta, 1984.* Alberta Research Council, Edmonton, AB, Report SWE 85/09.

Ashton, G.D. (1986). *River and Lake Ice Engineering.* Water Resources Publications, Littleton, Colorado, 485 pp.

Beltaos, S. (1995). *River Ice Jams.* Water Resources Publications, LLC, Highlands Ranch, Colorado, 372 pp.

Beltaos, S., Burrell, B.C. and Ismail, S. (1994). Ice and Sedimentation Processes in the Saint John River, Canada. *Proceedings of the Twelfth IAHR Symposium on Ice*, Trondheim, Norway, pp. 11-21.

Beltaos, S. and Krishnappan, B.G. (1982). Surges From Ice Jam Releases: A Case Study. *Canadian Journal of Civil Engineering*, Vol. 9, No. 2, pp. 276-284.

Blackburn, J.L. (2000). *Forecasting Open Water and Ice Related Flood Events Using Hydraulic Modeling Techniques.* M.Sc. Thesis, Department of Civil and Environmental Engineering, University of Alberta, Edmonton, AB.

Blackburn, J.L. and Hicks, F.E. (2003). Suitability of Dynamic Modeling for Flood Forecasting during Ice Jam Release Surge Events. *American Society of Civil Engineering: Journal of Cold Regions Engineering*, Vol. 17, No. 1, pp. 18-36.

Brunner, G.W. (2002). *HEC-RAS, River Analysis System User's Manual, Version 3.1.* US Army Cops of Engineers.

Carey, K.L. (1966). Observed Configuration and Computed Roughness of the Underside of River Ice, St. Croix Rvier, Wisconsin. U.S. Geol. Survey Prof. Paper, pp. B192–B198.

Chunge, J.A., Holly, F.M. Jr. and Verwey, A. (1980). *Practical Aspects of Computational River Hydraulics*. Pitman Publishing Company, London, England, 420 pp.

Chow, V.T. (1959). *Open Channel Hydraulics*. McGraw-Hill Book Company, New York, N.Y.

Doyle, P.F. (1977). *1977 Breakup and Subsequent Ice Jam at Fort McMurray*. Alberta Research Council, Edmonton, AB, Report SWE/77/01.

Doyle, P.F. and Andres, D.D. (1979). *1979 Spring Breakup and Ice Jamming on the Athabasca River Near Fort McMurray*. Alberta Research Council, Edmonton, AB, Report SWE-79/05.

Doyle, P.F. and Andres, D.D. (1978). *1978 Breakup in the Vicinity of Fort McMurray and Investigation of Two Athabasca River Ice Jams.* Alberta Research Council, Edmonton, AB, Report SWE-78/05.

Friesenhan, E.C. (2004). *Modeling of Historic Ice Jams on the Athabasca River at Fort McMurray*. M.Eng. Thesis, Department of Civil and Environmental Engineering, University of Alberta, Edmonton, AB.

Henderson, F.M. (1966). *Open Channel Flow*. MacMillan Series in Civil Engineering, MacMillan Publishing Co., New York, New York, 522 pp.

Henderson, F.M. and Gerard, R. (1981). Flood Waves Caused by Ice Jam Formation and Failure. *Proceedings, International Association for Hydraulic Research, International Symposium on Ice*. Quebec City, Quebec, Vol. 1, pp. 277-287.

Hicks, F.E. (1996). Hydraulic Flood Routing with Minimal Channel Data: Peace River, Canada. *Canadian Journal of Civil Engineering*, Vol. 23, No. 2, pp. 524-535.

Hicks, F.E. and Steffler, P.M. (1992). A Characteristic-Dissipative-Galerkin Scheme for Open Channel Flow. *ASCE Journal of Hydraulic Engineering*, Vol. 118, No. 2, pp. 337-352.

Hicks, F.E. and Steffler, P.M. (1990). *Finite Element Modeling of Open Channel Flow*. Water Resources Engineering Report No. 90-6, Department of Civil Engineering, University of Alberta, Edmonton, AB, 356 pp.

Hicks, F.E., McKay, K. and Shabayek, S. (1997). Modeling and Ice Jam Release Surge on the Saint John River, New Brunswick. *Proceedings, The 9th Workshop on River Ice*. Fredericton, NB, pp. 303-314.

Hicks, F.E., Steffler, P.M. and Gerard, R. (1991). Finite Element Modeling of Surge Propagation and an Application to the Hay River, N.W.T. *Canadian Journal of Civil Engineering*, Vol. 19, pp. 454-462.

Jasek, M. (2003). Ice Jam Release Surges, Ice Runs, and Breaking Fronts: Field Measurements, Physical Descriptions, and Research Needs. *Canadian Journal of Civil Engineering*, Vol. 30, pp. 113-127.

Keulegan, G.B. (1938). Laws of Turbulence in Open Channels. *Journal of Research of the National Bureau of Standards*, U.S. Department of Commerce, Vol. 21, pp. 707-741.

Khan, A.A., Steffler, P.M. and Gerard, R. (2000). Dam-Break Surges with Floating Debris. *Journal of Hydraulic Engineering*, Vol. 126, No. 5, pp. 375-379.

Liu, L. and Shen, H.T. (2004). Dynamics of Ice Jam Release Surges. *Proceedings, 17th International Symposium on Ice*. St. Petersburg, Russia, 8 pp.

Malcovish, C.D., Andres, D.D. and Mostert, P. (1988). *Observations of Breakup on the Athabasca River Near Fort McMurray, 1986 and 1987*. Alberta Research Council, Edmonton, AB, Report SWE-88/12.

Rickert, H.A. and Quazi, M.E. (1988). *Fort McMurray Ice Study, Breakup Observation Report 1988*. Alberta Environment, Technical Services Division, February 1989.

Rickert, H.A. and Quazi, M.E. (1982). *1982 Spring Breakup and Monitoring Report Athabasca and Clearwater Rivers at Fort McMurray*. Alberta Department of the Environment, Water Resources Management Services, Technical Services Division, December.

Robichaud, C. (2003). *Hydrometeorological Factors Influencing Breakup Ice Jam Occurrence at Fort McMurray, Alberta*. M.Sc. Thesis, Department of Civil and Environmental Engineering, University of Alberta, Edmonton, AB.

Schlichting, H. (1979). *Boundary Layer Theory. 7th Edition*. McGraw-Hill Book Company, New York, N.Y.

Van Der Vinne, P.G. (1994). *Characterization of the 1990 Ice Break-up Wave on the Athabasca River at Ft. McMurray*. Trillium Engineering and Hydrographics Inc., Edmonton, AB, Report SWE-94/12.

Watt, W.E. (ed.) (1989). *Hydrology of Floods in Canada*. National Research Council Canada, 245 pp.

Winhold, T. (1988). *Fort McMurray Ice Studies 1987 Breakup Observation Report.* Alberta Environment, Technical Services Division.

Wong, J., Beltaos, S. and Krishnappan, B.G. (1985). Laboratory Tests on Surges Created by Ice Jam Releases. *Canadian Journal of Civil Engineering*, Vol. 12, No. 4, pp. 930-933.

APPENDIX A

Table A-1. Measured data for station G140.

Time		W.L.[1]
(day hour)	(hr)	(m)
Apr 27 02 01:36	0.00	271.300
Apr 27 02 01:41	0.08	271.384
Apr 27 02 01:46	0.17	275.458
Apr 27 02 01:51	0.25	275.691
Apr 27 02 01:56	0.33	274.792
Apr 27 02 02:01	0.42	274.538
Apr 27 02 02:06	0.50	274.310
Apr 27 02 02:11	0.58	274.141
Apr 27 02 02:16	0.67	273.992
Apr 27 02 02:21	0.75	273.817
Apr 27 02 02:26	0.83	273.591
Apr 27 02 02:31	0.92	273.388
Apr 27 02 02:36	1.00	273.220
Apr 27 02 02:41	1.08	273.055
Apr 27 02 02:46	1.17	272.902
Apr 27 02 02:51	1.25	272.756
Apr 27 02 02:56	1.33	272.604
Apr 27 02 03:01	1.42	272.478
Apr 27 02 03:06	1.50	272.355
Apr 27 02 03:11	1.58	272.225
Apr 27 02 03:16	1.67	272.116
Apr 27 02 03:21	1.75	271.993
Apr 27 02 03:26	1.83	271.899
Apr 27 02 03:31	1.92	271.786
Apr 27 02 03:36	2.00	271.688
Apr 27 02 03:41	2.08	271.593
Apr 27 02 03:46	2.17	271.505
Apr 27 02 03:51	2.25	271.414
Apr 27 02 03:56	2.33	271.324
Apr 27 02 04:01	2.42	271.240
Apr 27 02 04:06	2.50	271.145
Apr 27 02 04:11	2.58	271.074
Apr 27 02 04:16	2.67	270.983
Apr 27 02 04:21	2.75	270.998
Apr 27 02 04:26	2.83	271.000
Apr 27 02 04:31	2.92	271.015
Apr 27 02 04:36	3.00	271.015
Apr 27 02 04:41	3.08	271.024
Apr 27 02 04:46	3.17	271.037
Apr 27 02 04:51	3.25	271.044
Apr 27 02 04:56	3.33	271.052
Apr 27 02 05:01	3.42	271.061
Apr 27 02 05:06	3.50	271.071
Apr 27 02 05:11	3.58	271.079
Apr 27 02 05:16	3.67	271.085
Apr 27 02 05:21	3.75	271.087
Apr 27 02 05:26	3.83	271.084
Apr 27 02 05:31	3.92	271.083

(1) Bed Elevation, 269.337 m

Time		W.L.[1]
(day hour)	(hr)	(m)
Apr 27 02 05:36	4.00	271.095
Apr 27 02 05:41	4.08	271.098
Apr 27 02 05:46	4.17	271.095
Apr 27 02 05:51	4.25	271.089
Apr 27 02 05:56	4.33	271.091
Apr 27 02 06:01	4.42	271.084
Apr 27 02 06:06	4.50	271.088
Apr 27 02 06:11	4.58	271.083
Apr 27 02 06:16	4.67	271.083
Apr 27 02 06:21	4.75	271.090
Apr 27 02 06:26	4.83	271.094
Apr 27 02 06:31	4.92	271.093
Apr 27 02 06:36	5.00	271.097
Apr 27 02 06:41	5.08	271.091
Apr 27 02 06:46	5.17	271.099
Apr 27 02 06:51	5.25	271.100
Apr 27 02 06:56	5.33	271.093
Apr 27 02 07:01	5.42	271.097
Apr 27 02 07:06	5.50	271.096
Apr 27 02 07:11	5.58	271.083
Apr 27 02 07:16	5.67	271.087
Apr 27 02 07:21	5.75	271.083
Apr 27 02 07:26	5.83	271.086
Apr 27 02 07:31	5.92	271.094
Apr 27 02 07:36	6.00	271.094
Apr 27 02 07:41	6.08	271.090
Apr 27 02 07:46	6.17	271.086
Apr 27 02 07:51	6.25	271.091
Apr 27 02 07:56	6.33	271.082
Apr 27 02 08:01	6.42	271.088
Apr 27 02 08:06	6.50	271.089
Apr 27 02 08:11	6.58	271.077
Apr 27 02 08:16	6.67	271.069
Apr 27 02 08:21	6.75	271.071
Apr 27 02 08:26	6.83	271.069
Apr 27 02 08:31	6.92	271.061
Apr 27 02 08:36	7.00	271.057
Apr 27 02 08:41	7.08	271.051
Apr 27 02 08:46	7.17	271.047
Apr 27 02 08:51	7.25	271.040
Apr 27 02 08:56	7.33	271.042
Apr 27 02 09:01	7.42	271.034
Apr 27 02 09:06	7.50	271.029
Apr 27 02 09:11	7.58	271.017
Apr 27 02 09:16	7.67	271.020
Apr 27 02 09:21	7.75	271.013
Apr 27 02 09:26	7.83	271.011
Apr 27 02 09:31	7.92	271.009

(1) Bed Elevation, 269.337 m

Table A-1 Continued. Measured data for station G140.

Time (day hour)	Time (hr)	W.L.[1] (m)
Apr 27 02 09:36	8.00	271.008
Apr 27 02 09:41	8.08	271.001
Apr 27 02 09:46	8.17	271.001
Apr 27 02 09:51	8.25	270.999
Apr 27 02 09:56	8.33	271.000
Apr 27 02 10:01	8.42	270.993
Apr 27 02 10:06	8.50	270.999
Apr 27 02 10:11	8.58	270.992
Apr 27 02 10:16	8.67	270.991
Apr 27 02 10:21	8.75	270.992
Apr 27 02 10:26	8.83	270.968
Apr 27 02 10:31	8.92	270.973
Apr 27 02 10:36	9.00	270.959
Apr 27 02 10:41	9.08	270.963
Apr 27 02 10:46	9.17	270.976
Apr 27 02 10:51	9.25	270.956
Apr 27 02 10:56	9.33	270.962
Apr 27 02 11:01	9.42	270.963
Apr 27 02 11:06	9.50	270.968
Apr 27 02 11:11	9.58	270.956
Apr 27 02 11:16	9.67	270.950
Apr 27 02 11:21	9.75	270.957
Apr 27 02 11:26	9.83	270.949
Apr 27 02 11:31	9.92	270.963
Apr 27 02 11:36	10.00	270.956
Apr 27 02 11:41	10.08	270.943
Apr 27 02 11:46	10.17	270.936
Apr 27 02 11:51	10.25	270.933
Apr 27 02 11:56	10.33	270.948
Apr 27 02 12:01	10.42	270.940
Apr 27 02 12:06	10.50	270.927
Apr 27 02 12:11	10.58	270.929
Apr 27 02 12:16	10.67	270.924
Apr 27 02 12:21	10.75	270.921
Apr 27 02 12:26	10.83	270.930
Apr 27 02 12:31	10.92	270.928
Apr 27 02 12:36	11.00	270.925
Apr 27 02 12:41	11.08	270.923
Apr 27 02 12:46	11.17	270.912
Apr 27 02 12:51	11.25	270.922
Apr 27 02 12:56	11.33	270.922
Apr 27 02 13:01	11.42	270.915
Apr 27 02 13:06	11.50	270.908
Apr 27 02 13:11	11.58	270.914
Apr 27 02 13:16	11.67	270.904
Apr 27 02 13:21	11.75	270.916
Apr 27 02 13:26	11.83	270.918
Apr 27 02 13:31	11.92	270.912

(1) Bed Elevation, 269.337 m

Time (day hour)	Time (hr)	W.L.[1] (m)
Apr 27 02 13:36	12.00	270.910
Apr 27 02 13:41	12.08	270.902
Apr 27 02 13:46	12.17	270.907
Apr 27 02 13:51	12.25	270.898
Apr 27 02 13:56	12.33	270.909
Apr 27 02 14:01	12.42	270.900
Apr 27 02 14:06	12.50	270.899
Apr 27 02 14:11	12.58	270.903
Apr 27 02 14:16	12.67	270.901
Apr 27 02 14:21	12.75	270.899
Apr 27 02 14:26	12.83	270.903
Apr 27 02 14:31	12.92	270.899
Apr 27 02 14:36	13.00	270.901
Apr 27 02 14:41	13.08	270.893
Apr 27 02 14:46	13.17	270.895
Apr 27 02 14:51	13.25	270.891
Apr 27 02 14:56	13.33	270.883
Apr 27 02 15:01	13.42	270.882

(1) Bed Elevation, 269.337 m

Table A-2. Measured data for station G135.

Time (day hour)	Time (hr)	W.L.[1] (m)
Apr 27 02 01:35	-0.01	263.957
Apr 27 02 01:40	0.07	263.937
Apr 27 02 01:45	0.15	263.926
Apr 27 02 01:50	0.24	263.922
Apr 27 02 01:55	0.32	263.920
Apr 27 02 02:00	0.40	263.920
Apr 27 02 02:05	0.49	263.924
Apr 27 02 02:10	0.57	263.931
Apr 27 02 02:15	0.65	264.450
Apr 27 02 02:20	0.74	265.505
Apr 27 02 02:25	0.82	264.968
Apr 27 02 02:30	0.90	264.893
Apr 27 02 02:35	0.99	264.827
Apr 27 02 02:40	1.07	264.699
Apr 27 02 02:45	1.15	264.618
Apr 27 02 02:50	1.24	264.488
Apr 27 02 02:55	1.32	264.325
Apr 27 02 03:00	1.40	264.180
Apr 27 02 03:05	1.49	264.048
Apr 27 02 03:10	1.57	263.922
Apr 27 02 03:15	1.65	263.810
Apr 27 02 03:20	1.74	263.711
Apr 27 02 03:25	1.82	263.630
Apr 27 02 03:30	1.90	263.540
Apr 27 02 03:35	1.99	263.467
Apr 27 02 03:40	2.07	263.399
Apr 27 02 03:45	2.15	263.340
Apr 27 02 03:50	2.24	263.276
Apr 27 02 03:55	2.32	263.228
Apr 27 02 04:00	2.40	263.171
Apr 27 02 04:05	2.49	263.123
Apr 27 02 04:10	2.57	263.089
Apr 27 02 04:15	2.65	263.051
Apr 27 02 04:20	2.74	263.025
Apr 27 02 04:25	2.82	263.006
Apr 27 02 04:30	2.90	262.988
Apr 27 02 04:35	2.99	262.953
Apr 27 02 04:40	3.07	262.942
Apr 27 02 04:45	3.15	262.929
Apr 27 02 04:50	3.24	262.925
Apr 27 02 04:55	3.32	262.904
Apr 27 02 05:00	3.40	262.897
Apr 27 02 05:05	3.49	262.890
Apr 27 02 05:10	3.57	262.882
Apr 27 02 05:15	3.65	262.891
Apr 27 02 05:20	3.74	262.880
Apr 27 02 05:25	3.82	262.877
Apr 27 02 05:30	3.90	262.871

(1) Bed Elevation, 261.723 m

Time (day hour)	Time (hr)	W.L.[1] (m)
Apr 27 02 05:35	3.99	262.873
Apr 27 02 05:40	4.07	262.873
Apr 27 02 05:45	4.15	262.873
Apr 27 02 05:50	4.24	262.878
Apr 27 02 05:55	4.32	262.873
Apr 27 02 06:00	4.40	262.877
Apr 27 02 06:05	4.49	262.880
Apr 27 02 06:10	4.57	262.890
Apr 27 02 06:15	4.65	262.885
Apr 27 02 06:20	4.74	262.889
Apr 27 02 06:25	4.82	262.897
Apr 27 02 06:30	4.90	262.902
Apr 27 02 06:35	4.99	262.897
Apr 27 02 06:40	5.07	262.899
Apr 27 02 06:45	5.15	262.909
Apr 27 02 06:50	5.24	262.899
Apr 27 02 06:55	5.32	262.897
Apr 27 02 07:00	5.40	262.906
Apr 27 02 07:05	5.49	262.905
Apr 27 02 07:10	5.57	262.905
Apr 27 02 07:15	5.65	262.905
Apr 27 02 07:20	5.74	262.905
Apr 27 02 07:25	5.82	262.906
Apr 27 02 07:30	5.90	262.902
Apr 27 02 07:35	5.99	262.904
Apr 27 02 07:40	6.07	262.908
Apr 27 02 07:45	6.15	262.894
Apr 27 02 07:50	6.24	262.898
Apr 27 02 07:55	6.32	262.898
Apr 27 02 08:00	6.40	262.900
Apr 27 02 08:05	6.49	262.891
Apr 27 02 08:10	6.57	262.902
Apr 27 02 08:15	6.65	262.898
Apr 27 02 08:20	6.74	262.895
Apr 27 02 08:25	6.82	262.898
Apr 27 02 08:30	6.90	262.893
Apr 27 02 08:35	6.99	262.888
Apr 27 02 08:40	7.07	262.886
Apr 27 02 08:45	7.15	262.880
Apr 27 02 08:50	7.24	262.878
Apr 27 02 08:55	7.32	262.880
Apr 27 02 09:00	7.40	262.879
Apr 27 02 09:05	7.49	262.881
Apr 27 02 09:10	7.57	262.878
Apr 27 02 09:15	7.65	262.869
Apr 27 02 09:20	7.74	262.869
Apr 27 02 09:25	7.82	262.866
Apr 27 02 09:30	7.90	262.854

(1) Bed Elevation, 261.723 m

Table A-2 Continued. Measured data for station G135.

Time		W.L.[1]
(day hour)	(hr)	(m)
Apr 27 02 09:35	7.99	262.858
Apr 27 02 09:40	8.07	262.851
Apr 27 02 09:45	8.15	262.853
Apr 27 02 09:50	8.24	262.847
Apr 27 02 09:55	8.32	262.846
Apr 27 02 10:00	8.40	262.847
Apr 27 02 10:05	8.49	262.844
Apr 27 02 10:10	8.57	262.832
Apr 27 02 10:15	8.65	262.828
Apr 27 02 10:20	8.74	262.821
Apr 27 02 10:25	8.82	262.826
Apr 27 02 10:30	8.90	262.812
Apr 27 02 10:35	8.99	262.818
Apr 27 02 10:40	9.07	262.817
Apr 27 02 10:45	9.15	262.814
Apr 27 02 10:50	9.24	262.807
Apr 27 02 10:55	9.32	262.809
Apr 27 02 11:00	9.40	262.802
Apr 27 02 11:05	9.49	262.810
Apr 27 02 11:10	9.57	262.804
Apr 27 02 11:15	9.65	262.799
Apr 27 02 11:20	9.74	262.799
Apr 27 02 11:25	9.82	262.795
Apr 27 02 11:30	9.90	262.784
Apr 27 02 11:35	9.99	262.779
Apr 27 02 11:40	10.07	262.782
Apr 27 02 11:45	10.15	262.792
Apr 27 02 11:50	10.24	262.777
Apr 27 02 11:55	10.32	262.777
Apr 27 02 12:00	10.40	262.775
Apr 27 02 12:05	10.49	262.771
Apr 27 02 12:10	10.57	262.771
Apr 27 02 12:15	10.65	262.768
Apr 27 02 12:20	10.74	262.762
Apr 27 02 12:25	10.82	262.760
Apr 27 02 12:30	10.90	262.766
Apr 27 02 12:35	10.99	262.773
Apr 27 02 12:40	11.07	262.768
Apr 27 02 12:45	11.15	262.764
Apr 27 02 12:50	11.24	262.764
Apr 27 02 12:55	11.32	262.755
Apr 27 02 13:00	11.40	262.762
Apr 27 02 13:05	11.49	262.759
Apr 27 02 13:10	11.57	262.764
Apr 27 02 13:15	11.65	262.763
Apr 27 02 13:20	11.74	262.762
Apr 27 02 13:25	11.82	262.753
Apr 27 02 13:30	11.90	262.761

(1) Bed Elevation, 261.723 m

Time		W.L.[1]
(day hour)	(hr)	(m)
Apr 27 02 13:35	11.99	262.768
Apr 27 02 13:40	12.07	262.752
Apr 27 02 13:45	12.15	262.748
Apr 27 02 13:50	12.24	262.759
Apr 27 02 13:55	12.32	262.759
Apr 27 02 14:00	12.40	262.756
Apr 27 02 14:05	12.49	262.763
Apr 27 02 14:10	12.57	262.761
Apr 27 02 14:15	12.65	262.761
Apr 27 02 14:20	12.74	262.761
Apr 27 02 14:25	12.82	262.750
Apr 27 02 14:30	12.90	262.752
Apr 27 02 14:35	12.99	262.753
Apr 27 02 14:40	13.07	262.751
Apr 27 02 14:45	13.15	262.763
Apr 27 02 14:50	13.24	262.759
Apr 27 02 14:55	13.32	262.756
Apr 27 02 15:00	13.40	262.759

(1) Bed Elevation, 261.723 m

Table A-3. Measured data for station 132 (Levellogger).

Time (day hour)	Time (hr)	W.L.[1] (m)
Apr 27 02 01:35	-0.01	258.262
Apr 27 02 01:40	0.07	258.432
Apr 27 02 01:45	0.15	258.682
Apr 27 02 01:50	0.24	258.562
Apr 27 02 01:55	0.32	258.572
Apr 27 02 02:00	0.40	258.612
Apr 27 02 02:05	0.49	258.632
Apr 27 02 02:10	0.57	258.662
Apr 27 02 02:15	0.65	258.682
Apr 27 02 02:20	0.74	258.702
Apr 27 02 02:25	0.82	258.822
Apr 27 02 02:30	0.90	259.712
Apr 27 02 02:35	0.99	259.692
Apr 27 02 02:40	1.07	259.682
Apr 27 02 02:45	1.15	259.692
Apr 27 02 02:50	1.24	259.712
Apr 27 02 02:55	1.32	259.712
Apr 27 02 03:00	1.40	259.732
Apr 27 02 03:05	1.49	259.722
Apr 27 02 03:10	1.57	259.602
Apr 27 02 03:15	1.65	259.422
Apr 27 02 03:20	1.74	259.232
Apr 27 02 03:25	1.82	259.072
Apr 27 02 03:30	1.90	258.962
Apr 27 02 03:35	1.99	258.862
Apr 27 02 03:40	2.07	258.792
Apr 27 02 03:45	2.15	258.702
Apr 27 02 03:50	2.24	258.622
Apr 27 02 03:55	2.32	258.522
Apr 27 02 04:00	2.40	258.492
Apr 27 02 04:05	2.49	258.402
Apr 27 02 04:10	2.57	258.332
Apr 27 02 04:15	2.65	258.242
Apr 27 02 04:20	2.74	258.152
Apr 27 02 04:25	2.82	258.102
Apr 27 02 04:30	2.90	258.052
Apr 27 02 04:35	2.99	257.992
Apr 27 02 04:40	3.07	257.942
Apr 27 02 04:45	3.15	257.922
Apr 27 02 04:50	3.24	257.872
Apr 27 02 04:55	3.32	257.852
Apr 27 02 05:00	3.40	257.832
Apr 27 02 05:05	3.49	257.812
Apr 27 02 05:10	3.57	257.792
Apr 27 02 05:15	3.65	257.782
Apr 27 02 05:20	3.74	257.762
Apr 27 02 05:25	3.82	257.762
Apr 27 02 05:30	3.90	257.742

(1) Bed Elevation, 256.422 m

Time (day hour)	Time (hr)	W.L.[1] (m)
Apr 27 02 05:35	3.99	257.742
Apr 27 02 05:40	4.07	257.722
Apr 27 02 05:45	4.15	257.732
Apr 27 02 05:50	4.24	257.712
Apr 27 02 05:55	4.32	257.712
Apr 27 02 06:00	4.40	257.722
Apr 27 02 06:05	4.49	257.712
Apr 27 02 06:10	4.57	257.712
Apr 27 02 06:15	4.65	257.712
Apr 27 02 06:20	4.74	257.712
Apr 27 02 06:25	4.82	257.712
Apr 27 02 06:30	4.90	257.712
Apr 27 02 06:35	4.99	257.712
Apr 27 02 06:40	5.07	257.722
Apr 27 02 06:45	5.15	257.712
Apr 27 02 06:50	5.24	257.732
Apr 27 02 06:55	5.32	257.722
Apr 27 02 07:00	5.40	257.742
Apr 27 02 07:05	5.49	257.732
Apr 27 02 07:10	5.57	257.732
Apr 27 02 07:15	5.65	257.742
Apr 27 02 07:20	5.74	257.742
Apr 27 02 07:25	5.82	257.742
Apr 27 02 07:30	5.90	257.742
Apr 27 02 07:35	5.99	257.742
Apr 27 02 07:40	6.07	257.742
Apr 27 02 07:45	6.15	257.742
Apr 27 02 07:50	6.24	257.742
Apr 27 02 07:55	6.32	257.742
Apr 27 02 08:00	6.40	257.742
Apr 27 02 08:05	6.49	257.742
Apr 27 02 08:10	6.57	257.742
Apr 27 02 08:15	6.65	257.742
Apr 27 02 08:20	6.74	257.742
Apr 27 02 08:25	6.82	257.722
Apr 27 02 08:30	6.90	257.742
Apr 27 02 08:35	6.99	257.732
Apr 27 02 08:40	7.07	257.722
Apr 27 02 08:45	7.15	257.722
Apr 27 02 08:50	7.24	257.712
Apr 27 02 08:55	7.32	257.712
Apr 27 02 09:00	7.40	257.712
Apr 27 02 09:05	7.49	257.712
Apr 27 02 09:10	7.57	257.712
Apr 27 02 09:15	7.65	257.712
Apr 27 02 09:20	7.74	257.712
Apr 27 02 09:25	7.82	257.692
Apr 27 02 09:30	7.90	257.692

(1) Bed Elevation, 256.422 m

Table A-3 Continued. Measured data for station 132 (Levellogger).

Time		W.L.[1]
(day hour)	(hr)	(m)
Apr 27 02 09:35	7.99	257.692
Apr 27 02 09:40	8.07	257.692
Apr 27 02 09:45	8.15	257.692
Apr 27 02 09:50	8.24	257.682
Apr 27 02 09:55	8.32	257.672
Apr 27 02 10:00	8.40	257.672
Apr 27 02 10:05	8.49	257.672
Apr 27 02 10:10	8.57	257.672
Apr 27 02 10:15	8.65	257.642
Apr 27 02 10:20	8.74	257.642
Apr 27 02 10:25	8.82	257.642
Apr 27 02 10:30	8.90	257.642
Apr 27 02 10:35	8.99	257.642
Apr 27 02 10:40	9.07	257.632
Apr 27 02 10:45	9.15	257.622
Apr 27 02 10:50	9.24	257.622
Apr 27 02 10:55	9.32	257.622
Apr 27 02 11:00	9.40	257.602
Apr 27 02 11:05	9.49	257.602
Apr 27 02 11:10	9.57	257.602
Apr 27 02 11:15	9.65	257.602
Apr 27 02 11:20	9.74	257.582
Apr 27 02 11:25	9.82	257.582
Apr 27 02 11:30	9.90	257.582
Apr 27 02 11:35	9.99	257.582
Apr 27 02 11:40	10.07	257.582
Apr 27 02 11:45	10.15	257.552
Apr 27 02 11:50	10.24	257.552
Apr 27 02 11:55	10.32	257.552
Apr 27 02 12:00	10.40	257.552
Apr 27 02 12:05	10.49	257.552
Apr 27 02 12:10	10.57	257.532
Apr 27 02 12:15	10.65	257.532
Apr 27 02 12:20	10.74	257.532
Apr 27 02 12:25	10.82	257.532
Apr 27 02 12:30	10.90	257.522
Apr 27 02 12:35	10.99	257.512
Apr 27 02 12:40	11.07	257.512
Apr 27 02 12:45	11.15	257.512
Apr 27 02 12:50	11.24	257.512
Apr 27 02 12:55	11.32	257.512
Apr 27 02 13:00	11.40	257.492
Apr 27 02 13:05	11.49	257.492
Apr 27 02 13:10	11.57	257.482
Apr 27 02 13:15	11.65	257.482
Apr 27 02 13:20	11.74	257.482
Apr 27 02 13:25	11.82	257.482
Apr 27 02 13:30	11.90	257.482

(1) Bed Elevation, 256.422 m

Time		W.L.[1]
(day hour)	(hr)	(m)
Apr 27 02 13:35	11.99	257.482
Apr 27 02 13:40	12.07	257.482
Apr 27 02 13:45	12.15	257.472
Apr 27 02 13:50	12.24	257.482
Apr 27 02 13:55	12.32	257.482
Apr 27 02 14:00	12.40	257.482
Apr 27 02 14:05	12.49	257.472
Apr 27 02 14:10	12.57	257.472
Apr 27 02 14:15	12.65	257.472
Apr 27 02 14:20	12.74	257.462
Apr 27 02 14:25	12.82	257.462
Apr 27 02 14:30	12.90	257.462
Apr 27 02 14:35	12.99	257.462
Apr 27 02 14:40	13.07	257.462
Apr 27 02 14:45	13.15	257.462
Apr 27 02 14:50	13.24	257.462
Apr 27 02 14:55	13.32	257.462
Apr 27 02 15:00	13.40	257.462

(1) Bed Elevation, 256.422 m

Table A-4. Measured data for station G130.

Time (day hour)	Time (hr)	W.L.[1] (m)
Apr 27 02 01:35	-0.01	257.513
Apr 27 02 01:40	0.07	257.521
Apr 27 02 01:45	0.15	257.522
Apr 27 02 01:50	0.24	257.595
Apr 27 02 01:55	0.32	257.654
Apr 27 02 02:00	0.40	257.726
Apr 27 02 02:05	0.49	257.720
Apr 27 02 02:10	0.57	257.706
Apr 27 02 02:15	0.65	257.693
Apr 27 02 02:20	0.74	257.689
Apr 27 02 02:25	0.82	257.680
Apr 27 02 02:30	0.90	257.680
Apr 27 02 02:35	0.99	257.687
Apr 27 02 02:40	1.07	257.704
Apr 27 02 02:45	1.15	258.745
Apr 27 02 02:50	1.24	258.511
Apr 27 02 02:55	1.32	258.863
Apr 27 02 03:00	1.40	258.904
Apr 27 02 03:05	1.49	258.809
Apr 27 02 03:10	1.57	258.751
Apr 27 02 03:15	1.65	258.749
Apr 27 02 03:20	1.74	258.721
Apr 27 02 03:25	1.82	258.705
Apr 27 02 03:30	1.90	258.679
Apr 27 02 03:35	1.99	258.571
Apr 27 02 03:40	2.07	258.405
Apr 27 02 03:45	2.15	258.244
Apr 27 02 03:50	2.24	258.147
Apr 27 02 03:55	2.32	258.016
Apr 27 02 04:00	2.40	257.901
Apr 27 02 04:05	2.49	257.823
Apr 27 02 04:10	2.57	257.731
Apr 27 02 04:15	2.65	257.657
Apr 27 02 04:20	2.74	257.566
Apr 27 02 04:25	2.82	257.509
Apr 27 02 04:30	2.90	257.414
Apr 27 02 04:35	2.99	257.353
Apr 27 02 04:40	3.07	257.290
Apr 27 02 04:45	3.15	257.216
Apr 27 02 04:50	3.24	257.163
Apr 27 02 04:55	3.32	257.096
Apr 27 02 05:00	3.40	257.031
Apr 27 02 05:05	3.49	257.000
Apr 27 02 05:10	3.57	256.952
Apr 27 02 05:15	3.65	256.896
Apr 27 02 05:20	3.74	256.857
Apr 27 02 05:25	3.82	256.800
Apr 27 02 05:30	3.90	256.780

(1) Bed Elevation, 255.048 m

Time (day hour)	Time (hr)	W.L.[1] (m)
Apr 27 02 05:35	3.99	256.730
Apr 27 02 05:40	4.07	256.700
Apr 27 02 05:45	4.15	256.715
Apr 27 02 05:50	4.24	256.687
Apr 27 02 05:55	4.32	256.680
Apr 27 02 06:00	4.40	256.652
Apr 27 02 06:05	4.49	256.641
Apr 27 02 06:10	4.57	256.624
Apr 27 02 06:15	4.65	256.608
Apr 27 02 06:20	4.74	256.575
Apr 27 02 06:25	4.82	256.583
Apr 27 02 06:30	4.90	256.572
Apr 27 02 06:35	4.99	256.569
Apr 27 02 06:40	5.07	256.571
Apr 27 02 06:45	5.15	256.588
Apr 27 02 06:50	5.24	256.574
Apr 27 02 06:55	5.32	256.582
Apr 27 02 07:00	5.40	256.594
Apr 27 02 07:05	5.49	256.550
Apr 27 02 07:10	5.57	256.578
Apr 27 02 07:15	5.65	256.581
Apr 27 02 07:20	5.74	256.562
Apr 27 02 07:25	5.82	256.573
Apr 27 02 07:30	5.90	256.605
Apr 27 02 07:35	5.99	256.604
Apr 27 02 07:40	6.07	256.591
Apr 27 02 07:45	6.15	256.600
Apr 27 02 07:50	6.24	256.587
Apr 27 02 07:55	6.32	256.569
Apr 27 02 08:00	6.40	256.582
Apr 27 02 08:05	6.49	256.580
Apr 27 02 08:10	6.57	256.613
Apr 27 02 08:15	6.65	256.589
Apr 27 02 08:20	6.74	256.601
Apr 27 02 08:25	6.82	256.605
Apr 27 02 08:30	6.90	256.598
Apr 27 02 08:35	6.99	256.591
Apr 27 02 08:40	7.07	256.593
Apr 27 02 08:45	7.15	256.574
Apr 27 02 08:50	7.24	256.576
Apr 27 02 08:55	7.32	256.593
Apr 27 02 09:00	7.40	256.581
Apr 27 02 09:05	7.49	256.603
Apr 27 02 09:10	7.57	256.557
Apr 27 02 09:15	7.65	256.600
Apr 27 02 09:20	7.74	256.577
Apr 27 02 09:25	7.82	256.570
Apr 27 02 09:30	7.90	256.544

(1) Bed Elevation, 255.048 m

Table A-4 Continued. Measured data for station G130.

Time (day hour)	Time (hr)	W.L.[1] (m)
Apr 27 02 09:35	7.99	256.550
Apr 27 02 09:40	8.07	256.566
Apr 27 02 09:45	8.15	256.570
Apr 27 02 09:50	8.24	256.569
Apr 27 02 09:55	8.32	256.556
Apr 27 02 10:00	8.40	256.545
Apr 27 02 10:05	8.49	256.550
Apr 27 02 10:10	8.57	256.550
Apr 27 02 10:15	8.65	256.562
Apr 27 02 10:20	8.74	256.537
Apr 27 02 10:25	8.82	256.537
Apr 27 02 10:30	8.90	256.547
Apr 27 02 10:35	8.99	256.532
Apr 27 02 10:40	9.07	256.538
Apr 27 02 10:45	9.15	256.529
Apr 27 02 10:50	9.24	256.520
Apr 27 02 10:55	9.32	256.514
Apr 27 02 11:00	9.40	256.516
Apr 27 02 11:05	9.49	256.503
Apr 27 02 11:10	9.57	256.516
Apr 27 02 11:15	9.65	256.496
Apr 27 02 11:20	9.74	256.492
Apr 27 02 11:25	9.82	256.481
Apr 27 02 11:30	9.90	256.493
Apr 27 02 11:35	9.99	256.482
Apr 27 02 11:40	10.07	256.462
Apr 27 02 11:45	10.15	256.464
Apr 27 02 11:50	10.24	256.429
Apr 27 02 11:55	10.32	256.448
Apr 27 02 12:00	10.40	256.437
Apr 27 02 12:05	10.49	256.426
Apr 27 02 12:10	10.57	256.426
Apr 27 02 12:15	10.65	256.417
Apr 27 02 12:20	10.74	256.398
Apr 27 02 12:25	10.82	256.439
Apr 27 02 12:30	10.90	256.416
Apr 27 02 12:35	10.99	256.404
Apr 27 02 12:40	11.07	256.398
Apr 27 02 12:45	11.15	256.376
Apr 27 02 12:50	11.24	256.376
Apr 27 02 12:55	11.32	256.370
Apr 27 02 13:00	11.40	256.359
Apr 27 02 13:05	11.49	256.377
Apr 27 02 13:10	11.57	256.379
Apr 27 02 13:15	11.65	256.379
Apr 27 02 13:20	11.74	256.392
Apr 27 02 13:25	11.82	256.379
Apr 27 02 13:30	11.90	256.377

(1) Bed Elevation, 255.048 m

Time (day hour)	Time (hr)	W.L.[1] (m)
Apr 27 02 13:35	11.99	256.375
Apr 27 02 13:40	12.07	256.368
Apr 27 02 13:45	12.15	256.348
Apr 27 02 13:50	12.24	256.353
Apr 27 02 13:55	12.32	256.370
Apr 27 02 14:00	12.40	256.355
Apr 27 02 14:05	12.49	256.344
Apr 27 02 14:10	12.57	256.346
Apr 27 02 14:15	12.65	256.342
Apr 27 02 14:20	12.74	256.333
Apr 27 02 14:25	12.82	256.348
Apr 27 02 14:30	12.90	256.344
Apr 27 02 14:35	12.99	256.348
Apr 27 02 14:40	13.07	256.327
Apr 27 02 14:45	13.15	256.307
Apr 27 02 14:50	13.24	256.331
Apr 27 02 14:55	13.32	256.348
Apr 27 02 15:00	13.40	256.346

(1) Bed Elevation, 255.048 m

Table A-5. Measured data for station 104.

Time		W.L.[1]
(day hour)	(hr)	(m)
Apr 27 02 01:36	0.00	244.611
Apr 27 02 01:41	0.08	244.612
Apr 27 02 01:46	0.17	244.622
Apr 27 02 01:51	0.25	244.632
Apr 27 02 01:56	0.33	244.626
Apr 27 02 02:01	0.42	244.629
Apr 27 02 02:06	0.50	244.632
Apr 27 02 02:11	0.58	244.637
Apr 27 02 02:16	0.67	244.641
Apr 27 02 02:21	0.75	244.650
Apr 27 02 02:26	0.83	244.647
Apr 27 02 02:31	0.92	244.652
Apr 27 02 02:36	1.00	244.659
Apr 27 02 02:41	1.08	244.658
Apr 27 02 02:46	1.17	244.662
Apr 27 02 02:51	1.25	244.665
Apr 27 02 02:56	1.33	244.670
Apr 27 02 03:01	1.42	244.677
Apr 27 02 03:06	1.50	244.680
Apr 27 02 03:11	1.58	244.683
Apr 27 02 03:16	1.67	244.689
Apr 27 02 03:21	1.75	244.696
Apr 27 02 03:26	1.83	244.707
Apr 27 02 03:31	1.92	244.727
Apr 27 02 03:36	2.00	244.781
Apr 27 02 03:41	2.08	244.902
Apr 27 02 03:46	2.17	245.139
Apr 27 02 03:51	2.25	245.321
Apr 27 02 03:56	2.33	245.345
Apr 27 02 04:01	2.42	245.375
Apr 27 02 04:06	2.50	245.414
Apr 27 02 04:11	2.58	245.462
Apr 27 02 04:16	2.67	245.493
Apr 27 02 04:21	2.75	245.462
Apr 27 02 04:26	2.83	245.460
Apr 27 02 04:31	2.92	245.404

(1) Bed Elevation, 242.275 m

Table A-6. Measured data for station 90 (RMWB-manual).

Time		W.L.[1]
(day hour)	(hr)	(m)
Apr 26 02 21:00	-4.60	241.420
Apr 27 02 04:00	2.40	241.670
Apr 27 02 05:15	3.65	241.800
Apr 27 02 05:30	3.90	242.100
Apr 27 02 05:45	4.15	242.300
Apr 27 02 06:00	4.40	242.600
Apr 27 02 06:10	4.57	242.800
Apr 27 02 06:30	4.90	242.600
Apr 27 02 07:30	5.90	242.300
Apr 27 02 08:30	6.90	242.200
Apr 27 02 09:30	7.90	242.100
Apr 27 02 10:30	8.90	242.000
Apr 27 02 12:30	10.90	241.900
Apr 27 02 13:30	11.90	241.900
Apr 27 02 14:30	12.90	241.900

(1) Bed Elevation, 238.629 m

Table A-7. Measured data for station 57 (WSC gauge).

Time (day hour)	Time (hr)	W.L.[1] (m)
Apr 27 02 01:30	-0.10	239.389
Apr 27 02 01:45	0.15	239.407
Apr 27 02 02:00	0.40	239.415
Apr 27 02 02:15	0.65	239.420
Apr 27 02 02:30	0.90	239.426
Apr 27 02 02:45	1.15	239.435
Apr 27 02 03:00	1.40	239.447
Apr 27 02 03:15	1.65	239.455
Apr 27 02 03:30	1.90	239.464
Apr 27 02 03:45	2.15	239.472
Apr 27 02 04:00	2.40	239.499
Apr 27 02 04:15	2.65	239.513
Apr 27 02 04:30	2.90	239.529
Apr 27 02 04:45	3.15	239.545
Apr 27 02 05:00	3.40	239.563
Apr 27 02 05:15	3.65	239.592
Apr 27 02 05:30	3.90	239.632
Apr 27 02 05:45	4.15	239.707
Apr 27 02 06:00	4.40	239.676
Apr 27 02 06:15	4.65	239.714
Apr 27 02 06:30	4.90	239.678
Apr 27 02 06:45	5.15	239.757
Apr 27 02 07:00	5.40	239.825
Apr 27 02 07:15	5.65	239.774
Apr 27 02 07:30	5.90	239.806
Apr 27 02 07:45	6.15	239.782
Apr 27 02 08:00	6.40	239.688
Apr 27 02 08:15	6.65	239.727
Apr 27 02 08:30	6.90	239.732
Apr 27 02 08:45	7.15	239.709
Apr 27 02 09:00	7.40	239.754
Apr 27 02 09:15	7.65	239.783
Apr 27 02 09:30	7.90	239.940
Apr 27 02 09:45	8.15	239.854
Apr 27 02 10:00	8.40	239.843
Apr 27 02 10:15	8.65	239.832
Apr 27 02 10:30	8.90	239.826
Apr 27 02 10:45	9.15	239.813
Apr 27 02 11:00	9.40	239.804
Apr 27 02 11:15	9.65	239.783
Apr 27 02 11:30	9.90	239.774
Apr 27 02 11:45	10.15	239.768
Apr 27 02 12:00	10.40	239.761
Apr 27 02 12:15	10.65	239.746
Apr 27 02 12:30	10.90	239.734
Apr 27 02 12:45	11.15	239.725
Apr 27 02 13:00	11.40	239.708
Apr 27 02 13:15	11.65	239.698
Apr 27 02 13:30	11.90	239.685
Apr 27 02 13:45	12.15	239.644
Apr 27 02 14:00	12.40	239.655
Apr 27 02 14:15	12.65	239.654
Apr 27 02 14:30	12.90	239.634
Apr 27 02 14:45	13.15	239.622
Apr 27 02 15:00	13.40	239.607

(1) Bed Elevation, 237.298 m